

**DEVELOPMENT OF METAL COMPLEXES FOR USE IN NON-
AQUEOUS REDOX FLOW BATTERIES AND C–H
FUNCTIONALIZATION OF *N*-HETEROCYCLES**

by

Pablo Cabrera Ventura

A dissertation submitted in partial fulfillment
of the requirements for the degree of
Doctor of Philosophy
(Chemistry)
in the University of Michigan
2017

Doctoral Committee:

Professor Melanie S. Sanford, Co-Chair
Professor Levi T. Thompson, Co-Chair
Professor John Montgomery
Professor Corey Stephenson

Pablo Cabrera Ventura
pabloco@umich.edu
orcid.org/0000-0003-1512-3399

© Pablo Cabrera Ventura 2017

Acknowledgements

The conclusion of this program is nothing but a collective effort that began prior to coming to the University of Michigan. God has blessed me with the opportunity to come to the University of Michigan and to be surrounded by many outstanding people that have guided me throughout my graduate career and to whom I owe enormous gratitude.

Melanie, I want to thank you for being an amazing advisor and mentor for me. I am very fortunate to have the opportunity to work in your lab. You have taught me how to think about chemistry in a new way. I feel very thankful for the many projects you let me try. You have been very positive and patient with me, even when research was going slow. Thank you for investing so much time in me. Even with your busy schedule, you always were able to find time to help me. You have gone above and beyond to help me achieve my aspirations as a chemist. Your incredible care for the lab has been instrumental for my development as a scientist.

I am grateful to my committee members Professors John Montgomery, Corey Stephenson, Levi Thompson and John Wolfe. Professor Montgomery, I had a great time during my rotation in your lab. I learned so much about nickel catalysis, air-sensitive techniques and NMR. I am also very thankful for your continual support. Professor Stephenson since you moved to Michigan, you have been incredibly helpful and have always gone out of your way to help me in research, ORP, and my career aspirations. Professor Thompson, it has been a pleasure working with you and your group. Our battery research collaboration has been one of the most valuable experiences in my PhD career. Professor Wolfe, thank you for your willingness to serve on my committee.

I am very thankful to all our members of the chemistry department staff. In particular, Margarita Bekiares, Liz Oxford, Cornelius Wright and Heather Hanosh for the countless academic and administrative support. I am extremely thankful to Dr. Eugenio Alvarado for your patience and help in teaching me NMR spectroscopy techniques. I'm thankful to Jim Windak and Paul Lennon for their quick turnaround and support in mass

spectrometry. I am very thankful to Dr. Jeff Kampf for working above and beyond to help me solve several X-ray structures. I am also grateful to Tracy Stevenson, Chris Peters, Laurie MacDonald, and Jon Boyd for their hard work in maintaining the Chemistry building. Roy Wentz, thank you for making outstanding battery H-cell glassware.

I would like to thank my lab mentors Drs. Amanda Cook, James Suttill, Laura Allen, Sarah Ryan, and Joseph Topczewski for all the advice that has helped me grow as a scientist. In particular, I want to thank James Suttill for his patience and help during the battery project. James, I had a blast working with you and learning a bunch of organometallic techniques from you. Laura, it was amazing to work with you in the photocatalysis project and to be around your contagious optimistic personality. Sarah, you brightened my days and always enjoyed hanging out in and outside of lab with you. I appreciate all your help in organic synthesis and in professional career advice. Joe, I am honored to have the opportunity to co-author an amazing paper with you.

I want to thank all the current and past Sanford lab members that I have had the opportunity to interact with as each of you have been instrumental in my career. Nomaan, it has been a pleasure working with such a smart person like you over the past five years. We've gone through a bunch of stuff together and I would say you've become one of my closest friends here at Michigan. You always find time to listen to me and give me great advice. Melissa, I am so fortunate to start and end my graduate career working with you. You have a natural chemistry instinct that has been instrumental to move forward our projects. I am excited to see all the great things you'll accomplish after grad school. James Bour, you are one of the smartest people I've encountered in graduate school and I am tremendously thankful for your ideas and suggestions, but most importantly, for our random chemistry conversations that have helped me learn about topics outside of our areas of research. Devin, you are the best desk-mate anyone could have. I had an incredible time working next to you. You are extremely talented chemist, very patient and always have time to help me out with editing, chemistry or anything. Ellen and Anuska, I am honored to have the opportunity to work with you in C-H activation projects and I look forward to seeing all you both will accomplish. Naoko, thank you for being a great friend and for all the gum you've given me. Christo, Eugene and Matt, thank you so much for always finding the time to help

me in my chemistry. Danielle, Naoko, Devin, Melissa, Eugene, Courtney, Koen and Andrew thank you so much for taking the time to edit my thesis chapters. I would like to acknowledge Thomas Dröge, Ansis Maleckis, Mónica Pérez, Rachel Brooner, Anna Wagner and Chelsea Huff for being amazing and welcoming lab-mates when I first joined the group. I want to thank Sydonie, Nicole, Ian, Sharmila, BJ, Liz, Monique, Curren and Katarina for always be there to help and to chat.

Prior to coming to Michigan I had the pleasure to interact with remarkable mentors that have impacted my academic career and life. Professor Kateri Ahrendt, thank you for taking the time to teach me organic chemistry while at Regis and for your suggestion to apply to the University of Michigan. Professor Paul Helquist, you have been an incredible role model for me and have taught me a lot about research in organic chemistry during my time in Notre Dame. Professor Seibert, thank you so much for believing in me and providing me incredible guidance in classes and life. Professor Paiz, you were an amazing mentor to me during my time in Guatemala.

Finally, quiero agradecer a mi familia y amigos de Guatemala por su amor y apoyo. Jackie, my lovely wife, thank you so much for your love, patience, understanding and support through this PhD program. I couldn't have done it without you. I am incredibly thankful to you because you've been by my side every second of this journey. Víctor y Mari, muchas gracias por su amor incondicional y por acompañarme durante esta etapa académica, por siempre escucharme y darme ánimos para seguir adelante. Víctor, Marisol y Fredy por amarme tanto y siempre estar pendiente de mi a pesar de la distancia. A mis sobrinos José, Manuel, Marisabel y Ana Lucia por su amor y cariño para conmigo. Maco, muchísimas gracias por darme la oportunidad de estudiar en Regis y apoyarme en este proceso académico.

Table of Contents

Acknowledgements	ii
List of Figures	vii
List of Tables	xi
Abstract	xiii
Chapter 1. Introduction	
1.1 Redox Flow Batteries	1
1.2 C–H Functionalization of Nitrogen Heterocycles	6
1.3 References	12
Chapter 2. Structure-Solubility-Electrochemistry Relationships of Bipyridine Chromium Complexes for Redox Flow Battery Applications	
2.1 Introduction	16
2.2 Results and Discussion	18
2.3 Conclusions	40
2.4 Perspective and Outlook	41
2.5 Experimental	41
2.6 References	80
Chapter 3. C–H Amination of Arenes and Heteroarenes Via Visible Light Photocatalysis	
3.1 Introduction	82
3.2 Background	83
3.3 Results and Discussion	85
3.4 Conclusions	93
3.5 Perspective and Outlook	94
3.6 Experimental	95
3.7 References	120

Chapter 4. Pd-Catalyzed Transannular C–H Arylation of Alicyclic Amines

4.1 Introduction	122
4.2 Results and Discussion	126
4.3 Conclusions	148
4.4 Experimental	149
4.5 References	209

Chapter 5. Ligand Effects on the Pd-Catalyzed Transannular C–H Functionalization of Azabicycloalkanes

5.1 Introduction	212
5.2 Results and Discussion	216
5.3 Conclusions	232
5.4 Perspective and Outlook	232
5.5 Experimental	233
5.6 References	285

List of Figures

Figure 1.1. General schematic of a RFB	3
Figure 1.2. Representative <i>N</i> -heterocycles in nature	7
Figure 1.3. Example of a Minisci reaction	8
Figure 1.4. Lidgett's C–H amination of biphenyl	8
Figure 1.5. A) Generic Jablonski diagram of a photoredox catalyst. B) Graphical illustration of the triplet excited state species for Ru(bpy) ₃ ²⁺	9
Figure 1.6. Reductive and oxidative quenching cycles in photoredox catalysis	10
Figure 1.7. C5–H functionalization of piperidine	11
Figure 1.8. Representative example of non-directed C–H functionalization of alicyclic amines	11
Figure 1.9. Representative example on the use of native functionalities	12
Figure 1.10. Transannular C–H arylation of alicyclic amines	12
Figure 2.1. Selected examples of MCCs used in non-aqueous RFBs	17
Figure 2.2. Cr-complex with electron-withdrawing ester bpy ligands and the corresponding cyclic voltammogram	19
Figure 2.3. Solubility of literature Cr complexes	20
Figure 2.4. Synthetic routes to the ester- and alkoxy-bpy ligands	21
Figure 2.5. Synthesis of ester- and alkoxy-bpy [Cr(Ln) ₃] ³⁺ complexes. ORTEP of [Cr(L15) ₃] ³⁺	21
Figure 2.6. Solubility of complexes with ligands L3-L9	23
Figure 2.7. Solubility of complexes with ligands L10-L14	24
Figure 2.8. Solubility of the alkoxy-bpy Cr(III) complexes	25
Figure 2.9. Redox active species in a bpy Cr complex non-aqueous RFB	25
Figure 2.10. Synthesis and solubility of Cr(0) bpy complexes	26
Figure 2.11. Solubility comparison of [Cr(L5) ₃] and [Cr(L11) ₃] across oxidation states	27

Figure 2.12. Representative cyclic voltammogram	28
Figure 2.13. CV of $[\text{Cr}(\text{L}1)_3]^{3+}$ in acetonitrile	29
Figure 2.14. CV of $[\text{Cr}(\text{L}11)_3]^{3+}$ in acetonitrile	32
Figure 2.15. A) CV of $[\text{Cr}(\text{L}6)_3]^{3+}$; B) CV of $[\text{Cr}(\text{L}14)_3]^{3+}$; C) CV of $[\text{Cr}(\text{L}8)_3]^{3+}$	33
Figure 2.16. A) CV of $[\text{Cr}(\text{L}15)_3]^{3+}$; B) CV of free ligand L15	34
Figure 2.17. A) CV of $[\text{Cr}(\text{L}5)_3]^0$; B) CV of $[\text{Cr}(\text{L}5)_3]^{3+}$	35
Figure 2.18. Photograph of an H-cell employed for charge and discharge experiments	37
Figure 2.19. CV of $[\text{Cr}(\text{L}11)_3]^0$	38
Figure 2.20. Charge/discharge cycling at ± 0.64 mA for $[\text{Cr}(\text{L}11)_3]^0$ in a H-cell	40
Figure 2.21. Absorbance Vs. Concentration plot for compound $[\text{Cr}(\text{L}1)_3]^{+3}$	69
Figure 2.22. A) Black cyclic voltammogram of a 5 mM solution of $[\text{Cr}(\text{L}12)_3]^{3+}$. B) Blue cyclic voltammogram of a 10 mM solution of ferrocene. C) Red cyclic voltammogram is from a mixture of $[\text{Cr}(\text{L}12)_3]^{3+}$ (5 mM) and ferrocene (10 mM)	72
Figure 3.1. Representative examples of arenes and heteroarenes bearing amine substituents	82
Figure 3.2. Selected examples of aromatic C–H amination protocols	83
Figure 3.3. A) Selected methods for the generation of <i>N</i> -centered radicals. B) Okada's work in photoredox reduction of <i>N</i> -acyloxyphthalimides	85
Figure 3.4. Proposed pathway to generate nitrogen radicals using visible light photocatalysis	85
Figure 3.5. Proposed catalytic cycle for the C–H amination protocol	90
Figure 3.6. Cyclic voltammograms of 27 (blue) and 1 (red)	92
Figure 3.7. Recent example of visible light photoredox C–H amination method	94
Figure 4.1. Representative C4-aryl piperidine drugs	122
Figure 4.2. A) Synthetic routes to 4-aryl piperidines. B) Synthesis of paroxetine analogs	123
Figure 4.3. Representative examples of C2–H functionalization of alicyclic amines	124
Figure 4.4. Representative examples of remote C–H functionalization of alicyclic amines	124
Figure 4.5. sp^3 -Nitrogen directed C–H Activation	125

Figure 4.6. Design principle for the transannular C–H activation reaction	126
Figure 4.7. Challenges associated with C4–H activation of piperidine	127
Figure 4.8. Initial work in Pd C–H functionalization of piperidine.	128
Figure 4.9. Attempt to employ pyridine directing group to functionalize piperidine	129
Figure 4.10. Use of amide directing group to functionalize piperidine	130
Figure 4.11. A) Structure of 3-azabicyclo[3.1.0]hexane. B) Synthesis of 8. C) Initial C–H Arylation of 8	131
Figure 4.12. Proposed mechanism for amination formation	132
Figure 4.13. Optimized conditions for C4-Arylation of piperidine analog 5	137
Figure 4.14. C–H arylation of bioactive bicyclic amines	140
Figure 4.15. Unsuccessful methods for directing group removal	141
Figure 4.16. Proposed mechanism for reductive deamination	142
Figure 4.17. Unsuccessful amines for transannular C–H arylation	143
Figure 4.18. Development of auxiliary directing groups	144
Figure 4.19. Thorpe-Ingold Effect in substrates	146
Figure 4.20. C–H arylation of substrate 27 and ¹ H NMR spectrum of isolated product 29	148
Figure 5.1. Relevance of representative bioactive azabicycloalkanes	212
Figure 5.2. Representative examples for the synthesis of azabicycloalkanes	213
Figure 5.3. Representative examples of arylated azabicycloalkanes and synthetic routes	214
Figure 5.4. Gaunt's C–H arylation of alkylamines	215
Figure 5.5. Transannular C–H functionalization of alicyclic amines	215
Figure 5.6. Ligand-less reactivity of benzo-isotropane substrate 1	217
Figure 5.7. Rate profile of 2a in the presence of 5 mol% quinaldic acid (red curve) and absence of ligand (blue curve)	220
Figure 5.8. A) Plausible off-cycle Pd species. B) Literature sp ³ -hybridized amine bound Pd complexes. C) X-Ray of analogous phenyl-piperidine substrate	221
Figure 5.9. Curve A: same-excess product-added reaction profile. Curve B: Ligand-less C–H arylation of 1 (parent reaction profile). Curve C: Time-shifted curve A to match parent reaction at 0.03 M 2a	222

Figure 5.10. Ligand-less reaction initial rates comparison of [2a] versus time plots. Blue line reaction without product 2b. Red line initial rates with 0.06 M 2b (50 mol %)	224
Figure 5.11. Ligand-added reaction initial rates comparison of [2a] versus time plots. Blue line initial rates without product 2b. Red line initial rates with 0.06 M 2b	225
Figure 5.12. Kinetic isotope effect for 1 and d_5 -1 with and without quinaldic acid	226
Figure 5.13. Catalyst recovery by addition of quinaldic acid after 4 hours	227
Figure 5.14. A) Reaction of 3 without ligand. B) Reaction of 3 with quinaldic acid	228
Figure 5.15. A) Scope in aryl iodide for tropane 4. B) Scope in azabicycloalkanes. C) Ligand addition on previously reported alicyclic amines	230
Figure 5.16. C–H functionalization of azabicyclo-nonane 10	232
Figure 5.17. Rate profile of 1 and 2a in the presence of 5 mol % quinaldic acid	251
Figure 5.18. Rate profile of 1 and 2a in the presence of 5 mol % picolinic acid	252
Figure 5.19. Rate profile of 1 and 2a without ligand	253
Figure 5.20. Reaction profile with added product at the reaction onset	254
Figure 5.21. Plot of initial rate of [2a] versus time with quinaldic acid additive	255
Figure 5.22. Plot of initial rate of [2a] versus time with picolinic acid additive	256
Figure 5.23. Plot of initial rate of [2a] versus time	257
Figure 5.24. Initial rate plot of [2a] versus time with quinaldic acid in the presence of 0.06 M 2b	258
Figure 5.25. Initial rate plot of [2a] versus time in the presence of 0.06 M 2b	259
Figure 5.26. KIE of 1 versus d_5 -1 without ligand	260
Figure 5.27. KIE of 1 versus d_5 -1 with quinaldic acid	261
Figure 5.28. Catalyst recovery by addition of 5 mol % picolinic acid after 240 minutes	263

List of Tables

Table 2.1. Potentials, peak current ratios and peak separations for $[\text{Cr}(\text{L}1)_3]^{3+}$, $[\text{Cr}(\text{L}2)_3]^{3+}$, $[\text{Cr}(\text{L}3)_3]^{3+}$ in acetonitrile	30
Table 2.2. Potentials, peak current ratios and peak separations for the ester- and alkoxy-bpy Cr(III) complexes in acetonitrile	31
Table 2.3. Potentials, peak current ratios and peak separations for the ester-bpy Cr(0) complexes in acetonitrile	35
Table 2.4. Standard serial solutions of complex $[\text{Cr}(\text{L}1)_3]^{+3}$ on acetonitrile	68
Table 2.5. Photometric measurements of stock solutions of $[\text{Cr}(\text{L}1)_3]^{+3}$ at $\lambda=420$ nm	69
Table 2.6. Maximum solubility of complex 3 in acetonitrile	70
Table 2.7. Solubility parameters and solubilities of metal complexes in acetonitrile	71
Table 3.1. Evaluation of <i>N</i> -acyloxyphthalimides with varying R groups	86
Table 3.2. Substrate scope in arene and heteroarene	88
Table 3.3. Selectivity in the C–H amination of naphthalene with different C–H amination methods	89
Table 3.4. Synthesis of nitrogen radical sources	91
Table 3.5. Evaluation of nitrogen sources with mesitylene as substrate	91
Table 3.6. Reaction optimization for <i>N</i> -acyloxysaccharine 27	93
Table 4.1. Optimization for 3-azabicyclo[3.1.0]hexane 8	132
Table 4.2. Substrate scope of aryl iodide	134
Table 4.3. Scope of aryl electrophile	134
Table 4.4. Optimization of piperidine substrate 5	136
Table 4.5. Amino reduction optimization conditions	137
Table 4.6. C–H arylation of alicyclic amines	138
Table 4.7. Optimization for SmI_2 reductive deamination	142
Table 4.8. Synthesis of new directing groups	144
Table 4.9. Substrates reactivity comparison at 150 °C	145

Table 4.10. Reactivity comparison of substrates at 130 °C	146
Table 5.1. Ligand evaluation with benzo-fused isotropane substrate 1	218
Table 5.2. Reaction optimization of 1 with quinaldic acid	219
Table 5.3. Addition of 2b to the C–H arylation of 1	223
Table 5.4. Ligand evaluation for substrate 1	249
Table 5.5. Experiments with precipitate 3 and supernatant	265
Table 5.6. Reaction optimization for 4	269

Abstract

Batteries represent a sustainable energy storage technology for the integration of renewable resources into the electrical grid. The first part of my research focused on the development of metal complexes as redox active materials for non-aqueous redox flow batteries. Flow batteries are rechargeable batteries based on solvated electroactive species that are flowed between storage tanks and electrochemical conversion cells to store or release electrical energy.

Chapter 2 describes a systematic study on the impact of the bipyridine ligand structure on the solubility and electrochemistry of $[\text{Cr}(\text{bpy})_3]$ complexes that afford six reversible redox couples over ~ 2 V and solubilities approaching 1 M. These studies reveal that solubility is highly dependent on the oxidation state of the metal complex with solubility differences up to 4 orders of magnitude between the Cr(0) and the Cr(III) complexes. In contrast, modifications to the metal complex have minimal impact on the electrochemical properties. Furthermore, this investigation led to the identification of a promising Cr complex that was evaluated in charge/discharge experiments affording a two-electron transfer at each of the electrodes with efficiencies of 70%.

The second part of my research is focused on the development of C–H functionalization methodologies. The conversion of carbon–hydrogen (C–H) bonds into new functional groups represents a powerful strategy for the synthesis of organic molecules. The advent of C–H functionalization has enabled medicinal chemists to utilize a late-stage functionalization approach to efficiently convert the C–H bonds in drug candidates to new chemical entities. Despite tremendous progress in the field, selective C–H functionalization of *N*-heterocycles remains challenging.

Chapter 3 describes a room-temperature photoredox-catalyzed method for the C–H amination of hetero(arenes). This chapter describes the design and development of *N*-trifluoroacetyloxyphthalimide as precursor to nitrogen-centered radical intermediates. *N*-trifluoroacetyloxyphthalimide is proposed to undergo a single electron reduction by the

photocatalyst leading to an imidyl radical. The C–H amination protocol addresses several limitations from previous methods such as the need for expensive oxidants and elevated temperatures. The mild reaction conditions enabled the preparation of several *N*-heterocyclic amine products, which are common motifs in bioactive molecules. Furthermore, the synthesis of *N*-trifluoroacetyloxysaccharine afforded highly electrophilic *N*-radicals, thereby permitting further reaction optimization to lower the photocatalyst and hetero(arene) loading.

Chapter 4 describes the development of a Pd-catalyzed transannular C–H arylation of alicyclic amines. A key design principle is the use of the nitrogen atom in these substrates to direct the Pd-catalyst to remote C–H bonds in the ring. This approach leverages the high-energy boat conformer species to achieve transannular C–H activation and subsequent C–C bond formation. The reaction exhibits high compatibility with a wide range of hetero(aryl) iodides in the diversification of 3-azabicyclo[3.1.0]hexane. Several alicyclic amines undergo C–H arylation in modest to good yields. The methodology was employed for the late-stage functionalization of bioactive molecules including amitifadine, varenicline and cytisine. Furthermore, several directing groups were synthesized which showed a wide range of reactivity toward the C4–H arylation of piperidine.

Chapter 5 describes the identification of pyridinecarboxylic acid ligands for the Pd-catalyzed C–H functionalization of azabicycloalkanes. The ligand additives were found to dramatically improve the reactivity. Kinetic studies reveal that the role of the ligand is to rescue deactivated Pd species. Reaction optimization enables the challenging distal C–H functionalization of diverse alkaloids such as tropane.

Chapter 1. Introduction

This dissertation explores the design and development of metal complexes for electrical energy storage devices (Chapter 2) and C–H functionalization methodologies (Chapter 3-5). Both projects utilize fundamental organic synthesis and physical organic chemistry concepts to optimize physical, electrochemical and chemical parameters. Furthermore, the use of electrochemical techniques enabled the rapid assessment of the redox properties of metal complexes and organic molecules across both areas of research.

1.1 Redox Flow Batteries

Electrical Energy Storage

The worldwide demand for electrical energy is expected to double by 2050.¹ This projection indicates that the production of electricity in the upcoming decades must become inexpensive, sustainable and reliable. As such, new strategies for energy production are being explored to minimize the dependence on dwindling fossil-fuel derivatives. A potential solution at the grid-level is to incorporate more renewable sources such as wind and solar power. However, the intermittent nature of renewable sources (*e.g.* day/night cycles) renders these technologies impractical. The combination of renewable energies with electrical energy storage devices (EES) offers a potential solution. EES devices are technologies capable of storing energy at high-energy production times and delivering it when the demand rises.^{1,2} EES systems are classified based on the fundamental method to store energy dividing them in five categories: mechanical storage (*i.e.* pump hydroelectric, compressed air, flywheels), electromagnetic storage (*i.e.* supercapitors), chemical storage (*i.e.* batteries), biological storage, and thermal energy storage (*i.e.* water tanks, aquifers, molten salt).³

In the U.S., pump hydroelectric storage (PHS) systems constitutes over 95% of energy storage capacity.⁴ These systems have been widely popularized due to the low-cost in infrastructure and reliable technology. However, PHS systems demand specific geographical conditions, as these systems are based on two interconnected water reservoirs at different elevations. At moments when electricity is inexpensive (off-peak hours) water is pumped to the high-elevation reservoir. Then, at peak electricity demand, water is released through a turbine to produce electricity with an overall round-trip efficiency of 70-80%.⁵ The remaining 5% of EES technologies comprises of compressed air, batteries, flywheels and thermal energy storage.

The fast-growing battery field possesses several advantages over other technologies including high round-trip efficiencies, long cycle-life, fast response time and low-pollution emissions. Batteries represent a suitable energy storage technology for the integration of renewable resources due to their compact size, low geographical requirements, and energy and power storage/delivery flexibility. The principal battery technologies for large-scale energy storage are sodium/sulfur, lead-acid, lithium-ion, and flow batteries.^{1,3} Of these, Na/S and Pb-acid batteries are mature technologies with several commercial applications. A major drawback in both systems is their temperature constraints.⁶ In the case of Pb-acid batteries, the ideal working temperature is approximately 27 °C; even a 5 °C change in temperature could lead to a 50% reduction in the battery life. In the case of Na/S, the device must be kept at temperatures above 270 °C, which is an energy-demanding process and represents a significant safety concern.

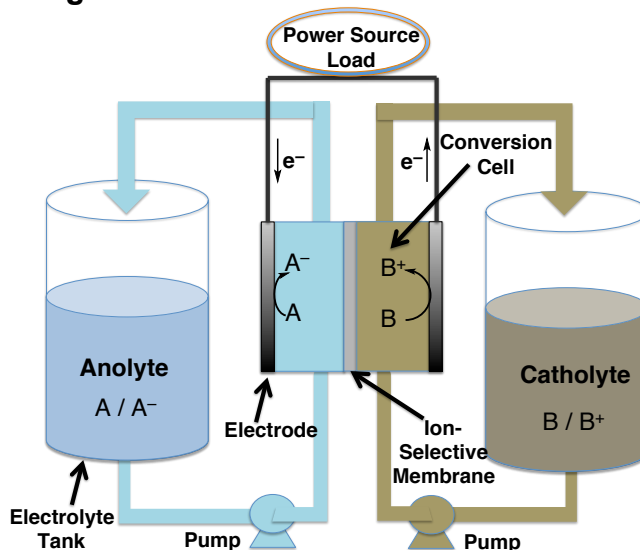
Flow Batteries

Redox flow batteries (RFBs) are rechargeable batteries based on one or two solvated electroactive species that undergo redox chemistries to hold or release electrical energy. The major advantage of RFBs over the conventional batteries is that the storage of the redox active species is decoupled from the electrodes, which allows for independent scaling of energy and power. As a result, these systems can achieve steady performance since the electrodes do not undergo physical or chemical changes. Consequently, the energy density is dependent on the volume and concentration of

active species in solution, while the power density is dependent on the electrode surface area, size, and electrochemical connection.

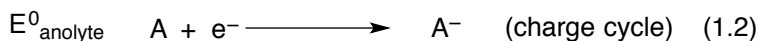
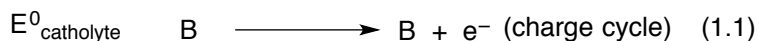
As shown in Figure 1.1, a RFB consists of three main components: a conversion cell, electrolyte tanks, and a flow system. An electrical power source (e.g. solar panels, wind turbines) is used to charge the RFB. During operation of the battery, the electrolyte solutions (A/A^- and B/B^+) are pumped in and out the reservoirs through the conversion cell where the electrochemical reactions occur. The storage reservoirs are usually larger than the cell in which electron transfer events occur. The conversion cell is comprised of high surface area inert electrodes and an ion-exchange membrane that allows passage of ions to maintain chemical balance, but prevents the catholyte and anolyte solutions from mixing. Electrons flow through the electrodes when a voltage difference is imposed driving redox reactions of the solvated active species. The electrolyte solution flow rate is a key factor that also contributes to the performance of the RFB as high flow rates increase battery capacity, but decrease the system efficiency by the increased pump consumption.⁷

Figure 1.1. General schematic of a RFB.



The liquid electrolyte is comprised of three main components: redox active species, supporting electrolyte, and solvent. The active species undergo oxidation state changes to store and deliver the energy. The nature of the active materials dictates the

cell potential, reversibility, and stability of the system. The electrolyte solutions are based on mixtures of high (catholyte) and low (anolyte) potential redox active materials such as zinc/bromine, iron/chromium, vanadium/vanadium and bromine/polysulfide.^{8,9} The overall cell potential of the battery is determined by the standard electrode potential of both half-cell reactions (equations 1.1-1.3).



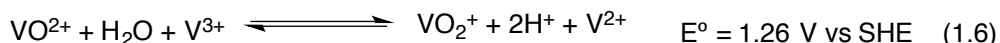
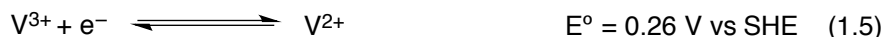
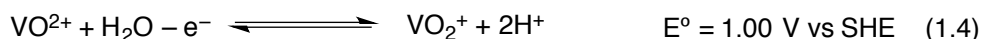
$$E^0_{\text{cell}} = E^0_{\text{catholyte}} + E^0_{\text{anolyte}} \quad (1.3)$$

The supporting electrolyte is the source of ions in the given solvent. These spectator ions enhance the conductivity of the electrolyte solution. Finally, the solvent is an important parameter that dictates the ionization capacity, maximum cell potential, and the solubility of the active species.

Aqueous RFBs

NASA developed the earliest redox flow batteries comprised of water-based electrolytes.¹⁰ One notable application of the aqueous chemistry is the zinc/bromine RFB. This battery system has good energy efficiency (80 %), low cost of materials, and well-developed technology to avoid active species crossover. In the catholyte, Br^- ions are converted to Br_3^- , and the anolyte, Zn^{2+} ions are deposited on a Zn electrode during the charging cycle. Due to the irreversible crossover of Br_2 , quaternary ammonium salts are circulated with the electrolyte to intercept Br_2 , which prevents crossover to the Zn electrode.^{9a} However, many of the aqueous technologies suffer from irreversible crossover, which leads to loss in battery efficiency. To overcome irreversible crossover, a single active species RFB was developed based on vanadium salts.¹¹ This all-vanadium aqueous RFB constitutes the state-of-the-art in the flow battery field with several commercial applications worldwide.^{12,13} At the positive electrode, V^{4+} is oxidized to V^{5+} releasing an electron during charge (eq. 1.4). The electron travels through an external circuit to the negative electrode, where V^{3+} is reduced to V^{2+} (eq. 1.5). In order

to maintain chemical balance, protons pass through the ion-selective membrane from the positive to the negative electrode.



These systems can achieve solubility up to 2M,¹⁴ with 80-90% coulombic efficiencies and 60-70% energy efficiencies at a 1.5 V charge/discharge potential in static H-cell set-ups (eq. 1.6).^{9a} The major disadvantage of the aqueous RFBs is the narrow potential window dictated by water electrolysis (~1.23 V), resulting in low energy densities of ~25 Wh L⁻¹.¹ Furthermore, the vanadium RFBs require the use of high concentrations of extremely corrosive supporting electrolytes such as sulfuric acid, hydrobromic acid, hydrochloric acid, or nitric acid.¹⁵

Non-aqueous RFBs

Non-aqueous systems have been proposed to alleviate some of the challenges associated with aqueous RFBs.¹⁶ Organic solvents offer dramatically wider voltage windows (~5 V for acetonitrile)¹⁷ and permit the use of a large number of organic and organometallic redox active species with tunable solubilities and redox properties. This offers exciting opportunities to improve the overall RFB energy efficiency.

The conceptual idea of a non-aqueous redox flow battery was introduced by Singh in 1984,¹⁶ but not demonstrated experimentally until Matsuda and coworkers reported the first non-aqueous RFB systems based on Ru(bpy)⁺², Ru(acac)₃ and Fe(bpy)⁺².¹⁸ Several reports on non-aqueous RFBs have been disclosed in the literature during the past two decades.¹⁹ The vast majority of publications focus on transition metal complexes bearing simple bipyridine²⁰, β-diketonate²¹, dithiolate²², cyclopentadienyl²³, and bipyridylimino isoindoline ligands²⁴. To date, the most soluble organometallic systems are in the range of 0.8 M to 1.0 M. Organic-based electrolytes have allowed the development of low equivalent weight catholyte and anolyte species with high performance and solubilities.²⁵

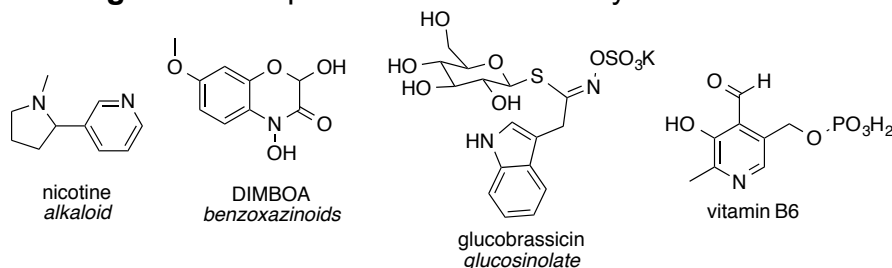
Despite their promise, non-aqueous systems remain largely underdeveloped due to the limited development of compatible cell components and membranes with organic solvents and high-performing redox active species with large potential window, high solubility, and long cycle-life stability.

Fundamental studies on the factors that affect redox-active electrolytes could provide valuable information toward the design and development of non-aqueous chemistries. Chapter 2 focuses on the systematic investigation of Cr^{3+} and Cr^0 complexes bearing functionalized bipyridine ligands to establish a series of solubility-electrochemistry-structure relationships with insights into chemical design principles for future classes of metal coordination complexes for non-aqueous RFBs.

1.2 C–H Functionalization of Nitrogen Heterocycles

Nitrogen heterocycles are ubiquitous molecules in nature with several classes of plant-derived natural products including alkaloids, benzoxazinoids, and glucosinolates (Figure 1.2).²⁶ In addition, biological processes within living organisms utilize *N*-heterocycles (vitamins, hormones, and enzymes). Given their prominence and bioactive properties, many *N*-heterocycles have been synthetically or biosynthetically prepared in pharmaceutical and agrochemical settings. As of 2014, 59% of U.S. FDA approved drugs had a nitrogen heterocycle in their structure.²⁷ This has led to significant interest in the development of new reactions to efficiently construct these amine cores. Classical approaches for the synthesis of saturated and aromatic *N*-heterocycles have focused on the development of 1) synthetic methodologies for the construction of amine scaffold²⁸ and 2) total synthesis of *N*-heterocyclic-based complex natural products.²⁹ Such approaches represent an iterative and resource-intensive strategy to prepare functionalized *N*-heterocycles. Furthermore, the production of libraries of compounds can be challenging, as *N*-heterocycles are often difficult to derivatize with traditional reactions.³⁰

Figure 1.2. Representative *N*-heterocycles in nature.

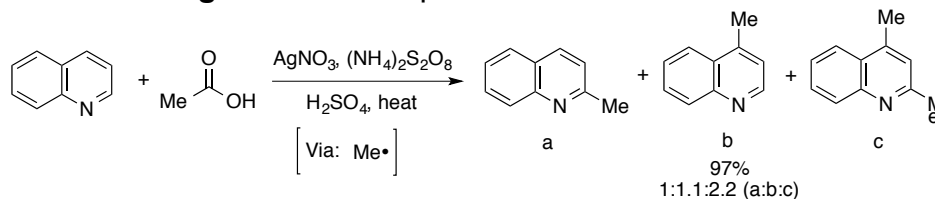


A more direct and efficient strategy is the C–H functionalization of *N*-heterocycles.^{31, 32} This approach has enabled 1) the development of late-state functionalization approaches for complex heteroarene diversification and 2) the increase in the synthetic scope of *N*-heterocycles.³³ Strategies to selectively C–H functionalize these molecules rely on 1) the innate properties of the substrate (activated C–H bonds, formation of stable radical intermediates, steric hindrance) or 2) directing groups (target nearby C–H bonds).

Radical aromatic substitution in *N*-heterocycles

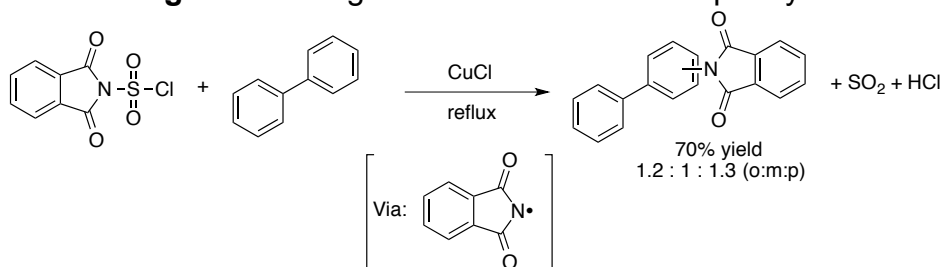
One of the first reports of radical additions to heteroaromatic bases was the addition of phenyl radicals to *ortho*- and *para*-positions of pyridine by the thermal decomposition of phenyl diazonium chloride.³⁴ Following this seminal work, several C–H functionalization methods that proceed via radical addition have been explored to elaborate important aromatic heterocyclic derivatives. One of the most utilized methods for radical heteroaromatic substitution is the Minisci reaction (Figure 1.3).³⁵ This reaction commonly employs mixtures of silver nitrate and ammonium persulfate in acid to oxidatively decarboxylate aliphatic carboxylic acids to generate alkyl radicals that further react with the heteroaromatic unit affording functionalized products with high-selectivity toward the electron-deficient C–H sites on the ring.

Figure 1.3. Example of a Minisci reaction.³⁵



Despite the great affinity of radical species for heteroarenes, it is quite difficult to control regioselectivity and reactivity. Combined with the limited exploration of radical sources aside from carbon radicals, this lack of control has largely prevented their use in industrial settings.³⁵ For example, the use of nitrogen centered radicals have been under utilized in $\text{C}(\text{sp}^2)\text{-H}$ functionalization.³⁶ Some of the first examples on the use of *N*-radicals was reported by Lidgett and co-workers where *N*-chlorosulfonylphthalimide was refluxed in biphenyl with added copper chloride to afford a mixture of C-H aminated products (Figure 1.4).³⁷ Other reports have employed analogous methods with the use of *N*-halo-amides and imides.³⁸ Since then, $\text{C}(\text{sp}^2)\text{-H}$ amination employing *N*-radicals has remained largely dormant.³⁹ In contrast, other methods for C-H amination employing transition metals⁴⁰ or metal-free oxidative couplings⁴¹ have seen great developments. However, these methods require reaction high temperatures, superstoichiometric oxidants, and specialized ligand scaffolds.

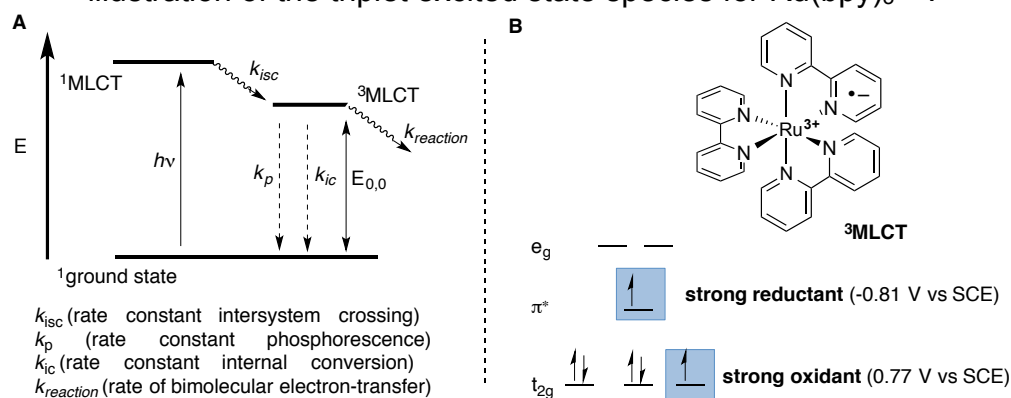
Figure 1.4. Lidgett's C-H amination of biphenyl.



Recently, visible light photoredox catalysis has gained interest due to the ability to control the generation, reactivity and selectivity of the radical species.⁴² The most commonly employed photocatalysts are homoleptic polypyridyl complexes of ruthenium and iridium, and aromatic organic molecules (acridiniums, eosin Y).⁴³ Upon exposure to visible light, the photocatalyst absorbs a photon, promoting an electron to a high-energy

excited state from the metal center to a ligand-based orbital (metal to ligand charge transfer; MLCT). The initial singlet excited species ($^1\text{MLCT}$) undergoes a rapid intersystem crossing to afford a long-lived triplet excited state species ($^3\text{MLCT}$; Figure 1.5 A). Although several other deactivation pathways can occur along the way (fluorescence, internal conversion, phosphorescence), the triplet excited state species can engage in bimolecular single-electron-transfer reactions with organic substrates (Figure 1.5 B). Notably, the triplet excited state is long-lived due to the spin-forbidden decay to the singlet ground state.

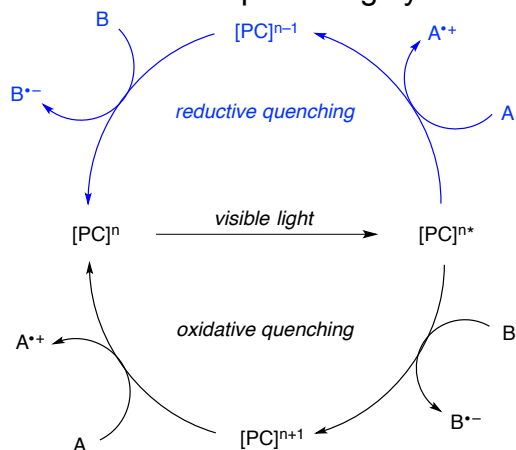
Figure 1.5. A) Generic Jablonski diagram of a photoredox catalyst. B) Graphical illustration of the triplet excited state species for $\text{Ru}(\text{bpy})_3^{2+*}$.



The nature of the organic or organometallic photocatalyst is key to reactivity. First, the lifetime of the excited species must be sufficiently long to engage in outer sphere bimolecular electron-transfer reactions. In general, iridium catalysts tend to have the longest lifetimes (~ 2000 ns), whereas the organic photoredox catalysts are in the range of 2-20 ns.^{42,43} Second, the redox potential of the photocatalyst excited state ($[\text{PC}]^*$) is important as it can provide an estimate of the ability to engage oxidative or reductive quenching cycles with organic substrates (Figure 1.6). Reductive quenching reactions employ the photocatalyst ($[\text{PC}]^*$) as the oxidant of electron-donating species (A). The reduced $[\text{PC}]^{n-1}$ can then serve as a reductant of electron-accepting species (B) and regenerate the $[\text{PC}]$. A similar mechanism applies to the oxidative quenching cycle, except that the catalyst initially functions as a reductant. Common organic reductive quenchers (A species) are tertiary amines, and oxidative quenchers (B

species) are aryl diazonium salts. Importantly, the redox potentials associated with the excited states cannot be directly measured, but a good approximation is obtained from cyclic voltammetry (CV) and the maximum emission wavelength of the catalyst.⁴⁴

Figure 1.6. Reductive and oxidative quenching cycles in photoredox catalysis.



Chapter 3 describes our efforts in the C–H amination of a wide range of *N*-heteroarenes and other arenes using visible light photoredox catalysis. Our method employs an iridium photocatalyst to engage with *N*-acyloxyphthalimides in an oxidative quenching cycle to produce nitrogen-centered radical intermediates. These *N*-radicals then react with hetero(arenes) to afford imide products.

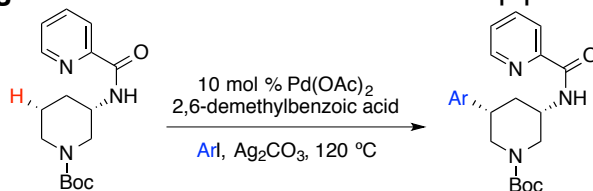
Transition metal catalyzed C–H functionalization of saturated *N*-Heterocycles

The C–H functionalization of saturated *N*-heterocycles (alicyclic amines) at C–H bonds in the ring or at adjacent alkyl chains remains challenging. This is in part due to the electron-rich properties of alicyclic amines, which have rendered them incompatible with metal catalysts (catalyst inhibition)⁴⁵ or strong oxidants (amine oxidation).⁴⁶ Furthermore, the selective activation of C(sp³)–H bonds is inherently more challenging than the activation of C(sp²)–H bonds, which has been attributed to the M–C bond strength differences in the C–H activated intermediate.⁴⁷

Traditional methods to C–H functionalize alicyclic amines have focused on the functionalization of the activated α-C–H bonds to the nitrogen atom. Strategies for α-C–H bond functionalization include deprotonation/functionalization of protected amines,⁴⁸

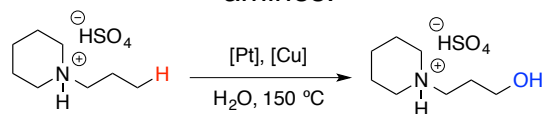
metal-carbenoid insertions,⁴⁹ transition metal directing groups,⁵⁰ and the use of reactive intermediates such as α -carbon radicals.⁵¹ Other approaches to functionalize remote C–H bonds in alicyclic amines include 1) the use of directing groups in the ring structure, 2) the use of non-directed strategies and 3) the use of innate functionalities in the amine scaffold. The use of directing groups within the ring structure has enabled the functionalization of several distal C–H bonds in alicyclic amines.⁵² Interestingly, the work by Maes functionalized the C5–H bond of piperidine through a ligand-directed approach (Figure 1.7).^{52C}

Figure 1.7. C5–H functionalization of piperidine.



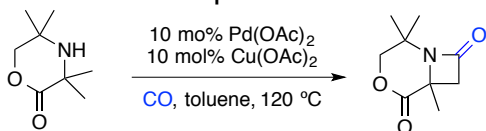
Non-directed strategies have been developed to functionalize terminal C–H sites in alkanes.⁵³ Recently this approach has been used for the remote functionalization of aliphatic cyclic and acyclic amines with the use of [Ir] and [Rh] catalysts.⁵⁴ Our group has recently explored the non-directed functionalization of aliphatic amines by the electrophilic activation of C–H bonds (Figure 1.8).^{55a} The use of protonated amines allowed the selective terminal C–H functionalization of several linear and cyclic alkyl amines by deactivation of reactive α -C–H bonds.

Figure 1.8. Representative example of non-directed C–H functionalization of alicyclic amines.



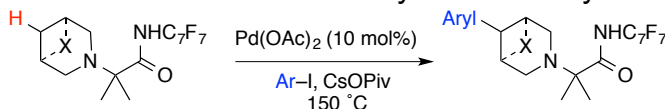
In contrast, the use of the native nitrogen atom on alicyclic amines to guide transition metals to selective C–H bonds has only been recently explored. Professor Matthew Gaunt at the University of Cambridge employed this strategy for the C–H functionalization of aliphatic amines at sites proximal to the nitrogen atom (Figure 1.9).⁵⁶

Figure 1.9. Representative example on the use of native functionalities.



Chapter 4 describes our work in the Pd-catalyzed transannular C–H arylation of variety of aliphatic cyclic and bicyclic amines (Figure 1.10). Our approach harnesses the strongly coordinating ability of the nitrogen atom to guide the Pd-catalyst to distal C–H bonds from the boat conformer. Chapter 5 describes the use of this transannular strategy for the functionalization of tropane and other azabicycloalkanes employing ligand additives for the Pd-catalyst.

Figure 1.10. Transannular C–H arylation of alicyclic amines.



1.3 References

- (1) Dunn, B.; Kamath, H.; Tarascon, J. M. *Science* **2011**, 334, 928.
- (2) Alotto, P.; Guarnieri, M.; Moro, F. *Renewable and Sustainable Energy Reviews* **2014**, 29, 325.
- (3) (a) Hameer, S.; van Niekerk, J. L. *Int. J. Energy Res.* **2015**, 39, 1179. (b) Aneke, M.; Wang, M. *Applied Energy* **2016**, 179, 350.
- (4) <https://energy.gov/sites/prod/files/2014/09/f18/Grid%20Energy%20Storage%20December%202013.pdf>. Accessed, April 20th, 1027.
- (5) Akinyele, D. O.; Rayudu, R. K. *Sustainable Energy Technologies and Assessments* **2014**, 8, 74.
- (6) Connolly, D. *A Review of Energy Storage Technologies: For the integration of fluctuating renewable energy.* **2010**.
- (7) Maa, X.; Zhanga, H.; Sunb, C.; Zoub, Y.; Zhang, T. *Journal of Power Sources* **2012**, 203, 153.
- (8) Weber, A. Z.; Mench, M. M.; Meyers, J. P.; Ross, P. N.; Gostick, J. T.; Liu, Q. *J. Appl. Electrochem.* **2011**, 41, 1137.
- (9) Ponce de León, C.; Frías-Ferrer, A.; González-García, J.; Szánto, D. A.; Walsh, F. C. *J. Power Sources* **2006**, 160, 716.
- (10) Thaller, L. H. *Electrically rechargeable redox flow cells*, NASA TM-X-71540, **1974**.

- (11) (a) Skyllas-Kazacos, M.; Rychick, M.; Robins, R. *All-vanadium redox battery*, US Patent 4,786,567, **1988**. (b) Sum, E.; Skyllas-Kazacos, M. *J. Power Sources* **1985**, *15*, 179. (c) Sum, E.; Rychcik, M.; Skyllas-Kazacos, M. *J. Power Sources* **1985**, *16*, 85.
- (12) <http://www.americanvanadium.com/cellcube.php>. Accessed April 22, 2017.
- (13) <http://www.ceic.unsw.edu.au/centers/vrb/>. Accessed April 22, 2017.
- (14) Rahman, F.; Skyllas-Kazacos, M. *J. Power Sources* **2009**, *189*, 1212.
- (15) Leung, P.; Li, X.; Ponce de Leon, C.; Berlouis, L.; Low, C. T. J.; Walsh, F. C. *RSC Adv.* **2012**, *2*, 10125.
- (16) Singh, P. *J. Power Sources* **1984**, *11*, 135.
- (17) Barrosse-Antle, L. E.; Bond, A. M.; Compton, R. G.; O'Mahony, A. M.; Rogers, E. I.; Silvester, D. S. *Chem. Asian J.* **2010**, *5*, 202.
- (18) Matsuda, Y.; Tanaka, K.; Okada, M.; Takasu, Y.; Morita, M.; Matsumura-Inoue, T. *J. Appl. Electrochem.* **1988**, *18*, 909.
- (19) (a) Perry, M. L.; Weber, A. Z. *J. Electrochem. Soc.* **2016**, *163*, A5064. (b) Gong, K.; Fang, Q.; Gu, S.; Li, S. F. Y.; Yan, Y. *Energy Environ. Sci.* **2015**, *8*, 3515.
- (20) Mun, J.; Lee, M.-J.; Park, J.-W.; Oh, D.-J.; Lee, D.-Y.; Doo, S.-G. *Electrochem. Solid-State Lett.* **2012**, *15*, A80.
- (21) Liu, Q.; Sleightholme, A. E. S.; Shinkle, A. A.; Li, Y.; Thompson, L. T. *Electrochemistry Communications* **2009**, *11*, 2312.
- (22) Cappillino, P. J.; Pratt, H. D.; Hudak, N. S.; Tomson, N. C.; Anderson, T. M.; Anstey, M. R. *Adv. Energy Mater.* **2014**, *4*, 1300566.
- (23) Wei, X.; Cosimbescu, L.; Xu, X.; Hu, J. Z.; Vijayakumar, M.; Feng, J.; Hu, M. Y.; Deng, X.; Xiao, J.; Liu, J.; et al. *Adv. Energy Mater.* **2015**, *5*, 1400678.
- (24) Sevov, C. S.; Fisher, S. L.; Thompson, L. T.; Sanford, M. S. *J. Am. Chem. Soc.* **2016**, *138*, 15378.
- (25) (a) Brushett, F. R.; Vaughey, J. T.; Jansen, A. N. *Adv. Energy Mater.* **2012**, *2*, 1390. (b) Sevov, C. S.; Samaroo, S. K.; Sanford, M. S. *Adv. Energy Mater.* **2016**, 1602027. (c) Sevov, C. S.; Hickey, D. P.; Cook, M. E.; Robinson, S. G.; Barnett, S.; Minter, S. D.; Sigman, M. S.; Sanford, M. S. *J. Am. Chem. Soc.* **2017**, *139*, 2924. (d) Wei, X.; Duan, W.; Huang, J.; Zhang, L.; Li, B.; Reed, D.; Xu, W.; Sprenkle, V.; Wang, W. *ACS Energy Lett.* **2016**, *1*, 705. (e) Duan, W.; Vemuri, R. S.; Milshtein, J. D.; Laramie, S.; et al. *J. Mater. Chem. A* **2016**, *4*, 5448.
- (26) Osbourn, A. E.; Lanzotti, V. *Plant-derived natural products*; 1st ed.; Springer-Verlag: New York, **2009**, pages 3-44.
- (27) Vitaku, E.; Smith, D. T.; Njardarson J. T. *J. Med. Chem.* **2014**, *57*, 10257.
- (28) Li, J. J. *Name reactions in heterocyclic chemistry*; 1st ed.; Wiley-Interscience: Hoboken, N.J., **2005**.

- (29) Majumdar, K. C.; Chattopadhyay, S. K. *Heterocycles in natural product synthesis*; 1st ed.; Wiley-VCH: Weinheim, **2011**.
- (30) Joule, J. A.; Mills, K. *Heterocyclic Chemistry*, 5th ed; Wiley: Chichester, **2010**.
- (31) Maes, J.; Maes, B. U. W. *Adv. Heterocycl. Chem.* **2016**, *120*, 137-194.
- (32) Wu, X. *Transition metal-catalyzed heterocycle synthesis via C-H activation*; 1st ed.; Wiley-VCH: Weinheim, 2016.
- (33) Cernak, T.; Dykstra, K. D.; Tyagarajan, S.; Vachal, P.; Krska, S. W. *Chem. Soc. Rev.* **2016**, *45*, 546.
- (34) Mohlau, R.; Berger, R. *Chem. Ber.* **1893**, *26*, 1994.
- (35) Duncton, M. A. J. *Med. Chem. Commun.* **2011**, *2*, 1135.
- (36) Zard, S. R. *Chem. Soc. Rev.* **2008**, *37*, 1603.
- (37) Lidgett, R. A.; Lynch, E. R.; McCall, E. B. *J. Chem. Soc.* **1965**, 3754.
- (38) (a) Lüning, U.; Skell, P. S. *Tetrahedron* **1985**, *41*, 4289. For *N*-tosyloxypthalimides see: (b) Cadogan, J. I. G.; Rowley, A. G. *J. Chem. Soc., Perkin Trans. 1*, **1975**, 1069.
- (39) Majority of the methods developed focused in radical cyclizations. For reviews see: (a) Esker, J. L.; Newcomb, M. *Adv. Heterocycl. Chem.* **1993**, *58*, 1. (b) Zard, S. Z. *Synlett*, **1996**, 1148.
- (40) (a) Shrestha, R.; Mukherjee, P.; Tan, Y.; Litman, Z. C.; Hartwig, J. F. *J. Am. Chem. Soc.* **2013**, *135*, 8480. (b) Boursalian, G. B.; Ngai, M.-Y.; Hojczyk, K. N.; Ritter, T. *J. Am. Chem. Soc.* **2013**, *135*, 13278.
- (41) (b) Kim, H. J.; Kim, J.; Cho, S. H.; Chang, S. *J. Am. Chem. Soc.* **2011**, *133*, 16382. (b) Kantak, A. A.; Potavathri, S.; Barham, R. A.; Romano, K. M.; DeBoef, B. *J. Am. Chem. Soc.* **2011**, *133*, 19960.
- (42) (a) Prier, C. K.; Rankic, D. A.; MacMillan, D. W. C. *Chem. Rev.* **2013**, *113*, 5322. (b) Narayanam, J. M. R.; Stephenson, C. R. J. *Chem. Soc. Rev.* **2010**, *40*, 102.
- (43) Romero, N. A.; Nicewicz, D. A. *Chem. Rev.* **2016**, *116*, 10075.
- (44) Tucker, J. W.; Stephenson, C. R. J. *J. Org. Chem.* **2012**, *77*, 1617.
- (45) Smalley, A. P.; Gaunt, M. J. *J. Am. Chem. Soc.* **2015**, *137*, 10632.
- (46) (a) Maes, B.U.W. *Chem. Eur. J.* **2012**, *18*, 10092. (b) Legacy, C. J.; Wang, A.; O'Day, B. J.; Emmert, M. H. *Angew. Chem. Int. Ed.* **2015**, *54*, 14907.
- (47) Jones, W. D.; Feher, F. *Acc. Chem. Res.* **1989**, *22*, 91.
- (48) Bode, J. W. *J. Org. Chem.* **2014**, *79*, 2809.
- (49) Davies, H. M. L.; Antoulinakis, E. G. *J. Organomet. Chem.* **2001**, *617-618*, 47.
- (50) (a) Spangler, J. E.; Kobayashi, Y.; Verma, P.; Wang, D.-H.; Yu, J.-Q. *J. Am. Chem. Soc.* **2015**, *137*, 11876. (b) Pastine, S. J.; Gribkov, D. V. & Sames, D. *J. Am. Chem. Soc.* **2006**, *128*, 14220.

(51) Shi, L.; Xia, W. *Chem. Soc. Rev.* **2012**, *41*, 7687.

(52) (a) Affron, D. P.; Davis, O. A.; Bull, J. A. *Org. Lett.* **2014**, *16*, 4956. (b) Ye, S.; Yang, W.; Coon, T.; Fanning, D.; Neubert, T.; Stamos, D.; Yu, J.-Q. *Chem. Eur. J.* **2016**, *22*, 4748. (c) Steijvoort, B. F. V.; Kaval, N.; Kulago, A. A.; Maes, B. U. W. *ACS Catal.* **2016**, *6*, 4486.

(53) Hartwig, J. F.; Larsen, M. A. *ACS Cent. Sci.*, **2016**, *2*, 281.

(54) (a) Lawrence, J. D.; Takahashi, M.; Bae, C.; Hartwig, J. F. *J. Am. Chem. Soc.* **2004**, *126*, 15334. (b) Li, Q.; Liskey, C. W.; Hartwig, J. F. *J. Am. Chem. Soc.* **2014**, *136*, 8755.

(55) (a) Lee, M.; Sanford, M. S. *J. Am. Chem. Soc.* **2015**, *137*, 12796. (b) Lee, M.; Sanford, M. S. *Org. Lett.* **2017**, *19*, 572. (c) Mbofana, C. T.; Chong, E.; Lawniczak, J.; Sanford, M. S. *Org. Lett.* **2016**, *18*, 4258.

(56) McNally, A.; Haffemayer, B.; Collins, B. S. L.; Gaunt, M. J. *Nature* **2014**, *510*, 129.

Chapter 2. Structure-Solubility-Electrochemistry Relationships of Bipyridine Chromium Complexes for Redox Flow Battery Applications¹

2.1 Introduction

Redox flow batteries (RFBs) are among the most promising electrical energy storage devices.² In these systems, external tanks store the energy in the form of soluble reduced and oxidized redox active species, thereby minimizing cross-contamination and self-discharge. The active species are circulated through a conversion cell to perform charging and discharging cycles. The physical separation of the active species and the electrodes allows for the independent scaling of energy capacity and power output. The energy density (E) in a RFB dictates the amount of energy that the device can store in Wh/L of electrolyte solution. The energy density (E) is directly proportional to the number of transferable electrons (n), the solubility (C_{active}) and the potential (V_{cell}) between the electro-active species (eq. 2.1).³

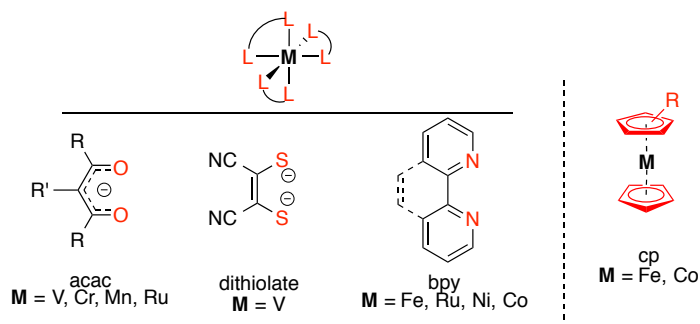
$$E \propto n \times C_{active} \times V_{cell} \times 0.5 \times F \quad (\text{Eq. 2.1})$$

State-of-the-art aqueous vanadium redox flow batteries have reached commercial and prototype applications. These flow batteries contain water-soluble vanadium salts of oxidation states (V^{2+}/V^{3+}) and (V^{4+}/V^{5+}) in aqueous acidic supporting electrolyte (HCl or H_2SO_4). These V-RFBs enable a storage system with one transferable electron per vanadium ion, high solubility of the active species, long-term cycling, and no detrimental capacity loss from crossover due to the use of vanadium in both half-cells.^{3a} However, aqueous-based electrolytes are limited by the electrochemical stability window of water (~ 1.23 V), rendering the overall battery energy density to ~ 25 Wh/L. The low energy density of these batteries translates to the need of

large infrastructures that can accommodate large amounts of redox active species, solvent and supporting electrolyte to achieve high-energy capacity.

Recently, a number of strategies have been employed to improve the energy density of these systems.^{2c} Our focus has been to improve the battery energy density by utilizing non-aqueous solvents that provide a wider electrochemical stability window (~5 V) in combination with metal coordination complex (MCCs, Figure 2.1) based electrolytes that have higher cell voltages (>2 V). Optimal redox active materials for RFBs should possess the following properties: (1) fast and reversible redox events that exceed the potential window of water; (2) robust chemical and electrochemical stability; (3) high solubility across multiple oxidation states. At the start of our investigation, non-aqueous RFB systems remained underexplored. Several MCCs have been developed bearing acetylacetonate (acac),⁴ dithiolate,⁵ cyclopentadienyl (Cp)⁶ and bipyridine (bpy)⁷ ligand scaffolds. However, these systems fell short for non-aqueous redox active materials, as the majority of the complexes only undergo a single electron transfer event (2 redox couples accessed during battery cycling) and demonstrate very low solubility. Although, a ferrocene derivative demonstrates high solubility (1.7 M in alkylcarbonate solvent mixtures), it possesses a low oxidation potential that is within the range of aqueous systems.^{6b} We reasoned that to fulfill all the requirements of ideal redox active material for non-aqueous RFBs, an initial survey of factors that impact solubility and electrochemistry of MCCs as a function of their structure could provide design principles for future generation electro-active materials.

Figure 2.1. Selected examples of MCCs used in non-aqueous RFBs.



This chapter focuses on the design, synthesis and electrochemical evaluation of chromium metal complexes bearing synthetic derivatives of the bpy scaffold to provide a number of structure-solubility-electrochemistry relationships that can be beneficial to the development of new MCCs for non-aqueous redox flow batteries. Our investigation led to the experimental demonstration that solubility as a function of oxidation state must be considered during the development of new electroactive materials. Finally, our investigation led to the identification of a promising MCC with multiple reversible redox events and good solubility across multiple oxidation states and its applicability to RFBs was demonstrated through charge/discharge cycling.

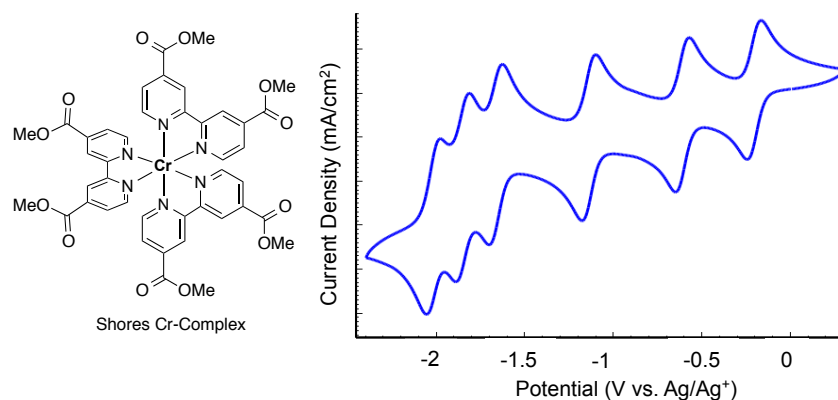
2.2 Results and Discussion

Studies with Bipyridine Cr-Complexes

Our laboratory, in partnership with the Thompson Lab of chemical engineering at The University of Michigan, first sought to identify a class of redox active metal complexes that were readily accessible by simple synthetic routes bearing earth-abundant transition metals. In addition, it was important that the ligands were modular, such that a variety of derivatives could be explored. Finally, we targeted redox active ligands that could serve as reservoirs for multiple electron transfer events in combination with the metal center. With these design criteria in mind, we selected bpy Cr complexes of the general class $[\text{Cr}(\text{bpy})_3]^{3+}$. Cr is an earth abundant first-row metal and the bpy ligand can be readily synthesized, modified, and scaled.

Cr has been previously used in other redox flow battery and electrochemical systems.⁸ In 2010, Shores and co-workers reported the synthesis and characterization of 4,4'-disubstituted-bipyridine chromium(III) complexes for application to photosensitizers.⁹ They demonstrated that the incorporation of an ester functional group at the 4,4'-position of the bipyridine ligand resulted in a chromium complex capable of six reversible electron transfers in acetonitrile, two more than the unsubstituted tris-bipyridine chromium(III) analogue (Figure 2.2). Such a redox active material is a desirable candidate for battery applications. As a result, these ester-substituted bpy Cr complexes represent an ideal target for a systematic study and optimization of the factors affecting solubility and electrochemistry.

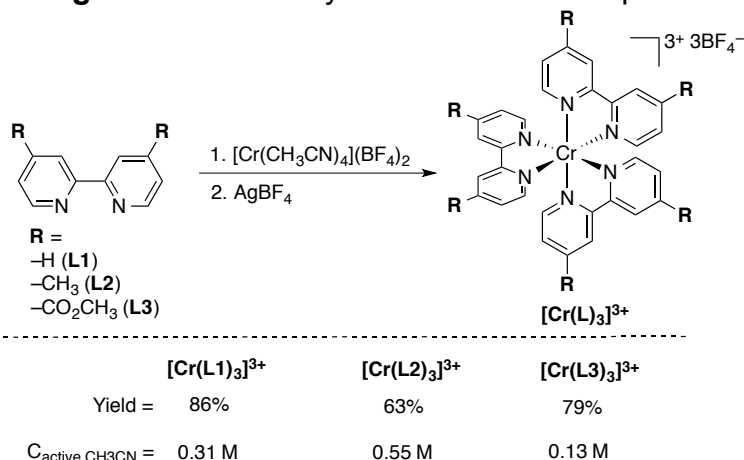
Figure 2.2. Cr-complex with electron-withdrawing ester bpy ligands and the corresponding cyclic voltammogram.



Our work commenced by synthesizing known bpy Cr complexes in order to thoroughly examine their solubility. The investigation of different organic solvents to improve on solubility and stability of redox active species is an important strategy to improve the energy density of a flow battery. In general, non-aqueous solvents for flow batteries must fulfill the following requirements: low viscosity, high dielectric constant and solvating properties, large electrochemical window, wide working temperature range and low toxicity. These parameters have led to the use of a limited number of organic solvents including acetonitrile, *N,N*-dimethylformamide, propylene carbonate, and 1,2-dimethoxyethane. Our investigation focused on the use of acetonitrile as it is the most commonly used solvent in non-aqueous RFBs and provides a high electrochemical window of ~ 5 V and suitable conductivity for our chromium complexes.¹⁰ The complexes were prepared by mixing 3 equiv of the corresponding ligand with $[\text{Cr}(\text{CH}_3\text{CN})_4](\text{BF}_4)_2$, followed by an *in situ* oxidation with AgBF_4 to afford the desired Cr(III) products (Figure 2.3).⁹ The compounds were characterized by elemental analysis and high-resolution mass spectrometry. Given that solubility is an important aspect of the overall energy density of a flow battery system (eq. 2.1), we sought to develop a reliable method to analyze the solubility of these benchmark molecules. UV-Vis spectroscopy proved to be a good method for determining the solubility of the complexes $[\text{Cr}(\text{L1})_3]^{3+}$, $[\text{Cr}(\text{L2})_3]^{3+}$, $[\text{Cr}(\text{L3})_3]^{3+}$ (details of the method are provided in the experimental section). As shown in Figure 2.3, $[\text{Cr}(\text{L1})_3]^{3+}$ and $[\text{Cr}(\text{L2})_3]^{3+}$ demonstrated reasonable solubility (0.31 M and 0.55 M in acetonitrile, respectively); however, these

complexes are limited to only 4 reversible redox couples.¹¹ In contrast, $[\text{Cr}(\text{L3})_3]^{3+}$ possesses 6 reversible redox couples but a relative low solubility (0.13 M in acetonitrile).

Figure 2.3. Solubility of literature Cr complexes.

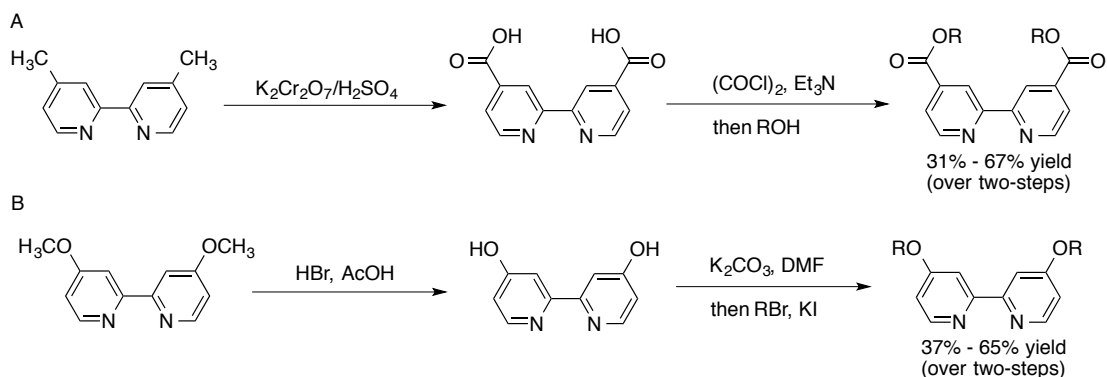


Given that $[\text{Cr}(\text{L3})_3]^{3+}$ had limited solubility, we sought to modify the ligand backbone to (1) understand the factors that impact solubility and electrochemistry in these systems and (2) identify a Cr complex that could be used for charge/discharge cycling experiments.

Synthesis of a New Library of Bpy-derived Cr(III) Complexes

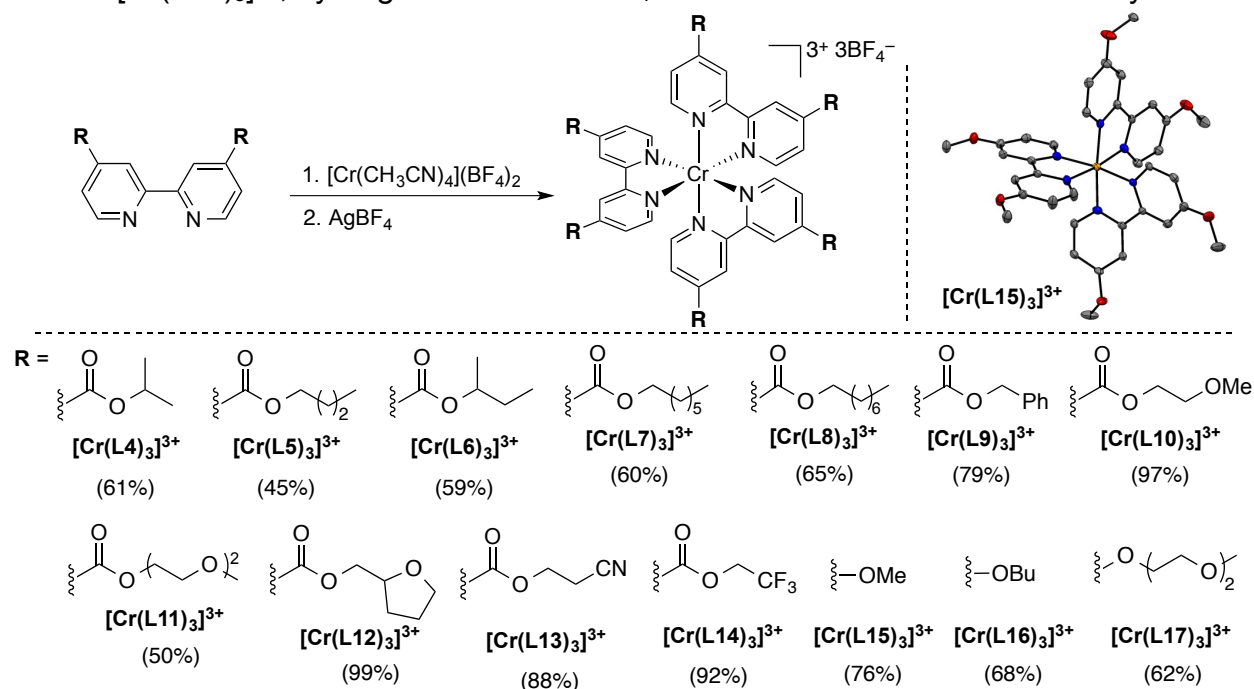
A series of ester-substituted bipyridine Cr(III) complexes was designed and synthesized with the aim of determining solubility and electrochemistry trends. The ester-bipyridine ligands were prepared in two synthetic steps from commercially available 4,4'-dimethylbipyridine with yields ranging from 31% to 67% (Figure 2.4 A). In addition, we targeted the synthesis of electron-donating alkoxy-substituted bipyridine Cr-complexes to gain insights on the impact of electronic effects in solubility and electrochemistry. As such, several 4,4'-alkoxy-substituted bipyridine ligands were prepared by a two-step sequence starting from the commercially available 4,4'-dimethoxybipyridine with yields ranging from 37% and 65% (Figure 2.4 B).

Figure 2.4. Synthetic routes to the ester- and alkoxy-bpy ligands.



These series of bpy ligands were reacted with $[\text{Cr}(\text{CH}_3\text{CN})_4](\text{BF}_4)_2$ followed by $1e^-$ oxidation with AgBF_4 to afford the desired Cr(III) complexes (Figure 2.5). The ester-bpy Cr complexes ($[\text{Cr}(\text{L4})_3]^{3+}$ to $[\text{Cr}(\text{L14})_3]^{3+}$) were prepared in yields ranging from 45% to 99% and were characterized by elemental analysis and high-resolution mass spectrometry. Similarly, the alkoxy-bpy complexes ($[\text{Cr}(\text{L15})_3]^{3+}$ to $[\text{Cr}(\text{L17})_3]^{3+}$) were obtained in high yield and purity. The solid-state structure of $[\text{Cr}(\text{L15})_3]^{3+}$ was utilized to further determine the structure of the complexes.

Figure 2.5. Synthesis of ester- and alkoxy-bpy $[\text{Cr}(\text{Ln})_3]^{3+}$ complexes. ORTEP of $[\text{Cr}(\text{L15})_3]^{3+}$, hydrogen atoms and BF_4^- counterions are omitted for clarity.



Solubility of the Synthetic Bpy Cr(III) Complexes

Non-aqueous RFBs have been limited by the low conductivity of organic solvent electrolytes, which can result in high overpotentials. In addition, the use of these non-aqueous solvents has limited the solubility of the electroactive species and supporting salts, which translates to low energy densities (eq 2.1). In the vanadium aqueous RFBs a typical battery includes redox active species with solubilities of ~2 M. This is because water at room temperature alone has a maximum concentration of 55.6 M and a high dielectric constant (80.1 at 23 °C)^{10b}, enabling high ionization and solvation of salts. In contrast, acetonitrile at room temperature has a maximum concentration of 19.2 M and dielectric constant of 37.5^{10b}. This intrinsically lower absolute concentration and reduced capability of salt ionization and solvation can limit the solubility of redox species in this solvent.

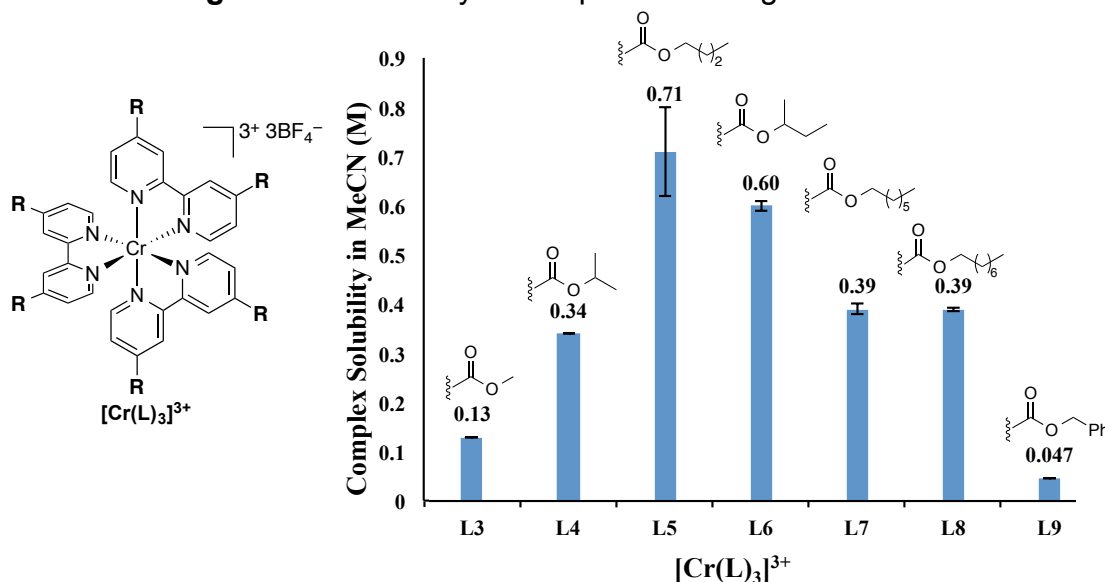
While solubility of the MCCs is a complex phenomenon, we rationalized that increasing the chain length and branching could enhance solubility by disrupting packing in the solid state.¹² In addition, we reasoned that replacing nonpolar methylene (-CH₂-) groups with more polar atoms such as oxygen or nitrogen could enhance solubility by increasing solvent/solute interactions. The solubility of all new Cr(III) complexes in acetonitrile was determined using UV-Vis spectroscopy. As discussed below, the solubility of these complexes ranges from 0.05 to 0.71 M.

Effect of Chain Length and Branching in the Ester-Bpy Cr(III) Complexes

First, we investigated the role of chain length in the ester-bpy complexes (Figure 2.6). We found that upon moving from methyl ester complex ([Cr(L3)₃]³⁺) to the butyl ester analog ([Cr(L5)₃]³⁺) the solubility increased by 0.6 M (from 0.13 M versus 0.71 M, respectively). [Cr(L5)₃]³⁺ was a pseudo-solid at room temperature and the addition of small amounts of acetonitrile readily converted the complex into a highly viscous solution. We hypothesized that this butyl ester complex was reaching a maximum solubility (equivalent to the density of the molecule). Further increasing the alkyl chain to the heptyl ([Cr(L7)₃]³⁺) and octyl ester ([Cr(L8)₃]³⁺) led to a decrease in solubility compared to the butyl ester (0.39 M for both MCCs). The identical solubility of these two complexes suggests that the observed solubility is a result of a lipophilic shell around

the complex, which offsets the effect of increasing chain length. We then looked at the effect of chain branching (Figure 2.6). Comparing the butyl ($[\text{Cr}(\text{L5})_3]^{3+}$) and sec-butyl ester derivatives ($[\text{Cr}(\text{L6})_3]^{3+}$), the sec-butyl chain showed a diminished solubility compared to the linear butyl ester complex (0.6 M versus 0.71 M). This result indicates that chain length has a more significant influence in solubility than branching in the 4-carbon chain compounds. Similarly, the isopropyl ester derivative ($[\text{Cr}(\text{L4})_3]^{3+}$) did not show a large increase in solubility despite the increase in chain branching compared to the methyl ester $[\text{Cr}(\text{L3})_3]^{3+}$ (0.34 versus 0.13 M). Finally, the benzyl ester complex ($[\text{Cr}(\text{L9})_3]^{3+}$) displayed very low solubility (0.05 M in acetonitrile). We hypothesize that the stabilizing π - π interactions of the aryl group offset the impact of chain length and branching in this benzyl complex. In addition, the low polarity of the phenyl ring could be contributing to the low solubility of complex $[\text{Cr}(\text{L9})_3]^{3+}$. As such, we next investigated the impact of polar functional groups in solubility.

Figure 2.6. Solubility of complexes with ligands L3-L9.

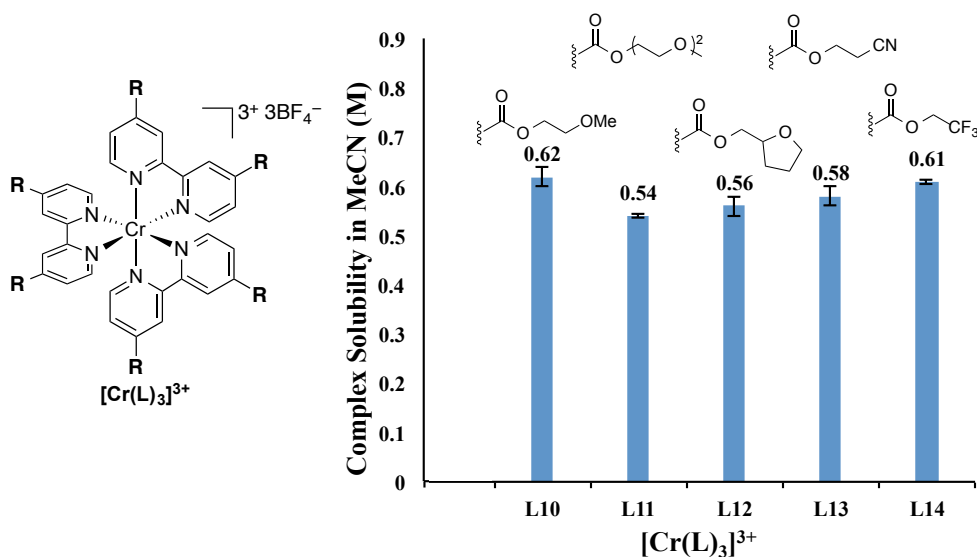


Effect of Polar Atoms in the Ester-Bpy Cr(III) Complexes

A comparison of the Cr(III) complexes with ligands L10–L12 allowed us to assess the impact of electronegative atoms on solubility (Figure 2.7). The 7-membered glycol ether chain of $[\text{Cr}(\text{L11})_3]^{3+}$ resulted in increased solubility of 0.54 M, compared to the analogous 7-membered all carbon chain complex ($[\text{Cr}(\text{L7})_3]^{3+}$, 0.39 M, Figure 2.6). However, increasing the chain branching in the tetrahydrofuranyl complex ($[\text{Cr}(\text{L12})_3]^{3+}$)

had minimal impact in solubility when compared to the linear ethylene glycol ether chains in $[\text{Cr}(\text{L10})_3]^{3+}$ and $[\text{Cr}(\text{L11})_3]^{3+}$ (0.56 M versus 0.62 M and 0.54 M, respectively). While we were surprised about the small changes in solubility across these polar functionalities, we hypothesized that these complexes were reaching an absolute maximum solubility. This hypothesis is further supported when comparing the four atom ester chains. For example, the butyl ester complex $[\text{Cr}(\text{L5})_3]^{3+}$ and the ether complex $[\text{Cr}(\text{L10})_3]^{3+}$, where the $-\text{CH}_2-$ unit is replaced for a polar $-\text{O}-$, have similar solubilities (0.71 versus 0.62 M, respectively). In addition, the incorporation of other electronegative groups such as $\text{CN}-$ and CF_3- resulted in solubilities within the range of the most soluble complexes (0.58 and 0.61 M, respectively), suggesting that our ligand derivatization has reached an absolute maximum solubility of approximately 0.6 to 0.7M in acetonitrile.

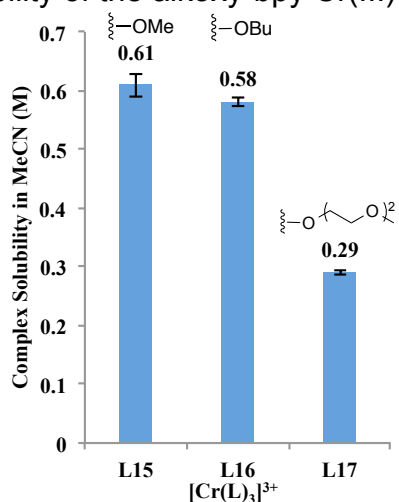
Figure 2.7. Solubility of complexes with ligands L10-L14.



Solubility of Alkoxy-Substituted Bpy Cr(III) Complexes

The solubility of the ether-bpy complexes is shown in Figure 2.8. Despite the differences in alkyl chain length, the methoxy ($[\text{Cr}(\text{L15})_3]^{3+}$) and *n*-butyloxy ($[\text{Cr}(\text{L16})_3]^{3+}$) substituents resulted in comparable solubilities to the highly soluble ester-bpy counterparts (0.61 and 0.58 M, respectively). It was surprising that, in this case, the compound with the glycol ether chain afforded a modest solubility of 0.29 M. This latter result cannot be explained at the moment, and further investigation is currently underway.

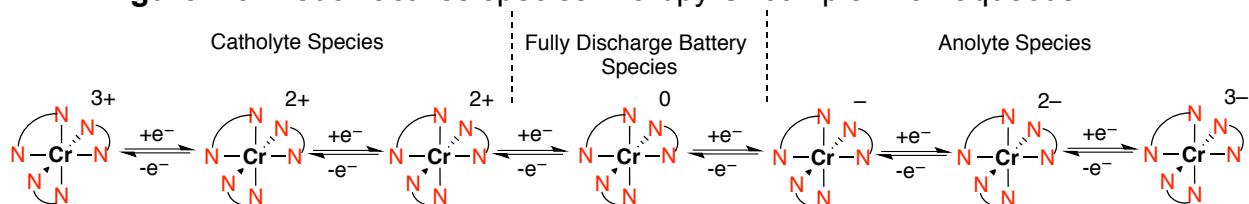
Figure 2.8. Solubility of the alkoxy-bpy Cr(III) complexes.



Synthesis and Solubility of Cr(0) Complexes

During the course of our investigation, we noticed in the literature that there is limited information about the solubility of redox active species for non-aqueous RFBs, despite the fact that this is a key parameter for the development of high-energy storage flow batteries. In addition most of the solubility information available was on the redox active starting materials.^{6b} However, this electroactive species undergoes a series of changes in oxidation state during the battery cycling. In our case as shown in Figure 2.9, the Cr(III) species will undergo 6 formal oxidation state changes. It is noted that these are formal oxidation states, as it has been reported by Wieghardt and co-workers that the Cr metal center remains Cr(III) and the redox chemistry occurs at the ligand (redox non-innocence).¹³ We hypothesized that many of these species would have drastically different solubilities due to their varying ionic character. In particular, the neutral species, which represent the active species of a fully discharged battery, were expected have a much lower solubility than the trications, due to the lack of ionic character.

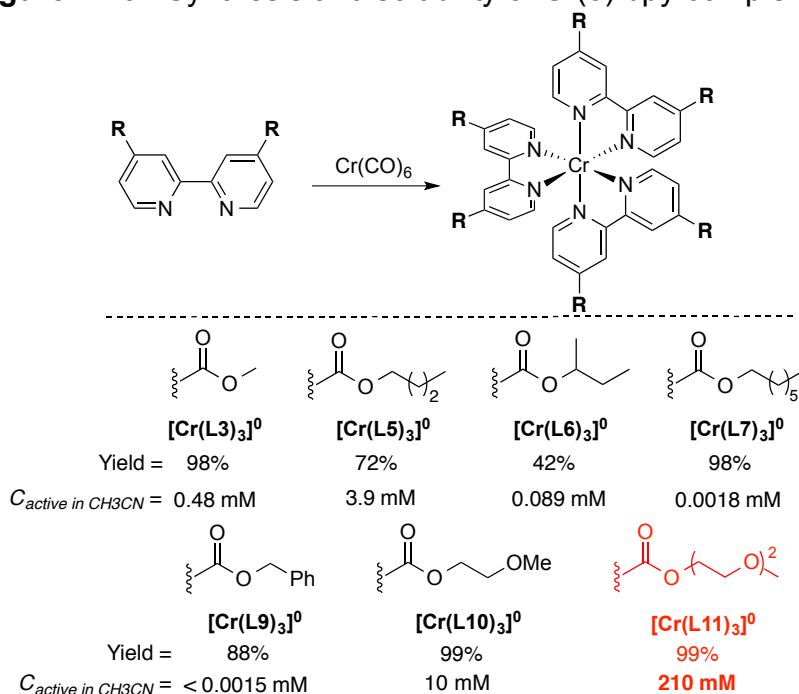
Figure 2.9. Redox active species in a bpy Cr complex non-aqueous RFB.



Our next objective was to investigate the solubility of a series of the ester-bpy Cr(0) complexes in acetonitrile. The neutral complexes from ligands L3, L5-L11 were prepared by refluxing 3 equiv of the ligand with $[\text{Cr}(\text{CO})_6]$ in degassed mesitylene. The

solubility of these air sensitive compounds was determined inside a N₂ glove-box using UV-Vis spectroscopy. As expected, these complexes had dramatically different solubilities than their Cr(III) analogues (Figures 2.6 and 2.7). As shown in Figure 2.10, the Cr(0) complexes afforded solubilities from insoluble (i.e. below spectrometer detection limit) to 210 mM. The alkyl ester derivatives (those of ligands L3, L5-L7) showed very poor solubilities in the millimolar range. Chain length effects were observed. For example, moving from the methyl ester complex [Cr(L3)₃]⁰ to the butyl ester [Cr(L5)₃]⁰ the solubility improved 8-fold (0.48 versus 3.9 mM, respectively). Similar to the Cr(III) complexes, extending the chain length to heptyl ester resulted in a decrease in solubility (0.0018 mM). Additionally, chain branching led to diminished solubility when comparing the butyl ([Cr(L5)₃]⁰) and iso-butyl ([Cr(L6)₃]⁰) ester complexes (3.9 mM versus 0.089 mM, respectively). Finally, the benzyl ester derivative yielded solubilities below the spectrometer detection limit (0.0015 mM).

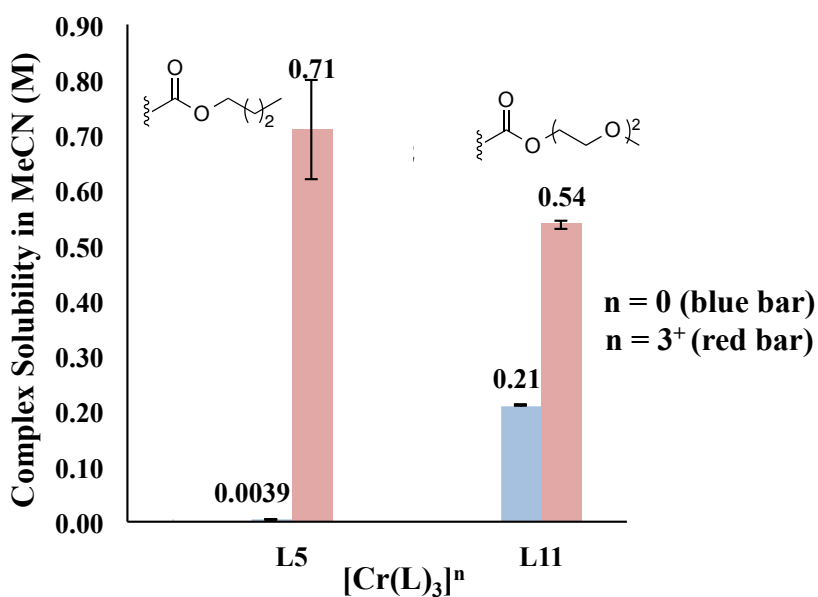
Figure 2.10. Synthesis and solubility of Cr(0) bpy complexes.



Notably, the incorporation of polar atoms in the ester functionality was effective in increasing solubility. For instance, incorporation of the methoxyethyl chain ([Cr(L10)₃]⁰) resulted in an ~2.5-fold increase in solubility when compared to the butyl ester counterpart (10 mM versus 3.9 mM). Furthermore, the methoxy(ethoxy)ethyl chain

$[\text{Cr}(\text{L11})_3]^0$) afforded the highest solubility from the series (210 mM). As shown in Figure 2.11, the most soluble complexes from the Cr(III) and Cr(0) series were those derived from the butyl ester ligand L5 and the methoxy(ethoxy)ethyl ligand L11, respectively. When comparing the solubilities at both oxidation states, it is clear that $[\text{Cr}(\text{L11})_3]^n$ is a particularly promising candidate for further battery experimentation. However, prior to advancing some of these complexes to battery cycling experiments, it was important to understand the effect of structural modifications on the electrochemical properties of the MCCs.

Figure 2.11. Solubility comparison of $[\text{Cr}(\text{L5})_3]$ and $[\text{Cr}(\text{L11})_3]$ across oxidation states.



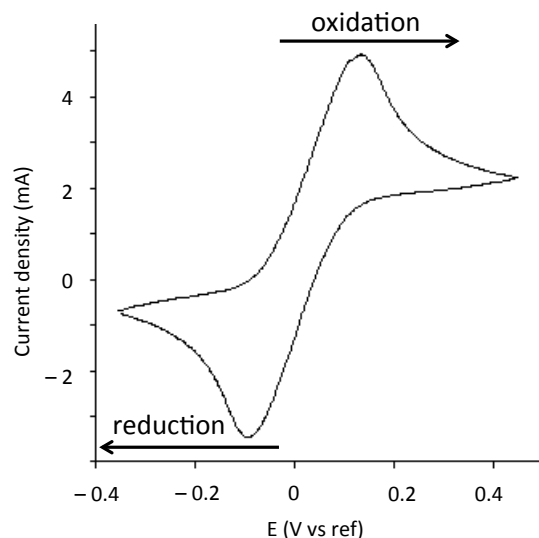
Cyclic Voltammetry of Bpy Cr(III) Complexes

Cyclic voltammetry (CV) is a technique used in the identification of promising redox active materials for redox flow batteries. It is an essential screening tool to quickly assess the electrochemical response of a molecules within a given voltage window. It is important to note that CV measurements do not necessarily correlate with cyclability in electrochemical evaluations over longer time frames. For that, bulk electrolysis charge/discharge experiments are required.

Voltammograms are obtained by utilizing a potentiostat. This instrument applies a potential between a working electrode and reference electrode, which is varied at a constant rate within an established voltage window and the current response between the working electrode and a counter electrode is recorded.¹⁴ In all of the CVs shown in

this chapter, peaks with a positive current response that appear when the voltage is swept towards the upper vertex potential correspond to oxidation reactions. When the voltage is swept towards the lower vertex potential, peaks with a negative current response correspond to reduction reactions (Figure 2.12).

Figure 2.12. Representative cyclic voltammogram.



Our systems utilized a three-electrode system with a working electrode (glassy carbon disk), a counter electrode (platinum) and a reference electrode (Ag/Ag^+). The supporting electrolyte for the experiments was TBABF_4 (tetrabutyl ammonium tetrafluoroborate). TBABF_4 is used as a conductivity-enhancing additive, and it was used in 10-fold excess to the concentration of the redox active species to prevent migration mass-transfer limitations at the double-layer electrode surface. In the present work, CV allowed us to obtain information about half-wave potentials, reversibility, and stability of chemical species. A ratio between the height of the anodic and cathodic peaks of a redox event close to 1 is indicative of a redox couple that is chemically reversible on the time scale of the CV experiment. Experimentally, the peak height ratios varied between 0.7 to 1.2. This is attributed to the error introduced by the assignment of the redox couple baseline. An irreversible peak indicates slow oxidation or reduction kinetics, or that upon electrochemical oxidation or reduction a subsequent irreversible chemical reaction occurs at the electrode surface.

Table 2.1 shows that the bipyridine $[\text{Cr}(\text{L1})_3]^{3+}$ and dimethylbipyridine $[\text{Cr}(\text{L2})_3]^{3+}$ complexes exhibit six well-defined redox couples across 2.3 and 2.1 V, respectively.

These values are consistent with those reported in the literature. As determined by the peak height current ratios, the first five redox couples are reversible. The 6th redox couple deviates significantly from unity with values of 1.62 and 2.11, respectively. Additionally, when the complexes are measured to potentials below -2.5 V, a new shoulder at -1.4 V is observed (Figure 2.13). We attribute this new peak to irreversible decomposition of the complexes. One possible pathway for decomposition is ligand shedding. This has been previously observed in literature reports.¹¹ As such, if these complexes were to be used in a symmetrical non-aqueous RFB (same compound in both half-cells) only the first four redox couples would be reversibly accessible. As reported, $[\text{Cr}(\text{L}3)_3]^{3+}$ with the ester-substituted bipyridine shows six couples within the acetonitrile solvent window. The electron-withdrawing nature of the ligands shifts the first redox couple to more positive potentials as compared to the parent $[\text{Cr}(\text{L}1)_3]^{3+}$ and $[\text{Cr}(\text{L}2)_3]^{3+}$ complexes (-0.20 V versus -0.56 V and -0.72 V, respectively). The six peaks are reversible and stable (CV time scale) even at low negative potentials (~ 2 V vs Ag/Ag^+).

Figure 2.13. CV of $[\text{Cr}(\text{L}1)_3]^{3+}$ in acetonitrile. Decomposition shoulder observed at -1.4 V when complex scanned to the most negative redox couple. CVs were taken in 0.1 M TBABF_4 in acetonitrile. Reference is Ag/Ag^+ with AgBF_4 (0.01M); working electrode is glassy carbon disk; counter electrode is platinum wire; scan rate is 100 mV s^{-1} ; temperature is 23 $^\circ\text{C}$.

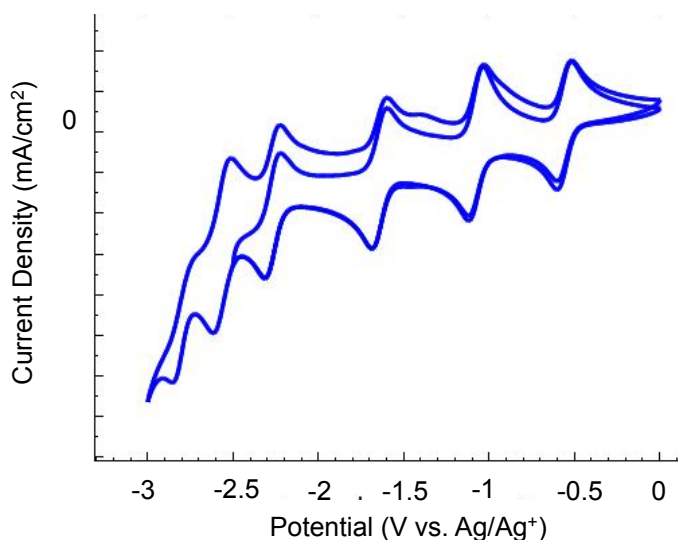


Table 2.1. Potentials, peak current ratios and peak separations for $[\text{Cr}(\text{L1})_3]^{3+}$, $[\text{Cr}(\text{L2})_3]^{3+}$, $[\text{Cr}(\text{L3})_3]^{3+}$ in acetonitrile. Reference is Ag/Ag^+ with AgBF_4 (0.01 M); supporting electrolyte is TBABF_4 (0.1 M); working electrode is glassy carbon disk; counter electrode is platinum wire; scan rate is 100 mV s^{-1} ; temperature is $23 \text{ }^\circ\text{C}$.

Compound		1 st	2 nd	3 rd	4 th	5 th	6 th
$[\text{Cr}(\text{L1})_3]^{3+}$	$E_{1/2}$ (V)	-0.56	-1.08	-1.65	-2.27	-2.58	-2.81
	$i_p^{\text{red}}/i_p^{\text{ox}}$	1.03	1.19	0.91	1.04	1.02	1.62
	ΔE_p (V)	0.084	0.077	0.077	0.077	0.084	0.084
$[\text{Cr}(\text{L2})_3]^{3+}$	$E_{1/2}$ (V)	-0.72	-1.22	-1.75	-2.34	-2.62	-2.84
	$i_p^{\text{red}}/i_p^{\text{ox}}$	0.94	0.98	0.94	1.04	1.05	2.11
	ΔE_p (V)	0.070	0.077	0.077	0.077	0.091	0.056
$[\text{Cr}(\text{L3})_3]^{3+}$	$E_{1/2}$ (V)	-0.20	-0.61	-1.14	-1.67	-1.86	-2.03
	$i_p^{\text{red}}/i_p^{\text{ox}}$	1.02	1.04	1.04	1.03	0.94	0.95
	ΔE_p (V)	0.070	0.070	0.077	0.063	0.056	0.056

As shown in Table 2.2, most modifications to the ester backbone had minimal effect on the electrochemistry of the complexes. The complexes show an average voltage window of 1.8 V. The first three redox couples have a larger voltage spacing of 0.5 V, whereas the last three couples are closer in potential. Widely spaced redox events are desirable for RFB applications, since the potential window of the cell (V_{cell}) is determined by the spacing between the highest and lowest potential redox couple.

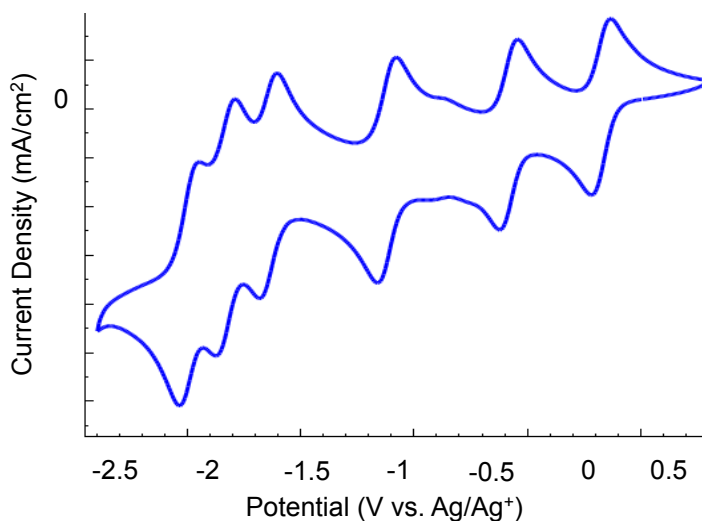
In general, high electrochemical reversibility is observed for most of the ester-bpy Cr(III) complexes. Therefore, these complexes should enable the design of a symmetrical RFB that stores a total of 3 electrons ($n = 3$, eq 2.1). Most notably, $[\text{Cr}(\text{L11})_3]$ displays excellent electrochemical properties as shown in the cyclic voltammogram (Figure 2.14). This complex was of interest as it afforded the highest solubility across different oxidation states. A small peak at approximately -0.8 V shows that a side electrochemical reaction has occurred. However, the relatively small side reaction is negligible with respect to the dominant electrochemical processes and when compared to the background double-layer charging at the electrode surface.

Table 2.2. Potentials, peak current ratios and peak separations for the ester- and alkoxy-bpy Cr(III) complexes in acetonitrile. Reference is Ag/Ag⁺ with AgBF₄ (0.01 M); supporting electrolyte is TBABF₄ (0.1 M); working electrode is glassy carbon disk; counter electrode is platinum wire; scan rate is 100 mV s⁻¹; temperature is 23 °C.

Compound		1st	2nd	3rd	4th	5th	6th
[Cr(L4)₃]³⁺	$E_{1/2}$ (V)	-0.17	-0.59	-1.22	-1.65	-1.85	-2.02
	i_p^{red}/i_p^{ox}	0.99	0.99	1.00	0.98	0.97	0.95
	ΔE_p (V)	0.060	0.060	0.065	0.060	0.045	0.050
[Cr(L5)₃]³⁺	$E_{1/2}$ (V)	-0.20	-0.61	-1.14	-1.67	-1.86	-2.04
	i_p^{red}/i_p^{ox}	0.99	0.96	0.99	0.94	0.97	1.02
	ΔE_p (V)	0.072	0.078	0.080	0.071	0.066	0.069
[Cr(L9)₃]³⁺	$E_{1/2}$ (V)	-0.17	-0.57	-1.11	-1.64	-1.82	-1.99
	i_p^{red}/i_p^{ox}	1.01	0.91	0.58	0.24	0.63	0.87
	ΔE_p (V)	0.078	0.078	0.070	0.083	0.066	0.072
[Cr(L10)₃]³⁺	$E_{1/2}$ (V)	-0.14	-0.57	-1.13	-1.67	-1.89	-2.07
	i_p^{red}/i_p^{ox}	0.58	1.11	0.95	1.29	0.87	0.52
	ΔE_p (V)	0.13	0.11	0.11	0.12	0.12	0.14
[Cr(L11)₃]³⁺	$E_{1/2}$ (V)	-0.17	-0.58	-1.12	-1.63	-1.82	-2.00
	i_p^{red}/i_p^{ox}	1.06	0.90	0.98	0.98	1.02	1.06
	ΔE_p (V)	0.084	0.070	0.084	0.063	0.056	0.070
[Cr(L12)₃]³⁺	$E_{1/2}$ (V)	-0.21	-0.61	-1.15	-1.68	-1.87	-2.04
	i_p^{red}/i_p^{ox}	0.99	0.96	1.01	0.95	0.96	0.99
	ΔE_p (V)	0.093	0.094	0.10	0.093	0.092	0.096
[Cr(L13)₃]³⁺	$E_{1/2}$ (V)	-0.17	-0.59	-1.12	-1.63	-1.83	-2.02
	i_p^{red}/i_p^{ox}	0.99	0.96	1.01	0.95	0.96	0.99
	ΔE_p (V)	0.14	0.13	0.13	0.14	0.14	0.14
[Cr(L15)₃]³⁺	$E_{1/2}$ (V)	-0.92	-1.36	-1.74	-2.30	-2.57	-2.80
	i_p^{red}/i_p^{ox}	0.70	0.79	0.65	0.75	0.92	0.47
	ΔE_p (V)	0.090	0.095	0.10	0.10	0.12	0.076
[Cr(L16)₃]³⁺	$E_{1/2}$ (V)	-0.94	-1.38	-1.76	-2.31	-2.57	-2.79
	i_p^{red}/i_p^{ox}	0.98	0.98	1.00	0.97	1.00	0.25
	ΔE_p (V)	0.077	0.063	0.070	0.070	0.063	0.042

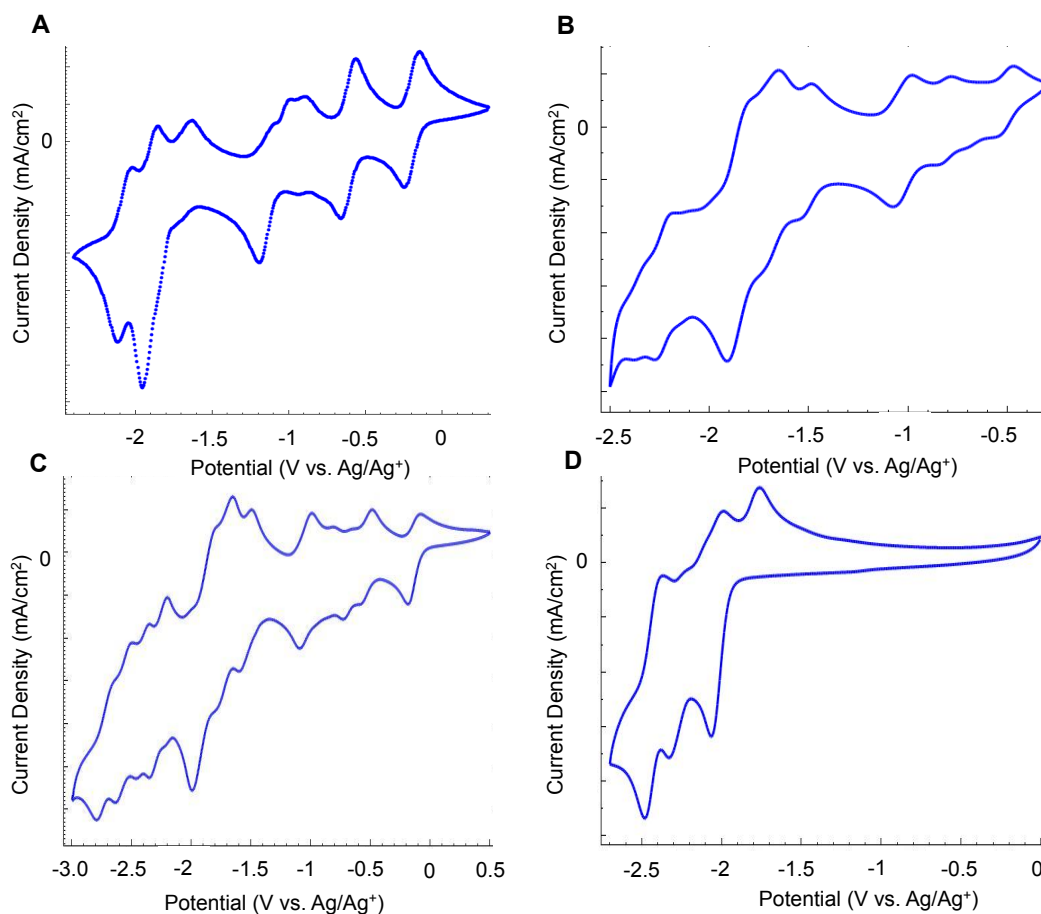
$[\text{Cr}(\text{L17})_3]^{3+}$	$E_{1/2}$ (V)	-0.93	-1.37	-1.76	-2.30	-2.55
	$i_p^{\text{red}}/i_p^{\text{ox}}$	0.87	1.03	0.90	1.01	0.73
	ΔE_p (V)	0.070	0.070	0.077	0.063	0.077

Figure 2.14. CV of $[\text{Cr}(\text{L11})_3]^{3+}$ in acetonitrile. CV was taken in 0.1 M TBABF₄ in acetonitrile. Reference is Ag/Ag⁺ with AgBF₄ (0.01M); working electrode is glassy carbon disk; counter electrode is platinum wire; scan rate is 100 mV s⁻¹; temperature is 23 °C.



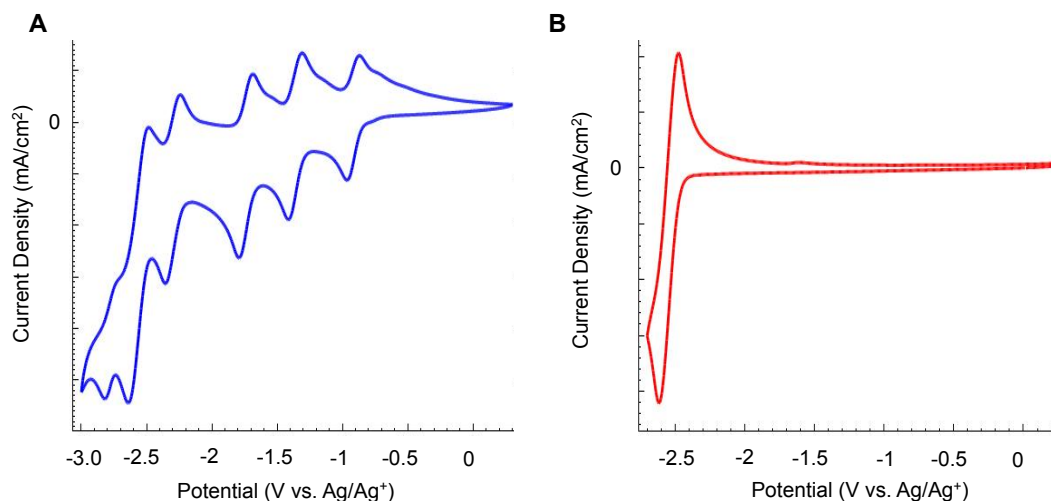
Complexes bearing *sec*-butyl ($[\text{Cr}(\text{L6})_3]^{3+}$), heptyl ($[\text{Cr}(\text{L7})_3]^{3+}$), octyl ($[\text{Cr}(\text{L8})_3]^{3+}$) and trifluoromethyl ($[\text{Cr}(\text{L14})_3]^{3+}$) chains exhibited irreversible electrochemistry (Figure 2.15). The high anodic currents observed around -2 V could be a result of free ligand reduction in solution. The cyclic voltammograms of the free bpy ligands show quasi-reversible peaks between -2 V and -2.5 V (Figure 2.15 D shows the CV of the free dimethyl ester-bpy ligand, L3). In the case of the perfluorinated complex, literature reports indicate that fluorinated alkyl chains decompose at highly reducing potentials.¹⁵

Figure 2.15. A) CV of $[\text{Cr}(\text{L6})_3]^{3+}$; B) CV of $[\text{Cr}(\text{L14})_3]^{3+}$; C) CV of $[\text{Cr}(\text{L8})_3]^{3+}$; D) CV of free ligand L3. CVs were taken in 0.1 M TBABF₄ in acetonitrile. Reference is Ag/Ag⁺ with AgBF₄ (0.01M); working electrode is glassy carbon disk; counter electrode is platinum wire; scan rate is 100 mV s⁻¹; temperature is 23 °C.



Finally, the alkoxy-bpy Cr(III) complexes show an initial reduction peak at around -0.9 V. This shift toward negative potentials is a reflection of the electron-donating properties of the ether substituent. These compounds exhibit four stable quasi-reversible redox events. Highly reducing potentials (beyond -2.5 V) resulted in decomposition of the complexes, as multiple small additional shoulders appeared (Figure 2.16 A). Additionally, the fifth peak in all the alkoxy-bpy Cr complexes showed a large cathodic and anodic current. The increase in current could be attributed to free ligand in solution. Indeed, CV of the free dimethoxy-bpy ligand (L15) shows a reversible redox couple around -2.6 V (Figure 2.16 B). Finally, the electron rich complex $[\text{Cr}(\text{L17})_3]^{3+}$ exhibited only five redox couples within the voltage window of acetonitrile.

Figure 2.16. A) CV of $[\text{Cr}(\text{L15})_3]^{3+}$; B) CV of free ligand L15. CVs were taken in 0.1 M TBABF₄ in acetonitrile. Reference is Ag/Ag⁺ with AgBF₄ (0.01M); working electrode is glassy carbon disk; counter electrode is platinum wire; scan rate is 100 mV s⁻¹; temperature is 23 °C.



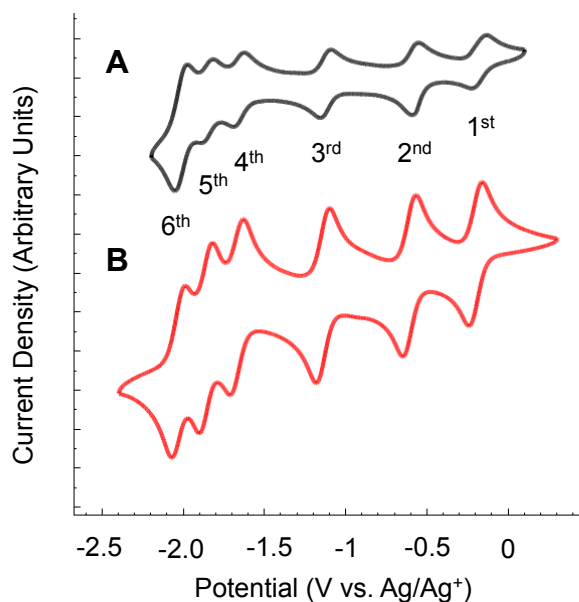
Cyclic Voltammetry of Bpy Cr(0) Complexes

Cyclic voltammetry of Cr(0) complexes showed similar electrochemical behavior to the Cr(III) analogues. Six reversible redox couples were observed and summarized in Table 2.3. The first three redox couples were widely spaced, whereas the last three couples were closer in voltage. Unlike the Cr(III) species, the sixth redox event showed a large increase in the peak current (Figure 2.17). The reason for this electrochemical response is unclear with the available information on these complexes. One possibility is that the neutral species has lower chemical stability in solution, thus leading to ligand shedding. In addition, the redox peaks reversibility in these complexes is reduced as determined by their corresponding current peak height ratio. Due to the poor solubility of the complexes most of the CVs were run at very low concentration, which led to low currents as compared to the background current. Complexes $\text{Cr}(\text{L6})_3]^0$, $[\text{Cr}(\text{L7})_3]^0$ and $[\text{Cr}(\text{L9})_3]^0$ could not be characterized by CV due to poor solubility.

Table 2.3. Potentials, peak current ratios and peak separations for the ester-bpy Cr(0) complexes in acetonitrile. Reference is Ag/Ag⁺ with AgBF₄ (0.01 M); supporting electrolyte is TBABF₄ (0.1 M); working electrode is glassy carbon disk; counter electrode is platinum wire; scan rate is 100 mV s⁻¹; temperature is 23 °C.

Compound		1 st	2 nd	3 rd	4 th	5 th	6 th
[Cr(L3) ₃] ⁰	E _{1/2} (V)	-0.18	-0.59	-1.12	-1.65	-1.83	-2.01
	i _p ^{red} /i _p ^{ox}	1.56	0.95	1.02	1.12	0.34	1.20
[Cr(L5) ₃] ⁰	E _{1/2} (V)	-0.18	-0.58	-1.13	-1.66	-1.85	-2.02
	i _p ^{red} /i _p ^{ox}	0.99	0.83	0.98	0.96	1.08	0.96
[Cr(L10) ₃] ⁰	E _{1/2} (V)	-0.17	-0.58	-1.12	-1.64	-1.82	-2.00
	i _p ^{red} /i _p ^{ox}	0.92	1.04	0.91	0.71	1.00	0.89
[Cr(L11) ₃] ⁰	E _{1/2} (V)	-0.18	-0.58	-1.14	-1.66	-1.86	-2.01
	i _p ^{red} /i _p ^{ox}	1.3	1.22	1.13	1.06	0.98	1.32

Figure 2.17. A) CV of [Cr(L5)₃]⁰; B) CV of [Cr(L5)₃]³⁺. CVs were taken in 0.1 M TBABF₄ in acetonitrile. Reference is Ag/Ag⁺ with AgBF₄ (0.01M); working electrode is glassy carbon disk; counter electrode is platinum wire; scan rate is 100 mV s⁻¹; temperature is 23 °C.



Summary of Solubility and Electrochemistry of Bpy Cr Complexes

In summary, our studies enabled us to establish trends in solubility and electrochemistry as function of the structure of the redox active species.

With regard to the solubility:

1) We identified drastic changes in solubility (~ 4 orders of magnitude) between two different oxidation states (Cr(III) versus Cr(0)) for MCCs bearing the same ligand framework.

2) Modification of the ligand backbone in the MCCs has a major impact on solubility. However, the solubility of these complexes is ultimately limited by the overall density and molecular weight of the complex itself. Therefore, the solubility of Cr(III) species was found to be relatively insensitive to chain substitution (maximum solubility resulted in ~0.6 M in acetonitrile).

3) The overall charge in the metal complexes dominates solubility. The 3+ charge of the Cr(III) complexes generally results in much higher solubility than that of the neutral Cr(0) analogues.

4) Cr(0) complexes showed that incorporation of polar functional groups (glycol ethers) in the ester backbone resulted in favorable increase in solubility compared to non-polar alkyl chains.

With regard to electrochemistry:

1) Changes in the structure of the MCC can impact the electrochemical properties and stability. The incorporation of highly aliphatic alkyl and perfluorinated chains resulted in irreversible electrochemical behavior and poor stability.

2) The electronic properties of the ligand (electron-donating or electron-withdrawing) can impact electrochemical stability, number of redox couples accessed, and cell voltage. In general, complexes bearing bpy ligands with electron-donating alkoxy substituents show lower stability and a lower number of reversible redox couples (four stable redox couples) over a 1.4 V window. In contrast, the ester-substituted complexes display enhanced electrochemical stability and six reversible redox couples over a 2 V window.

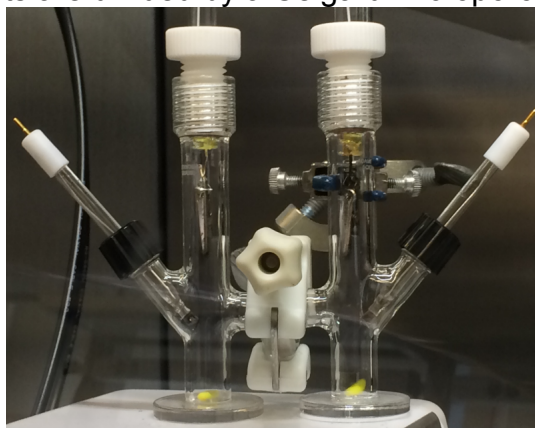
Charge and Discharge Cycling of $[\text{Cr}(\text{L11})_3]^0$

The systematic study on the solubility and electrochemistry of the Cr complexes bearing bpy ligands demonstrated the energy density of a flow battery containing these complexes to be directly related to solubility and the number of reversible redox states of Cr(0) complexes. We selected $[\text{Cr}(\text{L11})_3]^0$ as a promising candidate to move forward for charge/discharge experiments. The charge/discharge cycling in a static (non-flowing

cell) H-cell is an important electrochemical tool to preliminarily assess how these redox active species would perform in a practical RFB over long periods of time.

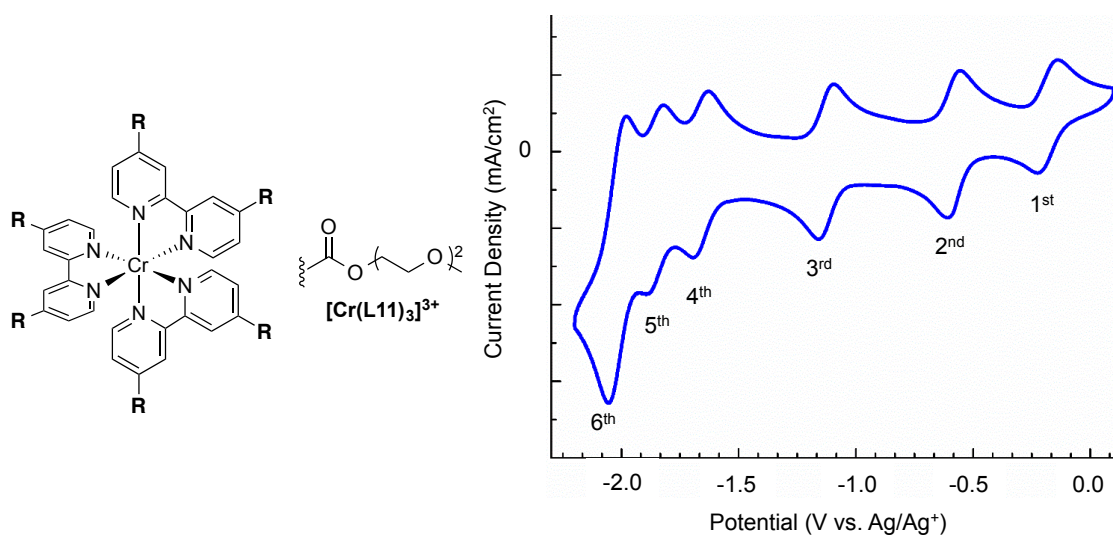
The experiments were performed in collaboration with the Thompson group in chemical engineering. H-cell charge/discharge experiments are designed to approximate the conditions of a battery while requiring a smaller quantity of material. An image of the cell is shown in Figure 2.18.^{4e} The charging step represents the input of energy in the form of electrical current to the system, while the discharge step involves the removal of this energy. The test can be performed under constant potential, constant current, or constant resistive load. Our experiments were performed in a N₂-filled glovebox under constant current in which the voltage response was recorded over time. A 4 electrode setup was used, with a graphite working electrode and Ag/Ag⁺ reference electrode placed in each compartment in order to record the absolute potential profiles at the positive and negative electrode during cycling. These correspond to the potentials of the redox couples observed in the cyclic voltammogram. A microporous plastic separator (Celgard) was employed to separate the two half cells. Stirring is extremely important in both compartments of the cell to minimize mass-transfer limitations at the electrodes. A large solution resistivity is observed in these H-cell experiments due to the large physical separation between the working and counter electrodes.

Figure 2.18. Photograph of an H-cell employed for charge and discharge experiments. Each compartment contains a graphite electrode and a Ag/Ag⁺ electrode. The compartments are divided by a Celgard microporous separator.



In collaboration with Dr. Xingyi Yang and Dr. Krista Hawthorne from the Thompson lab, we performed charge/discharge experiments with $[\text{Cr}(\text{L11})_3]^0$. Our initial design was to target multi-electron transfers given the attractive electrochemical profile of the Cr complex (6 reversible redox couples) to enable three-electron transfers between the electrode and metal complex. The objective was to add Cr(0) species in both compartments of the H-cell and allow the catholyte to undergo $3e^-$ oxidation to generate Cr(III) species, while in the anolyte the species would undergo a $3e^-$ reduction to generate Cr(3-) species. The discharging process is the reverse to regenerate the initial Cr(0) species in both half cells. As such, cutoff voltages were set to allow access to all redox couples. During charging, a voltage cutoff of 0 V (cathode) and -2.3 V (anode) was placed to avoid decomposition from accessing high potentials. During the discharge process a voltage cutoff of -1.2 V (cathode) and -1.35 V (anode) was placed. These voltage cutoffs were strategically placed based on the observed redox couples in the cyclic voltammogram in order to regenerate the Cr(0) complex (Figure 2.19).

Figure 2.19. CV of $[\text{Cr}(\text{L11})_3]^0$. CV was taken in 0.1 M TBABF₄ in acetonitrile. Reference is Ag/Ag⁺ with AgBF₄ (0.01M); working electrode is glassy carbon disk; counter electrode is platinum wire; scan rate is 100 mV s⁻¹; temperature is 23 °C.



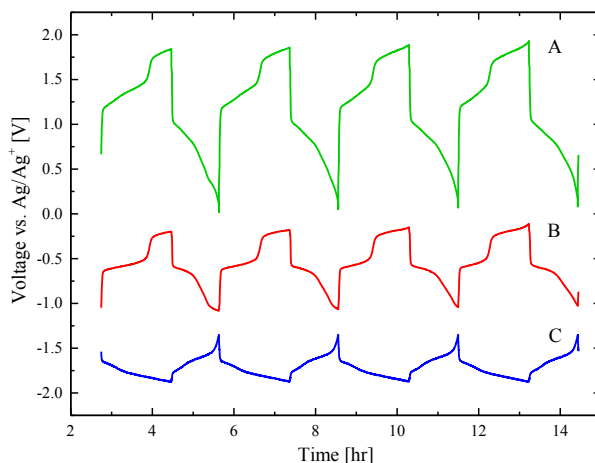
Overall, the experiment demonstrated that when the voltage reached the charging cutoffs the complex underwent decomposition, as it could not be subsequently discharged and cycled. This is an example of the importance of not only assessing stability by CV but also by bulk electrolysis and/or charge/discharge cycling. The

reactivity of the charged bulk solution can result in irreversible decomposition that during a CV experiment, due to the short time period, cannot be observed.

Given this preliminary result, we hypothesized that increasing the charging current could slow down degradation of the MCC as it would reside in the charged state for a shorter period of time. A charging current of 4.0 C enabled access to four of the six redox couples (two-electron transfers) as shown in Figure 2.20 A. The potential curve during charging exhibits two plateaus (1.1 and 1.7 V) that are indicative of two-electron charging. Discharge occurs smoothly without noticeable plateaus in the voltage curve to 0 V. Each of these plateaus corresponds to a single electron transfer process and can be understood by analyzing the individual potential profiles at the catholyte and anolyte (Figure 2.20 B and C, respectively). During charging two cathodic plateaus are observed at -0.6 and -0.2 V. These potentials are consistent with the 1st and 2nd redox couples in the CV (Figure 2.19). Similarly, the anolyte shows two subtle plateaus at voltages of -1.7 and -1.9 V. These potentials are consistent with the 4th and 5th redox couples in the CV. Overall, this electrochemical behavior demonstrates the first example of multi-electron cycling of MCCs in a symmetrical H-cell. The average coulombic efficiency for the cell was 68%. The energy density after charging the cell is 0.15 W h L^{-1} at ~27% state of charge (SOC). For the maximum $[\text{Cr}(\text{L11})_3]^0$ concentration (0.21 M), the total energy density would be 10.2 W h L^{-1} at the full state of charge (SOC).

The charge and discharge cycling could be repeated for only ten cycles. Inefficiencies of this un-optimized cycling experiment can be attributed to crossover of the active species through the Celgard separator, causing self-discharge. Additionally, it is likely that ligand shedding from the metal complex is reducing the capacity of the overall system. This problem is consistent with observations made during the CV studies. Finally, corrosion of the electrodes by the chemical and electrochemical interactions between the active species and supporting electrolyte could be another cause of degradation. Electrochemical decomposition of the redox active species is unlikely, as the mild voltage cutoffs protect the compound from high potentials; however, chemical degradation is still a possibility.

Figure 2.20. Charge/discharge cycling at ± 0.64 mA for $[\text{Cr}(\text{L11})_3]^0$ in a H-cell. Cycle 2 through 5 are shown. A) the total cell voltage; B) Catholyte potential; C) Anolyte potential. All potential curves are referenced versus Ag/Ag^+ electrode. Experiment performed with a graphite electrodes. Separator: Celgard 2325. Electrolyte: 0.01 M $[\text{Cr}(\text{L11})_3]^0$ and 0.5 M TBABF_4 in acetonitrile.



2.3 Conclusion

In conclusion, we have developed a series of chromium bipyridine complexes that undergo multiple redox events. The solubilities of these complexes can be significantly enhanced via ligand modification. These studies show that solubility in the $\text{Cr}(0)$ state is currently the limiting factor for achieving high energy densities. However, this solubility can be enhanced by 4 orders of magnitude through the incorporation of polar substituents in the ligand backbone. These substituents have minimal impact on the electrochemical behavior (as measured by cyclic voltammetry). These investigations led to the identification of complex $[\text{Cr}(\text{L11})_3]^0$ which was analyzed by charge/discharge cycling. The charge/discharge experiments are in agreement with the cyclic voltammetry, and demonstrate the accessibility of two redox couples at both the negative and positive electrodes in an H-cell. A symmetric, multielectron RFB offers opportunities to enhance the energy density of an RFB and to mitigate performance losses associated with crossover of the active species.

The advantages associated with complexes of general structure $[\text{Cr}(\text{L11})_3]^0$ and the outlined structure-solubility-electrochemistry relationship studies should prove useful for the development of new MCCs for non-aqueous flow batteries.

2.4 Perspective and Outlook

Challenges remain for non-aqueous RFBs to reach commercial prototypes. To further advance this field, it is important to continue the design and synthesis of robust redox active materials based on fundamental physical, organic and inorganic, properties. Using a single redox active species that acts both as catholyte and anolyte in a symmetric battery puts many requirements on the material. In my opinion, the independent development of catholyte and anolyte materials is more promising. This enables the independent optimization of the chemistry and electrochemistry of each half-cell. However, the final challenge will be to prove that both molecules are compatible in a full cell. Additionally, advances in cell design and engineering will provide opportunities to minimize mass transport issues, internal cell resistance, and combat the inherent poor conductivity of organic electrolytes. Finally, the development of organic-compatible membranes that allow passage of small ions in organic solvents across half-cells to maintain chemical balance, while preventing cross-over of redox-active species, will be a critical advance needed to move the field forward.

Our laboratory continues the development of new redox active materials through two different strategies: 1) the development of multidentate metal complexes and 2) the development of small redox-active organic molecules. To this end, we have shown that a combination of metal centers with less propensity for ligand exchange and tridentate non-innocent ligands afford stable multi-electron MCCs that can be charged and discharged for over 200 cycles.¹⁶ In addition, our lab continues exploring alkyl pyridinium and cyclopropenium cations as robust all-organic redox active materials for flow batteries.¹⁷

2.5 Experimental

Materials and Methods

All syntheses were conducted under an oxygen-free atmosphere in either a nitrogen filled glovebox or using standard Schlenk line techniques unless stated otherwise. Dichloromethane and diethyl ether were purified using an Innovative Technologies solvent purification system consisting of a copper catalyst, activated alumina, and molecular sieves. Triethylamine was purified by distillation

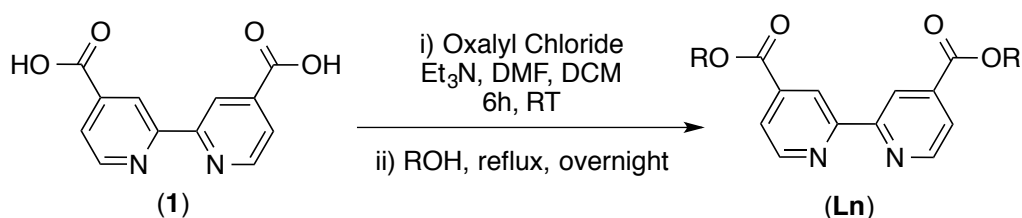
from CaH₂. The molecules [2,2'-bipyridine]-4,4'-dicarboxylic acid (**1**),¹⁸ [2,2'-bipyridine]-4,4'-dihydroxyl (**2**),¹⁹ 4,4'-dimethylester-2,2'-bipyridine (**L3**),²⁰ tetrakis(acetonitrile)chromium (II) tetrafluoroborate (**3**),²¹ tris(2,2'-bipyridine)chromium(III) tetrafluoroborate (**[Cr(L1)₃]³⁺**)⁹ and tris(4,4'-dimethylester-2,2'-bipyridine)chromium(III) tetrafluoroborate (**[Cr(L2)₃]³⁺**)⁹ were prepared according to published procedures. All remaining reagents were purchased from commercial sources and used as received. NMR spectra were obtained on Varian VNMRs 700, Varian VNMRs 500, Varian Inova 500, or Varian MR400 spectrometers. ¹H and ¹³C chemical shifts are reported in parts per million (ppm) relative to tetramethylsilane (Si(CH₃)₄), with the residual solvent peak used as an internal reference. NMR multiplicities are reported as follows: singlet (s), doublet (d), triplet (t), quartet (q), multiplet (m), broad signal (br). Coupling constants (*J*) are reported in hertz (Hz). Infrared (IR) spectroscopy on the Cr³⁺ complexes was performed with a Perkin-Elmer Spectrum BX FT-IR spectrometer using an ATR attachment. IR spectroscopy on the Cr⁰ complexes was performed with a Thermo Scientific Nicolet iS-10 spectrometer using KBr pellets. Melting points were determined with a Mel-Temp 3.0, Laboratory Devices Inc, USA instrument. Mass spectral data was obtained on a Micromass magnetic sector mass spectrometer in electrospray ionization mode. Elemental analyses were carried out at Atlantic Microlab in Norcross, GA. UV-Vis absorption data for Cr³⁺ complexes was collected on a Shimadzu UV-1601 UV-VIS spectrometer. UV-Vis absorption data for Cr⁰ complexes was collected on an Implen NanoPhotometer® P 300 UV/Vis spectrophotometer. Centrifugation was performed on a Sorval ST 16 centrifuge from ThermoScientific.

Electrochemical Analysis

All electrochemical analyses were carried out in an argon-filled or nitrogen-filled glovebox (MBraun). The supporting electrolyte was electrochemical grade tetrabutylammonium tetrafluoroborate (Sigma-Aldrich). The solvent was acetonitrile (Sigma-Aldrich, anhydrous 99.8%). Cyclic voltammetry was performed with an Autolab PGSTAT302N Potentiostat/Galvanostat (Ecochemie, Netherlands) and a 600D

Potentiostat (CH Instruments, US). Cyclic voltammetry was carried out in a three electrode electrochemical cell, consisting of a glassy carbon disk working electrode (0.07 cm^2 , BASi), a Ag/Ag^+ quasi-reference electrode (BASi) with 0.01 M AgBF_4 (Sigma-Aldrich) in acetonitrile separated by a glass frit, and a platinum wire counter electrode (23 cm, ALS). The glassy carbon disk electrode was polished using micron aluminum oxide polishing paper (9 micron and 0.3 micron, Fiber Instrument) and then sonicated in deionized water. All experiments were ran at a scan rate of 100 mV s^{-1} in an acetonitrile electrolyte containing 10 mM chromium complex and 0.1 M TBABF_4 , unless otherwise noted. Charge/discharge measurements were carried out with a Maccor 4000 Series Battery Tester in an H-cell. The H-cell was purchased from Adam's & Chittenden. A Celgard 2325 separator was soaked in 0.5 M TBABF_4 in acetonitrile for 24 h prior to cell assembly. For Cr complexes: The electrolyte contained 0.01 M chromium complex and 0.5 M TBABF_4 . Cells were charged at a current of 0.64 mA , with voltage cutoffs set on both the anode and cathode, referenced to a Ag/Ag^+ reference electrode placed in each side of the cell. The voltage cutoff during charging for the cathode was 0 V , and the voltage cutoff for the anode was -1.35 V . A charge limit of 0.001 Ah (4.0 Coulombs) was placed on the cell to protect the complex from overcharging. The discharge conditions were similar, with a discharge current of 0.64 mA , and voltage cutoffs of -1.2 V and -1.35 V for the cathode and anode, respectively.

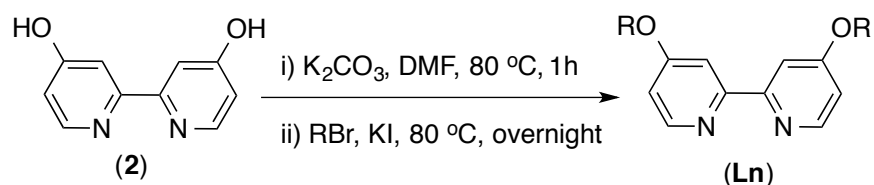
General Procedures



General Procedure 1: An oven dry three-necked flask was charged with [2,2'-bipyridine]-4,4'-dicarboxylic acid (1) (1.0 g , 4.09 mmol , 1.0 equiv), which was suspended in dry dichloromethane (30 mL). Triethylamine (3.44 mL , 24.54 mmol , 6.0 equiv) and DMF (50 uL , 0.65 mmol , 0.16 equiv) were subsequently added, followed by dropwise addition of oxalyl chloride (12.28 mmol , 3 equiv) under a nitrogen atmosphere. The reaction mixture was vigorously stirred for 6 h , then the corresponding alcohol

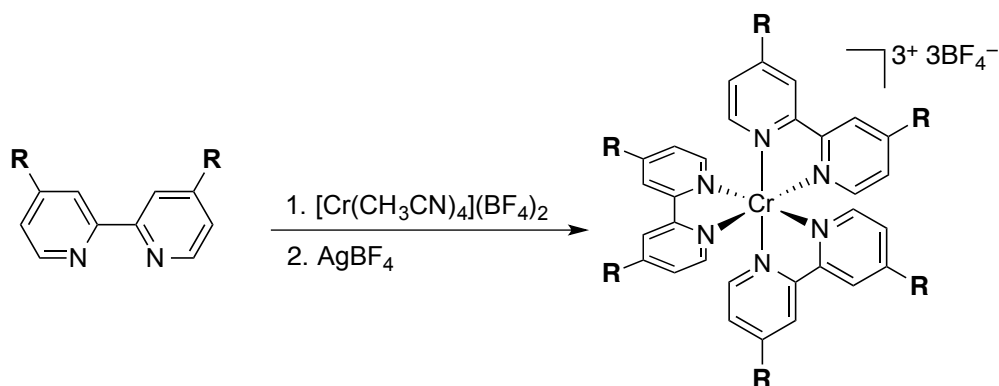
(12.28 mmol, 3.0 equiv) was added. The reaction mixture was refluxed for 12 h or until completion as indicated by thin layer chromatography. The reaction mixture was cooled to room temperature, a small amount of silica gel or basic aluminum oxide Brockmann I was added, and the volatiles were removed *in vacuo*. The ligands were then purified as described below.

Caution: Addition of the highly corrosive oxalyl chloride leads to an exothermic reaction and evolution of gasses. The reactions should remain under nitrogen atmosphere in a well-ventilated fume-hood.

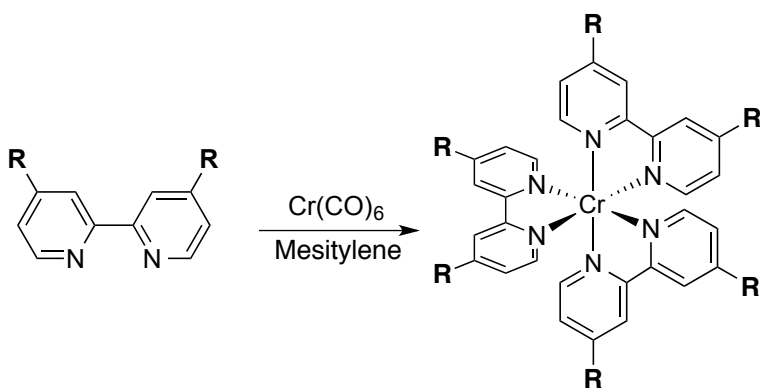


General Procedure 2: An oven dried Schlenk flask was charged with [2,2'-bipyridine]-4,4'-dihydroxyl (**2**) (1.0 g, 5.31 mmol, 1.0 equiv) and anhydrous K_2CO_3 (4.41 g, 31.9 mmol, 6.0 equiv). This mixture was suspended in dry DMF (80 mL, 0.07 M) and heated to 80 °C. After 1 h, the alkyl bromide (11.7 mmol, 2.2 equiv) and KI (1.94 g, 11.7 mmol, 2.2 equiv) were added. The resulting mixture was vigorously stirred overnight (~14 h) at 80 °C. The reaction was cooled to room temperature, and the solvent was removed under reduced pressure. The solid residue was suspended in chloroform (50 mL) and washed with water (4 × 25 mL). The organic layer was dried over anhydrous sodium sulfate, filtered and concentrated *in vacuo*. The ligands were purified as described below.

Caution: Handling of highly toxic alkyl halides should be performed inside a well-ventilated fume-hood.



General Procedure 3: Synthesis of $[\text{Cr}(\text{L})_3]^{3+}$ complexes. In a nitrogen-filled glovebox, a Schlenk tube containing a suspension of the appropriate bipyridine ligand (1.39 mmol, 3.3 equiv) in acetonitrile (14 mL, 0.03 M) was charged with $[\text{Cr}(\text{CH}_3\text{CN})_4](\text{BF}_4)_2$ (**3**) (0.16 g, 0.42 mmol, 1.0 equiv). The reaction mixture was vigorously stirred for 15 min until a dark green (for ester-bipyridine complexes) or a dark purple (for alkoxy-bipyridine complexes) solution formed. Silver tetrafluoroborate (0.08 g, 0.42 mmol, 1.0 equiv) was added in one portion, and the reaction mixture was stirred for 10 min to afford a light yellow/green solution and silver solid. The reaction was removed from the glovebox, and the solid was separated by centrifugation. The supernatant was decanted, concentrated, and filtered through glass fiber to remove any remaining silver solid. Each complex was further purified as described below.



General Procedure 4: Synthesis of $[\text{Cr}(\text{L})_3]^0$ Complexes. The neutral Cr^0 complexes were synthesized using a modification of a literature procedure.¹ A Schlenk flask was charged with the appropriate bipyridine ligand (2.22 mmol, 3 equiv), $\text{Cr}(\text{CO})_6$ (0.74 mmol, 1 equiv), and mesitylene (36 mL, 0.02 M solution in $\text{Cr}(\text{CO})_6$). The reaction mixture was degassed for 30 min by purging with N_2 , and then refluxed at 180 °C under

an inert atmosphere overnight. The dark purple mixture was allowed to cool to room temperature, and the mesitylene was removed *in vacuo* with heating. The remaining purple solid was dried *in vacuo* at 60 °C for 12 h to afford the desired complex as an air-sensitive dark purple solid.

Caution: While Cr(VI) is the most toxic oxidation state for chromium, the chromium (III) and (0) bipyridine complexes should be handled with appropriate personal protective equipment in a well-ventilated hood or inside of an inert atmosphere glove-box.

General Procedure 5: Solubility Determination of $[\text{Cr}(\text{L})_3]^{3+}$ Complexes. Stock solutions (2.0 mM) of each complex were prepared in acetonitrile, in triplicate, from which standard solutions of 0.5 mM, 1.0 mM, and 1.5 mM concentration were prepared by sequential dilution. A UV-Vis spectrum of the 2.0 mM stock solution was recorded and used to determine a suitable wavelength for absorbance measurements. Absorbances of the standard solutions were then measured at the determined wavelength and used to prepare an absorbance versus concentration calibration curve. Saturated solutions were then prepared by portion-wise addition of the desired compound to 300 μL of acetonitrile, with stirring, until a persistent suspension remained. The solution was filtered through cotton wool to remove any undissolved material, and three aliquots were diluted in acetonitrile to afford absorbances within the range of the calibration curve. Solubility studies were performed on the benchtop.

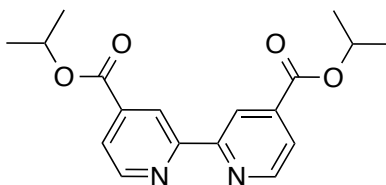
General Procedure 6: Solubility Determination of $[\text{Cr}(\text{L})_3]^0$ Complexes. Stock solutions (0.2 mM) of each complex were prepared in acetonitrile, in triplicate, from which standard solutions of 0.15 mM, 0.1 mM and 0.05 mM concentration were prepared by sequential dilution. A UV-vis spectrum of the 0.2 mM stock solution was recorded and used to determine a suitable wavelength for absorbance measurements. Absorbances of the standard solutions were then measured at the determined wavelength and used to prepare an absorbance versus concentration calibration curve. Saturated solutions were then prepared by portion-wise addition of the desired compound to 1 mL of acetonitrile, with stirring, until a persistent suspension remained. The solution was filtered through glass fiber to remove any undissolved material, and

three aliquots were diluted in acetonitrile to afford absorbances within the range of the calibration curve. These solubility studies were performed inside a nitrogen-filled glovebox.

General Procedure 6a: Solubility Approximation of $[\text{Cr}(\text{L6})_3]^0$ and $[\text{Cr}(\text{L7})_3]^0$. Due to the low solubility of the metal complexes $[\text{Cr}(\text{L6})_3]^0$ and $[\text{Cr}(\text{L7})_3]^0$, a modified procedure was employed. Saturated solutions were prepared in acetonitrile with vigorous stirring until a persistent suspension resulted. The solution was filtered through glass fiber to remove any undissolved material. The filtered solution was analyzed without any further dilution by UV-vis spectrometer. The solubility is obtained using Beer-Lambert's equation (see example for Cr^{3+} below). The highest and lowest molar extinction coefficients for analogous Cr^0 complexes ($10,000 \text{ L mol}^{-1} \text{ cm}^{-1}$ and $4,000 \text{ L mol}^{-1} \text{ cm}^{-1}$, respectively) are employed, affording an upper and lower solubility value with a path length cuvette of 1 cm, through which the average solubility is obtained.

Synthesis and Characterization

Synthesis of Ligands



L4. Ligand **L4** was synthesized from *iso*-propanol (1.10 g, 1.41 mL, 18.43 mmol, 3 equiv) following **General Procedure 1**. Purification via flash column chromatography (basic aluminum oxide Brockmann I, 1:1 EtOAc:Hex) furnished a red solid that was further recrystallized from $\text{CHCl}_3/\text{MeOH}$ (1:1) to afford **L4** as a light yellow solid (1.10 g, 3.35 mmol, 55% yield).

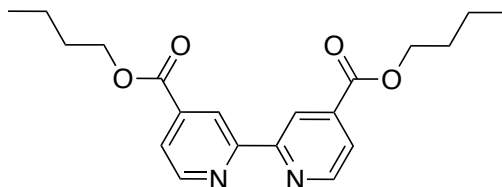
R_f : 0.77 (basic Al_2O_3 , 1:1 EtOAc:Hex)

IR (thin film, cm^{-1}): 2989, 1716, 1593, 1557, 1462, 1354, 1282, 1238, 1085, 916, 762.

MP: 116-117 °C

HRMS: ESI⁺ (m/z): $[\text{M}+\text{H}]^+$ calcd. for $\text{C}_{18}\text{H}_{21}\text{N}_2\text{O}_4$: 329.1496; found: 329.1490.

NMR: ^1H NMR (CDCl_3 , 700 MHz): δ 8.91 (app s, 2H), 8.85 (dd, $J = 0.8, 4.8$ Hz, 2H), 7.89 (dd, $J = 1.6, 4.8$ Hz, 2H), 5.31 (septet, $J = 6.4$, 2H), 1.41 (d, $J = 6.4$ Hz, 12H). ^{13}C NMR (CDCl_3 , 175.97 MHz): δ 164.6, 156.5, 150.0, 139.3, 123.1, 120.5, 69.6, 21.8.



L5. Ligand **L5** was synthesized from *n*-butanol (1.4 g, 1.7 mL, 18.43 mmol, 3 equiv) following **General Procedure 1**. Purification via flash column chromatography (basic aluminum oxide Brockmann I, 1:1 EtOAc:Hex) furnished an orange solid that was further recrystallized from $\text{CHCl}_3/\text{MeOH}$ (1:1) to afford **L5** as a white solid (1.10 g, 3.09 mmol, 50% yield).

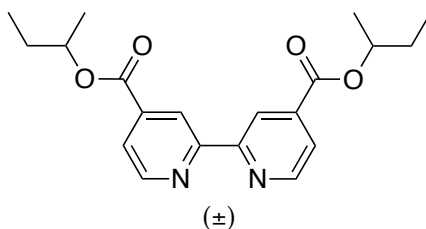
R_f : 1.00 (basic Al_2O_3 , 1:1 EtOAc:Hex)

IR (thin film, cm^{-1}): 2959, 1716, 1557, 1458, 1364, 1288, 1246, 1142, 959, 763.

MP: 104-106 °C

HRMS: ESI^+ (m/z): $[\text{M}+\text{H}]^+$ calcd. for $\text{C}_{20}\text{H}_{25}\text{N}_2\text{O}_4$, 357.1809; Found, 357.1814.

NMR: ^1H NMR (CDCl_3 , 400 MHz): δ 8.94 (dd, $J = 0.8, 1.6$ Hz, 2H), 8.87 (dd, $J = 0.8, 5.2$ Hz, 2H), 7.91 (dd, $J = 1.6, 5.2$ Hz, 2H), 4.40 (t, $J = 6.8$ Hz, 4H), 1.80 (m, 4H), 1.50 (m, 4H), 1.00 (t, $J = 7.6$ Hz, 6H). ^{13}C NMR (CDCl_3 , 175.97 MHz): δ 165.4, 156.7, 150.2, 139.1, 123.3, 120.7, 65.9, 30.8, 19.3, 13.9.



L6. Ligand **L6** was synthesized from racemic *sec*-butanol (1.37 g, 1.7 mL, 18.43 mmol, 3 equiv) following **General Procedure 1**. Purification via column chromatography (silica gel, 100% Hexanes to 2:3 EtOAc:Hex) afforded **L6** as a white solid (1.2 g, 3.37 mmol, 55% yield).

R_f : 0.76 (silica gel, 2:3 EtOAc:Hex)

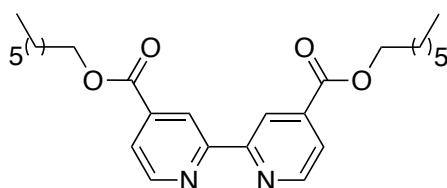
IR (thin film, cm^{-1}): 2976, 1716, 1700, 1558, 1281, 1254, 1109, 889, 756, 722.

MP: 41-43 °C

HRMS: ESI⁺ (m/z): [M+H]⁺ calcd. for C₂₀H₂₅N₂O₄: 357.1809 ; found: 357.1809.

NMR: ¹H NMR (CDCl₃, 700 MHz): δ 8.93 (app br s, 2 H), 8.86 (d, J = 4.9 Hz, 2H), 7.91 (dd, J = 1.4, 4.9 Hz, 2H), 5.16 (sextet, J = 6.3 Hz, 2H), 1.81 (app septet, J = 7 Hz, 2H), 1.71 (app septet, 2H), 1.38 (d, J = 6.3 Hz, 6H), 0.99 (t, J = 6.3 Hz, 6H).

¹³C NMR (CDCl₃, 175.95 MHz): δ 164.9, 156.7, 150.2, 139.6, 123.4, 120.7, 74.4, 29.0, 19.7, 10.0.



L7. Ligand **L7** was synthesized by refluxing [2,2'-bipyridine]-4,4'-dicarboxylic acid (**S1**) (2.5 g, 10.24 mmol) in *n*-heptanol (75.3 g, 92.0 mL, 0.65 mol) with catalytic sulfuric acid (1 mL) for 2 days. The reaction mixture was cooled to room temperature and the excess alcohol was removed by vacuum distillation. The residue was diluted in DCM (100 mL) and was extracted with 2M NaOH (3 x 25 mL) and water (20 mL). The aqueous layer was washed with DCM (2 x 25 mL). The combined organic extracts were dried over Na₂SO₄, filtered, and concentrated *in vacuo*. The residue was purified via column chromatography (silica gel, 100% Hexanes to 2:3 EtOAc:Hex) affording a colorless oil that was dried *in vacuo* overnight. A white solid formed and was collected on a fritted filter and washed with cold MeOH (3 x 5 mL). The resulting solid was then recrystallized from hot diethyl ether and acetonitrile to afford **L7** as a white solid (2.75 g, 6.24 mmol, 61% yield).

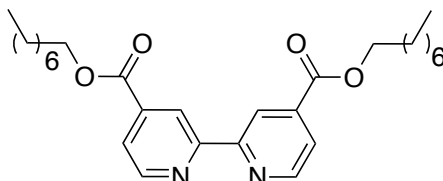
R_f: 0.84 (silica gel, 2:3 EtOAc:Hex)

IR (thin film, cm^{-1}): 2928, 2856, 1724, 1558, 1472, 1363, 1286, 1252, 1139, 953, 762, 721.

MP: 55-56 °C

HRMS: ESI⁺ (m/z): [M+H]⁺ calcd. for C₂₆H₃₇N₂O₄: 441.2748 ; found: 441.2756.

NMR: ^1H NMR (CDCl_3 , 700 MHz): δ 8.94 (app br s, 2H), 8.86 (d, $J = 4.9$ Hz, 2H), 7.90 (dd, $J = 1.4, 4.9$ Hz, 2H), 4.39 (t, $J = 7$ Hz, 4H), 1.81 (quintet, $J = 7$ Hz, 4H), 1.44 (quintet, $J = 7$ Hz, 4H), 1.37 (quintet, $J = 7$ Hz, 4H), 1.33-1.28 (multiple peaks, 8H), 0.89 (t, $J = 7$ Hz, 6H). ^{13}C NMR (CDCl_3 , 176 MHz): δ 165.4, 156.7, 150.2, 139.1, 123.4, 120.7, 66.2, 31.9, 29.1, 28.8, 26.1, 22.7, 14.2.



L8. Ligand **L8** was synthesized from *n*-octanol (3.20 g, 3.87 mL, 24.57 mmol, 3 equiv) following **General Procedure 1**. Purification via column chromatography (silica gel, 1:4 EtOAc:Hex) afforded **L8** as a white solid (1.65 g, 3.52, 43% yield).

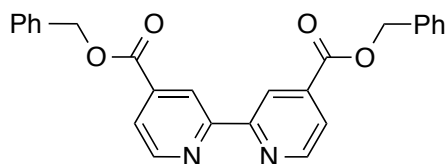
R_f : 0.46 (silica gel, 1:4 EtOAc:Hex)

IR (thin film, cm^{-1}): 2958, 2918, 2853, 1724, 1557, 1474, 1285, 1254, 1140, 1128, 951, 763, 722.

MP: 44-45 $^\circ\text{C}$

HRMS: ESI $^+$ (m/z): $[\text{M}+\text{H}]^+$ calcd. for $\text{C}_{28}\text{H}_{41}\text{N}_2\text{O}_4$: 469.3061; found: 469.3065.

NMR: ^1H NMR (CDCl_3 , 700 MHz): δ 8.96 (app br s, 2H), 8.87 (br d, $J = 4.9$ Hz, 2H), 7.91 (dd, $J = 1.4, 4.9$ Hz, 2H), 4.39 (t, $J = 7$ Hz, 4H), 1.81 (apparent quintet, $J = 7.2$ Hz, 4H), 1.45 (quintet, $J = 7.5$ Hz, 4H), 1.39-1.25 (multiple peaks, 16 H), 0.88 (t, $J = 7.0$ Hz, 6H). ^{13}C NMR (CDCl_3 , 175.95 MHz): δ 165.3, 156.5, 150.2, 139.3, 123.4, 120.8, 66.3, 31.9, 29.4, 29.3, 28.8, 26.1, 27.8, 14.2.



L9. Ligand **L9** was synthesized from benzyl alcohol (2.66 g, 2.55 mL, 24.6 mmol, 3 equiv) following **General Procedure 1**. Purification via column chromatography (basic aluminum oxide, 3:1 EtOAc:Hex) afforded **L9** as a white solid (1.98 g, 4.67, 57% yield).

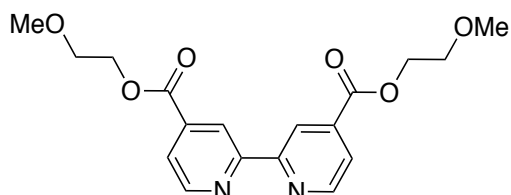
R_f : 0.9 (basic aluminum oxide, 3:1 EtOAc:Hex)

IR (thin film, cm^{-1}): 1712, 1590, 1558, 1360, 1282, 1242, 1128, 911, 760, 747.

MP: 99-100 $^\circ\text{C}$

HRMS: ESI⁺ (m/z): [M+H]⁺ calcd. for C₂₆H₂₁N₂O₄: 425.1496 ; found: 425.1508.

NMR: ¹H NMR (CDCl₃, 700 MHz): δ 8.97 (app. br s, 2H), 8.85 (dd, *J* = 4.9, 1.4 Hz, 2H), 7.92 (dd, *J* = 4.9, 1.4 Hz, 2H), 7.48 (d, *J* = 7 Hz, 4H), 7.41 (t, *J* = 7 Hz, 4H), 7.37 (d, *J* = 7 Hz, 2H), 5.44 (s, 4H). ¹³C NMR (CDCl₃, 175.95 MHz): δ 165.2, 156.6, 150.2, 138.8, 135.5, 128.8, 128.73, 128.66, 123.5, 120.8, 67.7.



L10. Ligand **L10** was synthesized from 2-methoxyethanol (0.965 g, 1 mL, 12.28 mmol, 3 equiv) following **General Procedure 1**. Purification via flash column chromatography (silica gel, 4:1 EtOAc:Hex) afforded **L10** as a white solid (0.53 g, 1.47 mmol, 36% yield).

R_f: 0.54 (silica gel, 4:1 EtOAc:Hex)

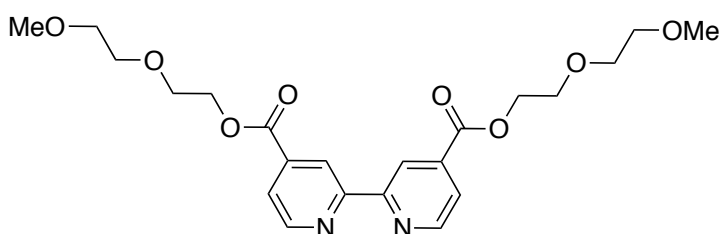
IR (thin film, cm⁻¹): 2903, 1725, 1555, 1458, 1373, 1360, 1283, 1253, 1119, 1024, 867, 759.

MP: 96-97 °C

HRMS: ESI⁺ (m/z): [M+H]⁺ calcd. for C₁₈H₂₁N₂O₆: 361.1394; found: 361.1392.

NMR: ¹H NMR (CDCl₃, 400 MHz): δ 8.97 (app br s, 2H), 8.86 (br d, *J* = 4.8 Hz, 2H), 7.92 (dd, *J* = 4.8, 1.6 Hz, 2H), 4.56 (m, 4H), 3.77 (m, 4H), 3.44 (s, 6H).

¹³C NMR (CDCl₃, 100.71 MHz): δ 165.3, 156.7, 150.2, 138.7, 123.5, 120.8, 70.4, 64.9, 59.2.



L11. Ligand **L11** was synthesized from 2-(2-methoxyethoxy)ethanol (2.97 g, 2.9 mL, 24.57 mmol, 3 equiv) following **General Procedure 1**. Purification via flash column chromatography (basic aluminum oxide Brockmann I, 3:1 EtOAc/Hex to 100 % EtOAc) afforded **L11** as a white solid (1.30 g, 2.90 mmol, 37% yield).

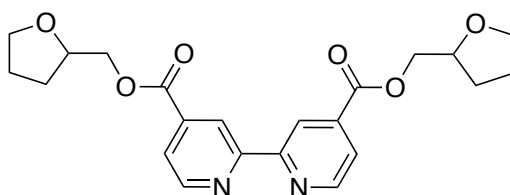
R_f: 0.71 (basic aluminum oxide, 100% EtOAc)

IR (thin film, cm^{-1}): 2891, 1726, 1556, 1460, 1249, 1108, 1027, 853, 760, 691.

MP: 81-83°C

HRMS: ESI⁺ (m/z): [M+H]⁺ calcd. for C₂₂H₂₉N₂O₈: 449.1918; found: 449.1917.

NMR: ¹H NMR (CDCl₃, 400 MHz): δ 8.97 (app br s, 2H), 8.86 (br d, J = 4.8, 2H), 7.92 (dd, J = 4.8, 1.6 Hz, 2H), 4.57 (m, 4H), 3.89 (m, 4H) 3.72 (m, 4H), 3.59 (m, 4H), 3.39 (s, 6H). ¹³C NMR (CDCl₃, 100.71 MHz): δ 165.3, 156.6, 150.2, 138.8, 123.5, 120.9, 72.1, 70.8, 69.2, 65.0, 59.3.



L12. Ligand **L12** was synthesized from racemic tetrahydrofurfuryl alcohol (1.89 g, 1.79 mL, 18.43 mmol, 3 equiv) following **General Procedure 1**. Purification via flash column chromatography (basic aluminum oxide Brockmann I, 3:1 EtOAc:Hex) afforded **L12** as a light yellow solid (1.94 g, 4.70 mmol, 77% yield).

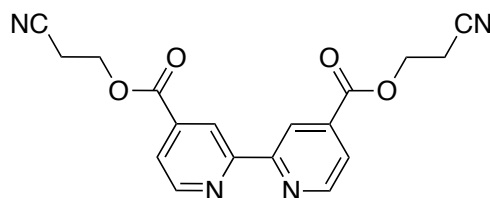
R_f: 0.62 (basic aluminum oxide, 3:1 EtOAc:Hex)

IR (thin film, cm^{-1}): 2875, 1717, 1700, 1654, 1558, 1368, 1290, 1256, 1080, 765.

MP: 103-105 °C

HRMS: ESI⁺ (m/z): [M+H]⁺ calcd. for C₂₂H₂₅N₂O₆: 413.1707; found: 413.1706.

NMR: ¹H NMR (CDCl₃, 700 MHz): δ 8.96 (dd, J = 1.5, 0.7 Hz, 2H), 8.85 (dd, J = 4.9, 0.7 Hz, 2H), 7.91 (dd, J = 4.9, 1.6 Hz, 2H), 4.43 (dd, J = 11.3, 3.7 Hz, 2H), 4.35 (dd, J = 11.3, 6.7 Hz, 2H), 4.30 (app dq, J = 6.9, 3.7 Hz, 2H), 3.93 (app td, J = 8.3, 6.8 Hz, 2H), 3.84 (ddd, J = 8.2, 7.5, 6.1 Hz, 2H), 2.10 (dddd, J = 12.5, 8.3, 7.2, 5.3 Hz, 2H), 2.02-1.91 (multiple peaks, 4H), 1.73 (app tdd, J = 12.4, 8.6, 7.1 Hz, 2H). ¹³C NMR (CDCl₃, 175.95 MHz): δ 165.3, 156.6, 150.2, 138.7, 123.4, 120.8, 76.5, 68.7, 67.8, 28.3, 25.9.



L13. Ligand **L13** was synthesized from 3-hydroxypropionitrile (0.87 g, 0.84 mL, 12.28 mmol, 3 equiv) following **General Procedure 1**. Purification via flash column

chromatography (silica gel, 4:1 EtOAc:Hex). The residue was washed with 0.3 M potassium carbonate (3 × 50 mL) to afford **L13** as a pale yellow solid (0.65 g, 1.86 mmol, 45% yield).

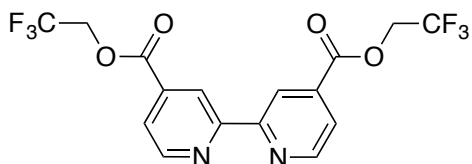
R_f: 0.54 (silica gel, 4:1 EtOAc:Hex)

IR (thin film, cm⁻¹): 1718, 1554, 1381, 1362, 1257, 1001, 858, 757, 691.

MP: 153-155 °C

HRMS: ESI⁺ (m/z): [M+H]⁺ calcd. for C₁₈H₁₅N₄O₄, 351.1088; found, 351.1092.

NMR: ¹H NMR (CDCl₃, 400 MHz): δ 8.98 (app br s, 2H), 8.90 (br d, *J* = 5.2 Hz, 2H), 7.93 (dd, *J* = 4.8, 1.6 Hz, 2H), 4.62 (t, *J* = 6.4 Hz, 4H), 2.91 (t, *J* = 6.4 Hz, 4H). ¹³C NMR (CDCl₃, 125.75 MHz): δ 164.7, 156.6, 150.5, 137.7, 123.5, 120.7, 116.6, 60.1, 18.3.



L14. Ligand **L14** was synthesized from trifluoroethanol (1.24 g, 0.90 mL, 12.28 mmol, 3 equiv) following **General Procedure 1**. Purification via flash column chromatography (silica gel, 1:2 EtOAc:Hex) afforded **L14** as a light pink solid (0.85 g, 2.08 mmol, 51% yield).

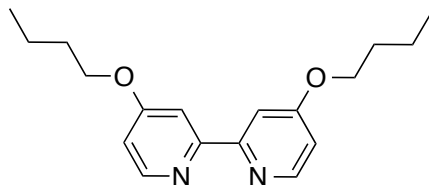
R_f: 0.46 (silica gel, 1:2 EtOAc:Hex)

IR (thin film, cm⁻¹): 2968, 1738, 1594, 1418, 1268, 1159, 960, 759, 704.

MP: 137-138 °C

HRMS: ESI⁺ (m/z): [M+H]⁺ calcd. for C₁₆H₁₁F₆N₂O₄: 409.0618; found: 409.0618.

NMR: ¹H NMR (CDCl₃, 400 MHz): δ 9.01 (dd, *J* = 1.6, 0.8 Hz, 2H), 8.92 (dd, *J* = 4.8, 0.8 Hz, 2H), 7.94 (dd, *J* = 4.8, 1.6 Hz, 2H), 4.78 (q, *J* = 8.4 Hz, 4H). ¹³C NMR (CDCl₃, 175.95 MHz): δ 163.6, 156.4, 150.3, 136.9, 123.4, 122.8 (q, *J* = 277 Hz), 120.7, 61.3 (q, *J* = 37 Hz). ¹⁹F NMR (CDCl₃, 376.87): δ -73.50 (t, *J* = 8.8 Hz).



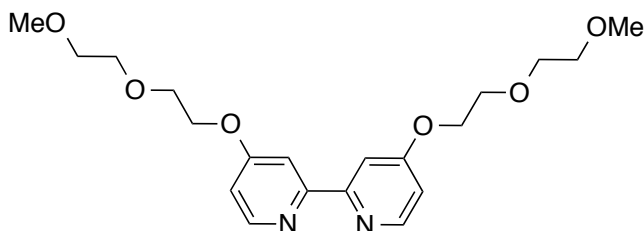
L16. Ligand **L16** was synthesized from *n*-bromobutane (0.41 g, 0.32 mL, 2.93 mmol, 2.2 equiv) following **General Procedure 2**. Purification of the off-white residue via recrystallization from CHCl₃:CH₃OH (v/v 1:1) afforded **L16** as a white solid (0.30 g, 1.00 mmol, 75% yield).

IR (thin film, cm⁻¹): 2953, 2872, 1561, 1459, 1300, 1242, 1003, 841, 745.

MP: 75-76 °C

HRMS: ESI⁺ (m/z): [M+H]⁺ calcd. for C₁₈H₂₅N₂O₂: 301.1911; found: 301.1915.

NMR: ¹H NMR (CDCl₃, 500 MHz): δ 8.45 (d, *J* = 5.5 Hz, 2H), 7.95 (d, *J* = 2.5 Hz, 2H), 6.82 (dd, *J* = 5.5, 2.5 Hz, 2H), 4.13 (t, *J* = 6.5 Hz, 4H), 1.80 (app quintet, *J* = 7.5 Hz, 4H), 1.51 (app sextet, *J* = 7.5 Hz, 4H), 0.98 (t, *J* = 7.5 Hz, 6H). ¹³C NMR (CDCl₃, 100.71 MHz): δ 166.3, 158.0, 150.2, 111.5, 106.8, 67.9, 31.2, 19.3, 14.0.



L17. Ligand **L17** was synthesized from 1-bromo-2-(2-methoxyethoxy)ethane (0.75 g, 0.55 mL, 4.09 mmol, 2.2 equiv) following **General Procedure 2**. Purification of the off-white residue via column chromatography (basic aluminum oxide Brockmann I, 4:1 EtOAc:Hex) afforded **L17** as a white solid (0.32 g, 0.82 mmol, 43% yield).

R_f: 0.4 (basic aluminum oxide, 4:1 EtOAc:Hex)

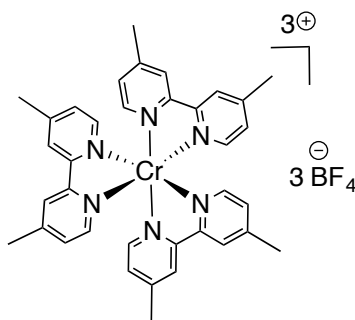
IR (thin film, cm⁻¹): 2878, 1584, 1563, 1471, 1443, 1297, 1242, 1103, 823.

MP: 48-50 °C

HRMS: ESI⁺ (m/z): [M+H]⁺ calcd. for C₂₀H₂₉N₂O₆: 393.2020; found: 393.2026.

NMR: ¹H NMR (CDCl₃, 500 MHz): δ 8.45 (d, *J* = 5.5 Hz, 2H), 7.98 (d, *J* = 2.5 Hz, 2H), 6.86 (dd, *J* = 5.5, 2.5 Hz, 2H), 4.30 (m, 4H), 3.90 (m, 4H), 3.72 (m, 4H), 3.57 (m, 4H), 3.38 (s, 6H). ¹³C NMR (CDCl₃, 100.71 MHz): δ 165.9, 157.9, 150.3, 111.6, 106.8, 72.1, 71.0, 69.5, 67.6, 59.2.

Synthesis of $[\text{Cr}(\text{L})_3]^{3+}$ Complexes



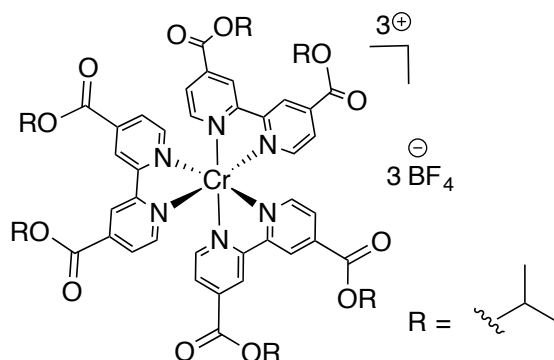
$[\text{Cr}(\text{L}2)_3]^{3+}$. This complex was synthesized from 4,4'-dimethyl-2,2'-bipyridine (0.50 g, 2.71 mmol) and **3** (0.32 g, 0.82 mmol) following **General Procedure 3**. The yellow solution was concentrated *in vacuo* and mixed with diethyl ether (200 mL), resulting in the precipitation of a yellow solid and a brown oil. The supernatant was decanted, and the remaining material was then dissolved in dichloromethane (10 mL) and precipitated with diethyl ether (200 mL). The bright yellow solid was collected by filtration, washed with diethyl ether (2×100 mL), and dried overnight *in vacuo* to afford **$[\text{Cr}(\text{L}2)_3]^{3+}$** as a bright yellow powder (0.44 g, 0.52 mmol, 63% yield).

IR (thin film, cm^{-1}): 1618, 1555, 1029, 836.

MP: 181 °C (Dec.)

HRMS: ESI⁺ (m/z): $[\text{M} - 3\text{BF}_4]^{3+}$ calcd. for $\text{C}_{36}\text{H}_{36}\text{N}_6\text{Cr}$: 201.4130; found: 201.4128.

Elemental Analysis: Analysis (calcd., found for $\text{C}_{36}\text{H}_{36}\text{N}_6\text{CrB}_3\text{F}_{12}(\text{CH}_2\text{Cl}_2)_{0.5}$): C (48.30, 48.52), H (4.11, 4.49), N (9.26, 9.39).



$[\text{Cr}(\text{L}4)_3]^{3+}$. This complex was synthesized from **L4** (0.90 g, 2.74 mmol) and **3** (0.32 g, 0.83 mmol) following **General Procedure 3**. The yellow solution was concentrated *in vacuo* and the resulting residue was recrystallized from $\text{CH}_3\text{CN}:\text{Et}_2\text{O}$ (v/v 1:10) to afford

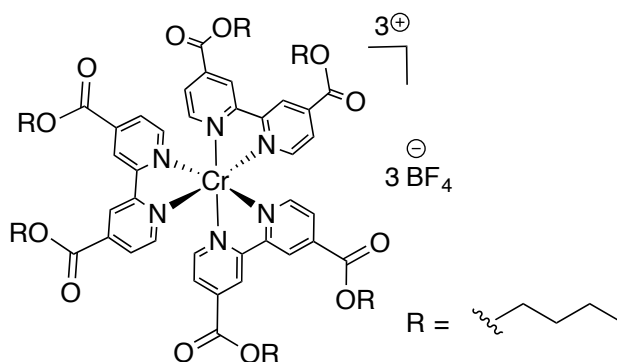
a mixture of a yellow powder and a brown oily residue. The supernatant was decanted, and the remaining material was dissolved in dichloromethane (10 mL) and precipitated with diethyl ether (100 mL). The resulting yellow powder was collected by filtration, dried overnight *in vacuo* to afford **[Cr(L4)₃]³⁺** as a bright yellow solid (0.68 g, 0.51 mmol, 61% yield).

IR (thin film, cm⁻¹): 1719, 1559, 1261, 1029, 763.

MP: 189 °C (Dec.)

HRMS: ESI⁺ (m/z): [M – 3BF₄]³⁺ calcd. for C₅₄H₆₀N₆O₁₂Cr: 345.4553; found: 345.4558.

Elemental Analysis: Analysis (calcd., found for C₅₄H₆₀N₆O₁₂CrB₃F₁₂(CH₂Cl₂)_{0.5}): C (48.85, 48.67), H (4.59, 4.98), N (6.27, 6.02).



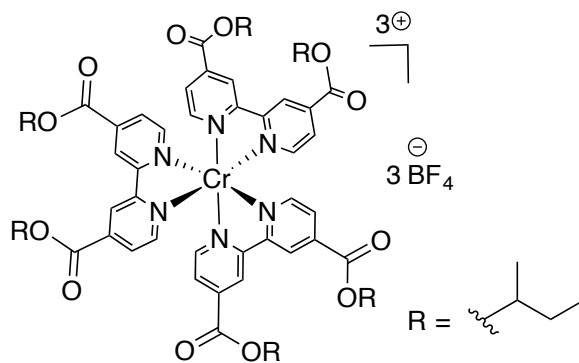
[Cr(L5)₃]³⁺. This complex was synthesized from **L5** (1.00 g, 2.81 mmol) and **3** (0.33 g, 0.85 mmol) following **General Procedure 3**. The yellow/green solution was concentrated *in vacuo*, and the residue was recrystallized from CH₃CN:Et₂O (v/v 1:10). The supernatant was decanted, and the resulting yellow solid was washed with diethyl ether (3 × 50 mL) and dried *in vacuo* overnight to afford **[Cr(L5)₃]³⁺** as a bright yellow solid (0.53 g, 0.38 mmol, 45% yield).

IR (thin film, cm⁻¹): 1726, 1407, 1233, 1029, 762.

MP: 167 °C (Dec.)

HRMS: ESI⁺ (m/z): [M – 3BF₄]³⁺ calcd. for C₆₀H₇₂N₆O₁₂Cr: 373.4866; found: 373.4870.

Elemental Analysis: Analysis (calcd., found for C₆₀H₇₂N₆O₁₂CrB₃F₁₂): C (52.16, 51.73), H (5.25, 5.24), N (6.08, 6.14).



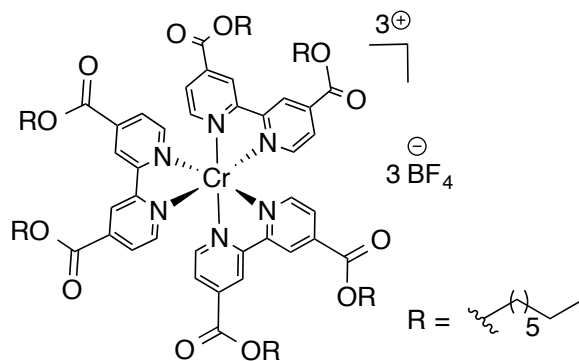
[Cr(L6)₃]³⁺. This complex was synthesized from **L6** (0.53 g, 1.49 mmol) and **3** (0.19 g, 0.48 mmol) following **General Procedure 3**. The yellow solution was concentrated to a minimal amount of solvent, and Et₂O (20 mL) was added to precipitate a yellow solid. The yellow solid was washed with Et₂O (3 x 30 mL), and recrystallized by vapor diffusion of diethyl ether into an acetonitrile solution of the Cr complex. The product was dried overnight *in vacuo* to afford **[Cr(L6)₃]³⁺** as a yellow powder (0.39 g, 0.28 mmol, 59% yield).

IR (thin film, cm⁻¹): 2975, 1717, 1559, 1407, 1259, 1234, 1033, 864, 763, 716.

MP: 165 °C (Dec.)

HRMS: ESI⁺ (m/z): [M – 3BF₄]³⁺ calcd. for C₆₀H₇₂N₆O₁₂Cr: 373.4866; found: 373.4878.

Elemental Analysis: Analysis (calcd., found for C₆₀H₇₂N₆O₁₂CrB₃F₁₂): C (52.16, 51.96), H (5.25, 5.27), N (6.08, 5.85).



[Cr(L7)₃]³⁺. This complex was synthesized from **L7** (0.53 g, 1.20 mmol) and **3** (0.15 g, 0.39 mmol) following **General Procedure 3**. The yellow solution was concentrated *in vacuo* to a sticky yellow solid. The solid was diluted in dichloromethane (10 mL), and the product was precipitated with diethyl ether. The supernatant was decanted, and the remaining yellow solid was washed with a small amount of diethyl ether. The product

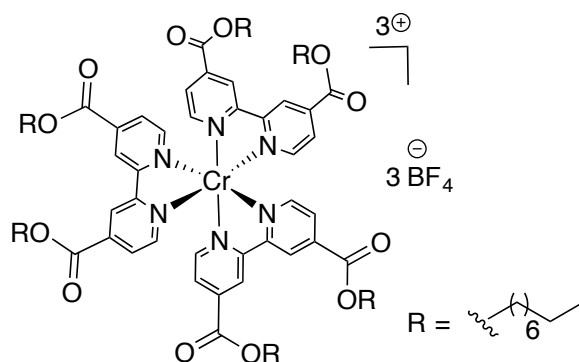
was dried overnight *in vacuo* to afford $[\text{Cr}(\text{L7})_3]^{3+}$ as a yellow solid (0.38 g, 0.23 mmol, 60% yield).

IR (thin film, cm^{-1}): 2926, 2361, 1732, 1559, 1407, 1258, 1234, 1034, 763, 708.

MP: 150-152 °C

HRMS: ESI⁺ (m/z): $[\text{M} - 3\text{BF}_4]^{3+}$ calcd. for $\text{C}_{78}\text{H}_{108}\text{N}_6\text{O}_{12}\text{Cr}$: 457.5805; found: 457.5816.

Elemental Analysis: Analysis (calcd., found for $\text{C}_{78}\text{H}_{108}\text{N}_6\text{O}_{12}\text{CrB}_3\text{F}_{12}(\text{CH}_2\text{Cl}_2)_{0.5}$): C (56.24, 56.57), H (6.55, 6.51), N (5.01, 4.95).



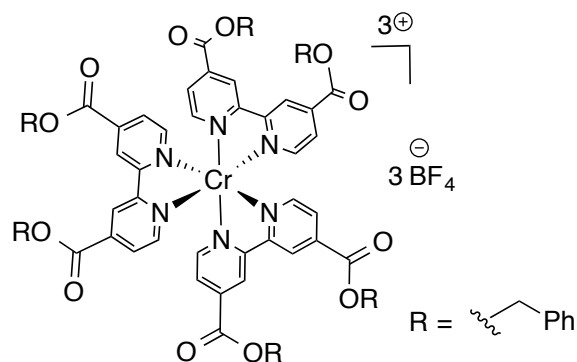
$[\text{Cr}(\text{L8})_3]^{3+}$. This complex was synthesized from **L8** (1.27 g, 2.71 mmol) and **3** (0.32 g, 0.82 mmol) following **General Procedure 3**. The yellow solution was concentrated *in vacuo* to afford a sticky orange solid. This residue was diluted with dichloromethane (10 mL), and the product was precipitated with diethyl ether (50 mL) to give a yellow solid, which was collected by filtration. The solid was washed with diethyl ether (3 × 50 mL) and dried overnight *in vacuo* to afford $[\text{Cr}(\text{L8})_3]^{3+}$ as a dark yellow powder (0.77 g, 0.44 mmol, 65% yield).

IR (thin film, cm^{-1}): 2924, 2855, 1731, 1560, 1257, 1036, 764.

MP: 135 °C (Dec.)

HRMS: ESI⁺ (m/z): $[\text{M} - 3\text{BF}_4]^{3+}$ calcd. for $\text{C}_{84}\text{H}_{120}\text{N}_6\text{O}_{12}\text{Cr}$: 485.6118; found: 485.6111.

Elemental Analysis: Analysis (calcd., found for $\text{C}_{84}\text{H}_{120}\text{N}_6\text{O}_{12}\text{CrB}_3\text{F}_{12}(\text{CH}_2\text{Cl}_2)_{0.75}$): C (57.12, 57.11), H (6.87, 7.10), N (4.72, 4.72).



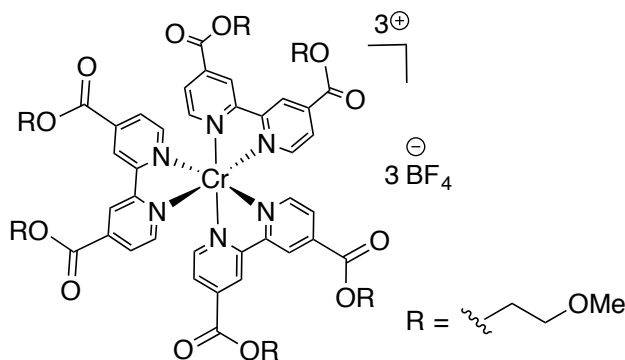
[Cr(L9)₃]³⁺. This complex was synthesized from **L9** (0.75 g, 1.77 mmol) and **3** (0.27g, 0.54 mol) following **General Procedure 3**. The orange solution was concentrated *in vacuo*, and the resulting residue was recrystallized by vapor diffusion of diethyl ether into an acetonitrile solution of the Cr complex. The resulting solid was collected by filtration and washed with diethyl ether (3 x 20 mL) and dried *in vacuo* overnight to afford **[Cr(L9)₃]³⁺** as a yellow solid (0.68 g, 0.43 mmol, 79% yield).

IR (thin film, cm⁻¹): 3094, 1731, 1624, 1410, 1258, 1234, 1053, 1036, 760.

MP: 260 °C (Dec.)

HRMS: ESI⁺ (m/z): [M – 3BF₄]³⁺ calcd. for C₇₈H₆₀CrN₆O₁₂: 441.4553; found: 441.4569.

Elemental Analysis: Analysis (calcd., found for C₇₈H₆₀B₃CrF₁₂N₆O₁₂): C (59.08, 58.94), H (3.81, 3.94), N (5.30, 5.39).



[Cr(L10)₃]³⁺. This complex was synthesized from **L10** (0.50 g, 1.386 mmol) and **3** (0.16 g, 0.42 mmol) following **General Procedure 3**. The yellow solution was concentrated to a minimal amount of solvent, and the diethyl ether (200 mL) was added, resulting in the precipitation of a yellow solid and a brown oil. The supernatant was decanted, the remaining material was dissolved in a small amount of dichloromethane (10 mL) and precipitated with diethyl ether (200 mL). The yellow solid was collected by filtration,

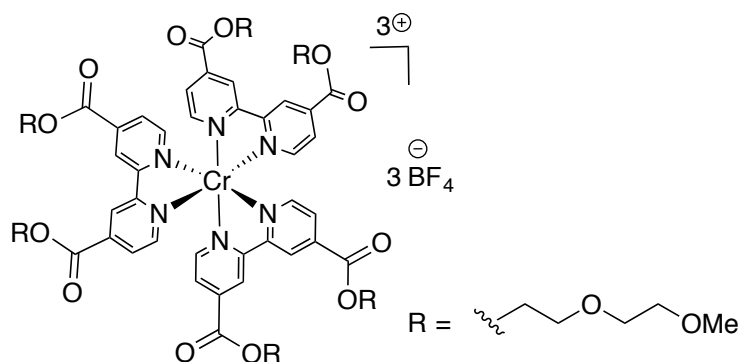
washed with diethyl ether (2 × 100 mL), and dried overnight *in vacuo* to afford **[Cr(L10)₃]³⁺** as a bright yellow powder (0.60 g, 0.41 mmol, 97% yield).

IR (thin film, cm⁻¹): 1734, 1559, 1261, 1024, 764.

MP: 127 °C (Dec.)

HRMS: ESI⁺ (m/z): [M – 3BF₄]³⁺ calcd. for C₅₄H₆₀N₆O₁₈Cr: 377.4451; found: 377.4451.

Elemental Analysis: Analysis (calcd., found for C₅₄H₆₀N₆O₁₈CrB₃F₁₂(CH₂Cl₂)): C (44.68, 44.34), H (4.23, 4.17), N (5.68, 5.65).



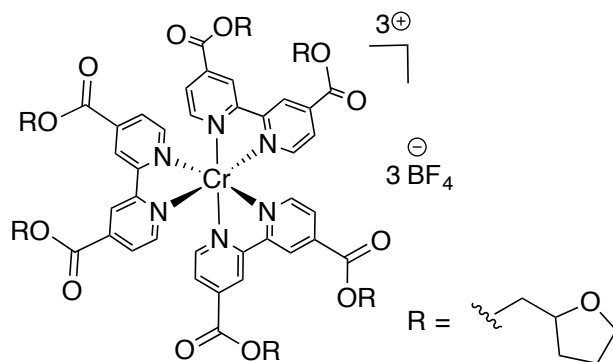
[Cr(L11)₃]³⁺. This complex was synthesized from **L11** (0.67 g, 1.49 mmol) and **3** (0.18 g, 0.45 mmol) following **General Procedure 3**. The yellow solution was concentrated, and the resulting residue was dissolved in acetonitrile (5 mL) and layered with diethyl ether (15 mL), which resulted in separation of a dark yellow oil. The oil was diluted with dichloromethane (10 mL) and diethyl ether (100 mL) was added to precipitate a yellow residue. The residue was washed with diethyl ether (4 × 100 mL) to furnish a dark yellow powder. This powder was dried *in vacuo* overnight to afford **[Cr(L11)₃]³⁺** as a dark yellow solid (0.39 g, 0.22 mmol, 50% yield).

IR (thin film, cm⁻¹): 1730, 1562, 1258, 1030, 762.

MP: 50-51 °C.

HRMS: ESI⁺ (m/z): [M – 3BF₄]³⁺ calcd. for C₆₆H₈₄N₆O₂₄Cr: 465.4975; found: 465.4982.

Elemental Analysis: Analysis (calcd., found for C₆₆H₈₄N₆O₂₄CrB₃F₁₂(CH₂Cl₂)): C (46.18, 46.19), H (4.97, 5.14), N (4.82, 5.09).



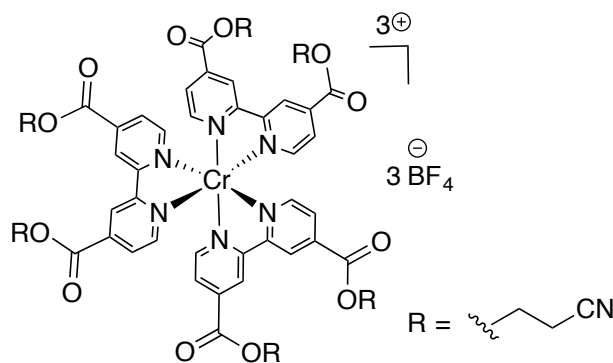
[Cr(L12)₃]³⁺. This complex was synthesized from **L12** (1.10 g, 2.67 mmol) and **3** (0.32 g, 0.81 mmol) following **General Procedure 3**. The yellow solution was concentrated *in vacuo*. The residue was dissolved in acetonitrile (5 mL), and this solution was layered with diethyl ether (15 mL), which resulted in the separation of a dark yellow oil. The oil was diluted with dichloromethane (10 mL), and diethyl ether (100 mL) was added to precipitate the product. The residue was washed with diethyl ether (2 × 100 mL) to furnish a yellow powder. This powder was collected by filtration and dried *in vacuo* overnight to afford **[Cr(L12)₃]³⁺** as a yellow solid (1.32 g, 0.81 mmol, quantitative yield).

IR (thin film, cm⁻¹): 1729, 1563, 1254, 1030, 762.

MP: 102 °C (Dec.)

HRMS: ESI⁺ (m/z): [M – 3BF₄]³⁺ calcd. for C₆₆H₇₂N₆O₁₈Cr: 429.4764; found: 429.4763.

Elemental Analysis: Analysis (calcd., found for C₆₆H₇₂N₆O₁₈CrB₃F₁₂(CH₂Cl₂)): C (49.23, 49.55), H (4.56, 4.77), N (5.14, 5.12).



[Cr(L13)₃]³⁺. This complex was synthesized from **L13** (0.71 g, 2.01 mmol) and **3** (0.24 g, 0.61 mmol) following **General Procedure 3**. The yellow/green solution was concentrated, and the residue was recrystallized by vapor diffusion of diethyl ether into an acetonitrile solution of the Cr complex. The solid was washed twice with CH₂Cl₂:Et₂O

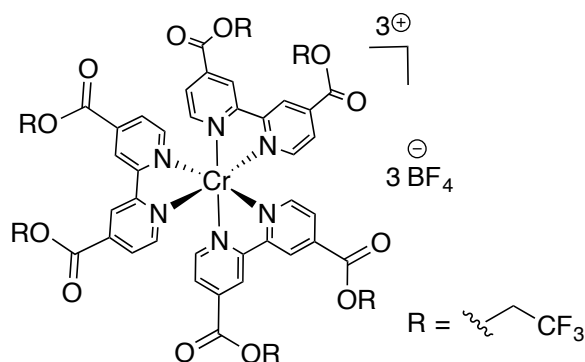
(v/v 1:3). The product was then dried overnight *in vacuo* to afford $[\text{Cr}(\text{L13})_3]^{3+}$ as a dark orange powder (0.75 g, 0.53 mmol, 88% yield).

IR (thin film, cm^{-1}): 1732, 1563, 1029, 762.

MP: 83 °C (Dec.)

HRMS: ESI⁺ (m/z): $[\text{M} - 3\text{BF}_4]^{3+}$ calcd for $\text{C}_{54}\text{H}_{42}\text{N}_{12}\text{O}_{12}\text{Cr}$: 367.4145; found: 367.4134

Elemental Analysis: Analysis (calcd., found for $\text{C}_{54}\text{H}_{42}\text{N}_{12}\text{O}_{12}\text{CrB}_3\text{F}_{12}(\text{CH}_2\text{Cl}_2)_{0.5}$): C (46.56, 46.79), H (3.08, 3.21), N(11.96, 11.93).



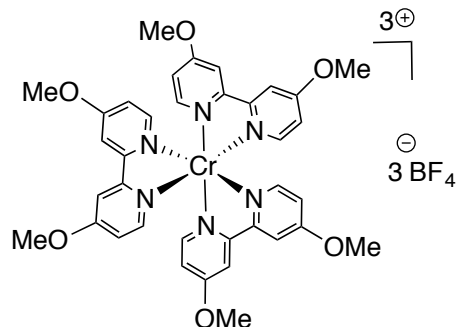
$[\text{Cr}(\text{L14})_3]^{3+}$. This complex was synthesized from **L14** (0.77 g, 1.88 mmol) and **3** (0.22 g, 0.57 mmol) following **General Procedure 3**. The yellow solution was concentrated *in vacuo*, and the residue was purified by sequential crystallizations from dichloromethane (5 mL) and diethyl ether (15 mL). The resulting yellow powder was dried overnight *in vacuo* to afford $[\text{Cr}(\text{L14})_3]^{3+}$ as a bright yellow powder (0.85 g, 0.52 mmol, 92% yield).

IR (thin film, cm^{-1}): 1750, 1410, 1163, 1034, 760.

MP: 91 °C (Dec.)

HRMS: ESI⁺ (m/z): $[\text{M} - 3\text{BF}_4]^{3+}$ calcd. for $\text{C}_{48}\text{H}_{30}\text{N}_6\text{O}_{12}\text{CrF}_{18}$: 425.3674; found: 425.3672.

Elemental Analysis: Analysis (calcd., found for $\text{C}_{48}\text{H}_{30}\text{N}_6\text{O}_{12}\text{CrB}_3\text{F}_{30}(\text{CH}_2\text{Cl}_2)$): C (36.28, 36.15), H (1.99, 2.11), N (5.18, 5.26).



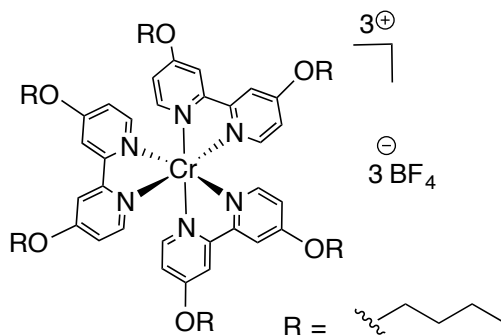
[Cr(L15)₃]³⁺. This complex was synthesized from 4,4'-dimethoxy-2,2'-bipyridine (0.55 g, 2.54 mmol) and **3** (0.30 g, 0.77 mmol) following **General Procedure 3**. The orange solution was concentrated, and the crude mixture was recrystallized from CH₃CN:Et₂O (v/v 1:5). The resulting yellow solid was then washed with diethyl ether (2 × 50 mL) and dried *in vacuo* overnight to afford **[Cr(L15)₃]³⁺** as a bright yellow powder (0.56 g, 0.58 mmol, 76% yield).

IR (thin film, cm⁻¹): 1609, 1498, 1023, 836.

MP: 151°C (Dec.)

HRMS: ESI⁺ (m/z): [M – 3BF₄]³⁺ calcd. for C₃₆H₃₆N₆O₆Cr: 233.4028; found: 233.4026.

Elemental Analysis: Analysis (calcd., found for C₃₆H₃₆N₆O₆CrB₃F₁₂): C (44.99, 44.84), H (3.78, 4.08), N (8.74, 8.46).



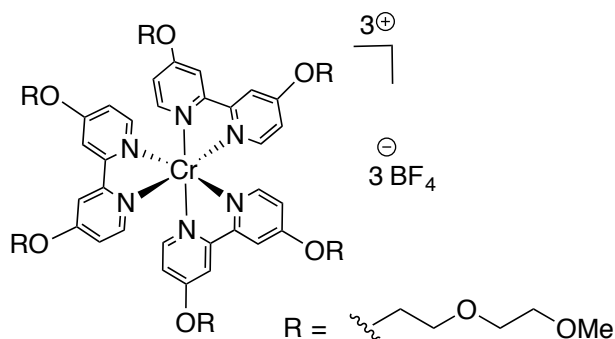
[Cr(L16)₃]³⁺. This complex was synthesized from **L16** (1.00 g, 3.33 mmol) and **3** (0.39 g, 1.01 mmol) following **General Procedure 3**. The yellow solution was concentrated *in vacuo*, and the residue was recrystallized by vapor diffusion of diethyl ether into an acetonitrile solution of the Cr complex. This crystalline product was dried overnight *in vacuo* to afford **[Cr(L16)₃]³⁺** as orange crystals suitable for analysis via single crystal X-ray diffraction (0.83 g, 0.68 mmol, 68% yield)

IR (thin film, cm⁻¹): 2959, 1608, 1448, 1022, 842.

MP: 194-195 °C

HRMS: ESI⁺ (m/z): [M – 3BF₄]³⁺ calcd. for C₅₄H₇₂N₆O₆Cr: 317.4967; found: 317.4971.

Elemental Analysis: Analysis (calcd., found for C₅₄H₇₂N₆O₆CrB₃F₁₂): C (53.44, 53.19), H (5.98, 5.93), N (6.92, 6.97).



[Cr(L17)₃]³⁺. This complex was synthesized from **L17** (0.34 g, 0.858 mmol) and **3** (0.10 g, 0.26 mmol) following **General Procedure 3**. The orange solution was concentrated to minimal amount of solvent (~5 mL), and the addition of diethyl ether (200 mL) resulted in the formation of a pale orange precipitate. This solid was washed with diethyl ether (3 x 100 mL) and dried *in vacuo* overnight to afford **[Cr(L17)₃]³⁺** as a pale orange solid (0.24 g, 0.16 mmol, 62% yield).

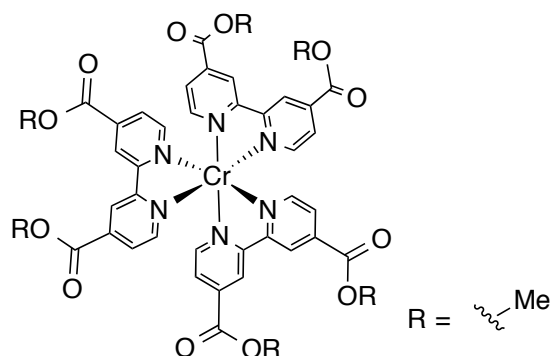
IR (thin film, cm⁻¹): 2883, 1609, 1554, 1443, 1235, 1020, 843.

MP: 49 °C (Dec.)

HRMS: ESI⁺ (m/z): [M – 3BF₄]³⁺ calcd. for C₆₀H₈₄N₆O₁₈Cr: 409.5077; found: 409.5078.

Elemental Analysis: Analysis (calcd., found for C₆₀H₈₄N₆O₁₈CrB₃F₁₂): C (48.37, 48.16), H (5.68, 5.73), N (5.64, 5.61).

Synthesis of Cr⁰-Complexes



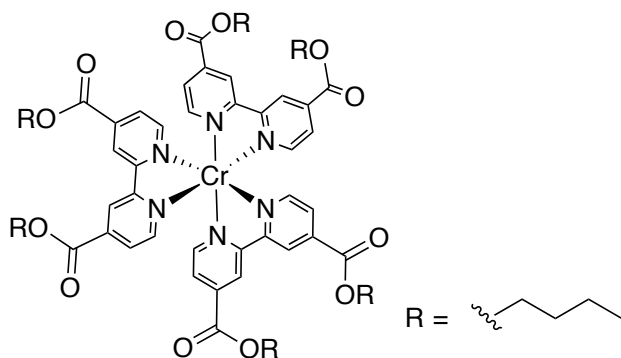
[Cr(L3)₃]⁰. This complex was synthesized from **L3** (0.50 g, 1.84 mmol) following the **General Procedure 4** to afford **[Cr(L3)₃]⁰** as a dark purple solid (0.52 g, 0.60 mmol, 98% yield).

IR (KBr pellet, ν , cm⁻¹): 2949, 1714, 1559, 1444, 1209, 946, 757, 543.

MP: 159 °C (Dec.)

HRMS: ESI⁺ (m/z): [M]⁺ calcd. for C₄₂H₃₆N₆O₁₂Cr: 868.1791; found: 868.1812.

Elemental Analysis: Analysis (calcd., found for C₄₂H₃₆N₆O₁₂Cr(C₉H₁₂)_{0.25}): C (59.13, 58.98), H (4.37, 4.58), N (9.35, 9.19).



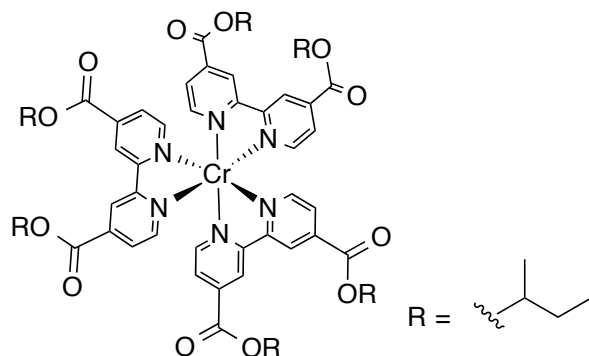
[Cr(L5)₃]⁰. This complex was synthesized from **L5** (2.00 g, 5.61 mmol) following **General Procedure 4**. The purple solid was washed with dry pentane (60 mL), the supernatant was decanted by cannula filtration, and the residue was dried overnight to afford **[Cr(L5)₃]⁰** as a dark purple solid (1.5 g, 1.33 mmol, 72% yield).

IR (KBr pellet, ν , cm⁻¹): 2958, 1709, 1558, 1271, 1110, 939, 755.

MP: 153-155 °C

HRMS: ESI⁺ (m/z): [M]⁺ calcd. for C₆₀H₇₂N₆O₁₂Cr: 1120.4608; found: 1120.4572.

Elemental Analysis: Analysis (calcd., found for $C_{60}H_{72}N_6O_{12}Cr$): C (64.27, 63.99), H (6.47, 6.27), N (7.50, 7.44).

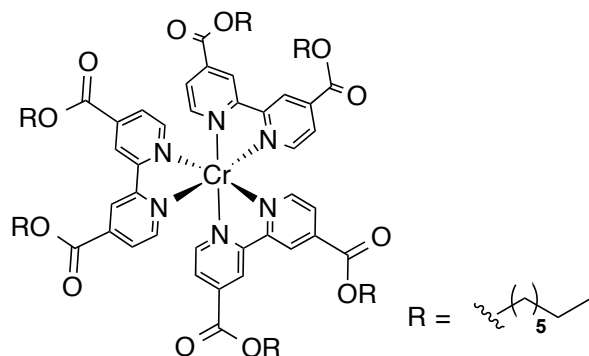


$[Cr(L6)_3]^0$. This complex was synthesized from **L6** (0.40 g, 1.11 mmol) following **General Procedure 4**. The purple solid was washed with dry acetonitrile (10 mL) and then dried *in vacuo* overnight to afford $[Cr(L6)_3]^0$ as a purple solid (0.18 g, 0.16 mmol, 42% yield).

IR (KBr pellet, ν , cm^{-1}): 2971, 2934, 1697, 1554, 1459, 1270, 1204, 1091, 940, 755.

MP: 115-117 °C (Dec.)

Elemental Analysis: Analysis (calcd., found for $C_{60}H_{72}CrN_6O_{12}$): C (64.27, 64.31), H (6.47, 6.57), N (7.50, 7.46).



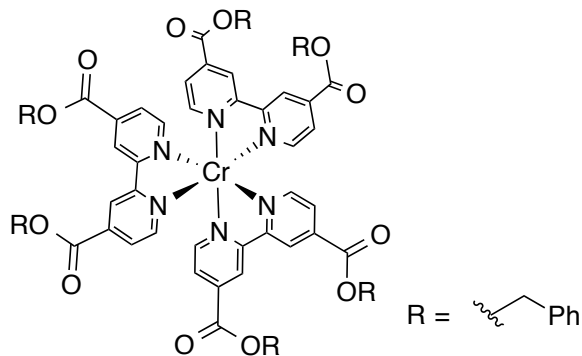
$[Cr(L7)_3]^0$. This complex was synthesized from **L7** (0.15 g, 0.34 mmol) following **General Procedure 4** to afford $[Cr(L7)_3]^0$ as a light purple solid (0.153 g, 0.33 mmol, 98% yield).

IR (KBr pellet, ν , cm^{-1}): 2956, 2929, 2856, 1727, 1594, 1395, 1254, 981, 763, 692.

MP: 55-57 °C

HRMS: ESI⁺ (m/z): $[M]^+$ calcd. for $C_{78}H_{108}CrN_6O_{12}$: 1372.7425; found: 1372.7385.

Elemental Analysis: Analysis (calcd., found for $C_{78}H_{108}CrN_6O_{12}$): C (68.20, 68.11), H (7.92, 7.81), N (6.12, 6.16).

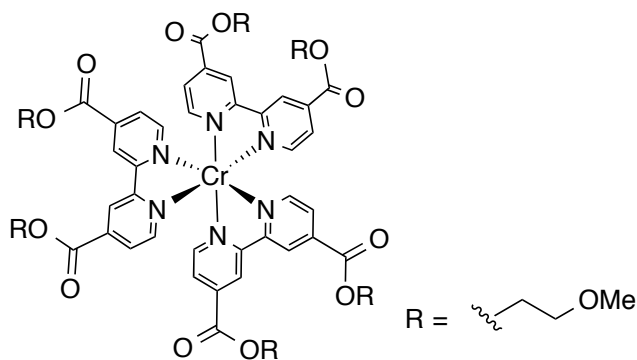


$[Cr(L9)_3]^0$. This complex was synthesized from **L9** (1 g, 2.36 mmol) following **General Procedure 4** to afford $[Cr(L9)_3]^0$ as a purple solid (0.92 g, 0.7 mmol, 88% yield).

IR (KBr pellet, ν , cm^{-1}): 3031, 1723, 1648, 1559, 1261, 1244, 1133, 949, 761, 697.

MP: 228 °C (dec.)

Elemental Analysis: Analysis (calcd., found for $C_{78}H_{60}CrN_6O_{12}$): C (70.69, 70.28), H (4.56, 4.75), N (6.34, 6.33).



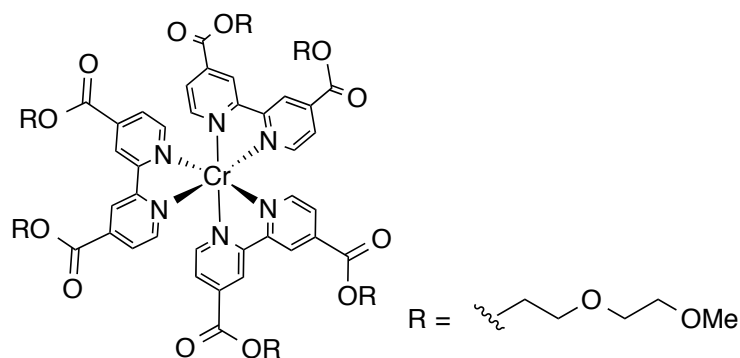
$[Cr(L10)_3]^0$. This complex was synthesized from **L10** (0.8 g, 2.22 mmol) following **General Procedure 4** to afford $[Cr(L10)_3]^0$ as a dark purple solid (0.83 g, 0.74 mmol, quantitative yield).

IR (KBr pellet, ν , cm^{-1}): 2921, 2824, 1711, 1558, 1374, 1321, 1203, 1119, 943, 764.

MP: 75-77 °C

HRMS: ESI⁺ (m/z): $[M]^+$ calcd. for $C_{54}H_{60}N_6O_{18}Cr$: 1132.3364; found: 1132.3402.

Elemental Analysis: Analysis (calcd., found for $C_{54}H_{60}N_6O_{18}Cr$): C (57.24, 57.28), H (5.34, 5.12), N (7.42, 7.37).



[Cr(L11)₃]⁰. This complex was synthesized from **L11** (1 g, 2.23 mmol) following **General Procedure 4** to afford **[Cr(L11)₃]⁰** as a dark purple solid (1.03 g, 0.74 mmol, quantitative yield).

IR (KBr pellet, cm⁻¹): 2890, 1709, 1557, 1202, 1112, 972, 853, 761, 692.

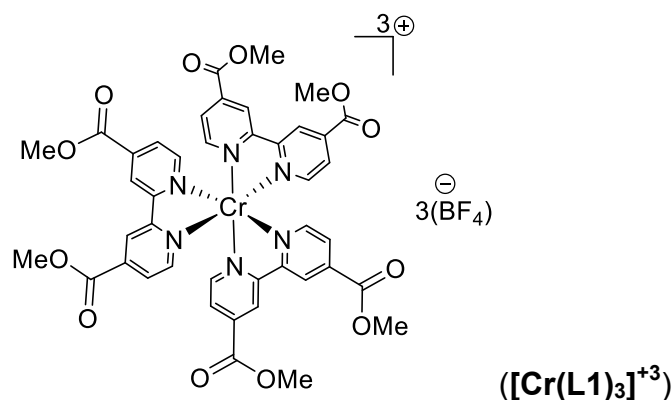
MP: 68-70 °C

HRMS: ESI⁺ (m/z): [M]⁺ calcd. for C₆₆H₈₄N₆O₂₄Cr: 1396.4937; found: 1396.4871.

Elemental Analysis: Analysis (calcd., found for C₆₆H₈₄N₆O₂₄Cr(C₉H₁₂)_{0.25}): C (57.43, 57.54), H (6.14, 6.00), N (5.89, 6.00).

Solubility Studies of Metal Complexes

Representative example of solubility studies (using General Procedure 4)



Serial dilutions were prepared in triplicate according to the formula $C_1V_1 = C_2V_2$ using calibrated volumetric glassware.

Table 2.4. Standard serial solutions of complex **[Cr(L1)₃]⁺³** on acetonitrile.

Concentration (mM)	Vol. of CH ₃ CN (mL)	Mass/Vol. needed
2.0	10	23.43 mg of [Cr(L1)₃]⁺³
1.5	5	3.75 mL of 2.0 mM stock solution
1.0	5	2.50 mL of 2.0 mM stock solution
0.5	5	2.50 mL of 1.0 mM standard solution

The quantitative analysis was carried on a Shimadzu UV-1601 spectrophotometer. The spectrum mode was used to obtain the UV-Vis absorbance spectrum of a 2.0 mM stock solution of $[\text{Cr}(\text{L1})_3]^{+3}$ over a continuous range (300-1100 nm). This analysis was used to determine a suitable wavelength for absorbance measurements: $\lambda_{\text{max}} = 420 \text{ nm}$.

Two rectangular spectrophotometer cells (Starna Cells, pathlength: 0.5 and 1.0 cm) were employed for the analysis.

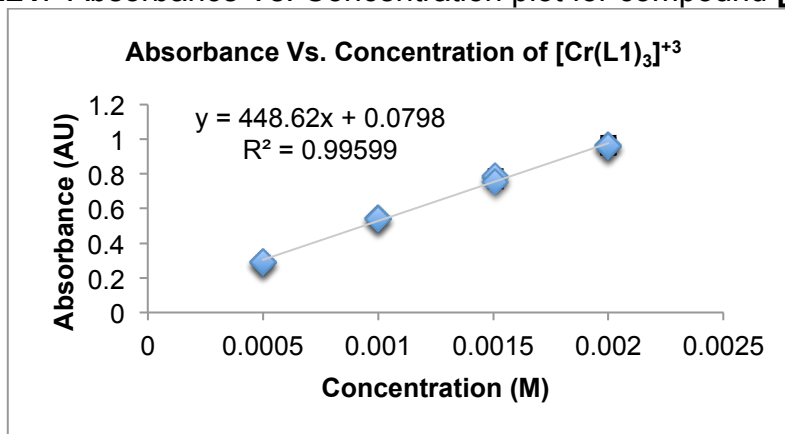
Once the suitable wavelength was chosen, the standard solution absorbances were determined by photometric mode, measuring the absorbances at the predetermined wavelength (in this case $\lambda = 420 \text{ nm}$). Measurements were performed starting from the most dilute solutions through to the most concentrated.

Table 2.5. Photometric measurements of stock solutions of $[\text{Cr}(\text{L1})_3]^{+3}$ at $\lambda = 420 \text{ nm}$.

Exp. No.	Concentration of Stock Solution (mM)	Absorbance
1	0.5	0.289
2	0.5	0.293
3	0.5	0.290
4	1.0	0.541
5	1.0	0.546
6	1.0	0.537
7	1.5	0.775
8	1.5	0.788
9	1.5	0.753
10	2.0	0.958
11	2.0	0.969
12	2.0	0.961

The acquired data was plotted such that absorbance vs. concentration is used to obtain a calibration curve equation for the indicated metal complex $[\text{Cr}(\text{L1})_3]^{+3}$ (Figure 2.21).

Figure 2.21. Absorbance Vs. Concentration plot for compound $[\text{Cr}(\text{L1})_3]^{+3}$.



The plot afforded a Beer-Lambert equation for compound $[\text{Cr}(\text{L1})_3]^{+3}$,

$$Y = 448.62X + 0.0789 \quad (\text{Eq. 2.2})$$

Then, saturated solutions were prepared by portion-wise addition of the desired compound to 300 μL of acetonitrile, with stirring, until a persistent suspension resulted. The solution was then filtered through cotton wool to remove any insoluble material and three aliquots, of 60 μL each, were individually diluted in 5 mL of acetonitrile to afford absorbances within the range of the calibration curve (0.289-0.961 AU) at the predetermined wavelength ($\lambda = 420 \text{ nm}$). The concentration of the diluted solution (X), which was prepared from the saturated solution aliquot, was determined by back-calculation using the measured absorbance (Y) and Eq. 2.2.

Lastly, the concentration of the dilute solutions was converted to the maximum solubility of the saturated solution in acetonitrile (Table 2.6). The average and the standard deviation of the runs were calculated to give the maximum solubility of $[\text{Cr}(\text{L1})_3]^{+3}$ as **0.1331 \pm 0.0004 M**.

Table 2.6. Maximum solubility of complex **3** in acetonitrile.

Experiment run	Absorbance (Y from Eq. 1)	Concentration of aliquot (X from Eq. 1)	Maximum solubility of $[\text{Cr}(\text{L1})_3]^{+3}$ in CH_3CN (mM)
Saturated solution 1	0.792	1.601 mM	133.5
Saturated solution 2	0.790	1.597 mM	133.1
Saturated solution 3	0.788	1.592 mM	132.7

Solubility of Metal Complexes

The following solubilities of the metal complexes on acetonitrile were determined using General Procedure 5. Any deviations from this procedure are disclosed in each individual case.

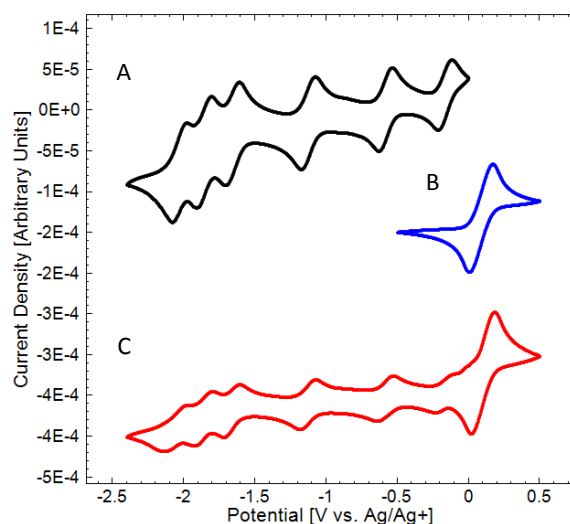
Table 2.7. Solubility parameters and solubilities of metal complexes in acetonitrile.

Complex	λ_{\max} (nm)	Standard Dilutions (mM)	Saturated Solution Dilution	Max. solubility in MeCN (M)
[Cr(L1) ₃] ³⁺	403	2.0, 1.5, 1.0, 0.5	30.0 μ L to 5 mL	0.307 \pm 0.001
[Cr(L2) ₃] ³⁺	418	2.0, 1.5, 1.0, 0.5	10.0 μ L to 5 mL	0.553 \pm 0.001
[Cr(L3) ₃] ³⁺	420	2.0, 1.5, 1.0, 0.5	60.0 μ L to 5 mL	0.1330 \pm 0.0004
[Cr(L4) ₃] ³⁺	419	2.0, 1.5, 1.0, 0.5	20.0 μ L to 5 mL	0.341 \pm 0.001
[Cr(L5) ₃] ³⁺	420	2.0, 1.5, 1.0, 0.5	10.0 μ L to 5 mL	0.71 \pm 0.09
[Cr(L6) ₃] ³⁺	419	1.5, 1.0, 0.5	10.0 μ L to 5 mL	0.60 \pm 0.01
[Cr(L7) ₃] ³⁺	418	2.0, 1.5, 1.0, 0.5	15.0 μ L to 5 mL	0.39 \pm 0.01
[Cr(L8) ₃] ³⁺	417	2.0, 1.5, 1.0, 0.5	10.0 μ L to 5 mL	0.394 \pm 0.003
[Cr(L9) ₃] ³⁺	419	2.0, 1.5, 1.0, 0.5	40 μ L to 2 mL	0.0469 \pm 0.0006
[Cr(L10) ₃] ³⁺	420	2.0, 1.5, 1.0, 0.5	10.0 μ L to 5 mL	0.62 \pm 0.02
[Cr(L11) ₃] ³⁺	420	2.0, 1.5, 1.0, 0.5	5.0 μ L to 2 mL	0.539 \pm 0.003
[Cr(L12) ₃] ³⁺	421	2.0, 1.5, 1.0, 0.5	10.0 μ L to 5 mL	0.56 \pm 0.02
[Cr(L13) ₃] ³⁺	421	2.0, 1.5, 1.0, 0.5	10.0 μ L to 5 mL	0.58 \pm 0.02
[Cr(L14) ₃] ³⁺	418	1.5, 1.0, 0.5, 0.25	10.0 μ L to 5 mL then 2.0 mL to 5 mL	0.611 \pm 0.006
[Cr(L15) ₃] ³⁺	462	1.5, 1.0, 0.5, 0.25	10.0 μ L to 10 mL	0.61 \pm 0.02
[Cr(L16) ₃] ³⁺	464	10.0, 7.5, 5.0, 2.5	50.0 μ L to 2 mL, then 0.5 mL to 1 mL	0.577 \pm 0.001
[Cr(L17) ₃] ³⁺	462	10.0, 5.0, 2.5, 7.5	30.0 μ L to 2 mL	0.289 \pm 0.004
[Cr(L3) ₃] ⁰	562	0.2, 0.15, 0.1, 0.05	200.0 μ L to 1 mL	4.8 \times 10 ⁻⁴ \pm 1.3 \times 10 ⁻⁵
[Cr(L5) ₃] ⁰	556	0.15, 0.1, 0.05, 0.025	30.0 μ L to 2 mL	0.0039 \pm 2.5 \times 10 ⁻⁵
[Cr(L6) ₃] ⁰	557	See General Procedure 6a		8.9 \times 10 ⁻⁵ \pm 5.0 \times 10 ⁻⁵
[Cr(L7) ₃] ⁰	562	See General Procedure 6a		1.8 \times 10 ⁻⁵ \pm 1.0 \times 10 ⁻⁵
[Cr(L9) ₃] ⁰	Solubility determined by the lower detection limit of Implen Nanodrop UV-vis (2 ng/ μ L)			1.5 \times 10 ⁻⁶
[Cr(L10) ₃] ⁰	561	0.2, 0.15, 0.1, 0.05	30.0 μ L to 2 mL	0.010 \pm 4.2 \times 10 ⁻⁶
[Cr(L11) ₃] ⁰	566	0.2, 0.15, 0.1, 0.05	5.0 μ L to 10 mL	0.21 \pm 1.4 \times 10 ⁻³

Cyclic Voltammograms of Cr Complexes

Cyclic voltammogram of $[\text{Cr}(\text{L12})_3]^{3+}$ with added ferrocene as an internal and external reference.

Figure 2.22. A) Black cyclic voltammogram of a 5 mM solution of $[\text{Cr}(\text{L12})_3]^{3+}$. B) Blue cyclic voltammogram of a 10 mM solution of ferrocene. C) Red cyclic voltammogram is from a mixture of $[\text{Cr}(\text{L12})_3]^{3+}$ (5 mM) and ferrocene (10 mM). CVs in 0.1 M TBABF₄ in acetonitrile. Reference is Ag/Ag⁺ with AgBF₄ (0.01M); Working electrode is glassy carbon disk; Counter electrode is platinum wire; CV conducted at 23 °C at a scan rate of 100 mV s⁻¹.



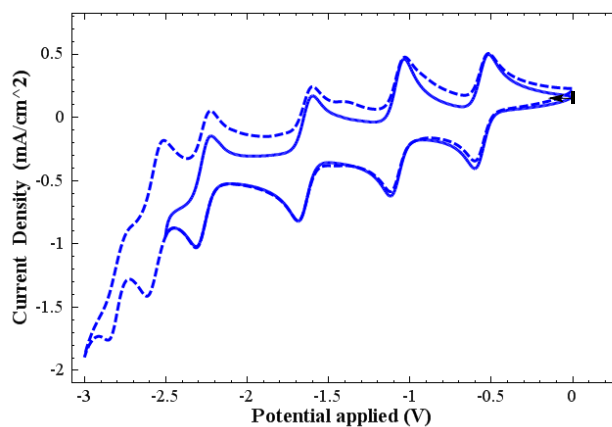
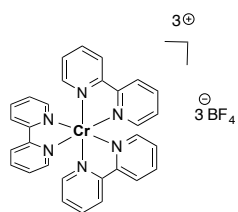
$E_{1/2}$ ferrocene = 0.09 V vs. Ag/Ag⁺ with AgBF₄ (0.01 M) in acetonitrile.

Corrected values for the half wave potential of $[\text{Cr}(\text{L12})_3]^{3+}$ versus Fc/Fc⁺:

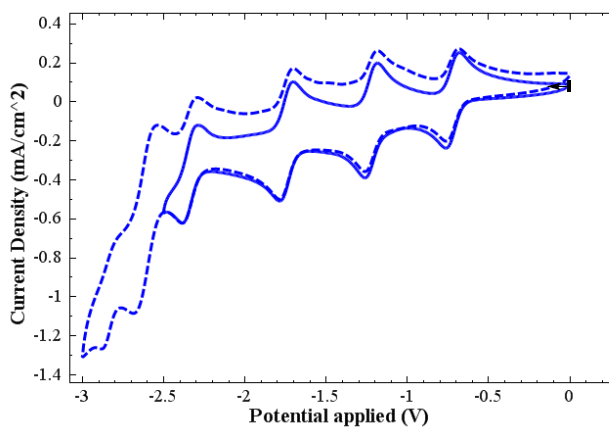
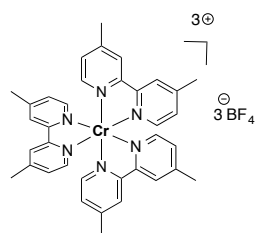
		1 st	2 nd	3 rd	4 th	5 th	6 th
$[\text{Cr}(\text{L12})_3]^{3+}$	$E_{1/2}$ (V)	-0.3	-0.61	-1.15	-1.68	-1.87	-2.04

Note: In the following CVs bar indicates the starting potential and arrow indicates sweeping direction. The cyclic voltammograms correspond to one full scan of the complex (between the 2nd and 10th scan) in the shown potential window. All potential scans beyond the first scan overlay well.

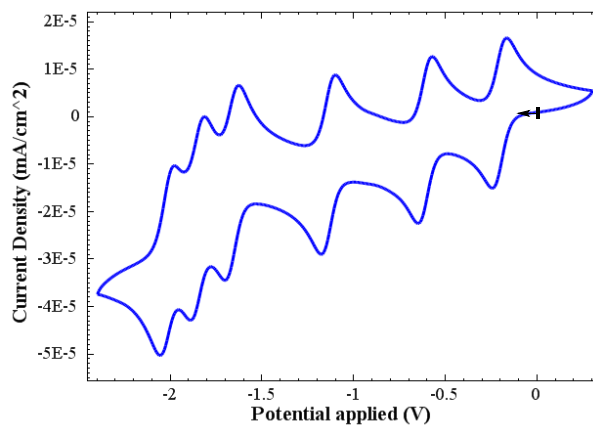
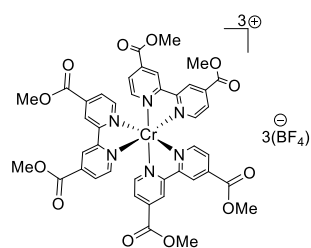
Cyclic voltammogram of $[\text{Cr}(\text{L1})_3]^{3+}$



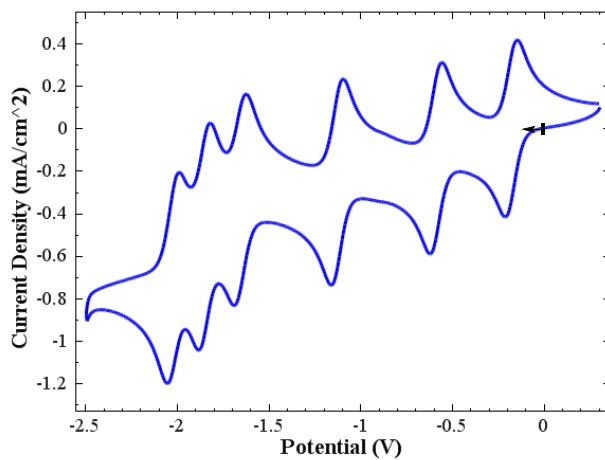
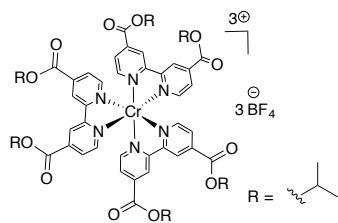
Cyclic voltammogram of $[\text{Cr}(\text{L2})_3]^{3+}$



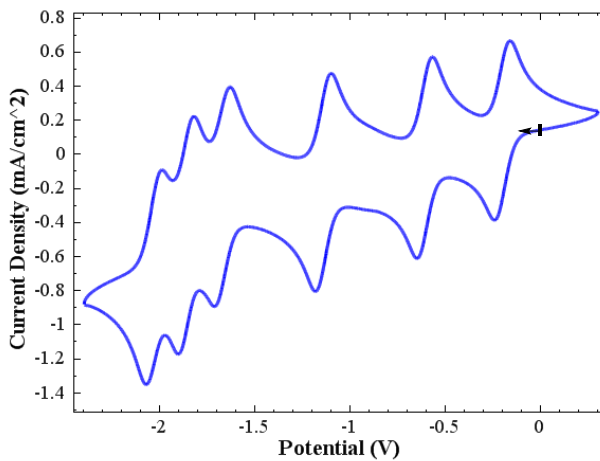
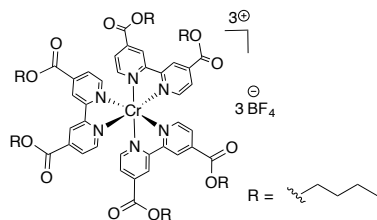
Cyclic voltammogram of $[\text{Cr}(\text{L3})_3]^{3+}$



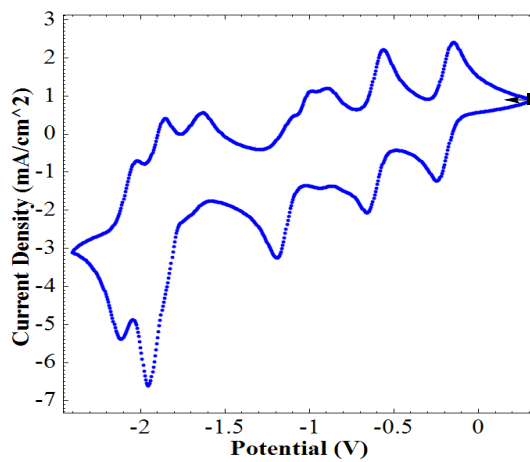
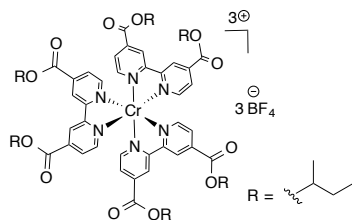
Cyclic voltammogram of $[\text{Cr}(\text{L4})_3]^{3+}$



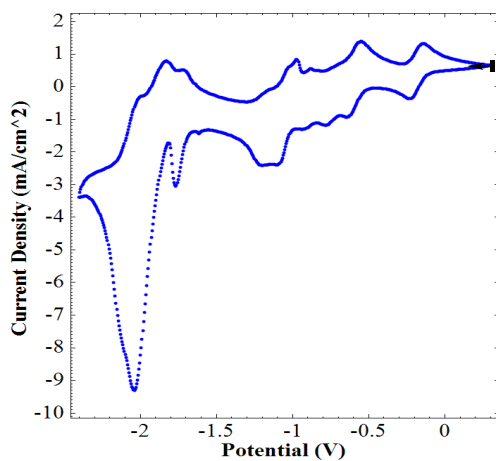
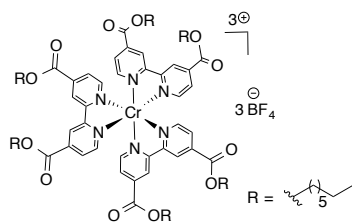
Cyclic voltammogram of $[\text{Cr}(\text{L5})_3]^{3+}$



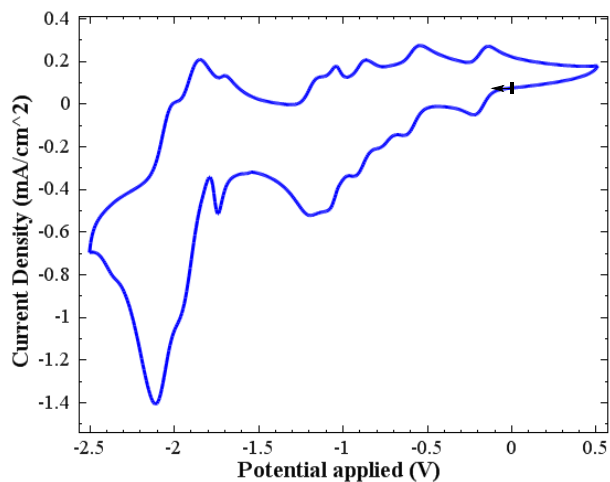
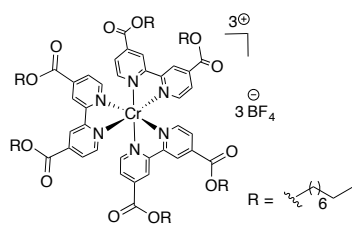
Cyclic voltammogram of $[\text{Cr}(\text{L6})_3]^{3+}$



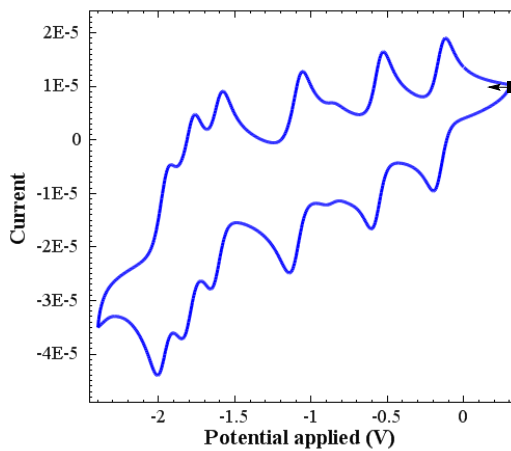
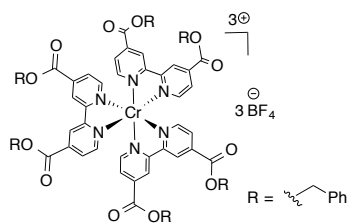
Cyclic voltammogram of $[\text{Cr}(\text{L7})_3]^{3+}$



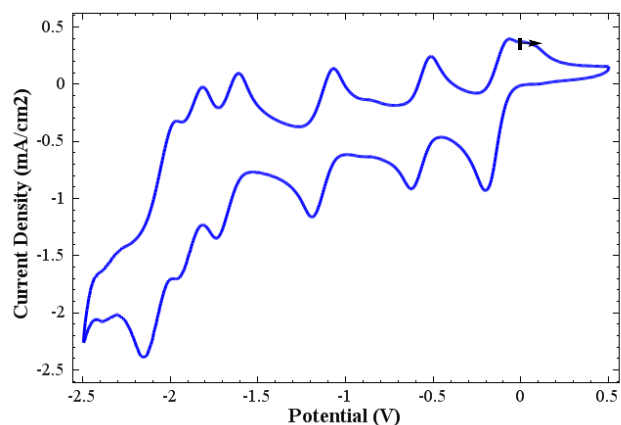
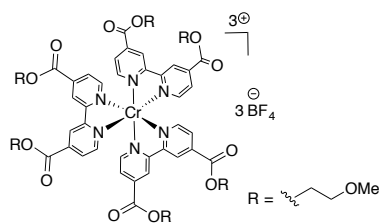
Cyclic voltammogram of $[\text{Cr}(\text{L8})_3]^{3+}$



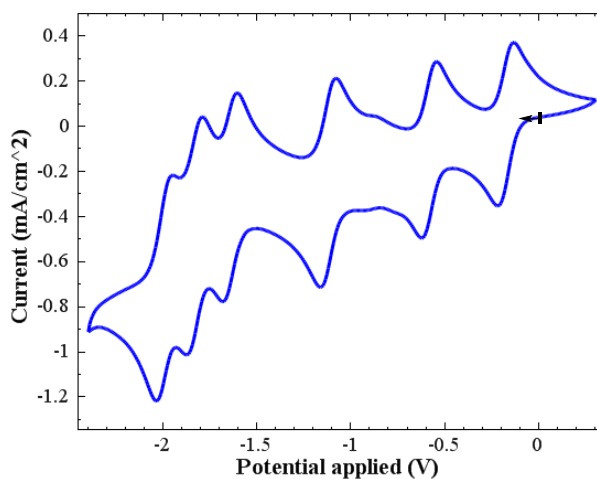
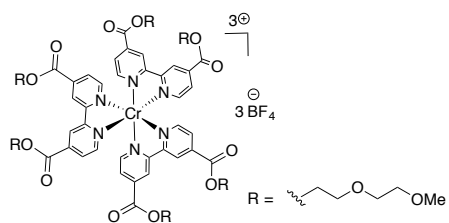
Cyclic voltammogram of $[\text{Cr}(\text{L9})_3]^{3+}$



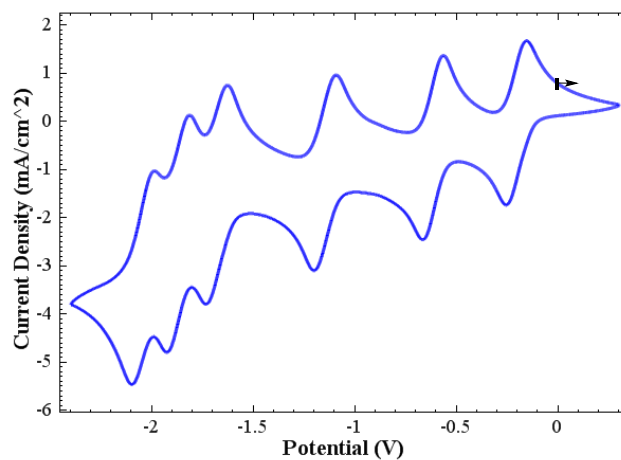
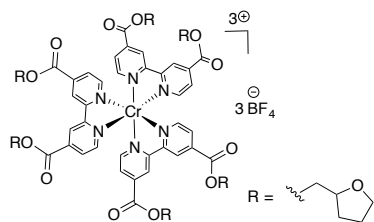
Cyclic voltammogram of $[\text{Cr}(\text{L10})_3]^{3+}$



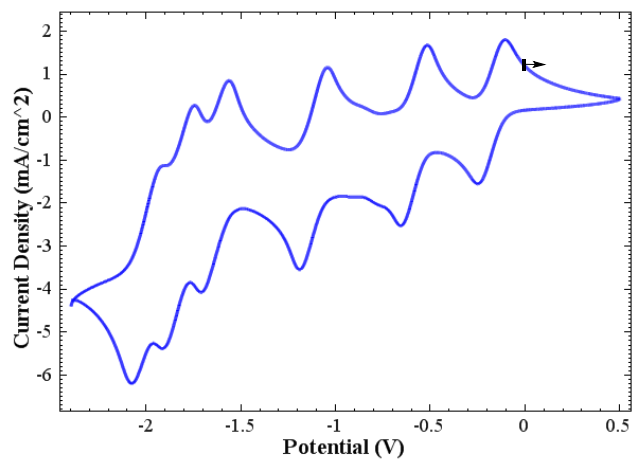
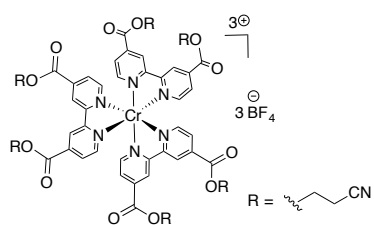
Cyclic voltammogram of $[\text{Cr}(\text{L11})_3]^{3+}$



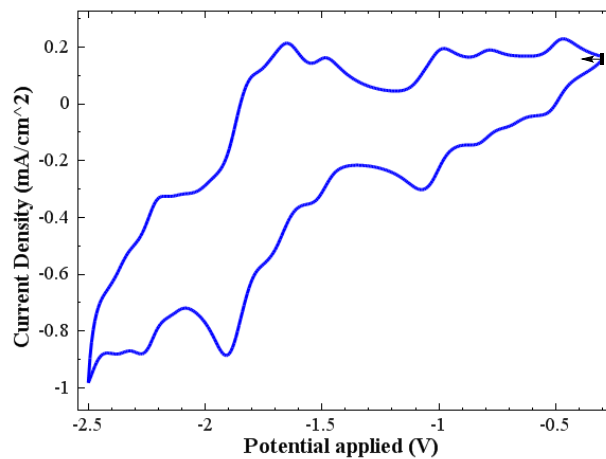
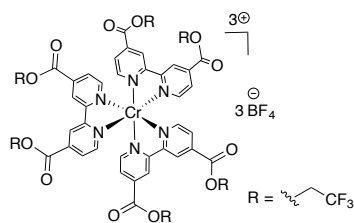
Cyclic voltammogram of $[\text{Cr}(\text{L12})_3]^{3+}$



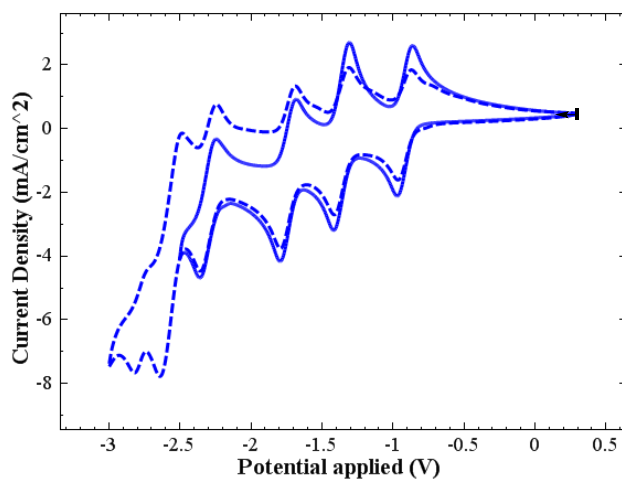
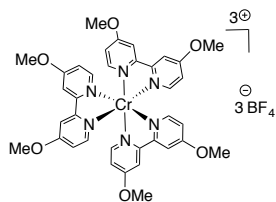
Cyclic voltammogram of $[\text{Cr}(\text{L13})_3]^{3+}$



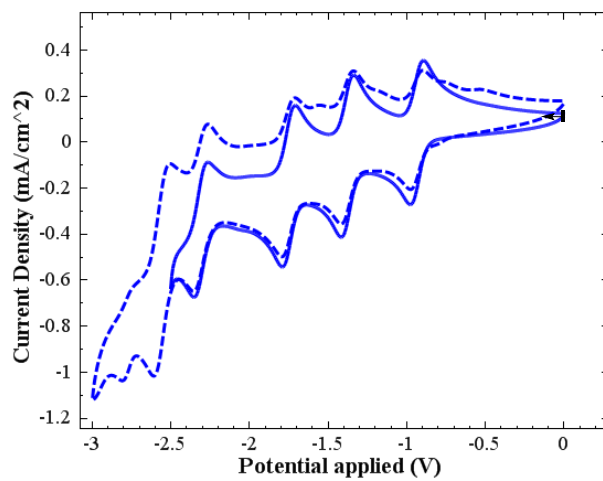
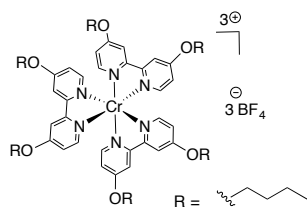
Cyclic voltammogram of $[\text{Cr}(\text{L14})_3]^{3+}$



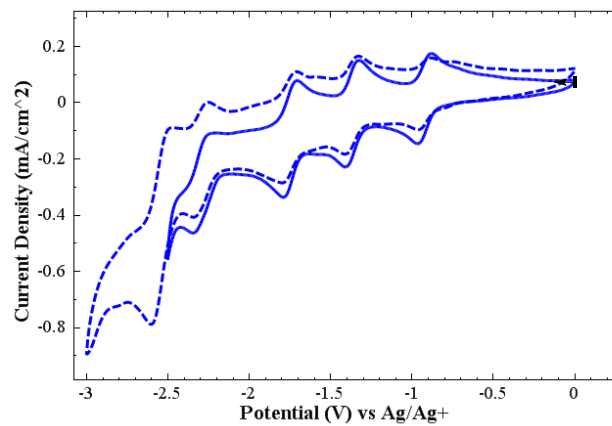
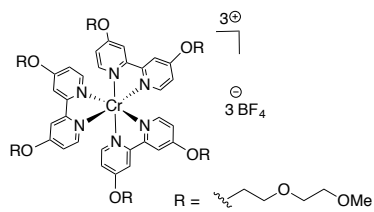
Cyclic voltammogram of $[\text{Cr}(\text{L15})_3]^{3+}$



Cyclic voltammogram of $[\text{Cr}(\text{L16})_3]^{3+}$

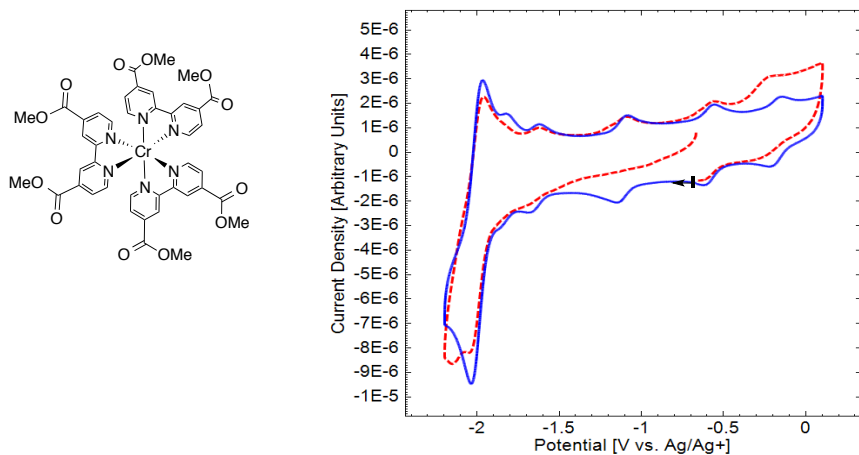


Cyclic voltammogram of $[\text{Cr}(\text{L17})_3]^{3+}$

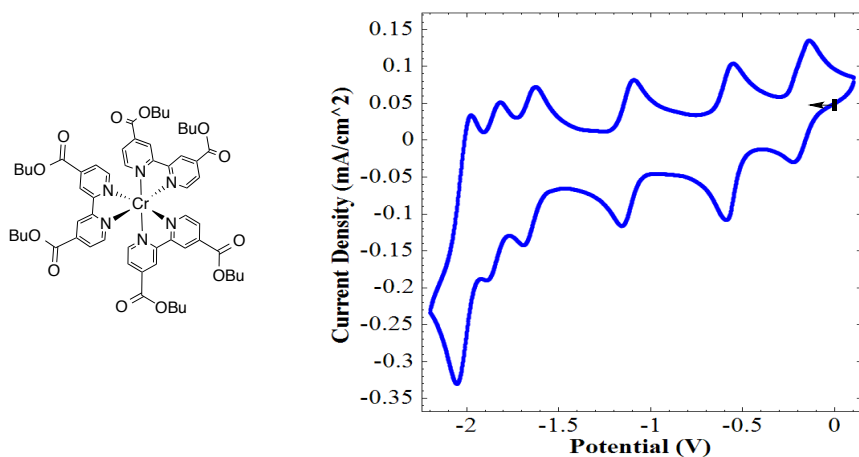


Cyclic voltammogram of $[\text{Cr}(\text{L3})_3]^0$

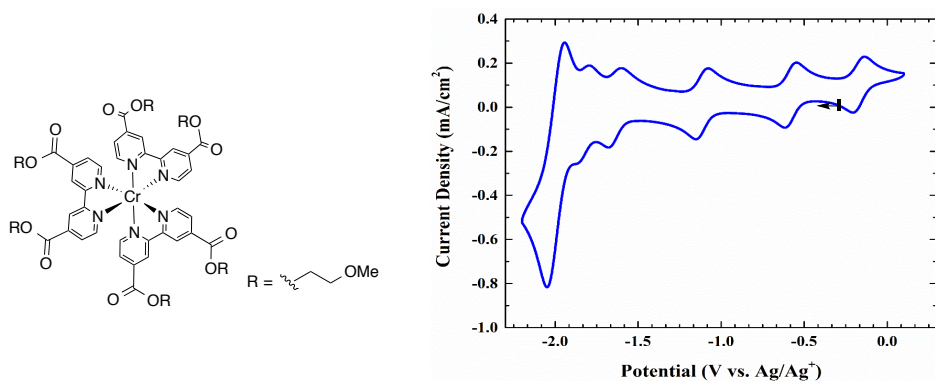
Note: Red dotted CV is the 1st scan starting at the open circuit potential. Blue CV is the 3rd scan. For the rest of Cr(0) complexes one full scan between 2nd and 10th are shown for clarity. All scans beyond the first one overlay well.



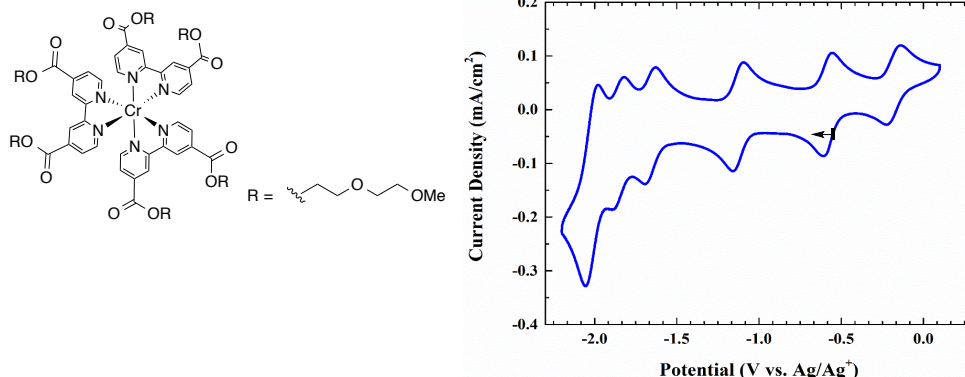
Cyclic voltammogram of $[\text{Cr}(\text{L5})_3]^0$



Cyclic voltammogram of $[\text{Cr}(\text{L10})_3]^0$



Cyclic voltammogram of $[\text{Cr}(\text{L11})_3]^0$



2.6 References

- (1) Portion of this chapter is adapted with permission from: (a) Cabrera, P. J.; Yang, X.; Suttill, J. A.; Brooner, R. E. M.; Thompson, L. T.; Sanford, M. S. *Inorg. Chem.* **2015**, *54*, 10214. (b) Cabrera, P. J.; Yang, X.; Suttill, J. A.; Hawthorne, K. L. Brooner, R. E. M.; Sanford, M. S.; Thompson, L. T. *J. Phys. Chem. C*, **2015**, *119*, 15882.
- (2) (a) Dunn, B.; Kamath, H.; Tarascon, J.-M. *Science*, **2011**, *334*, 928. (b) Yang, Z.; Zhang, J.; Kintner-Meyer, M. C. W.; Lu, X.; Choi, D.; Lemmon, J. P.; Liu, J. *Chem. Rev.*, **2011**, *111*, 3577. (c) Shin, S.-H.; Yun, S.-H.; Moon, S.-H. *RSC Adv.* **2013**, *3*, 9095.
- (3) (a) Ponce de Leon, C.; Frías-Ferrer, A.; González-García, J.; Szanto, D. A.; Walsh, F. C. *J. Power Sources* **2006**, *160*, 716. (b) Huang, Q.; Wang, Q. *ChemPlusChem* **2015**, *80*, 312.
- (4) (a) Zhang, D.; Lan, H.; Li, Y. *J. Power Sources* **2012**, *217*, 199. (b) Liu, Q.; Sleightholme, A. E. S.; Shinkle, A. A.; Li, Y.; Thompson, L. T. *Electrochem. Commun.* **2009**, *11*, 2312. (c) Sleightholme, A. E. S.; Shinkle, A. A.; Liu, Q.; Li, Y.; Monroe, C. W.; Thompson, L. T. *J. Power Sources* **2011**, *196*, 5742. (d) Yamamura, T.; Shiokawa, Y.; Yamana, H.; Moriyama, H. *Electrochim. Acta* **2002**, *48*, 43. (e) Suttill, J. A.; Kucharyson, J. F.; Escalante-Garcia, I. L.; Cabrera, P. J.; James, B. R.; Savinell, R. F.; Sanford, M. S.; Thompson, L. T. *J. Mater. Chem. A* **2015**, *3*, 7929.
- (5) Cappillino, P. J.; Pratt, H. D.; Hudak, N. S.; Tomson, N. C.; Anderson, T. M.; Anstey, M. R. *Adv. Energy Mater.* **2014**, *4*, 1300566.
- (6) (a) Hwang, B.; Park, M.-S.; Kim, K. *ChemSusChem* **2015**, *8*, 310. (b) Wei, X. L.; Cosimbescu, L.; Xu, W.; Hu, J. Z.; Vijayakumar, M.; Feng, J.; Hu, M. Y.; Deng, X. C.; Xiao, J.; Liu, J.; Sprenkle, V.; Wang, W. *Adv. Energy Mater.* **2015**, *5*, 1400678.
- (7) (a) Matsuda, Y.; Morita, T. M.; Tanaka, K.; Okada, M.; Matsumura-Inoue, T. *Denki Kagaku* **1985**, *53*, 632. (b) Matsuda, Y.; Tanaka, K.; Okada, M.; Takasu, Y.; Morita, M.; Matsumura-Inoue, T. *J. Appl. Electrochem.* **1988**, *18*, 909. (c) Morita, M.; Tanaka, Y.; Tanaka, K.; Matsuda, Y.; Matsumura-Inoue, T. *Bull. Chem. Soc. Jpn.* **1988**, *61*, 2711. (d) Mun, J.; Lee, M.-J.; Park, J.-W.; Oh, D.-J.; Lee, D.-Y.; Doo, S.-G. *Electrochem. Solid-State Lett.* **2012**, *15*, A80. (e) Chakrabarti, M. H.; Dryfe, R. A. W.; Roberts, E. P. L. *Electrochim. Acta* **2007**, *52*, 2189. (f) Kim, J.-H.; Kim, K. J.; Park, M.-S.; Lee, N. J.; Hwang, U.; Kim, H.; Kim, Y.-J. *Electrochem. Commun.* **2011**, *13*, 997. (g) Chakrabarti, M. H.; Lindfield Roberts, E. P.; Saleem, M. *Int. J. Green Energy* **2010**, *7*, 445. (h) Xing, X.; Zhang, D.; Li, Y. *J. Power Sources* **2015**, *279*, 205. (i)

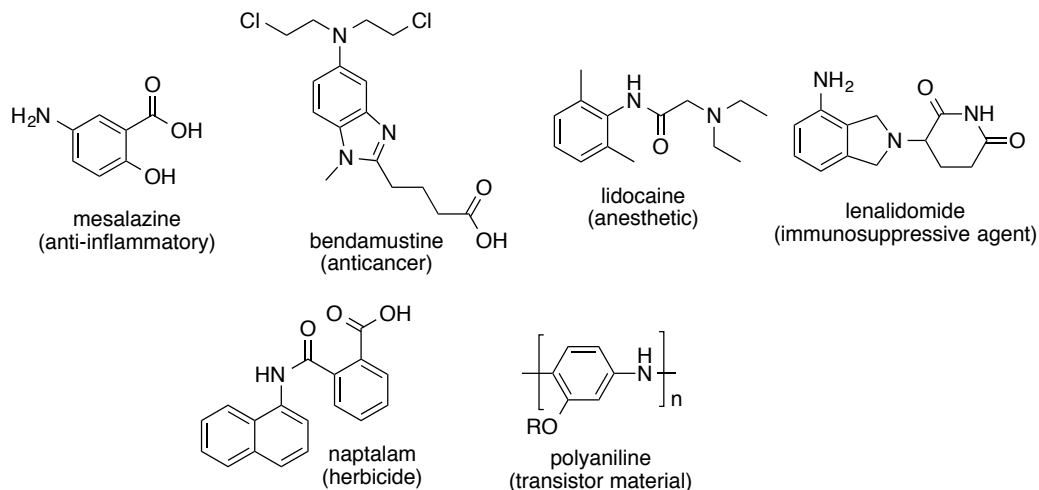
- Park, M.-S.; Lee, N. J.; Lee, S.-W.; Kim, K. J.; Oh, D.-J.; Kim, Y.-J. *ACS Appl. Mater. Interfaces* **2014**, *6*, 10729.
- (8) (a) Bae, C.-H.; Roberts, E.; Dryfe, R. *Electrochim. Acta* **2002**, *48*, 279. (b) Liu, Q.; Shinkle, A. A.; Li, Y.; Monroe, C. W.; Thompson, L. T.; Sleightholme, A. E. S. *Electrochem. Commun.* **2010**, *12*, 1634.
- (9) McDaniel, A. M.; Tseng, H.-W.; Damrauer, N. H.; Shores, M. P. *Inorg. Chem.* **2010**, *49*, 7981.
- (10) (a) Barrosse-Antle, L. E.; Bond, A. M.; Compton, R. G.; O'Mahony, A. M.; Rogers, E. I.; Silvester, D. S. *Chem. Asian J.* **2010**, *5*, 202. (b) Gong, K.; Fang, Q.; Gu, S.; Li, S. F. Y.; Yan, Y. *Energy Environ. Sci.* **2015**, *8*, 3515. (c) https://depts.washington.edu/eooptic/linkfiles/dielectric_chart%5B1%5D.pdf, Accessed: March 30th, 2017.
- (11) Hughes, M. C.; Rao, J. M.; Macero, D. J. *Inorg. Chim. Acta* **1979**, *35*, L321.
- (12) (a) Anslyn, E. V.; Dougherty, D. A. *Modern Physical Organic Chemistry*, 1st ed.; University Science Books: CA, 2005; p 153–202. (b) Palmer, D. S.; Llinas, A.; Morao, I.; Day, G. M.; Goodman, J. M.; Glen, R. C.; Mitchell, J. B. O. *Mol. Pharmaceutics* **2008**, *5*, 266.
- (13) Scarborough, C. C.; Sproules, S.; Weyhermüller, T.; DeBeer, S.; Wieghardt, K. *Inorg. Chem.* **2011**, *50*, 12446.
- (14) Bard, A. J.; Faulkner, L. R. *Electrochemical Methods: Fundamentals and Applications*, 2nd ed.; Wiley: New York, 2001.
- (15) Barker, D. J.; Brewin, D. H.; Dahm, R. H.; Hoy, L. R. J. *Electrochim. Acta* **1978**, *23*, 1107.
- (16) Sevov, C. S.; Fisher, S. L.; Thompson, L. T.; Sanford, M. S. *J. Am. Chem. Soc.* **2016**, *138*, 15378.
- (17) (a) Sevov, C. S.; Samaroo, S. K.; Sanford, M. S. *Adv. Energy Mater.* **2016**, 1602027 (b) Sevov, C. S.; Hickey, D. P.; Cook, M. E.; Robinson, S. G.; Barnett, S.; Minter, S. D.; Sigman, M. S.; Sanford, M. S. *J. Am. Chem. Soc.* **2017**, *139*, 2924
- (18) Hoertz, P. G.; Staniszewski, A.; Marton, A.; Higgins, G. T.; Incarvito, C. D.; Rheingold, A. L.; Meyer, G. J. *J. Am. Chem. Soc.* **2006**, *128*, 8234.
- (19) Hong, Y.-R.; Gorman, C. B. *J. Org. Chem.* **2003**, *68*, 9019.
- (20) Garelli, N.; Vierling, P. *J. Org. Chem.* **1992**, *57*, 3046.
- (21) Henriques, R. T.; Herdtweck, E.; Kühn, F. E.; Lopes, A. D.; Mink, J.; Romão, C. C. *J. Chem. Soc., Dalton Trans.* **1998**, 1293.

Chapter 3. C–H Amination of Arenes and Heteroarenes Via Visible Light Photocatalysis¹

3.1 Introduction

The selective conversion of C–H bonds into functional groups is a highly desired transformation in the manufacture of pharmaceuticals, agrochemicals and materials science (Figure 3.1). C–H amination, or the direct transformation of a C–H bond into a C–N bond, has become an area of increased interest due to the prevalence of nitrogen in natural products and materials.² As of 2010, ~67% of the top 200 pharmaceuticals by US retail sales contained nitrogen atoms.^{3a}

Figure 3.1. Representative examples of arenes and heteroarenes bearing amine substituents.

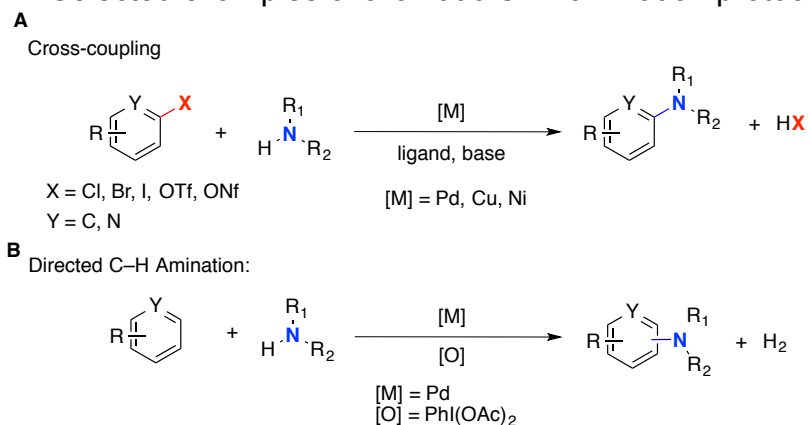


In particular, aromatic amines are widely prevalent in pharmaceutical agents, and 58% of the small-molecule best-selling drugs contain a $\text{C}(\text{sp}^2)\text{--N}$ bond.^{3b} As such, the development of methods to synthesize aryl amines is of high importance. One of the most utilized methods for aromatic C–H amination is the nitration of arenes with nitric and sulfuric acid mixtures followed by reduction of the nitro group, typically by a

heterogeneous hydrogenation catalyst (Pd/C, PtO₂, Raney-Ni).⁴ Other methods for C–N bond formation such as nucleophilic aromatic substitution and cross coupling reactions (Buchwald-Hartwig,⁵ Ullman,⁶ Chan-Lam⁷) require pre-functionalized C–X bonds (e.g. X = halides, triflate, nitro) on the aromatic system (Figure 3.2 A).

Recent efforts have focused on the direct amination of aromatic C–H bonds catalyzed by transition metals. Most of these methodologies employ directing groups to achieve *ortho*-C–H aminations⁸ or engineered systems that afford intramolecular C–H amination products.⁹ Non-directed intermolecular C–H amination reactions are much less common due to major challenges in selectivity. Recent reports on transition metal catalyzed intermolecular C–H amination by Hartwig¹⁰ and Ritter,¹¹ and metal-free methods by Chang¹² and DeBoef¹³ have demonstrated the feasibility of such transformations. However, these reactions typically require super stoichiometric amounts of oxidants, high temperatures, expensive nitrogen sources, and/or specialized catalyst scaffolds (Figure 3.2 B).

Figure 3.2. Selected examples of aromatic C–H amination protocols.



3.2 Background

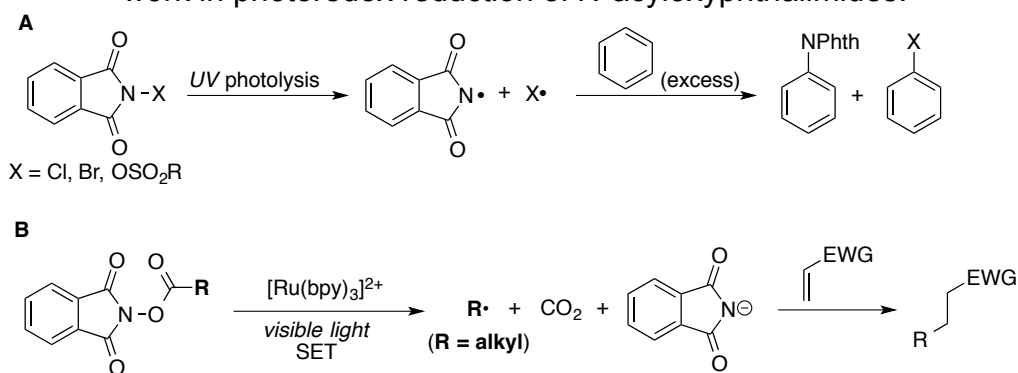
The *in situ* formation of nitrogen-centered radicals by traditional methods such as UV-photolysis, heat or radical initiators have usually focused on the use of halogenated amines and amides that can subsequently react with substrates.¹⁴ Lidget and coworkers first demonstrated the free-radical C–H amination of aromatic compounds utilizing *N*-chlorosulphonylphthalimide at high temperatures (180-250 °C) in the presence CuCl via phthalimido-radicals.¹⁵ Later, Cadogan¹⁶ and Abramovich¹⁷ showed that UV-photolysis

could be used for aromatic C–H aminations utilizing *N*-tosylphthalimide as the radical source. Skell subsequently demonstrated that UV-photolysis could also promote the C–H amination of arenes utilizing *N*-bromophthalimide as the nitrogen source, but with competitive C–H bromination.¹⁸ All these reactions require harsh reaction conditions and solvent quantities of the arene. In addition, these methods led to competing side reactions (Figure 3.3 A).

An underexplored method to generate nitrogen-centered radicals is through the use of visible light photocatalysis. This approach relies on the ability of metal complexes or organic dyes to undergo photoexcitation with visible light and facile intersystem crossing to access a long-lived triplet photoexcited state that undergoes single-electron transfer (SET) with organic substrates.¹⁹ Photocatalysis offers several attractive features, as these reactions are commonly setup at room temperature and without the use of strong oxidants or reductants.¹⁹

A seminal report by Okada demonstrated that the photocatalyst $[\text{Ru}(\text{bpy})_3]^{2+}$ can reduce *N*-acyloxyphthalimides through an outer sphere single electron transfer (SET) releasing CO_2 , phthalimide, and alkyl radicals (Figure 3.3 B). The alkyl radicals were further reacted with H-atom sources, diphenyldiselenide, or vinylketones.²⁰ Overman recently utilized this approach in the total synthesis of (–)-aplyviolene^{21a} as well as in subsequent publications on the formation of quaternary carbon centers via conjugate addition of tertiary alkyl radicals to electron deficient alkenes.^{21b,c} Overman's work exemplifies the mild conditions and high selectivity that can be achieved using photoredox catalysis. These reports on the photocatalyzed reduction of *N*-acyloxyphthalimides provided the basis for the studies described in this chapter. At the time we began our work, visible light photoredox catalysis for $\text{C}(\text{sp}^2)\text{--H}$ amination was not reported.

Figure 3.3. A) Selected methods for the generation of *N*-centered radicals. B) Okada's work in photoredox reduction of *N*-acyloxyphthalimides.



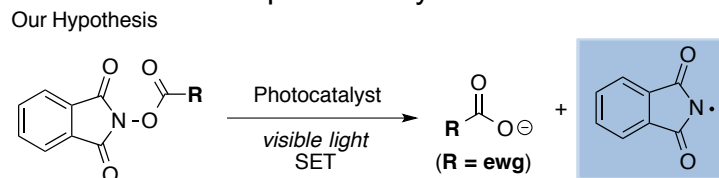
This chapter describes our work in the use of visible light photoredox catalysts to achieve the C–H amination of a range of arenes and heteroarenes. In addition, several modifications to the nitrogen radical source led to the development of saccharine-based *N*-radical precursors that displayed improved reactivity due to their highly electrophilic properties.

3.3 Results and Discussion

Development of Visible Light C–H Amination of Arenes and Heteroarenes Via Photoredox Catalysis

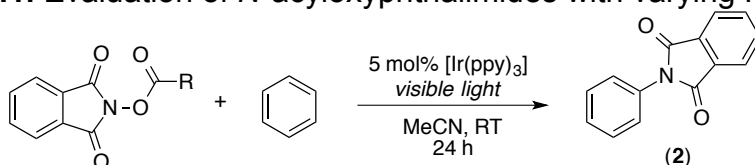
Inspired by the work of Okada and the literature precedent for the generation of phthalimido-radicals by UV-photolysis, my colleague Dr. Laura Allen envisioned that modification of the electronic structure of *N*-acyloxyphthalimides by incorporation electron-withdrawing groups at the *R* position could alter the fragmentation process. Specifically, she hypothesized that enhancing the leaving group ability of the carboxylate would enable release of a carboxylate anion along with phthalimidyl radicals (Fig. 3.4).

Figure 3.4. Proposed pathway to generate nitrogen radicals using visible light photocatalysis.



Dr. Allen prepared a range of *N*-acyloxyphthalimides with varying electronics in the R group (Table 3.1). These substrates were reacted with benzene in the presence of visible light and the strongly reducing photocatalyst tris[2-phenylpyridinato-C₂,N]iridium(III) (Ir(ppy)₃). The incorporation of a CF₃ group in the *N*-acyloxyphthalimide (**1**) afforded an 81% yield of the C–H amination product **2** (Table 3.1 entry 1). Other, *N*-acyloxyphthalimides with less electron-withdrawing substituents bearing a perfluorinated arene and phenyl group (**1a** and **1b**, respectively) resulted in lower yields of the C–H aminated product (53% and 8%, respectively; entries 2 and 3). This is particularly important because *N*-trifluoroacyloxyphthalimide (**1**) can be prepared from *N*-hydroxyphthalimide and trifluoroacetic anhydride. Subsequent optimization demonstrated that the maximum yield of aminated product was obtained when 10 equiv of the arene, 1 equiv of *N*-trifluoroacyloxyphthalimide (**1**), and 5 mol % of Ir(ppy)₃ were reacted in acetonitrile at room temperature for 24 h in the presence of visible light. Control experiments show that no product is formed in the absence of photocatalyst or visible light (Table 3.1 entries 4 and 5).

Table 3.1. Evaluation of *N*-acyloxyphthalimides with varying R groups.



Entry	<i>N</i> -acyloxyphthalimide (R)	Modification	Yield of 2 ^a
1	1 (CF ₃)	-----	81%
2	1a (C ₆ F ₅)	-----	53%
3	1b (Ph)	-----	8%
4	1 (CF ₃)	No Ir(ppy) ₃	not detected
5	1 (CF ₃)	No visible light	not detected

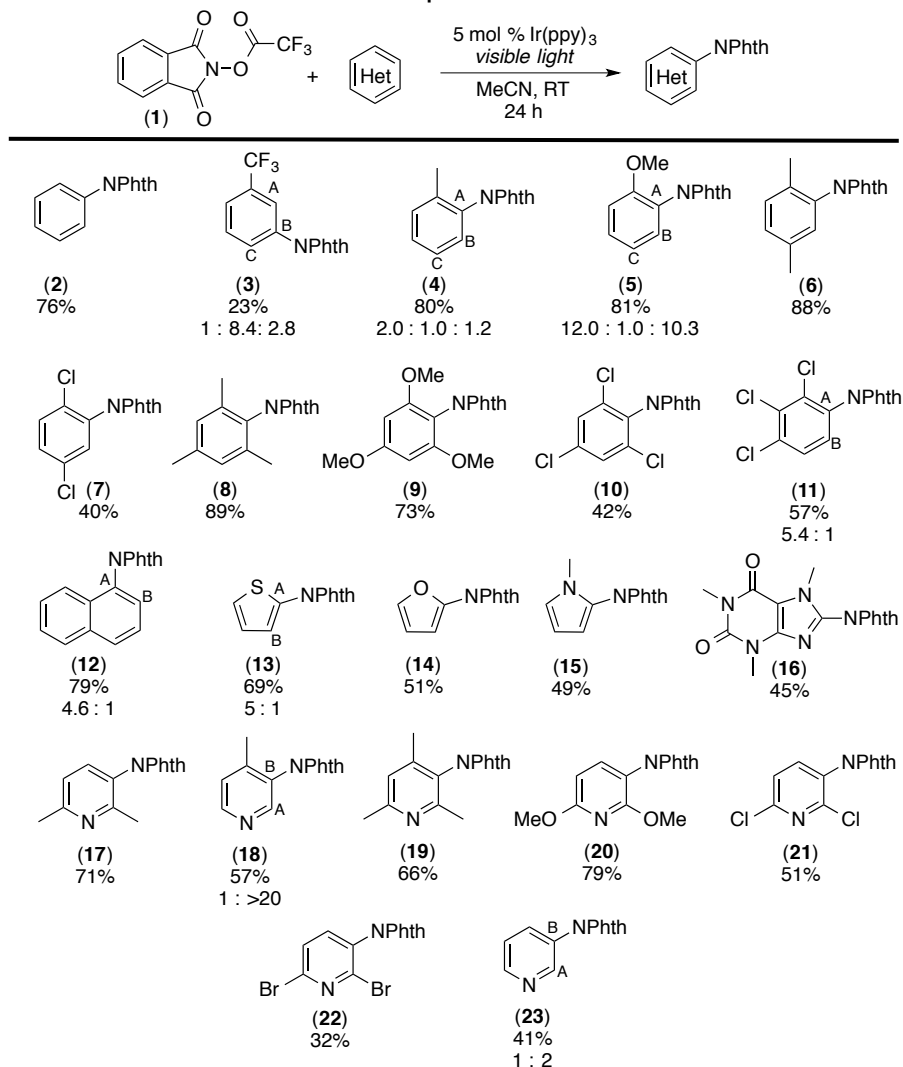
^a Conditions: 1 equiv of **1**, 5 mol% Ir(ppy)₃, 10 equiv benzene, MeCN (0.1 M), visible light, room temperature, 24h. Calibrated GC yields.

Substrate Scope of the Reaction

We next examined the scope of arenes and heteroarenes that participate in this C–H amination reaction. A wide range of mono-, di- and tri-substituted arenes underwent C–H amination under these conditions, providing access to diverse aniline

products (Table 3.2). The site selectivity of these reactions is consistent with that anticipated for a radical aromatic substitution pathway.²² For instance, arene substrates bearing electron-donating substituents such as alkyl and alkoxy groups gave moderate to high levels of *ortho/para* selectivity (e.g., products **4** and **5**). In contrast, electron-withdrawing substituents, such as trifluoromethyl, provided mainly *meta*-functionalized aminated products (**3**). However, arenes bearing electron-withdrawing substituents afforded lower yields than those with electron-donating groups. This is further evidence for a pathway involving electrophilic nitrogen radicals. Finally, it is noteworthy that this reaction is high yielding and selective for C(sp²)-H bonds in the presence of benzylic C(sp³)-H bonds (cf, **4**, **6**, **8**, **17**, **18**, **19**). In addition, a variety of tri-substituted arenes afforded high yields of the desired product (**8**, **9**, **10**, **11**, **19**). This is particularly important as comparable transition-metal catalyzed C-H functionalization methods tend to be highly sensitive to sterics.

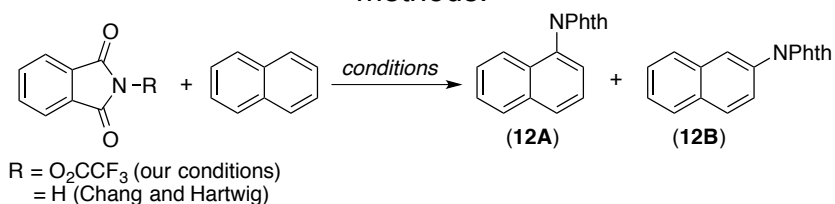
Given the mild reaction conditions, we hypothesized our protocol could be compatible with a range of heterocycles. Gratifyingly, a variety of 5-membered heterocycles such as thiophene (**13**), furan (**14**), *N*-methylpyrrole (**15**) and caffeine (**16**) underwent selective C-H amination at the 2-position of the arene in moderate to high yields under our optimal conditions. In addition, pyridine derivatives are viable substrates for this transformation, providing *meta*-substituted products in high selectivity (products **17**, **18**). Furthermore, pyridine derivatives bearing halides were compatible with our reaction conditions (products **21** and **22** required 20 equiv of heteroarene). Finally, pyridine was functionalized in good yield generating the *meta*-aminated isomer as the major product (**23**). Notably, there does not appear to be any catalyst inhibition with these pyridine substrates, presumably because [Ir] contains strongly coordinated cyclometalated phenylpyridine ligands.

Table 3.2. Substrate scope in arene and heteroarene.

Conditions: **1** (1 equiv), arene (10 equiv), Ir(ppy)₃ (5 mol%), visible light, MeCN (0.1 M), room temperature, 24h. Isolated yields. For products **21-23**, 20 equivalents of heteroarene and MeCN (0.2 M) were used.

Next, we compared the site selectivity of this reaction to that of other C–H amination reactions reported in the literature using naphthalene as a representative substrate. As shown in Table 3.3 entry 1, our reaction conditions afforded isomer **12A** as a major product with a 7 : 1 ratio (**12A** : **12B**). In comparison, Chang and co-workers report that their reaction conditions (PhI(OAc)₂/phthalimide) provide 68% yield of aminated naphthalene (**12**) with a 1 : 1 ratio (**12A** : **12B**; entry 2).¹² In our hands, Hartwig’s Pd-catalyzed conditions afforded a 23% yield of **12** with a 1 : 7 selectivity favoring isomer **12B** (entry 3).¹⁰ Overall, these results demonstrate that our method is complementary to previously published methods.

Table 3.3 Selectivity in the C–H amination of naphthalene with different C–H amination methods.



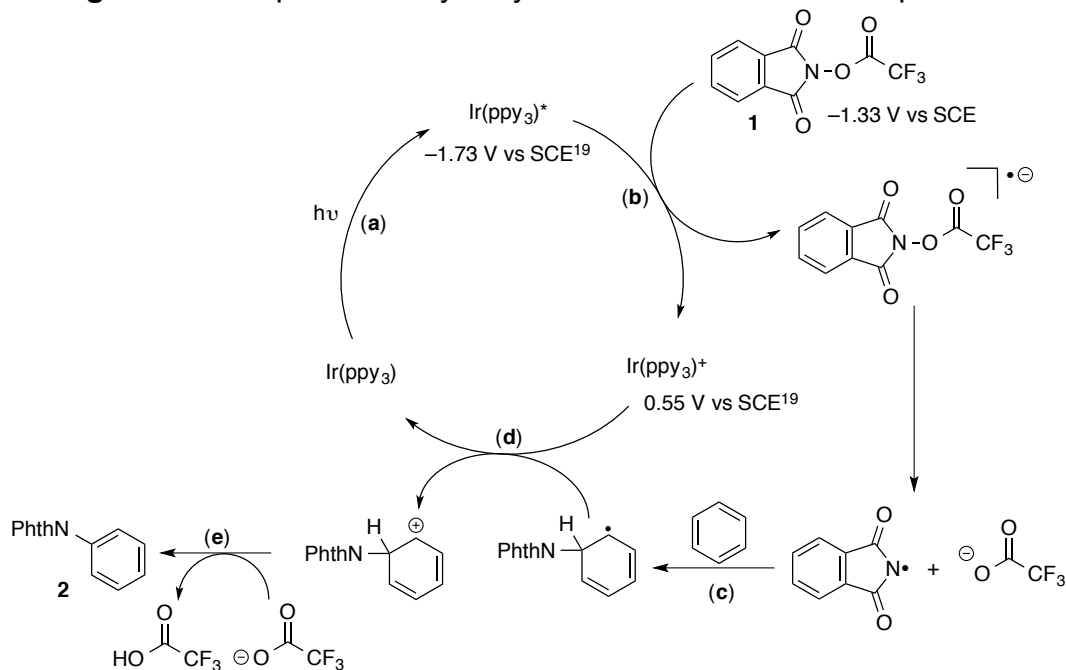
Entry	Conditions	Yield	12A : 12B
1 ^a	Our standard conditions	79%	7 : 1
2 ^b	PhthNH, PhI(OAc) ₂	68%	1 : 1
3 ^c	PhthNH, PhI(OAc) ₂ , Pd(OAc) ₂ , P ^t Bu ₃	23%	1 : 7

^aConditions: **1** (1 equiv), Ir(ppy)₃ (5 mol %), naphthalene (10 equiv), MeCN (0.1 M in **1**), visible light, 24 h, rt. Yield determined by GC using neopentylbenzene as a standard. ^bReference 12. ^cConditions analogous to those in reference 10 were used as follows: Phthalimide (0.1 mmol, 1.0 equiv), Pd(OAc)₂/P^tBu₃ (10 mol%), naphthalene (5 mL), PhI(OAc)₂ (6.0 equiv total, 2.0 equiv at t = 0, 9, 24 h), 100 °C, 33 h.

Proposed Reaction Mechanism

A proposed catalytic cycle for the current transformation is shown in Figure 3.5. This cycle begins with visible light photoexcitation of Ir(ppy)₃ to generate Ir(ppy)₃^{*} (step a). Single electron transfer from Ir(ppy)₃^{*} to **1** then results in fragmentation of the *N*-acyloxyphthalimide to generate an *N*-centered phthalimidyl radical (PhthN•), trifluoroacetate, and Ir(ppy)₃⁺ (step b). The arene intercepts the PhthN• forming a neutral radical intermediate (step c) which can be oxidized by Ir(ppy)₃⁺, returning the photocatalyst to its ground state (step d). The trifluoroacetate anion, formed upon reductive cleavage of the N–O bond, deprotonates the cationic Wheland intermediate, providing 1 equiv of aminated product and trifluoroacetic acid (step e).

Figure 3.5. Proposed catalytic cycle for the C–H amination protocol.



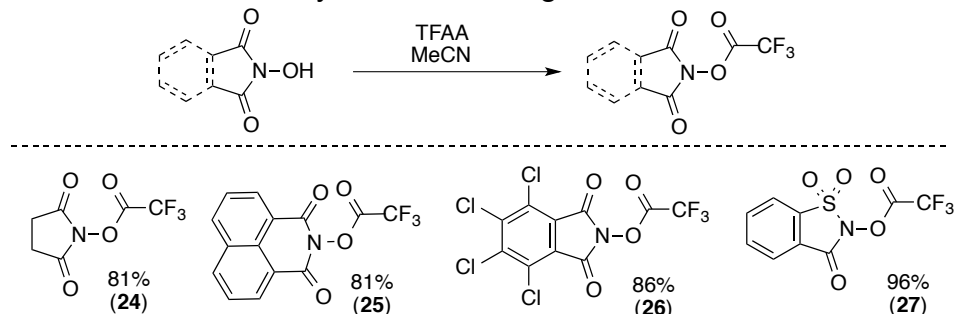
Analysis of the reduction potential of the *N*-trifluoroacetoxyphthalimide (-1.33 V vs SCE) by cyclic voltammetry indicated that the excited state of Ir(ppy)₃ (-1.73 V vs SCE¹⁹) is sufficiently reducing to support the single electron transfer from Ir(ppy)₃* to **1** (step b). This is in agreement with other literature reports of the reduction of *N*-acyloxyphthalimides.^{20,23} In addition, we identified that light is essential for the reaction to proceed. Experiments when light is halted demonstrate that product formation stops, and reaction progress only recommences after light is turned back on. This is in agreement with visible light promoting photoexcitation of Ir(ppy)₃ (step a). However, this experiment does not rule out the possibility of a radical chain mechanism.²⁴

Development of Nitrogen Radical Sources

Although this method enabled the functionalization of several (hetero)arenes, we recognize that the requirements for excess arene and relatively high catalyst loading, as well as the use of a single nitrogen radical source are drawbacks of the method. In an effort to improve reactivity, we hypothesized that using other nitrogen radical sources with varying electronic properties could improve the methodology. In particular, we hoped that the incorporation of electron deficient groups around the imide could shift the reduction potential of the *N*-acyloxyimide, thus enabling: (1) the use of simpler photocatalysts and (2) an increase in reaction yields by enhancing the nitrogen radical

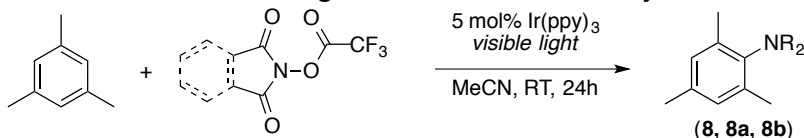
affinity for nucleophilic arenes and heteroarenes. To test this hypothesis, four different *N*-acyloxyimides were prepared from the corresponding *N*-hydroxyimide in high yields (81-96%; Table 3.4).

Table 3.4. Synthesis of nitrogen radical sources.



Initial screening revealed that **24** and **25** behaved very similar to **1**, and no reaction improvement was observed, despite optimization. However, **26** and **27** showed more promising results. Subjecting these imides to the reaction conditions in the presence of mesitylene resulted in good yields of the aminated product (Table 3.5). Although **26** and **27** led to lower isolated yields than **1**, we were pleased to observe the formation of product. Given the high yield of aminated product **8b**, we continued optimization with the *N*-acyloxysaccharine **27**.

Table 3.5. Evaluation of nitrogen sources with mesitylene as substrate.



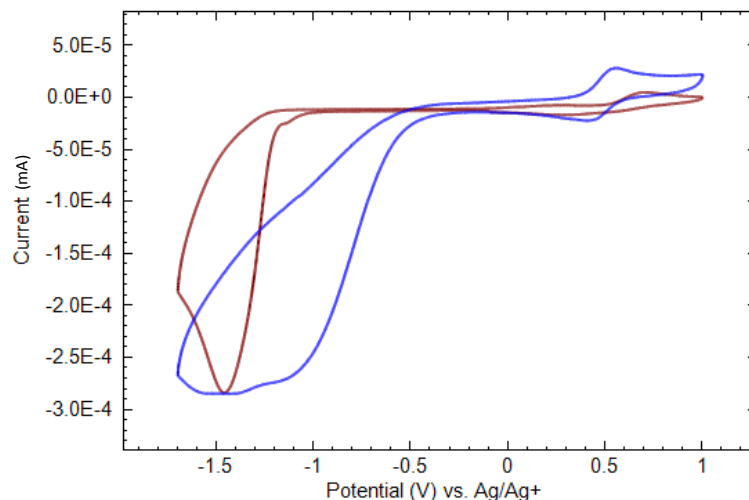
Entry	N-source	Yield ^a
1	26	41% (8a)
2	27	74% (8b)
3	1	89% (8)

^aConditions: N-source (1 equiv), mesitylene (10 equiv), Ir(ppy)₃ (5 mol%), MeCN (0.1 M), rt. Isolated yield. **8**: NR₂ is phthalimide, **8a**: NR₂ is tetrachlorophthalimide, **8b**: NR₂ is saccharine.

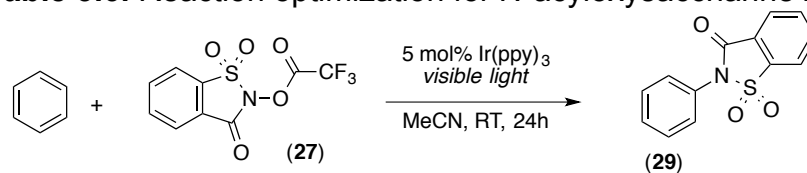
We hypothesized that an optimal photocatalyst must be identified first, such that the photocatalyst and the amine source have a good potential match. As shown in Table 3.6, a variety of photocatalysts with varying redox potentials were tested (entries 1-5). [Ru(d^tbubpy)₃]²⁺ was identified as the best photocatalyst for the reaction (entry 3), affording 49% uncalibrated GC yield of **29**. [Ru(d^tbubpy)₃]²⁺ has a lower excited state

reduction potential than Ir(ppy)₃ due to its less electron-donating ligands. This yield improvement validates our hypothesis that substrate **27** and [Ru(d^tbubpy)₃]²⁺ have a better voltage match. Furthermore, the cyclic voltammograms of **27** and **1** show that *N*-acyloxysaccharine **27** is easier to reduce, thus rendering the nitrogen radicals more electrophilic (compare onset redox potentials in Figure 3.6).

Figure 3.6. Cyclic voltammograms of **27** (blue) and **1** (red). CVs done with 0.1 M TBABF₄ in acetonitrile. Reference electrode Ag/Ag⁺, 100 mV/s scan rate, 23 °C.



Further reaction optimization demonstrated that a good yield of **29** was maintained when the catalyst loading was lowered to 1 mol % (entry 7, 44% yield). Finally, we were able to decrease the arene substrate to 1 equiv in the presence of 2.5 equiv of **27**. Under these conditions, the desired aminated product **29** was obtained in 65% isolated yield.

Table 3.6. Reaction optimization for *N*-acyloxysaccharine **27**.

Entry	Photocatalyst	Benzene (equiv)	27 (equiv)	GC Yield ^a
1	[Ru(bpy) ₃] ²⁺ (5 mol%)	10	1	31%
2	[Ru(dmbpy) ₃] ²⁺ (5 mol%)	10	1	49%
3	[Ru(dtBubpy) ₃] ²⁺ (5 mol%)	10	1	49%
4	[Ir(ppy)(bpy) ₂] ⁺ (5 mol%)	10	1	31%
5	[Ir(ppy) ₃] (5 mol%)	10	1	29%
6	[Ru(dtBubpy) ₃] ²⁺ (2.5 mol%)	10	1	34%
7	[Ru(dtBubpy) ₃] ²⁺ (1 mol%)	10	1	44%
8	[Ru(dtBubpy) ₃] ²⁺ (1 mol%)	5	1	51%
9	[Ru(dtBubpy) ₃] ²⁺ (1 mol%)	1	1	44%
10	[Ru(dtBubpy) ₃] ²⁺ (1 mol%)	1	2.5	61%

^aConditions: Reaction set up with the equivalents shown in each entry, MeCN (0.1 M), RT, 24h. GC yields based on a calibration curve for *N*-phenylphthalimide.

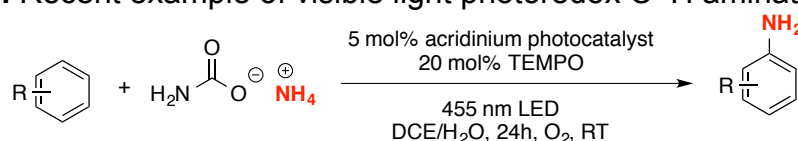
3.4 Conclusions

In summary, this chapter has described a mild visible light photocatalyzed method for the C–H amination of arenes and heteroarenes. The reaction employs *N*-trifluoroacyloxypthalimide as the nitrogen radical precursor. *N*-Trifluoroacyloxypthalimide is proposed to undergo a single electron reduction by the photocatalyst (Ir(ppy)₃), leading to trifluoroacetate and the reactive imidyl radical. A wide range of arenes with different functionalities were compatible with the system. In addition, the mild reaction conditions allowed the use heteroarenes substrates, affording modest to excellent yields of the aminated product. Finally, several new nitrogen-sources including an *N*-trifluoroacyloxysaccharine were developed. The formation of highly electrophilic saccharine based radicals enabled further reaction optimization to lower the catalyst loading and reduce the amount of arene required.

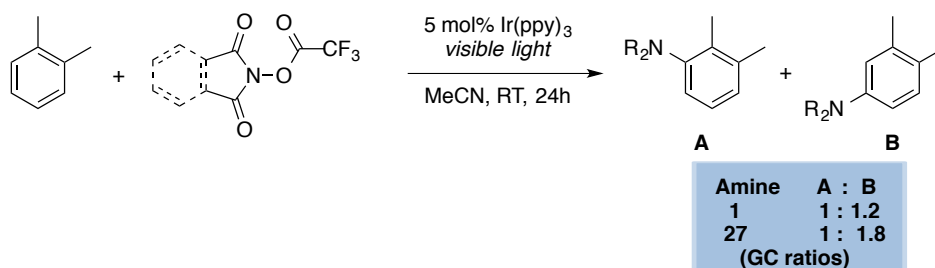
3.5 Perspective and Outlook

An important aspect of C–H amination of arenes and heteroarenes is the ability to control site-selectivity between similar C–H bonds. Due to the reactive nature of nitrogen radicals, they typically react to form multiple isomeric products. Since our methodology was published, we were pleased to see that several groups have published in the fields of C–H amination using nitrogen-centered radicals and also employing photocatalysis.²⁵ However, many of them still afford isomeric mixtures of aminated products. Very recently a major breakthrough came from the lab of Professor Nicewicz at UNC, Chapel Hill. His method employs photoredox catalysis and a nitroxyl radical to achieve selective C–H amination of arenes and heteroarenes with a variety of amines including ammonia surrogate (Figure 3.7).²⁶

Figure 3.7. Recent example of visible light photoredox C–H amination method.



However, the Nicewicz method only works on a moderate scope of substrates and several regioisomers are still observed. In general, selective C–H amination methods that employ radicals are rare. In order to improve the selectivity of this reaction, one avenue is to utilize nitrogen radicals with varying electronic or steric properties that could discriminate between C–H bonds. We began to explore this concept by the use of a *N*-acyloxysaccharine, which affords highly electrophilic radicals. We hypothesized that by decreasing the electron density of the nitrogen centered radical we could enhance its affinity for the most electron-rich C–H bond. Preliminary results suggest that with optimization of reaction conditions site selectivity can be improved through this strategy.

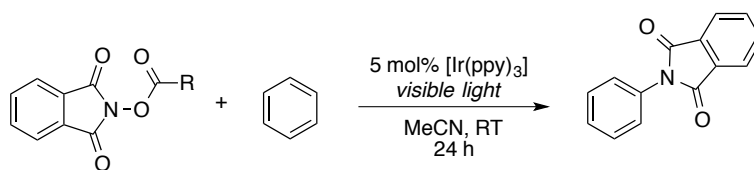


3.6 Experimental

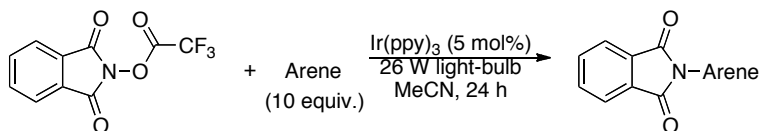
Materials and Methods

All reagents were purchased from common suppliers and dried over P_2O_5 prior to use unless otherwise noted. Tris[2-phenylpyridinato- $C_{2,N}$]iridium(III) ($Ir(ppy)_3$) was purchased from Sigma Aldrich. Ethyl acetate (EtOAc) and hexanes for column chromatography were purchased from VWR. Silica gel for flash column chromatography was purchased from Dynamic Adsorbents. $CDCl_3$ was purchased from Cambridge Isotope Laboratories, Inc. Thin layer chromatography (TLC) was performed on Merck TLC plates pre-coated with silica gel 60 F254. NMR spectra were recorded on a Varian 700 (699.76 MHz for 1H ; 175.95 MHz for ^{13}C), Varian 500 (500.10 MHz for 1H ; 125.75 MHz for ^{13}C , 470.56 MHz for ^{19}F), or Varian MR400 (400.52 MHz for 1H ; 100.71 for ^{13}C ; 376.87 MHz for ^{19}F) with the residual solvent peak ($CDCl_3$: 1H : $\delta = 7.26$ ppm, ^{13}C : $\delta = 77.16$ ppm) as the internal reference unless otherwise noted. Chemical shifts are reported in parts per million (ppm) (δ) relative to tetramethylsilane. Multiplicities are reported as follows: br (broad resonance), s (singlet), d (doublet), t (triplet), q (quartet), m (multiplet). Coupling constants (J) are reported in Hz. Infrared (IR) spectroscopy was performed on a Perkin-Elmer Spectrum BX FT-IR spectrometer and peaks are reported in cm^{-1} . Melting points were determined with a Mel-Temp 3.0, a Laboratory Devices Inc, USA instrument and are uncorrected. High-resolution mass spectra were recorded on a Micromass AutoSpec Ultima Magnetic Sector mass spectrometer. Gas chromatography was carried out on a Shimadzu 17A using a Restek Rtx®-5 (Crossbond 5% diphenyl - 95% dimethyl polysiloxane; 15 m, 0.25 mm ID, 0.25 μm df) column. All stock solutions were made using volumetric glassware. All reagents were weighed out in a nitrogen-filled drybox with exclusion of air and moisture, unless otherwise noted.

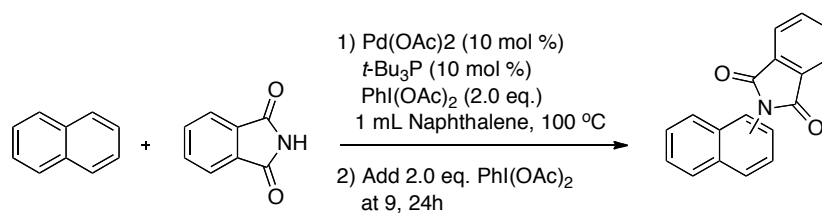
General Procedures



General Procedure A: General procedure for optimization reactions. In a N_2 -filled drybox, substituted N-acyloxyphthalimide **1** (0.05 mmol, 1.0 equiv) and $\text{Ir}(\text{ppy})_3$ (0.0025 mmol, 5 mol%) were weighed into a 4-mL scintillation vial equipped with a micro stir bar. Acetonitrile (0.5 mL, 0.1 M solution in **1**) was then added followed by benzene (0.5 mmol, 44 μL 10.0 equiv). The reaction vial was sealed with a Teflon-lined cap, removed from the N_2 -filled drybox, and placed on a stir-plate. Two 26 W compact fluorescent light bulbs were placed on opposite sides of the vial at approximately 5 cm distance. The reaction mixture was stirred at room temperature for 24 h. It was then diluted with CH_2Cl_2 (3.0 mL) and an internal standard (neopentylbenzene, 0.0579 mmol, 10 μL , 1.16 equiv) was added. An aliquot (~ 0.6 mL) was removed for analysis, and yields were determined by GC.

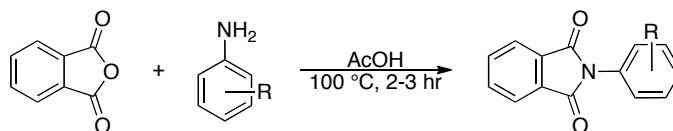


General procedure B: Substrate scope isolation. In a N_2 -filled drybox, trifluoroacetyl N-acyloxyphthalimide (**1**) (0.25 mmol, 65 mg, 1.0 equiv) and $\text{Ir}(\text{ppy})_3$ (0.0125 mmol, 8.0 mg, 0.05 equiv) were weighed into a 4-mL scintillation vial equipped with a micro stir bar. Acetonitrile (2.5 mL, 0.1 M solution **1**) was then added followed by the arene substrate (2.5 mmol, 10.0 equiv). The reaction vial was sealed with a Teflon-lined cap, removed from the N_2 -filled drybox, and placed on a stir-plate. Two 26 W compact fluorescent light bulbs were placed on opposite sides of the vial at approximately 5 cm distance. The reaction mixture was stirred at room temperature for the indicated time.



General Procedure C: Sterically controlled Pd-catalyzed C–H amination reaction.

In a N₂-filled drybox, Pd(OAc)₂ (0.01 mmol, 0.10 equiv), P^{*t*}Bu₃ (0.01 mmol, 0.1 equiv), phthalimide (0.1 mmol, 1 equiv) and PhI(OAc)₂ (0.2 mmol, 2 equiv) were weighed into a 4-mL scintillation vial equipped with a micro stir bar. Naphthalene (1.14 g, 8.90 mmol, 89 equiv) was subsequently added, the vial was then sealed with a Teflon-lined cap, removed from the N₂-filled drybox, and placed in a sand bath preheated to 100 °C on the benchtop and vigorously stirred. At 9 h and 24 h, the reaction was cooled to RT, taken back into the N₂-filled drybox, and more PhI(OAc)₂ (0.2 mmol, 2 equiv) was added at each time point. The reaction was again sealed with a Teflon-lined screwcap, and placed back in the pre-heated sand bath and vigorously stirred at 100 °C for a total of 33 h. The reaction mixture was then cooled down to RT, diluted with EtOAc (1.5 mL), and a GC standard (neopentylbenzene, 10 uL, 0.0579 mmol, 0.56 equiv) was added. An aliquot (~0.8 mL) was removed for analysis, and yields and isomeric ratios were determined based on a calibration curve of authentic samples by GC.

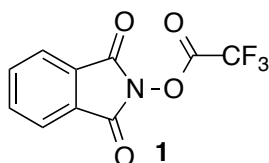


General Procedure D: Synthesis of authentic samples. Phthalic anhydride (60 mg, 0.40 mmol, 1.0 equiv) was added to a 20 mL vial equipped with a magnetic stir bar. Acetic acid (1.00 mL) was added via syringe followed by the appropriate aniline derivative (0.40 mmol, 1.0 equiv). The reaction was heated at 100 °C for 2-3 h, and then the reaction mixture was quenched with water, upon which time a white solid precipitated from solution. The precipitate was collected via vacuum filtration, washed with water, and dried *in vacuo* to give the desired product.

General Procedure E: Synthesis of N-trifluoroacetoxy imides. The corresponding *N*-hydroxyimide (1.0 equiv) was added to an oven-dried Schlenk flask equipped with a

magnetic stir bar, and the flask was evacuated and back-filled with nitrogen. Dry acetonitrile (1 M in N-hydroxyimide) and trifluoroacetic anhydride (2.0 equiv) were then added via syringe, and the mixture was stirred at room temperature for 4 to 6 h. The volatiles were then removed *in vacuo*, and the remaining white solid was dried *in vacuo* for an additional 12 h.

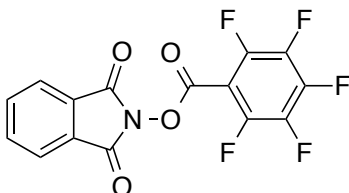
Characterization



N-(trifluoromethyl)acyloxyphthalimide (1): General procedure **E** was followed using N-hydroxyphthalimide (1 g, 6.12 mmol). The product was obtained as a moisture sensitive white solid (1.16 g, 80% yield).

NMR: ^1H NMR (C_6D_6 , 400 MHz): δ 7.09 (dd, $J = 3.2, 5.6$ Hz, 2H), 6.67 (dd, $J = 2.8, 5.6$ Hz, 2H). ^{13}C NMR (C_6D_6 , 175.95 MHz): δ 160.2, 155.3 (q, $J = 45$ Hz), 134.6, 128.5, 124.0, 114.7 (q, $J = 286$ Hz) ^{19}F NMR (C_6D_6 , 400 MHz): δ -72.6.

HRMS EI (m/z): M^+ calcd for $\text{C}_{10}\text{H}_4\text{F}_3\text{NO}_4$: 259.0088; found: 259.0092.



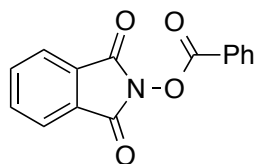
1,3-dioxoisindolin-2-yl 2,3,4,5,6-pentafluorobenzoate (1a):

In a 250 mL round bottom flask equipped with magnetic stir bar was added N-hydroxyphthalimide (4.29 mmol, 700 mg, 1.0 equiv) and dicyclohexylcarbodiimide (4.29 mmol, 885 mg, 1.0 equiv). Ethyl acetate (125 mL) was then added followed by pentafluorobenzoic acid (4.29 mmol, 910 mg, 1.0 equiv) and the reaction was stirred at room temperature, open to air for 3 h, during which time the reaction mixture became cloudy and a white solid precipitated from the solution. The white solid was removed via vacuum filtration and the filtrate was dried with MgSO_4 and further dried *in vacuo* to give the crude product. Recrystallization of the crude solid from hot ethanol provided the pure

substituted N-acyloxyphthalimide. The product was obtained as a white solid (1127 mg, 73% yield).

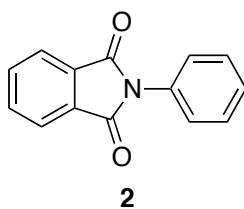
NMR: ^1H NMR (CDCl_3 , 700 MHz): δ 7.94 (dd, $J = 5.6, 2.8$ Hz, 2H), 7.84 (dd, $J = 5.6, 2.8$ Hz, 2H). ^{13}C NMR (CDCl_3 , 175.95 MHz): δ 161.3, 156.1 (m), 147.5-145.8 (m), 145.8-144.2 (m), 139.0-137.3 (m), 135.2, 128.9, 124.4, 103.4 (td, $J = 14, 5$ Hz). ^{19}F NMR (CDCl_3 , 376.87 MHz): δ -132.8 – -132.9 (m), -143.3 (tt, $J = 21, 7$ Hz), -158.8 – -158.9 (m).

HRMS EI (m/z): M^+ calcd for $\text{C}_{15}\text{H}_4\text{F}_5\text{NO}_4$: 357.0060; found: 357.0058. MP: 111-112 °C.



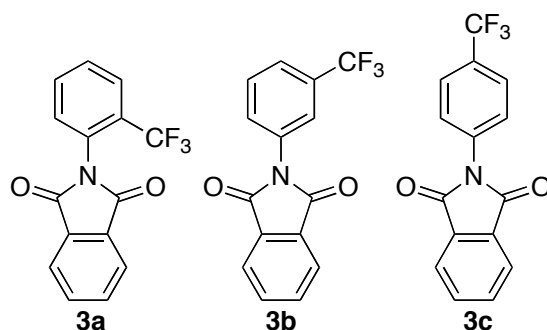
1,3-dioxoisindolin-2-yl benzoate (1b): In a 250 mL round bottom flask equipped with magnetic stir bar was added N-hydroxyphthalimide (4.29 mmol, 700 mg, 1.0 equiv) and dicyclohexylcarbodiimide (4.29 mmol, 885 mg, 1.0 equiv). Ethyl acetate (125 mL) was then added followed by benzoic acid (4.29 mmol, 524 mg, 1.0 equiv) and the reaction was stirred at room temperature, open to air for 3 h, during which time the reaction mixture became cloudy and a white solid precipitated from the solution. The white solid was removed via vacuum filtration and the filtrate was dried with MgSO_4 and further dried *in vacuo* to give the crude product. Recrystallization of the crude solid from hot ethanol provided the pure substituted N-acyloxyphthalimide. The product was obtained as a white solid (805 mg, 70% yield). The structure of **1b** was confirmed by comparison of ^1H and ^{13}C NMR data to that reported in the literature.²⁷

NMR: ^1H NMR (CDCl_3 , 700 MHz): δ 8.21-8.19 (m, 2H), 7.94-7.92 (m, 2H), 7.83-7.80 (m, 2H), 7.70 (tt, $J = 7.7, 1.4$ Hz, 1H), 7.55-7.53 (m, 2H). ^{13}C NMR (CDCl_3 , 175.95 MHz): δ 162.9, 162.2, 135.0, 134.9, 130.8, 129.2, 129.0, 125.4, 124.2.



N-phenylphthalimide (2): General procedure **B** was followed using benzene (2.5 mmol, 195 mg, 0.22 mL) as the arene substrate. After 24 h, the volatiles were removed *in vacuo*, and the crude mixture was purified by column chromatography to afford **2** as a white solid in 76% yield (95 mg). The structure of **2** was confirmed by comparison of ^1H and ^{13}C NMR data to that reported in the literature.²⁸

NMR: ^1H (CDCl_3 , 700 MHz): δ 7.96 (dd, $J = 4.9, 2.8$ Hz, 2H), 7.79 (dd, $J = 4.9, 2.8$ Hz, 2H), 7.51 (t, $J = 7.7$ Hz, 2H), 7.45-7.44 (m, 2H), 7.42-7.40 (m, 1H). ^{13}C NMR (CDCl_3 , 175.95 MHz): δ 167.4, 134.5, 131.9, 131.8, 129.2, 128.2, 126.7, 123.9.



N-(trifluoromethylbenzene)phthalimide (3): General procedure **B** was followed using trifluorotoluene (2.5 mmol, 365 mg, 0.31 mL) as the arene substrate. After 24 h, the volatiles were evaporated *in vacuo* and the crude mixture was purified by column chromatography to give a mixture of **3a**, **3b**, and **3c** as a white solid. The structures of **3a**, **3b**, and **3c** were determined by synthesis of authentic samples (using general procedure **D**). Isomer ratios were determined by ^{19}F NMR spectroscopy.

Isolated Yield: 23% (17 mg, 1.0: 8.4: 2.8)

R_f (isolated mixture of isomers): 0.47 (30% EtOAc/70% hexanes)

IR (ν , cm^{-1}): (isolated mixture of isomers): 2921, 2852, 1708, 1494, 1453, 1375, 1313, 1109, 1062, 875, 804.

HRMS (isolated mixture of isomers): EI (m/z) M^+ calcd for $\text{C}_{15}\text{H}_8\text{F}_3\text{NO}_2$: 291.0507; found: 291.0514.

3a: NMR: ^1H NMR (CDCl_3 , 700 MHz): δ 7.97-7.94 (m, 2H), 7.84 (d, $J = 7.7$ Hz, 1H), 7.82-7.79 (m, 2H), 7.71 (t, $J = 7.7$ Hz, 1H), 7.63 (t, $J = 7.7$ Hz, 1H), 7.37 (d, $J = 7.7$ Hz, 1H). ^{13}C NMR (CDCl_3 , 175.95 MHz): δ 167.2, 134.6, 133.3, 132.0, 131.8, 130.2, 129.9 (q, $J = 2$ Hz), 129.7 (q, $J = 31$ Hz), 127.7 (q, $J = 5$ Hz), 124.1, 123.1 (q, $J = 273$ Hz), ^{19}F NMR (CDCl_3 , 376.87 MHz): δ -61.42 (s).

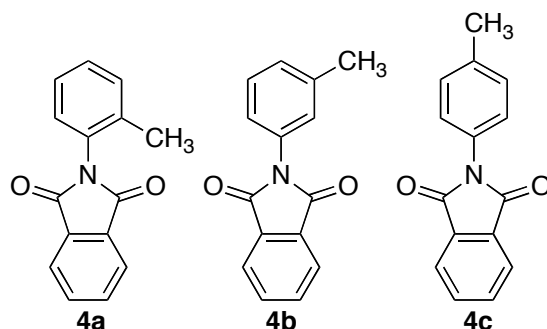
mp: 103-105 °C.

3b: NMR: ^1H NMR (CDCl_3 , 700 MHz): δ 8.00-7.97 (m, 2H), 7.84-7.78 (m, 2H), 7.78 (br s, 1H), 7.67 (m, 3H). ^{13}C NMR (CDCl_3 , 175.95 MHz): δ 167.1, 135.1, 132.7, 132.0 (q, $J = 33$ Hz), 131.8, 130.0, 129.9, 125.0 (q, $J = 4$ Hz), 124.3, 123.9 (q, $J = 273$ Hz), 123.7 (q, $J = 4$ Hz). ^{19}F NMR (CDCl_3 , 376.87 MHz): δ -62.69 (s).

mp: 84-87 °C.

3c: NMR: ^1H NMR (CDCl_3 , 700 MHz): δ 8.00-7.97 (m, 2H), 7.84-7.81 (m, 2H), 7.78 (d, $J = 8.4$ Hz, 2H), 7.65 (d, $J = 8.4$ Hz, 2H). ^{13}C NMR (CDCl_3 , 175.95 MHz): δ 166.9, 135.1, 134.9, 131.7, 130.0 (q, $J = 33$ Hz), 126.6, 126.4 (q, $J = 4$ Hz), 124.2, 124.0 (q, $J = 272$ Hz). ^{19}F NMR (CDCl_3 , 470.56 MHz): δ -62.66 (s).

mp: 216-218 °C.



N-(tolyl)phthalimide (4): General procedure **B** was followed using toluene (2.5 mmol, 230 mg, 0.27 mL) as the arene substrate. After 24 h, the volatiles were evaporated *in vacuo* and the crude mixture was purified by column chromatography to give a mixture of **4a**, **4b**, and **4c** as a white solid. The structures of **4a**, **4b**, and **4c** were confirmed by synthesis of authentic samples (using general procedure **D**) and isomer ratios were determined by ^1H NMR spectroscopy.

Isolated Yield: 80% (47 mg, 2.0: 1.0: 1.2)

R_f (isolated mixture of isomers): 0.77 (30% EtOAc/70% hexanes)

IR (ν , cm^{-1}): (isolated mixture of isomers): 1708, 1465, 1377, 1110, 1080, 884, 770, 715.

HRMS (isolated mixture of isomers): EI (m/z) M^+ calcd for $C_{15}H_{11}NO_2$: 237.0790; found: 237.0793.

4a: NMR: 1H NMR ($CDCl_3$, 700 MHz): δ 7.96 (dd, $J = 4.9, 2.8$ Hz, 2H), 7.80 (dd, $J = 4.9, 2.8$ Hz, 2H), 7.38-7.32 (m, 3H), 7.21 (d, $J = 7.7$ Hz) 2.22 (s, 3H). ^{13}C NMR ($CDCl_3$, 175.95 MHz): δ 167.5, 136.7, 134.5, 132.2, 131.3, 130.7, 129.6, 128.9, 127.0, 123.9, 18.2.

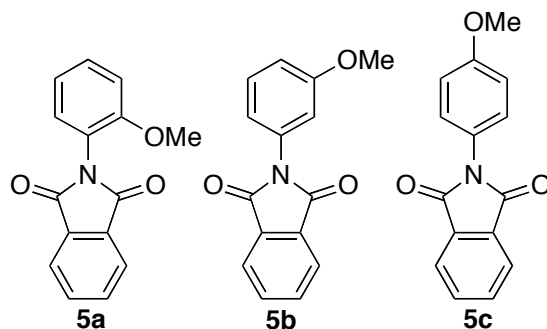
mp: 151-152 °C.

4b: NMR: 1H NMR ($CDCl_3$, 700 MHz): δ 7.96-7.95 (m, 2H), 7.79-7.78 (m, 2H), 7.40 (t, $J = 7.7$ Hz, 1H), 7.24-7.22 (m, 3H), 2.42 (s, 3H). ^{13}C NMR ($CDCl_3$, 175.95 MHz): δ 167.5, 139.3, 134.5, 131.9, 131.6, 129.2, 129.1, 127.4, 123.9, 123.8, 21.6.

mp: 146-147 °C.

4c: NMR: 1H NMR ($CDCl_3$, 700 MHz): δ 7.96-7.94 (m, 2H), 7.80-7.77 (m, 2H), 7.31 (s, 4H), 2.41 (s, 3H). ^{13}C NMR ($CDCl_3$, 175.95 MHz): δ 167.6, 138.3, 134.5, 132.0, 129.9, 129.1, 126.6, 123.8, 21.4.

mp: 173-175 °C.



N-(methoxybenzene)phthalimide (5): General procedure **B** was followed using anisole (2.5 mmol, 270 mg, 0.27 mL) as the arene substrate. After 24 h, the volatiles were evaporated *in vacuo* and the crude mixture was purified by column chromatography to give a mixture of **5a**, **5b**, and **5c** as a white solid. The structures of **5a**, **5b**, and **5c** were confirmed by synthesis of authentic samples (using general procedure **D**) and isomer ratios were determined by 1H NMR spectroscopy.

Isolated Yield: 81% (51 mg, 12: 1: 10.3)

R_f (isolated mixture of isomers): 0.54 (100% CH_2Cl_2)

IR (ν , cm^{-1}); (isolated mixture of isomers): 1703, 1505, 1384, 1251, 1113, 1021, 883, 768, 712.

HRMS: EI (m/z); (isolated mixture of isomers): M^+ calcd for $\text{C}_{15}\text{H}_{11}\text{NO}_3$: 253.0739; found: 253.0746

5a: NMR: ^1H NMR (CDCl_3 , 700 MHz): δ 7.95 (dd, $J = 5.6, 2.8$ Hz, 2H), 7.78 (dd, $J = 5.6, 2.8$ Hz, 2H), 7.45-7.43 (m, 1H), 7.26 (dd, $J = 7.7, 1.4$ Hz, 1H), 7.08 (td, $J = 7.7, 1.4$ Hz, 1H), 7.05-7.06 (m, 1H), 3.80 (s, 3H). ^{13}C NMR (CDCl_3 , 175.95 MHz): δ 167.5, 155.6, 134.2, 132.4, 130.8, 130.1, 123.8, 121.0, 120.4, 112.3, 56.0.

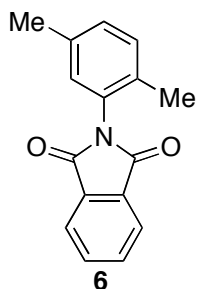
mp: 129-130 $^\circ\text{C}$.

5b: NMR: ^1H NMR (CDCl_3 , 700 MHz): δ 7.96 (dd, $J = 5.6, 2.8$ Hz, 2H), 7.80 (dd, $J = 5.6, 2.8$ Hz, 2H), 7.41 (t, $J = 7.7$ Hz, 1H), 7.03 (ddd, $J = 7.7, 2.1, 0.7$ Hz, 1H), 6.99 (t, $J = 2.1$ Hz, 1H) 6.96 (ddd, $J = 7.7, 2.1, 0.7$ Hz, 1H), 3.84 (s, 3H). ^{13}C NMR (CDCl_3 , 175.95 MHz): δ 167.4, 160.2, 134.6, 132.8, 131.9, 130.0, 123.9, 119.0, 114.3, 112.5, 55.6.

mp: 92-94 $^\circ\text{C}$.

5c: NMR: ^1H NMR (CDCl_3 , 700 MHz): δ 7.95 (dd, $J = 5.6, 2.8$ Hz, 2H), 7.78 (dd, $J = 5.6, 2.8$ Hz, 2H), 7.34-7.33 (m, 2H), 7.03-7.01 (m, 2H), 3.85 (s, 3H). ^{13}C NMR (CDCl_3 , 175.95 MHz): δ 167.7, 159.4, 134.4, 132.0, 128.1, 124.4, 123.8, 114.6, 55.7.

mp: 131-132 $^\circ\text{C}$.



1-N-phthalimido-2,4-dimethylbenzene (6): General procedure **B** was followed using 1,4-dimethylbenzene (2.5 mmol, 265 mg, 0.31 mL) as the arene substrate. After 24 h, the reaction was diluted with EtOAc, and triethylamine (1 mL) was added to quench trifluoroacetic acid. The reaction mixture was concentrated *in vacuo*, and the residue was purified via column chromatography. The crude product was dissolved in EtOAc (~10 mL) and washed with 2M NaOH (3 x 10 mL). The organic layer was dried over Na_2SO_4 , and the volatiles were evaporated *in vacuo* to give **6** as a white solid.

Isolated Yield: 88% (55 mg)

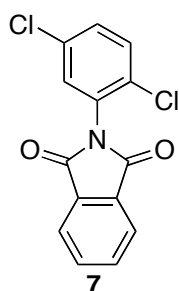
R_f: 0.52 (50% hexane/50% Et₂O)

IR (ν , cm⁻¹): 2921, 2851, 1716, 1507, 1370, 1238, 1112, 1082, 873, 819, 717.

mp: 137-139 °C

HRMS: ESI⁺ (m/z): [M+H]⁺ calcd for C₁₆H₁₄NO₂: 252.1019; found: 252.1016.

NMR: ¹H (CDCl₃, 700 MHz): δ 7.97-7.94 (m, 2H), 7.80-7.77 (m, 2H), 7.25 (d, *J* = 7.7 Hz, 1H), 7.18 (dd, *J* = 7.7, 1.4 Hz, 1H), 7.03 (s, 1H), 2.36 (s, 3H), 2.16 (s, 3H). ¹³C NMR (CDCl₃, 175.95 MHz): δ 167.5, 136.8, 134.4, 133.4, 132.2, 131.0, 130.5, 130.4, 129.3, 123.8, 20.9, 17.6.



1-N-phthalimido-2,4-dichlorobenzene (7): General procedure **B** was followed using 1,4-dichlorobenzene (2.5 mmol, 370 mg) as the arene substrate. After 24 h, the reaction was diluted with EtOAc, and triethylamine (1 mL) was added to quench trifluoroacetic acid. The reaction mixture was concentrated *in vacuo*, and the residue was purified via column chromatography, followed by diluting the product in EtOAc (10 mL) and washing with 2M NaOH (3 x 10 mL). The organic layer was dried over Na₂SO₄, and the volatiles were evaporated *in vacuo* to give **7** as a white solid.

Isolated Yield: 40% (29 mg)

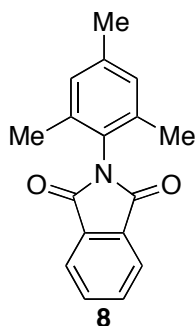
R_f: 0.41 (25% EtOAc/75% hexanes)

IR (ν , cm⁻¹): 1719, 1473, 1412, 1217, 1094, 1078, 864, 815, 710.

mp: 177-179 °C

HRMS: ESI⁺ (m/z) [M+H]⁺ calcd for C₁₄H₈Cl₂NO₂: 291.9927; found: 291.9923

NMR: ¹H (CDCl₃, 700 MHz): δ 8.00-7.97 (m, 2H), 7.84-7.81 (m, 2H), 7.51 (d, *J* = 8.4 Hz, 1H), 7.42 (dd, *J* = 8.4, 2.8 Hz, 1H), 7.37 (d, *J* = 2.8 Hz, 1H). ¹³C NMR (CDCl₃, 175.95 MHz): δ 166.3, 134.8, 133.3, 131.9, 131.9, 131.3, 130.9, 130.9, 130.8, 124.3.



1-N-phthalimido-2,4,6-trimethylbenzene (8): General procedure **B** was followed using 1,3,5-trimethylbenzene (2.5 mmol, 300 mg, 0.35 mL) as the arene substrate. After 24 h, the reaction was diluted with EtOAc and triethylamine (1 mL) was added to quench trifluoroacetic acid. The reaction mixture was concentrated *in vacuo*, and the residue was purified via column chromatography to give **8** as a white solid.

Isolated Yield: 89% (59 mg)

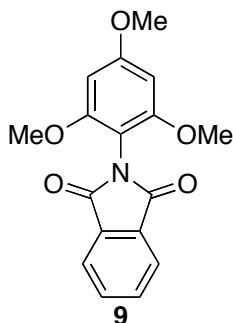
R_f: 0.48 (25% EtOAc/75% hexanes)

IR (ν, cm⁻¹): 2919, 1718, 1489, 1464, 1375, 1113, 1038, 882, 852.

mp: 154-156 °C

HRMS: ESI⁺(m/z): [M+H]⁺ calcd for C₁₇H₁₆NO₂: 266.1176; found: 266.1172

NMR: ¹H (CDCl₃, 700 MHz): δ 7.97-7.96 (m, 2H), 7.80-7.79 (m, 2H), 7.01 (s, 2H), 2.34 (s, 3H), 2.13 (s, 6H). ¹³C NMR (CDCl₃, 175.95 MHz): δ 167.5, 139.4, 136.6, 134.4, 132.1, 129.4, 127.2, 123.8, 21.2, 18.1.



1-N-phthalimido-2,4,6-trimethoxybenzene (9): General procedure **B** was followed using 1,3,5-trimethoxybenzene (2.5 mmol, 420 mg) as the arene substrate. After 24 h, the volatiles were evaporated *in vacuo* and the crude mixture was purified by column chromatography to give **9** as a light yellow crystalline solid.

Isolated Yield: 73% (57 mg)

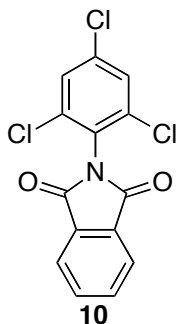
R_f: 0.24 (30% EtOAc/70% hexanes)

IR (ν , cm^{-1}): 2922, 1785, 1731, 1711, 1591, 1515, 1463, 1423, 1388, 1341, 1239, 1206, 1164, 1130, 1104, 1084, 1033, 946, 882, 817, 716.

mp: 195-196 °C

HRMS: EI (m/z) M^+ calcd for $\text{C}_{17}\text{H}_{15}\text{NO}_5$: 313.0950; found: 313.0946.

NMR: ^1H (CDCl_3 , 700 MHz): δ 7.92-7.89 (m, 2H), 7.75-7.72 (m, 2H), 6.21 (s, 2H), 3.83 (s, 3H), 3.74 (s, 6H). ^{13}C NMR (CDCl_3 , 175.95 MHz): δ 167.8, 162.2, 157.7, 133.9, 132.6, 123.5, 101.8, 91.2, 56.1, 55.6.



1-N-phthalimido-2,4,5-trichlorobenzene (10): General procedure **B** was followed using 1,3,5-trichlorobenzene (2.5 mmol, 454 mg) as the arene substrate. After 24 h, the volatiles were evaporated *in vacuo* and the crude mixture was purified by column chromatography to give **10** as a white solid.

Isolated Yield: 42% (34 mg)

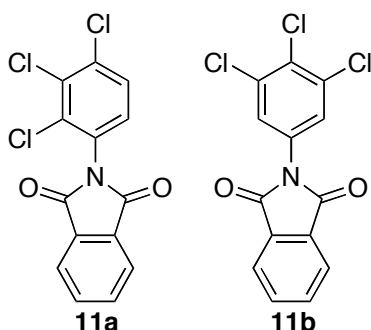
R_f: 0.65 (30% EtOAc/70% Hexanes)

IR (ν , cm^{-1}): 3085, 2926, 1723, 1555, 1466, 1364, 1224, 1100, 872, 788.

mp: 146-147 °C

HRMS: EI (m/z): M^+ calcd for $\text{C}_{14}\text{H}_6\text{Cl}_3\text{NO}_2$: 324.9464; found: 324.9464.

NMR: ^1H (CDCl_3 , 700 MHz): δ 8.00-7.98 (m, 2H), 7.85-7.82 (m, 2H), 7.51 (s, 2H). ^{13}C NMR (CDCl_3 , 175.95 MHz): 165.6, 136.6, 136.3, 134.9, 131.9, 128.9, 127.2, 124.4.



N-(1,2,3-trichlorobenzene)phthalimide (11): General procedure **B** was followed using 1,2,3-trichlorobenzene (2.5 mmol, 454 mg) as the arene substrate. After 24 h, the volatiles were evaporated *in vacuo* and the crude mixture was purified by column chromatography to give to give **11a** and **11b** as white solids (57% total yield; 5.4: 1). The regioisomeric ratio was determined by the amount of **11a** and **11b** separated by column chromatography.

11a:

Isolated yield: 48% (39 mg)

R_f: 0.47 (30% Ethyl Acetate, 70% hexanes)

IR (ν, cm⁻¹): 1716, 1451, 1373, 1097, 881, 823, 791, 709.

mp: 176-177 °C.

HRMS: EI (m/z): M⁺ calcd for C₁₄H₆Cl₃NO₂: 324.9464; found: 324.9464.

NMR: ¹H NMR (CDCl₃, 700 MHz): δ 7.98 (dd, *J* = 5.6, 2.8 Hz, 2H), 7.83 (dd, *J* = 5.6, 2.8 Hz, 2H), 7.54 (d, *J* = 8.4 Hz, 1H), 7.24 (d, *J* = 8.4 Hz, 1H). ¹³C NMR (CDCl₃, 175.95 MHz): δ 166.3, 135.7, 134.9, 134.2, 133.4, 131.8, 129.9, 128.9, 128.8, 124.3.

11b:

Isolated yield: 9% (7 mg)

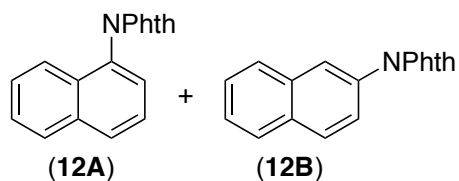
R_f: 0.50 (30% Ethyl Acetate, 70% Hexane)

mp: 207-209 °C

IR (ν, cm⁻¹): 1719, 1589, 1555, 1439, 1376, 1227, 1163, 1095, 1081, 857, 787, 709.

HRMS EI (m/z): M⁺ calcd for C₁₄H₆Cl₃NO₂: 324.9464; found: 324.9461.

NMR: ¹H NMR (CDCl₃, 700 MHz): δ 7.98 (dd, *J* = 5.6, 3.5 Hz, 2H), 7.83 (dd, *J* = 5.6, 3.5 Hz, 2H) 7.62 (s, 2H). ¹³C NMR (CDCl₃, 175.95 MHz): δ 166.4, 135.1, 134.6, 131.3, 131.2, 131.0, 126.4, 124.3.



N-Phthalimidonaphthalene (12): General procedure **B** was followed using naphthalene (2.5 mmol, 320 mg) as the arene substrate. After 24 h, the reaction was diluted with EtOAc, and triethylamine (1 mL) was added to quench trifluoroacetic acid. The reaction mixture was concentrated *in vacuo*, and the residue was purified via column chromatography. The product was further purified by dissolving it in EtOAc (~10 mL) and washing with 2M NaOH (3 x 10 mL). The organic layer was dried over Na₂SO₄, and the volatiles were evaporated *in vacuo* to give a mixture of **12a** and **12b** as a white solid. The structures of **12a** and **12b** were confirmed by synthesis of authentic samples (using general procedure **D**) and isomer ratios were determined by ¹H NMR spectroscopy

Crude ratio: 7.1 : 1.0 (GC)

Isolated Yield: 79% (54 mg, 4.6 : 1 by ¹H NMR)

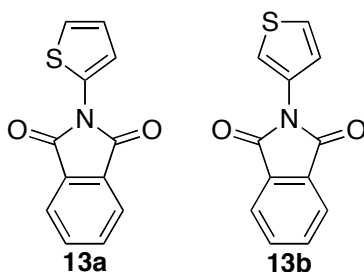
R_f (isolated mixture of isomers): 0.41 (25% EtOAc/75% hexanes)

IR (ν, cm⁻¹); (isolated mixture of isomers): 1707, 1540, 1466, 1401, 1374, 1108, 1084.

HRMS; (isolated mixture of isomers): ESI⁺ (m/z) [M+H]⁺ calcd for C₁₈H₁₂NO₂: 274.0863; found: 274.0860

NMR: 12a: ¹H NMR (CDCl₃, 700 MHz): δ 8.03-8.02 (m, 2H), 8.00 (d, *J* = 8.4 Hz, 1H), 7.96 (d, *J* = 8.4 Hz, 1H), 7.85-7.84 (m, 2H), 7.63-7.59 (m, 2H), 7.55-7.47 (multiple peaks, 3H). ¹³C NMR (CDCl₃, 175.95 MHz): δ 167.9, 134.6, 134.6, 132.2, 130.4, 130.1, 129.7, 128.3, 127.3, 127.1, 126.7, 125.6, 124.1, 122.6.

12b: ¹H NMR (CDCl₃, 700 MHz): δ 8.00-7.98 (multiple peaks, 3H), 7.95 (d, *J* = 1.4 Hz, 1H), 7.91-7.89 (m, 2H), 7.83-7.80 (m, 2H), 7.56-7.52 (multiple peaks, 3H). ¹³C NMR (CDCl₃, 175.95 MHz): δ 167.6, 134.6, 133.4, 132.7, 131.9, 129.2, 129.1, 128.4, 127.9, 126.8, 126.7, 125.7, 124.3, 123.9



N-Phthalimidothiophene (13): General procedure **B** was followed using thiophene (2.5 mmol, 210 mg, 0.20 mL) as the arene substrate. After 24 h, the volatiles were evaporated *in vacuo* and the crude mixture was purified by column chromatography to give a mixture of **13a** and **13b** as a yellow solid.

Isolated Yield: 69% (40 mg, 4.6 : 1)

R_f; (isolated mixture of isomers): 0.50 (30% EtOAc/70% Hexanes)

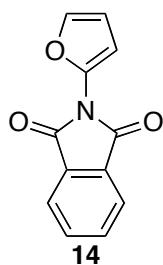
IR (ν , cm^{-1}); (isolated mixture of isomers): 3114, 2921, 1710, 1529, 1446, 1375, 1323, 1243, 1108, 1061, 882, 779, 677

mp (isolated mixture of isomers): 162-164 °C

HRMS (isolated mixture of isomers): ESI⁺ (m/z) [M+H]⁺ calcd for C₁₂H₈NO₂S: 230.0270; found: 230.0265.

NMR: 13a: ¹H NMR (CDCl₃, 700 MHz): δ 7.95-7.93 (m, 2H), 7.78-7.77 (m, 2H), 7.53 (dd, J = 5.2, 1.4 Hz, 1H), 7.22 (dd, J = 5.5, 1.4 Hz, 1H), 7.06 (dd, J = 5.5, 3.8 Hz, 1H).

¹³C NMR (CDCl₃, 175.95 MHz): δ 166.1, 134.8, 132.4, 131.5, 125.4, 124.0, 122.0, 120.5.



2-N-Phthalimidofuran (14): General procedure **B** was followed using furan (2.5 mmol, 170 mg, 0.18 mL) as the arene substrate. After 24 h, the volatiles were evaporated *in vacuo* and the crude mixture was purified by column chromatography to give **14** as a white solid.

Isolated Yield: 51% (27 mg)

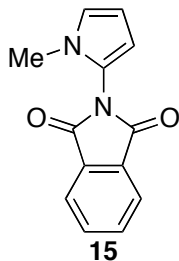
R_f: 0.57 (25% EtOAc/75% hexanes)

IR (ν , cm^{-1}): 1728, 1603, 1497, 1388, 1222, 1152, 1082, 882, 713.

mp: 162-164 °C

HRMS: ESI⁺ (m/z) [M+H]⁺ calcd for C₁₂H₈NO₃: 214.0499; found: 214.0489

NMR: ¹H NMR (CDCl₃, 700 MHz): δ 7.99-7.96 (m, 2H), 7.83-7.80 (m, 2H), 7.47 (dd, *J* = 1.4, 2.1 Hz, 1H), 6.55 (dd, *J* = 2.1, 3.5 Hz, 1H), 6.46 (dd, *J* = 1.4, 3.5 Hz, 1H) ¹³C NMR (CDCl₃, 175.95 MHz): δ 166.3, 141.8, 138.0, 134.9, 131.7, 124.3, 111.6, 106.8.



1-methyl-2-N-phthalimidopyrrole (15): General procedure **B** was followed using N-methylpyrrole (2.5 mmol, 203 mg, 0.22 mL) as the arene substrate. After 24 h, the volatiles were evaporated *in vacuo* and the crude mixture was purified by column chromatography to give **15** as a white solid.

Isolated Yield: 51% (28 mg)

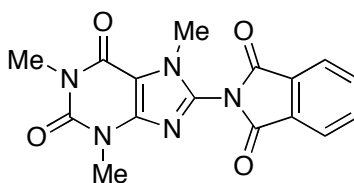
R_f: 0.35 (30% EtOAc/70% hexanes)

IR (ν , cm^{-1}): 2162, 1718, 1553, 1496, 1369, 1291, 1237, 1080, 880, 798.

mp: 172-173 °C

HRMS: ESI⁺ (m/z): [M+H]⁺ calcd for C₁₃H₁₁N₂O₂: 227.0815; found: 227.0815

NMR: ¹H (CDCl₃, 400 MHz): δ 7.99-7.95 (m, 2H), 7.84-7.79 (m, 2H), 6.72 (dd, *J* = 2.8, 2.1 Hz, 1H), 6.24 (dd, *J* = 4.2, 2.8 Hz, 1H), 6.20 (dd, *J* = 4.2, 2.1 Hz, 1H), 3.48 (s, 3H). ¹³C NMR (CDCl₃, 175.9 MHz): δ 167.8, 134.7, 131.9, 124.1, 122.3, 118.7, 107.7, 107.7, 33.4.



16

8-(N-phthalimido)caffeine (16): General procedure **B** was followed using caffeine (2.5 mmol, 486 mg) as the arene substrate. After 24 h, the reaction was diluted with EtOAc, and triethylamine (1 mL) was added to quench trifluoroacetic acid. The reaction mixture was concentrated *in vacuo*, and the residue was purified via column chromatography. The product was further purified by recrystallization from CHCl₃/Et₂O to give **16** as a white solid.

Isolated Yield: 45% (38 mg)

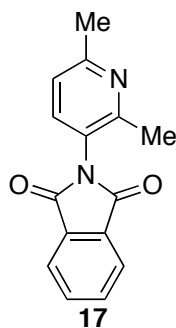
R_f: 0.44 (100% Et₂O)

IR (ν, cm⁻¹): 1734, 1706, 1654, 1506, 1445, 1221, 1055, 1033, 879, 717.

mp: 228-229 °C

HRMS: ESI⁺ (m/z) [M+H]⁺ calcd for C₁₆H₁₄N₅O₄: 340.1040; found: 340.1033.

NMR: ¹H NMR (CDCl₃, 700 MHz): δ 8.02 (dd, *J* = 5.6, 2.8 Hz, 2H), 7.89 (dd, *J* = 5.6, 2.8 Hz, 2H), 3.90 (s, 3H), 3.59 (s, 3H), 3.44 (s, 3H). ¹³C NMR (CDCl₃, 175.95 MHz): δ 165.6, 153.4, 151.6, 147.0, 137.1, 135.6, 131.6, 124.9, 108.3, 32.5, 30.1, 28.2.



17

2,6-dimethyl-3-(N-phthalimido)pyridine (17): General procedure **B** was followed using 2,6-dimethylpyridine (2.5 mmol, 268 mg, 0.29 mL) as the arene substrate. After 24 h, the reaction was diluted with EtOAc, and triethylamine (1 mL) was added to quench trifluoroacetic acid. The volatiles were evaporated *in vacuo* and the crude mixture was purified by column chromatography to give **17** as a light brown solid.

Isolated Yield: 71% (34 mg)

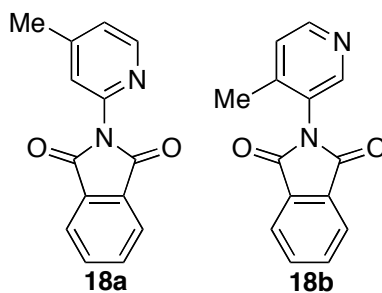
R_f: 0.33 (20% NEt₃/20% EtOAc/60% hexanes)

IR (ν , cm⁻¹): 2922, 2851, 1723, 1578, 1464, 1373, 1226, 1106, 885, 720

mp: 160-161 °C

HRMS: ESI⁺ (m/z) [M+H]⁺ calcd for C₁₅H₁₃N₂O₂: 253.0972; found: 253.0970

NMR: ¹H NMR (CDCl₃, 700 MHz): δ 7.96 (dd, *J* = 5.6, 3.5 Hz, 2H), 7.81 (dd, *J* = 5.6, 3.5 Hz, 2H), 7.41 (d, *J* = 8.4 Hz, 1H), 7.14 (d, *J* = 8.4 Hz, 1H), 2.60 (s, 3H), 2.41 (s, 3H). ¹³C NMR (CDCl₃, 175.95 MHz): δ 167.1, 159.2, 156.1, 136.8, 134.7, 132.1, 124.4, 124.1, 121.6, 24.5, 21.4.



N-Phthalimido-4-picoline (18): General procedure **B** was followed using 4-methylpyridine (2.5 mmol, 233 mg, 0.24 mL) as the arene substrate. After 24 h, the reaction was diluted with EtOAc, and triethylamine (1 mL) was added to quench trifluoroacetic acid. The reaction mixture was concentrated *in vacuo* and the residue was purified via column chromatography to give a mixture of **18a** and **18b** as a light brown solid. The structures of **18a** and **18b** were confirmed by synthesis of authentic samples (using general procedure **D**) and isomer ratios were determined by ¹H NMR spectroscopy.

Crude ratio: 1.0 : 7.2 (GC)

Isolated Yield: 57% (34 mg; 1: >20 ¹H NMR)

R_f (isolated mixture of isomers): 0.26 (20% NEt₃/20% EtOAc/60% hexanes)

IR (ν , cm⁻¹) (isolated mixture of isomers): 2924, 1709, 1598, 1502, 1422, 1378, 1240, 1080, 843, 708.

mp (isolated mixture of isomers): 147-149 °C

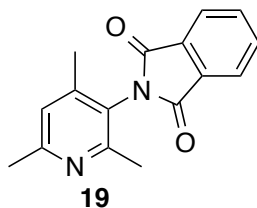
HRMS (isolated mixture of isomers) ESI⁺ (m/z): [M+H]⁺ calcd for C₁₄H₁₁N₂O₂: 239.0815; found: 239.0820.

18a: NMR: ^1H NMR (CDCl_3 , 700 MHz): δ 8.54 (d, $J = 4.9$ Hz, 1H), 7.98-7.96 (m, 2H), 7.81-7.79 (m, 2H), 7.25 (s, 1H), 7.19 (d, $J = 4.9$ Hz, 1H), 2.45 (s, 3H). ^{13}C NMR (CDCl_3 , 175.95 MHz): δ 166.9, 150.1, 149.4, 146.2, 134.7, 131.9, 124.7, 124.1, 123.0, 21.2.

mp: 145-146 °C

18b: NMR: ^1H NMR (CDCl_3 , 700 MHz): δ 8.55 (d, $J = 4.9$ Hz, 1H), 8.44 (s, 1H), 7.99-7.96 (m, 2H), 7.84-7.82 (m, 2H), 7.31 (d, $J = 4.9$ Hz, 1H), 2.25 (s, 3H) ^{13}C NMR (CDCl_3 , 175.95 MHz): δ 167.1, 150.2, 149.6, 146.1, 134.8, 132.0, 128.2, 125.9, 124.2, 18.0.

mp: 147-148 °C



2,4,6-trimethyl-3-(N-phthalimido)pyridine (19): General procedure **B** was followed using 2,4,6-trimethylpyridine (2.5 mmol, 302 mg, 0.33 mL) as the arene substrate. After 24 h, the reaction was diluted with EtOAc, and triethylamine (1 mL) was added to quench trifluoroacetic acid. The reaction mixture was concentrated *in vacuo* and the residue was purified via column chromatography to give **19** as a white solid.

Isolated Yield: 66 % (44 mg)

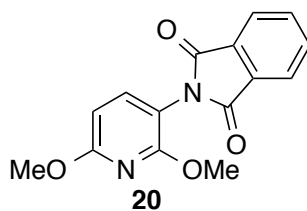
R_f: 0.45 (20% NEt_3 /20% EtOAc/60% hexanes)

IR (v, cm^{-1}): 2925, 2361, 1723, 1603, 1466, 1373, 1112, 866, 716.

mp: 112-113 °C

HRMS: ESI^+ (m/z) [$\text{M}+\text{H}$] $^+$ calcd for $\text{C}_{16}\text{H}_{14}\text{N}_2\text{O}_2$: 267.1128; found: 267.1132

NMR: ^1H NMR (CDCl_3 , 700 MHz): δ 7.97-7.95 (m, 2H), 7.83-7.80 (m, 2H), 7.00 (s, 1H), 2.53 (s, 3H), 2.35 (s, 3H), 2.12 (s, 3H). ^{13}C NMR (CDCl_3 , 175.95 MHz): δ 167.0, 158.8, 156.3, 146.4, 134.7, 132.0, 124.1, 124.0, 123.3, 24.3, 21.1, 17.8.



2,6-dimethoxy-3-(N-phthalimido)pyridine (20): General procedure **B** was followed using 2,6-dimethoxypyridine (2.5 mmol, 348 mg, 0.33 mL) as the arene substrate. After 24 h, the reaction was diluted with EtOAc, and triethylamine (1 mL) was added to quench trifluoroacetic acid. The reaction mixture was concentrated *in vacuo* and the residue was purified via column chromatography. The product was further purified by dissolving in DCM (~15 mL) and washing with 1M NaOH (3 x 6 mL). The organic layer was dried over Na₂SO₄, and the volatiles were evaporated *in vacuo* to give **20** as a white solid.

Isolated Yield: 79 % (56 mg)

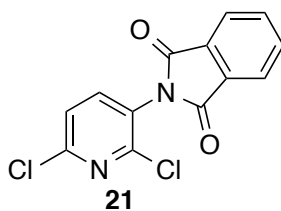
R_f: 0.63 (20% NEt₃/20% EtOAc/60% hexanes)

IR (ν, cm⁻¹): 2952, 2361, 1732, 1705, 1586, 1392, 1315, 1084, 1008, 880, 721

mp: 159-160 °C

HRMS: ESI⁺ (m/z) [M+H]⁺ calcd for C₁₅H₁₂N₂O₄: 285.0870; found: 285.0860

NMR: ¹H NMR (CDCl₃, 700 MHz): δ 7.95-7.92 (m, 2H), 7.79-7.77 (m, 2H), 7.45 (d, *J* = 8.4 Hz, 1H), 6.43 (d, *J* = 8.4 Hz, 1H), 3.96 (s, 3H), 3.92 (s, 3H). ¹³C NMR (CDCl₃, 175.95 MHz): δ 167.5, 163.4, 158.6, 141.0, 134.3, 132.3, 123.9, 106.6, 101.8, 54.1, 54.0.



2,6-dichloro-3-(N-phthalimido)pyridine (21): A modification from general procedure **B** was followed using 2,6-dichloropyridine (5 mmol, 740 mg, 20 equiv) as the arene substrate and acetonitrile (1.25 mL, 0.2 M solution **1**). After 24 h, the reaction was diluted with EtOAc, and triethylamine (1 mL) was added to quench trifluoroacetic acid. The reaction mixture was concentrated *in vacuo* and the residue was purified via column chromatography. The product was further purified by dissolving in DCM (~15 mL) and washing with 1M NaOH (3 x 6 mL). The organic layer was dried over Na₂SO₄, and the volatiles were evaporated *in vacuo* to give **21** as a light brown solid.

Isolated Yield: 51 % (38 mg)

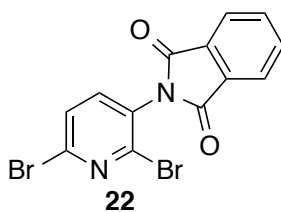
R_f: 0.36 (20% NEt₃/20% EtOAc/60% hexanes)

IR (ν, cm⁻¹): 2922, 2852, 1790, 1721, 1552, 1442, 1377, 1140, 1080, 826, 710

mp: 115-117 °C

HRMS: ESI⁺ (m/z) [M+H]⁺ calcd for C₁₃H₆Cl₂N₂O₂: 292.9879; found: 292.9879

NMR: ¹H NMR (CDCl₃, 700 MHz): δ 8.00-7.97 (m, 2H), 7.86-7.83 (m, 2H), 7.67 (d, *J* = 7.7 Hz, 1H), 7.45 (d, *J* = 7.7 Hz, 1H). ¹³C NMR (CDCl₃, 175.95 MHz): δ 166.0, 151.0, 149.6, 141.4, 135.0, 131.8, 126.0, 124.4, 124.0.



2,6-dibromo-3-(N-phthalimido)pyridine (22): A modification from general procedure **B** was followed using 2,6-dibromopyridine (5 mmol, 1.18 g, 20 equiv) as the arene substrate and acetonitrile (1.25 mL, 0.2 M in **1**). After 24 h, the reaction was diluted with EtOAc, and triethylamine (1 mL) was added to quench trifluoroacetic acid. The reaction mixture was concentrated *in vacuo* and the residue was purified via column chromatography. The crude product was dissolved in DCM (~15 mL) and washed with

1M NaOH (3 x 6 mL). The organic layer was dried over Na₂SO₄, and the volatiles were evaporated *in vacuo* to give **22** as a light brown solid.

Isolated Yield: 32 % (30 mg)

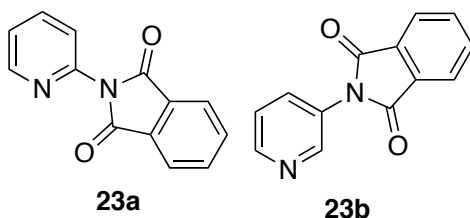
R_f: 0.36 (20% NEt₃/20% EtOAc/60% hexanes)

IR (ν, cm⁻¹): 2922, 2852, 1745, 1718, 1432, 1374, 1340, 1112, 1083, 855, 712.

mp: 157-159 °C

HRMS: ESI⁺ (m/z) [M+H]⁺ calcd for C₁₃H₆Br₂N₂O₂: 380.8869; found: 380.8859

NMR: ¹H NMR (CDCl₃, 700 MHz): δ 8.00-7.98 (m, 2H), 7.86-7.83 (m, 2H), 7.62 (d, *J* = 7.7 Hz, 1H), 7.50 (d, *J* = 7.7 Hz, 1H). ¹³C NMR (CDCl₃, 175.95 MHz): δ 166.0, 142.1, 141.2, 140.7, 135.1, 131.8, 129.0, 128.1, 124.4.



N-phthalimidopyridine (23): A modification from general procedure **B** was followed using pyridine (5 mmol, 393 mg, 0.40 mL, 20 equiv) as the arene substrate and acetonitrile (1.25 mL, 0.2 M solution **1**). After 24 h, the reaction was diluted with EtOAc, and triethylamine (1 mL) was added to quench trifluoroacetic acid. The reaction mixture was concentrated *in vacuo* and the residue was run through a plug of silica gel (~250 mL, 1:1:3 v/v, Et₃N:EtOAc:Hex). The mixture of products were further purified by dissolving in DCM (~15 mL) and washing with 1M NaOH (3 x 6 mL). The organic layer was dried over Na₂SO₄, and the volatiles were evaporated *in vacuo* to give a mixture of **23a** and **23b**. Isomer ratios were determined by ¹H NMR spectroscopy. The product mixture was separated via silica gel column chromatography to afford **23a** as a light yellow solid and **23b** as a white solid.

¹H NMR ratio (mixture of isolated products): 1 : 2

Isolated Yield (total of **23a** & **23b**): 41 % (23 mg)

23a:

R_f: 0.63 (50% DCM/50% Et₂O)

IR (ν, cm⁻¹): 2919, 2850, 1709, 1585, 1464, 1438, 1379, 1112, 1082, 882, 778, 711.

mp: 201-203 °C

HRMS: ESI⁺ (m/z) [M+H]⁺ calcd for C₁₃H₈N₂O₂: 225.0659; found: 225.0659

NMR: ¹H NMR (CD₃CN, 700 MHz): δ 8.64 (dd, *J* = 2.1, 4.9 Hz, 1H), 7.98 (td, *J* = 2.1, 7.7Hz, 1H), 7.96-7.93 (m, 2H), 7.89-7.87 (m, 2H), 7.47-7.46 (m, 2H). ¹³C NMR (CD₃CN, 175.95 MHz): δ 167.8, 150.5, 147.3, 139.5, 135.7, 132.9, 124.9, 124.5, 123.7.

23b:

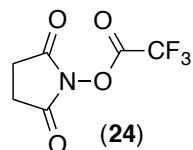
R_f: 0.37 (50% DCM/50% Et₂O)

IR (u, cm⁻¹): 2919, 2851, 1781, 1700, 1578, 1479, 1427, 1378, 1107, 879, 792, 708

mp: 155-156 °C

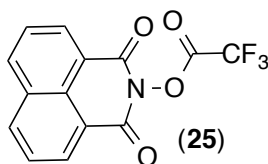
HRMS: ESI⁺ (m/z) [M+H]⁺ calcd for C₁₃H₈N₂O₂: 225.0659; found: 225.0662

NMR: ¹H NMR (CD₃CN, 700 MHz): δ 8.70 (br s, 1H), 8.63 (br s, 1H), 7.97-7.95 (m, 2H), 7.90-7.85 (m, 3H), 7.53 (dd, *J* = 4.9, 8.4 Hz, 1H). ¹³C NMR (CD₃CN, 175.95 MHz): δ 168.0, 149.8, 148.7, 135.8, 135.2, 132.8, 130.1, 124.8, 124.5.



N-trifluoroacetyloxysuccinimide (24): General procedure **E** was followed using N-hydroxysuccinimide (1g, 8.7 mmol). The product was obtained as a moisture sensitive white solid (1.5 g, 81% yield).

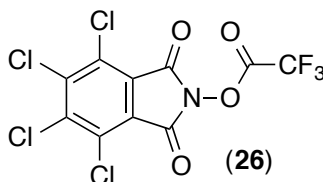
NMR: ¹H NMR (700 MHz, Benzene-*d*₆) δ 1.38 (s, 1H). ¹³C NMR (176 MHz, Benzene-*d*₆) δ 166.66, 154.44 (q, *J* = 45.5 Hz), 114.63 (q, *J* = 286.0 Hz), 24.99. ¹⁹F NMR (377 MHz, Benzene-*d*₆): δ -72.81 (s, 3 F).



N-trifluoroacetyloxynaphthalimide (25): General procedure **E** was followed using N-hydroxynaphthalimide (1 g, 8.7 mmol). The product was obtained as a moisture sensitive white solid (1.5 g, 81% yield).

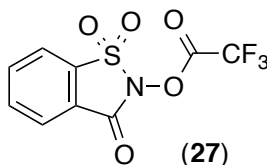
NMR: ¹H NMR (700 MHz, Benzene-*d*₆) δ 8.17 (dd, *J* = 7.2, 1.2 Hz, 2H), 7.28 (dd, *J* = 8.3, 1.1 Hz, 2H), 6.86 (dd, *J* = 8.3, 7.2 Hz, 2H). ¹³C NMR (176 MHz, Benzene-*d*₆) δ 157.95,

134.33, 131.59, 131.35, 127.92, 126.37, 121.69 (Note: The acyl carbonyl signal and the CF_3 were not observed in the spectrum in the time of acquisition). ^{19}F NMR (377 MHz, Benzene- d_6): δ -72.5 (s, 3 F).



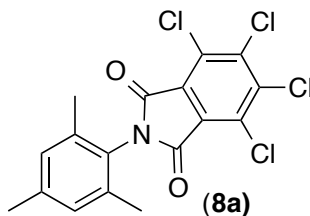
N-trifluoroacetyloxytetrachlorophthalimide (26): General procedure **E** was followed using N-hydroxytetrachlorophthalimide (1g, 4.7 mmol). The product was obtained as a moisture sensitive white solid (1.6 g, 86% yield).

NMR: ^{13}C NMR (176 MHz, Chloroform- d) δ 155.90, 141.83, 131.08, 124.19 (Note: the acyl carbonyl signal and the CF_3 were not observed in the spectrum at the given acquisition time). ^{19}F NMR (377 MHz, Chloroform- d) δ -71.96.



N-trifluoroacetyloxysaccharine (27): General procedure **E** was followed using N-hydroxysaccharine (made following a reported procedure²⁹) (0.35 g, 1.76 mmol). The product was obtained as a moisture sensitive white solid (500 mg, 96% yield).

NMR: ^1H NMR (401 MHz, Chloroform- d) δ 8.18 (dt, J = 7.5, 1.0 Hz, 1H), 8.09 – 7.91 (m, 3H). ^{13}C NMR (176 MHz, Chloroform- d) δ 156.55, 153.86 (q, J = 46.0 Hz), 136.94, 136.63, 135.51, 126.47, 124.59, 122.25, 113.94 (q, J = 286.5 Hz). ^{19}F NMR (377 MHz, Chloroform- d) δ -71.78.



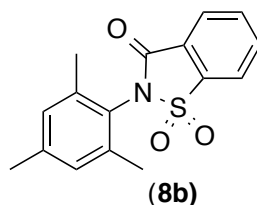
1-N-tetrachlorophthalimido-2,4,6-trimethylbenzene (8a): A modified general procedure **B** was followed using 1,3,5-trimethylbenzene (2 mmol, 0.24 g, 0.28 mL) as the arene substrate and N-trifluoroacetyloxytetrachlorophthalimide **26** (0.2 mmol, 0.079 g,

1 equiv). After 24 h, the reaction was diluted with EtOAc and triethylamine (1 mL) was added to quench trifluoroacetic acid. The reaction mixture was concentrated *in vacuo*, and the residue was purified via column chromatography to give **8a** as a white solid.

Isolated Yield: 41% (33 mg)

R_f: 0.5 (25% EtOAc/75% hexanes)

NMR: ¹H NMR (700 MHz, Chloroform-*d*) δ 7.00 (s, 2H), 2.34 (s, 3H), 2.10 (s, 6H). ¹³C NMR (176 MHz, Chloroform-*d*) δ 162.46, 140.46, 139.79, 136.13, 130.05, 129.38, 127.44, 126.26, 21.12, 17.93.

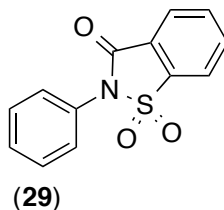


1-N-o-benzoicsulfimidyl-2,4,6-trimethylbenzene (8b): A modified general procedure **B** was followed using 1,3,5-trimethylbenzene (2 mmol, 0.24 g, 0.28 mL) as the arene substrate and N-trifluoroacyloxysaccharine **27** (0.2 mmol, 0.06 g, 1 equiv). After 24 h, the reaction was diluted with EtOAc and triethylamine (1 mL) was added to quench trifluoroacetic acid. The reaction mixture was concentrated *in vacuo*, and the residue was purified via column chromatography to give **8b** as a white solid.

Isolated Yield: 74% (45 mg)

R_f: 0.45 (25% EtOAc/75% hexanes)

NMR: ¹H NMR (700 MHz, Chloroform-*d*) δ 8.17 (d, *J* = 7.6 Hz, 1H), 8.00 (d, *J* = 7.6 Hz, 1H), 7.93 (app. t, *J* = 7.6 Hz, 1H), 7.91 – 7.86 (m, 1H), 7.03 (s, 2H), 2.34 (s, 3H), 2.29 (s, 6H). ¹³C NMR (176 MHz, Chloroform-*d*) δ 158.27, 140.70, 139.40, 138.37, 134.96, 134.30, 129.93, 127.06, 125.63, 123.40, 121.18, 21.15, 18.36.



1-N-o-benzoicsulfimidyl-benzene (29): A modified general procedure **B** was followed using benzene (0.08 mmol, 6.24 mg, 7.2 μL, 1 equiv) as the arene substrate, N-trifluoroacyloxysaccharine **27** (0.2 mmol, 0.06 g, 2.5 equiv) and [Ru(dtBubpy)₃](PF₆)₂ (1

mol%, 1 mg). After 24 h, the reaction was diluted with EtOAc and triethylamine (1 mL) was added to quench trifluoroacetic acid. The reaction mixture was concentrated *in vacuo*, and the residue was purified via column chromatography to give **29** as a white solid. The isolated product NMR matches previous literature report.¹²

Isolated Yield: 65% (14 mg)

NMR: ¹H NMR (401 MHz, Chloroform-*d*) δ 8.17 (m, 1H), 8.01 (m, 1H), 7.97 – 7.85 (m, 2H), 7.60 – 7.49 (m, 5H).

3.7. References

(1) This chapter is adapted with permission from: Allen, L. J.; Cabrera, P. J.; Lee, M.; Sanford, M. S. *J. Am. Chem. Soc.* **2014**, *136*, 5607.

(2) Zalatan, D. N.; Bois, J. D. *Top. Curr. Chem.* **2009**, *292*, 347.

(3) (a) McGrath, N. A.; Brichacek, M.; Njardarson, J. T. *J. Chem. Educ.* **2010**, *87*, 1348. (b) <https://www.forbes.com/sites/simonking/2013/01/28/the-best-selling-drugs-of-all-time-humira-joins-the-elite/#2145f8235110>. Accessed: March 25th, 2017.

(4) Larock, R. C. *Comprehensive Organic Transformations*, Wiley-VCH Publishers: New York, 1999; pp. 821-827. Carey, F. A.; Sundberg, R. J. In *Advanced Organic Chemistry Part A*, Springer Press: New York, 2007, pp. 771-779.

(5) (a) Muci, A. R.; Buchwald, S. L. *Top. Curr. Chem.* **2002**, 131–209. (b) Hartwig, J. F. *Acc. Chem. Res.* **2008**, *41*, 1534.

(6) Wolf, C.; Liu, S.; Mei, X.; August, A. T.; Casimir, M. D. *J. Org. Chem.* **2006**, *71*, 3270.

(7) Lam, P.; Clark, C. G.; Saubern, S.; Adams, J.; Winters, M. P.; Chan, D. M.; Combs, A. *Tetrahedron letters* **1998**, *39*, 2941.

(8) Thu, H.-Y.; Yu, W.-Y.; Che, C.-M. *J. Am. Chem. Soc.* **2006**, *128*, 9048.

(9) Tsang, W. C. P.; Zheng, N.; Buchwald, S. L. *J. Am. Chem. Soc.* **2005**, *127*, 14560.

(10) Shrestha, R.; Mukherjee, P.; Tan, Y.; Litman, Z. C.; Hartwig, J. F. *J. Am. Chem. Soc.* **2013**, *135*, 8480.

(11) Boursalian, G. B.; Ngai, M.-Y.; Hojczyk, K. N.; Ritter, T. *J. Am. Chem. Soc.* **2013**, *135*, 13278.

(12) Kim, H. J.; Kim, J.; Cho, S. H.; Chang, S. *J. Am. Chem. Soc.* **2011**, *133*, 16382.

(13) Kantak, A. A.; Potavathri, S.; Barham, R. A.; Romano, K. M.; DeBoef, B. *J. Am. Chem. Soc.* **2011**, *133*, 19960.

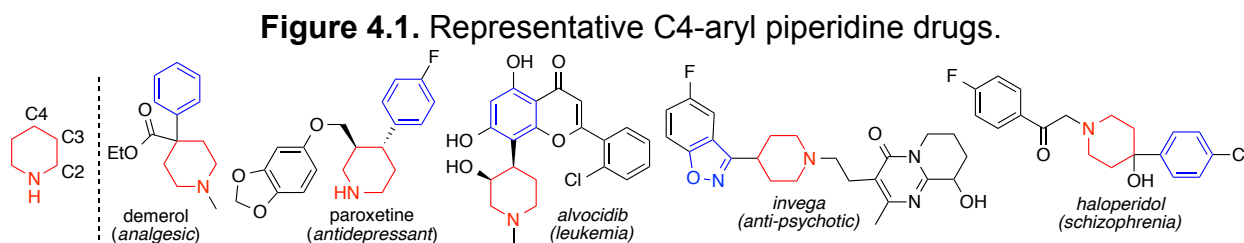
(14) For a review on this area: Zard, S. R. *Chem. Soc. Rev.* **2008**, *37*, 1603.

- (15) Lidgett, R. A.; Lynch, E. R.; McCall, E. B. *J. Chem. Soc.* **1965**, 3754.
- (16) Cadogan, J. I. G.; Rowley, A. G. *J. Chem. Soc., Perkin Trans. 1*, **1975**, 1069.
- (17) Abramovitch, R. A.; Beckert, J. M.; Chinnassamy, P.; Xiaohua, H.; Pennington, W.; Sanjivamurthy, A. R. V. *Heterocycles*, **1989**, 28, 623.
- (18) Lüning, U.; Skell, P. S. *Tetrahedron* **1985**, 41, 4289.
- (19) (a) Prier, C. K.; Rankic, D. A.; MacMillan, D. W. C. *Chem. Rev.* **2013**, 113, 5322. (b) Narayanam, J. M. R.; Stephenson, C. R. J. *Chem. Soc. Rev.* **2010**, 40, 102.
- (20) Okada, K.; Okamoto, K.; Morita, N.; Okubo, K.; Oda, M. *J. Am. Chem. Soc.* **1991**, 113, 9401.
- (21) (a) Schnermann, M. J.; Overman, L. E. *Angew. Chem. Int. Ed.* **2012**, 51, 9576. (b) Lackner, G. L.; Quasdorf, K. W.; Overman, L. E. *J. Am. Chem. Soc.* **2013**, 135, 15342. (c) Pratsch, G.; Lackner, G. L.; Overman, L. E. *J. Org. Chem.* **2015**, 80, 6025.
- (22) (a) Minisci, F. *Synthesis* **1973**, 1973, 1. (b) Martínez-Barrasa, V.; García de Viedma, A.; Burgos, C.; Alvarez-Builla, J. *Org. Lett.* **2000**, 2, 3933. (c) Nagib, D. A.; MacMillan, D. W. C. *Nature* **2011**, 480, 224.
- (23) (a) Cornella, J.; Edwards, J. T.; Qin, T.; Kawamura, S.; Wang, J.; Pan, C.-M.; Gianatassio, R.; Schmidt, M.; Eastgate, M. D.; Baran, P. S. *J. Am. Chem. Soc.* **2016**, 138, 2174. (b) Tang, Q.; Liu, X.; Liu, S.; Xie, H.; Liu, W.; Zeng, J.; Cheng, P. *RSC Adv.* **2015**, 5, 89009.
- (24) Cismesia, M. A.; Yoon, T. P. *Chem. Sci.*, **2015**, 6, 5426.
- (25) Xiong, T.; Zhang, Q. *Chem. Soc. Rev.* **2016**, 45, 3069.
- (26) Romero, N. A.; Margrey, K. A.; Tay, N. E.; Nicewicz, D. A. *Science* **2015**, 349, 1326.
- (27) Tan, B.; Toda, N.; Barbas, C. F. *Angew. Chem. Int. Ed.* **2012**, 51, 12538.
- (28) Kantak, A. A.; Potavathri, S.; Barham, R. A.; Romano, K. M.; DeBoef, B. *J. Am. Chem. Soc.* **2011**, 133, 19960.
- (29) Nagasawa, H. T.; Kawle, S. P.; Elberling, J. A.; DeMaster, E. G.; Fukuto, J. M. *J. Med. Chem.* **1995**, 38, 1865.

Chapter 4. Pd-Catalyzed Transannular C–H Arylation of Alicyclic Amines¹

4.1 Introduction

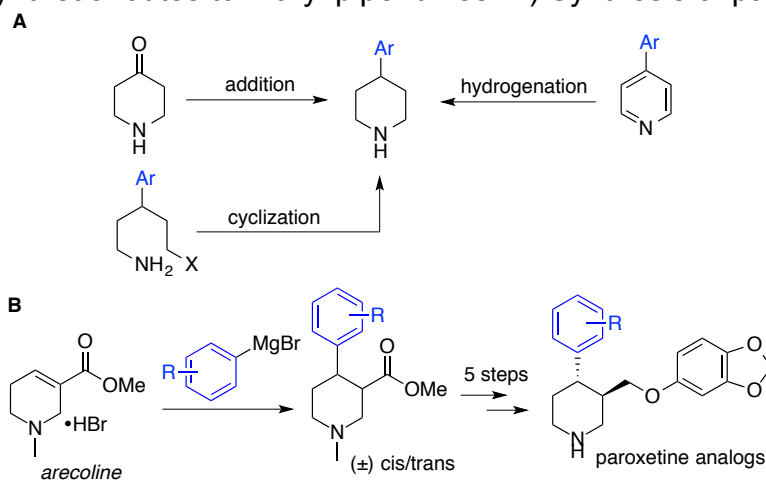
Saturated nitrogen heterocycles (or alicyclic amines) are prevalent motifs in pharmaceuticals, agrochemicals, materials, and natural products. For example, piperidine, a six-membered alicyclic amine, is the second most common ring structure in pharmaceutical agents.² A recent analysis of small-molecule FDA approved drugs revealed that 58% of piperidine drugs contain a substituent at the distal C4 position.³ Aromatic substituents at the C4 position of piperidine are especially common in active pharmaceutical ingredients (Figure 4.1). These include commercial treatments for pain (demerol), depression (paroxetine), leukemia (alvocidib), schizophrenia (invega and haloperidol).



Common synthetic routes to access 4-aryl piperidines include 1) addition of aryl Grignards to pre-functionalized piperdines, 2) hydrogenation of 4-aryl pyridines, and 3) cyclization of acyclic precursors (Figure 4.2 A).⁴ However, these existing approaches have major drawbacks, including the requirement for pre-functionalized starting materials and the need for multi-step sequences to access derivatives for structure-activity relationship studies (SAR).^{5a,b} For example, SAR studies in analogs of the

antidepressant drug paroxetine with varying aryl groups in the C4 position of piperidine requires five synthetic steps after initial installation of the aromatic unit (Figure 4.2 B).⁵ Furthermore, the synthetic difficulty of accessing functionalized amines increases exponentially as the alicyclic amine becomes more complex in structure.

Figure 4.2 A) Synthetic routes to 4-aryl piperidines. B) Synthesis of paroxetine analogs.



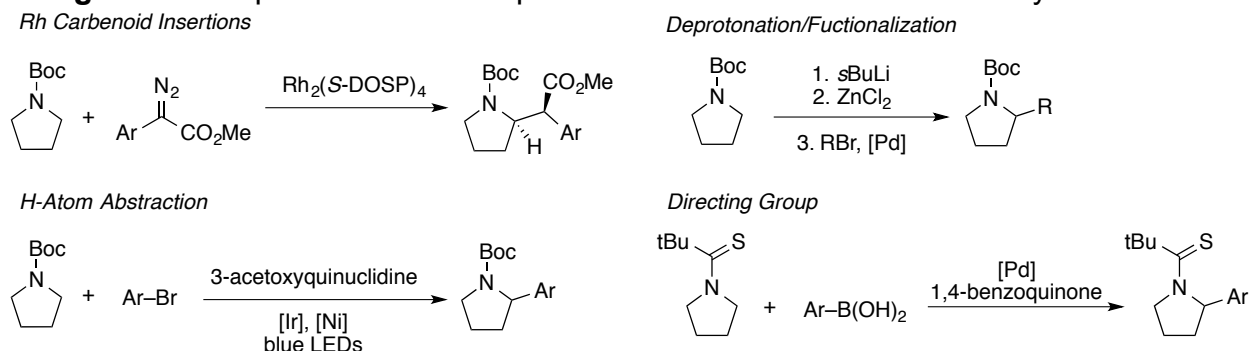
C–H Functionalization of Alicyclic amines

The advent of C–H functionalization has enabled medicinal chemists to utilize a late-stage functionalization approach to convert the C–H bonds in drug candidates to new chemical entities in a fast and efficient manner.⁶ Strategies to selectively C–H functionalize molecules rely on 1) the innate properties of the substrate (activated C–H bonds, formation of stable radical intermediates, steric hindrance) or 2) directing groups (target nearby C–H bonds). However, when molecular complexity increases, such as in biologically active compounds, selective C–H bond functionalization becomes more challenging.

Despite tremendous progress in C–H functionalization, methods for the functionalization of alicyclic amines remain scarce. The vast majority of literature reports have focused on exploiting the innate properties of alicyclic amines to functionalize the C2 position.⁷ Due to the electron-donating properties of the nitrogen atom, selective functionalization of electron-rich α -C–H bonds by metal carbenoid insertions⁸ and H-atom abstractions⁹ have been demonstrated (Figure 4.3, left). Additionally, the highly

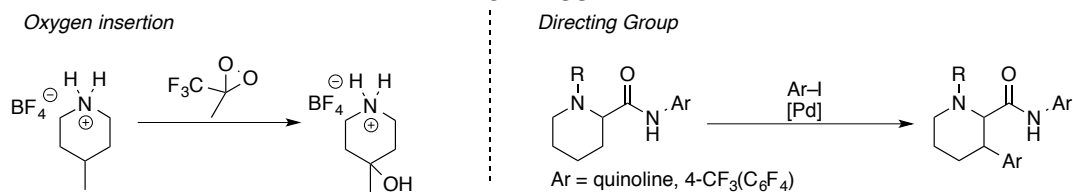
acidic nature of these C–H bonds has also allowed the development of selective C2–H bond deprotonation/functionalization strategies.¹⁰ Very recently, the use of directing groups on the N-atom has allowed the selective arylation of C2–H bonds in a variety of alicyclic amines (Figure 4.3, right).¹¹

Figure 4.3. Representative examples of C2–H functionalization of alicyclic amines.



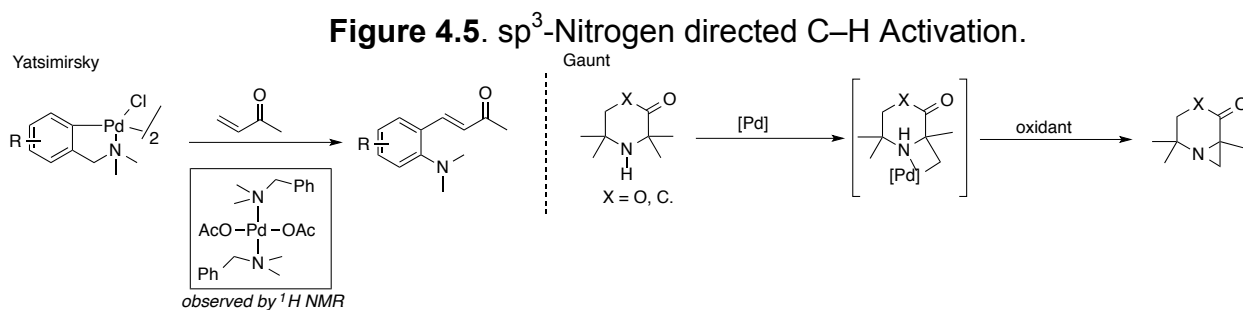
Existing methods for the C–H functionalization of saturated nitrogen heterocycles at sites remote to nitrogen are rare. This has been accomplished by H-atom abstraction methods or through the use of directing groups (Figure 4.4). Asensio and co-workers demonstrated that protonation of alicyclic amines deactivates the highly activated C2–H bonds, thus enabling oxygen insertion with methyl(trifluoromethyl)dioxirane at distal sites of several cyclic and acyclic amines.¹² Directing groups have also allowed the functionalization of adjacent C–H bonds at remote positions from nitrogen.¹³

Figure 4.4. Representative examples of remote C–H functionalization of alicyclic amines.



In contrast, methods that leverage the innate nitrogen functionality in alicyclic amines to direct transition metals to reactive C–H bonds is underexplored. Using native functionalities within a complex molecule can become a powerful tool to promote site selective C–H functionalization without the need of external directing groups.⁶

Stoichiometric studies by Yatsimirsky demonstrated that the nitrogen atom in *N,N*-dimethylbenzylamines can cyclometallate with Pd(II) salts at adjacent C(sp²)-H bonds to promote a variety of C-C bond forming reactions.¹⁴ This ground-breaking work elucidated the C-H activation mechanism of this stoichiometric reaction and demonstrated that a major challenge in utilizing basic amine nitrogen substrates is the formation of off-cycle Pd(X)₂(amine)₂ species (Figure 4.5, left). This strategy was then translated to catalysis.¹⁵ Very recently, Gaunt and co-workers have developed several protocols to functionalize exocyclic pendant alkyl chains of nitrogen heterocycles (Figure 4.5, right).¹⁶ This strategy leverages the secondary, bulky sp³ amine as a directing group to activate C(sp³)-H bonds by the formation of four- or five-member palladacycles. The authors propose that steric repulsion of the bulky amine substrate destabilizes formation of Pd(X)₂(amine)₂ complexes, thus promoting the C(sp³)-H cleavage through the monoligated species.



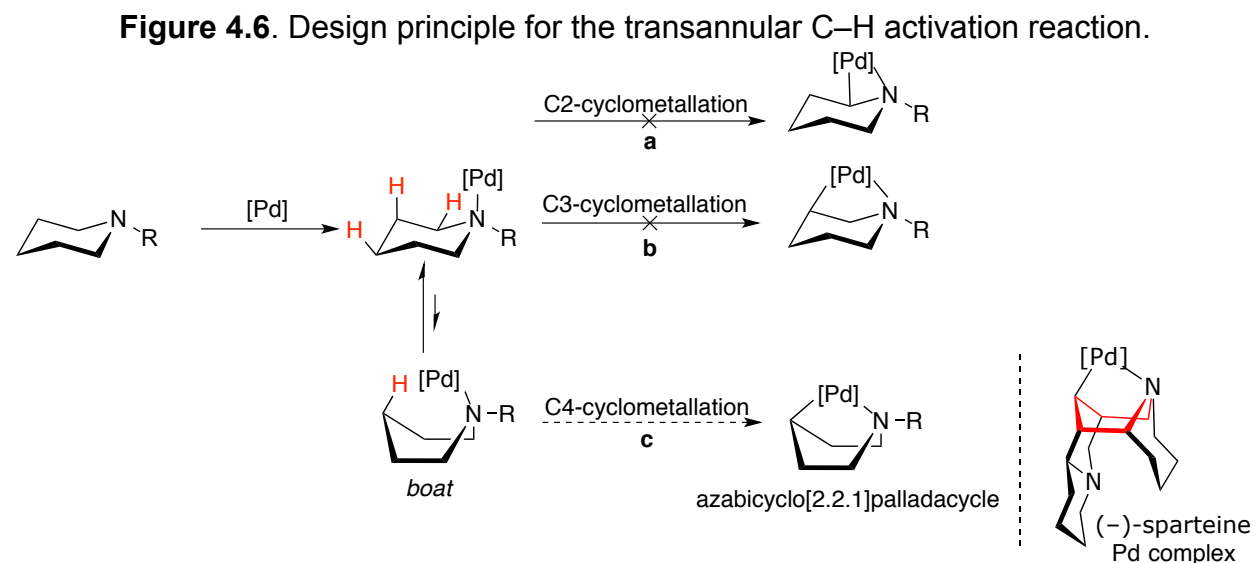
To our knowledge, there are no available metal-catalyzed methods for selective C-H functionalization of alicyclic amines that harness the strongly donating properties of the sp³-nitrogen atom in cyclic amine substrates to direct metal catalysts at specific C-H bonds remote from the nitrogen.

This chapter focuses on the development of this strategy by leveraging the energetically disfavored boat conformation of these cyclic substrates to achieve transannular C-H activation and subsequent C-C bond formation. Additionally, this chapter includes the substrate scope, limitations of the protocol, and the design and synthesis of several auxiliary-directing groups to promote C-H activation.

4.2 Results and Discussion

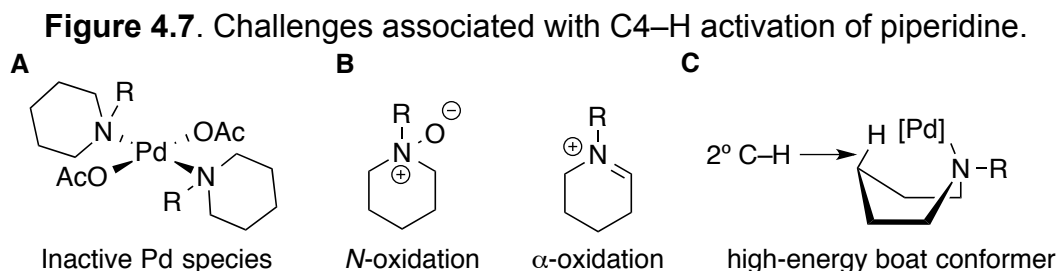
Design Principle

Inspired by the work in sp^3 -nitrogen directed C–H functionalization and the stoichiometric reactivity of alkylamine Pd complexes, my colleague Dr. Joseph Topczewski proposed the use of the nitrogen atom in piperidine to direct the palladium catalyst to the ring system. Upon coordination of the catalyst to the amine, Pd could interact with the C2–H, C3–H or C4–H bonds (Figure 4.6). However, highly strained cyclometallated Pd complexes would result from C2–H or C3–H bond activation (3 and 4 member palladacycles). In contrast, piperidine’s rapid conformational changes could bring the remote C4–H bonds in close proximity to palladium via the boat conformer. This in turn could enable a transannular C4–H activation affording an azabicyclo[2.2.1]palladacycle intermediate that could be further reacted to forge new C–FG bonds (FG = functional group).



This proposal is supported by the work of Bercaw, which demonstrated that (–)-sparteine in the presence of stoichiometric $\text{Pd}(\text{OAc})_2$ generates an analogous azabicyclo[2.2.1]palladacycle.¹⁷ Nonetheless, this proposal has several challenges that must be addressed. First, the intrinsic azaphilicity of Pd could lead to formation of inactive Pd species (Figure 4.7 A). The formation of analogous Pd species has been

observed in the *ortho*-palladation of *N,N*-dimethylbenzylamine.¹⁸ Second, amines are prone to oxidation at nitrogen or at adjacent C–H bonds.¹⁹ Furthermore, alkylamines are known to undergo undesired β -hydride elimination pathways upon coordination to Pd (Figure 4.7 B).²⁰ Third, Pd must intercept the high-energy boat conformer species (energy barrier for piperidine chair inversion is 10.4 kcal/mol)²¹ and undergo C–H cleavage of an unactivated secondary C(sp³)–H bond (Figure 4.7 C).



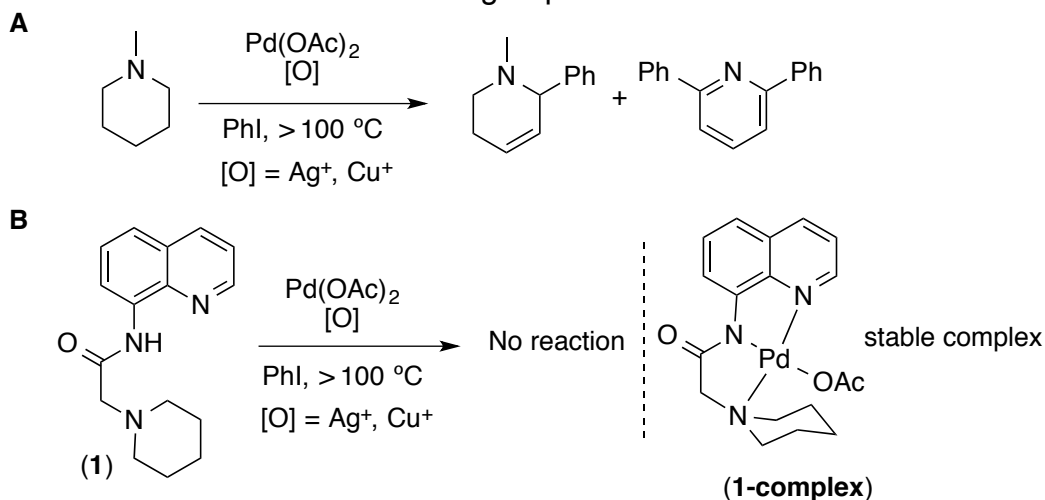
Initial Work

Initial work by Noam Saper, Melissa Lee and Dr. Joseph Topczewski focused on the use of *N*-methyl piperidine as a starting substrate (Figure 4.8 A). Subjecting *N*-methyl piperidine to C–H activation conditions of related Pd-catalyzed C(sp³)–H arylation methods²² led to the formation of undesired C2–H arylated products. These α -arylated products are consistent with a mechanism triggered by an initial α -oxidation of piperidine.²³

Due to the side reactions observed for *N*-methyl piperidine, the incorporation of pendant directing groups was explored next. Several bidentate coordinating directing groups have been utilized for the functionalization of C(sp³)–H bonds. These chelating groups have been shown to improve reactivity by slowing down undesired side reactions (e.g. β -hydride elimination), increasing the stability of Pd intermediates, and favoring cyclometallation.²⁴ A quinoline-based directing group, popularized by Daugulis, was incorporated to piperidine (**1**, Figure 4.8 B). This substrate was subjected to a variety of reaction conditions, however no functionalized product was observed. Stoichiometric studies reveal that reaction of Pd(OAc)₂ with **1** produces a stable square planar complex without open coordination sites necessary for C–H activation (**1**-

complex). **1-complex** shows exceptional thermal and chemical stability as no reactivity was observed under a variety of reaction conditions.

Figure 4.8. Initial work in Pd C–H functionalization of piperidine. A) Attempts to functionalize *N*-methylpiperidine. B) Attempts to utilize a bidentate auxiliary directing group.

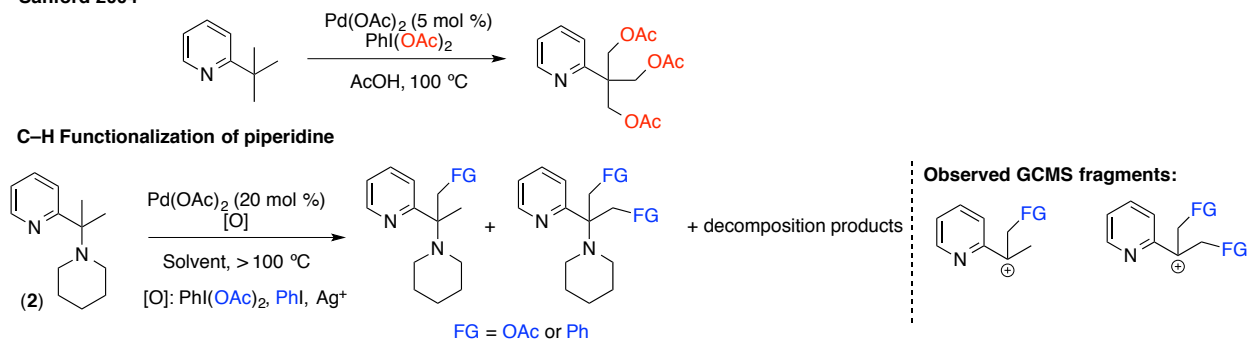


The lack of reactivity in **1-complex** prompted us to investigate monodentate pendant directing groups that could facilitate the desired transformation. In the area of directed Pd-catalyzed C–H functionalization, directing groups derived from pyridines, oximes, carboxylates and amides have enabled the selective functionalization of nearby C–H bonds.²⁵ It is important to note that the piperidine nitrogen must remain sp^3 -hybridized, otherwise planarization of the ring will prevent access to the boat conformer.

Our group has utilized pyridine as a directing group to undergo $C(sp^3)$ -H functionalization reactions (Figure 4.9, top).²⁶ Furthermore, we developed an analogous piperidine substrate bearing a pyridine directing group (**2**, Figure 4.9, bottom). However, under a variety of C–H activation conditions, functionalization at the methyl C–H bonds was observed along with several unidentifiable byproducts.

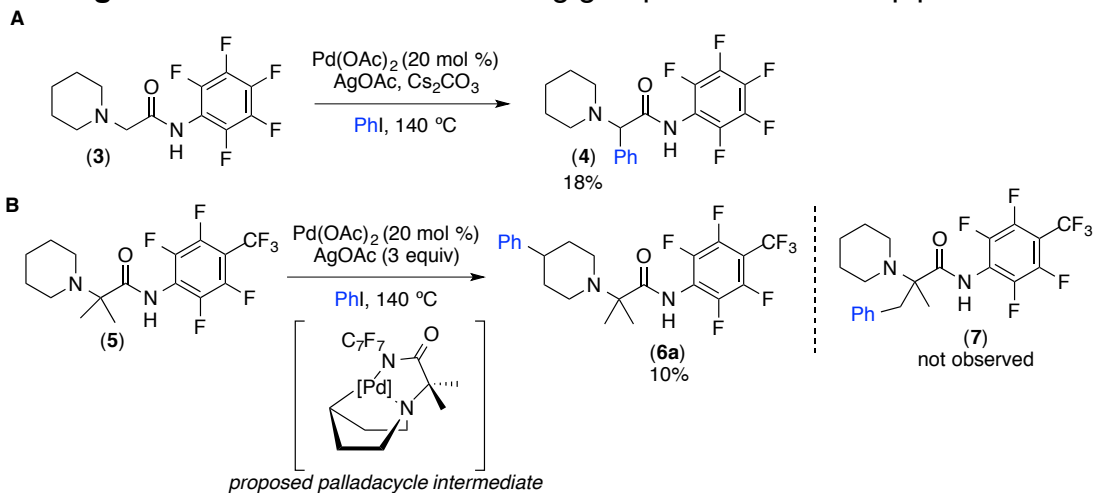
Figure 4.9. Attempt to employ pyridine directing group to functionalize piperidine.

Sanford 2004



As such, we turned our attention to anionic directing groups that have proven successful in C–H functionalization. The Yu Group has developed a perfluorinated amide that, upon deprotonation, tightly coordinates Pd and enables the functionalization of sp^2 and sp^3 C–H bonds.²⁷ We synthesized a piperidine substrate bearing the perfluorinated amide (**3**, Figure 4.10 A). This substrate was subjected to a variety of C–H arylation conditions and isolation of the observed product demonstrated that arylation occurred at the methylene carbon (**4**). Additionally, S_NAr on the perfluorinated ring was observed.²⁸ Given these results, the next generation substrate contained gem-dimethyl substituents to block this reactive α -methylene position and a 4- $\text{CF}_3(\text{C}_6\text{F}_4)$ amide, developed by Yu, to prevent S_NAr (**5**, Figure 4.10 B). Gratifyingly, subjecting this substrate to typical C–H arylation conditions employing Pd(OAc)_2 and AgOAc in neat phenyl iodide²⁹ afforded the desired product in 10% yield (**6a**). Product **6a** was confirmed by comparing NMR and GCMS data with an independently synthesized authentic product. Interestingly, products derived from C–H functionalization of the methyl groups (**7**) were not observed in this reaction. This result indicates that the substrate coordinates to Pd in a bidentate fashion, positioning the catalyst away from the α -methyl C–H bonds. This result differs from other reports where α -methyl sites are functionalized with this amide directing group.³⁰

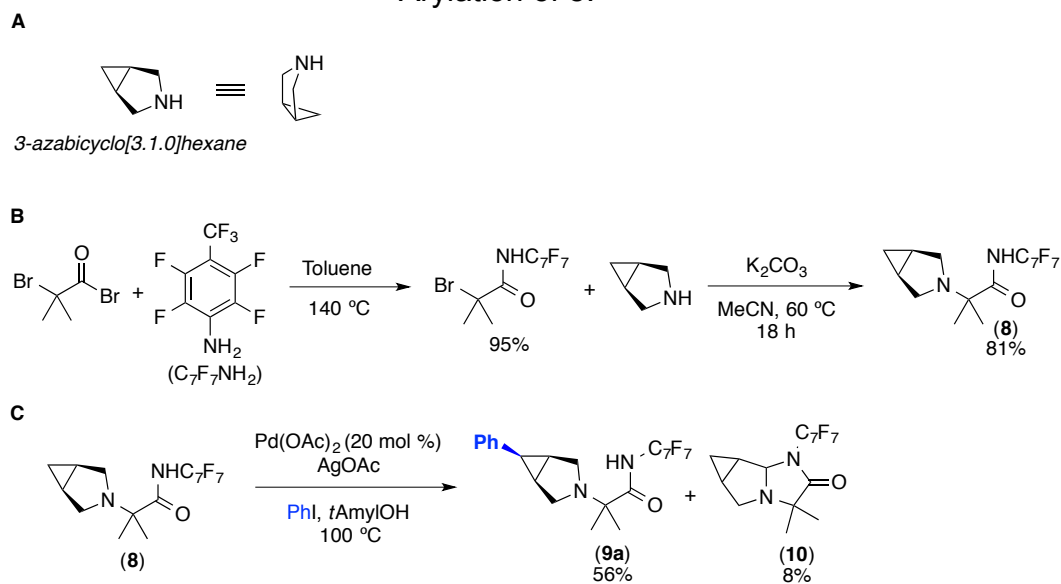
Figure 4.10. Use of amide directing group to functionalize piperidine.



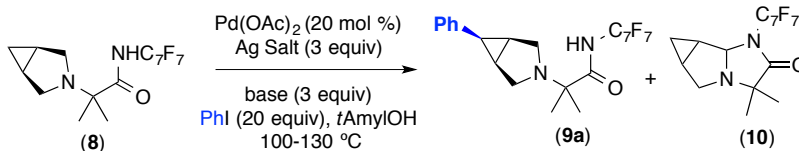
3-Azabicyclo[3.1.0]hexane Optimization

Despite our efforts to improve the reactivity of **5**, the arylated piperidine product remained in low yields. We attributed the poor reactivity in piperidine to the requirement of accessing the high-energy boat conformer species and the challenging cleavage of strong C–H bonds, which in related reactions is typically the rate limiting step. Therefore, we reasoned that selecting a more reactive substrate would facilitate reaction optimization. We chose to continue our reaction development with 3-azabicyclo[3.1.0]hexane, as the substrate is pre-arranged in a boat-like conformer and the cyclopropane C–H bonds, due to the high *s*-character, are more reactive toward C–H activation than other secondary C(sp³)–H bonds (Figure 4.11 A).³¹ This substrate (**8**) was prepared from commercially available reagents in two steps in high yield (Figure 4.11 B). Subjecting **8** to the C–H arylation conditions furnished 56% yield of product (**9a**). Interestingly, aminor byproducts from product and starting material (**10**) were observed (Figure 4.11 C).

Figure 4.11. A) Structure of 3-azabicyclo[3.1.0]hexane. B) Synthesis of **8**. C) Initial C–H Arylation of **8**.



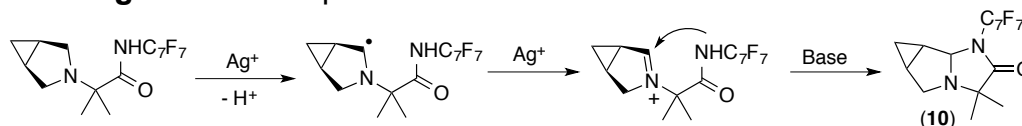
We found that re-subjecting aminal **10** to the reaction conditions did not furnish product. This led us to further investigate reaction conditions to 1) improve yield of the desired product (**9a**) and 2) prevent aminal formation. As show in Table 4.1, we explored a variety of Ag^+ salts and bases in the presence of 20 mol % $\text{Pd}(\text{OAc})_2$. We found that AgTFA , Ag_2CO_3 and Ag_2O led to formation of higher amount of aminal byproduct than AgOAc (compare entries 1-3 versus 4). Further optimization with AgOAc revealed that addition of carboxylate bases such as KOPiv increased the yield of **9a** (83%, entry 7); however, lowering the amount of Pd to 10 mol % resulted in a drastic drop in yield to 35% (entry 8). Increasing the temperature to 130 °C improved the yield of the desired product **9a** (61%, entry 9), while also increasing the amount of aminal byproduct **10** (9%).

Table 4.1. Optimization for 3-azabicyclo[3.1.0]hexane **8**^a

Entry	Temp.	Pd(OAc) ₂ (mol %)	Ag ⁺	Base	Conversion	Yield	
						9a	10
1	100 °C	20%	AgTFA	-----	94%	21%	44%
2	100 °C	20%	Ag ₂ CO ₃	-----	75%	36%	11%
3	100 °C	20%	Ag ₂ O	-----	84%	21%	21%
4	100 °C	20%	AgOAc	-----	73%	56%	6%
5	100 °C	20%	AgOAc	K ₂ CO ₃	67%	6%	17%
6	100 °C	20%	AgOAc	KOAc	86%	78%	3%
7	100 °C	20%	AgOAc	KOPiv	94%	83%	8%
8	100 °C	10%	AgOAc	KOPiv	75%	35%	7%
9	130 °C	10%	AgOAc	KOPiv	99%	61%	9%
10	130 °C	0%	AgOAc	KOPiv	85%	nd	28%
11	130 °C	10%	-----	KOPiv	99%	43%	4%
12 ^b	130 °C	10%	-----	CsOPiv	99%	93%	< 4%
13 ^c	130 °C	10%	-----	CsOPiv	99%	87%	< 2%

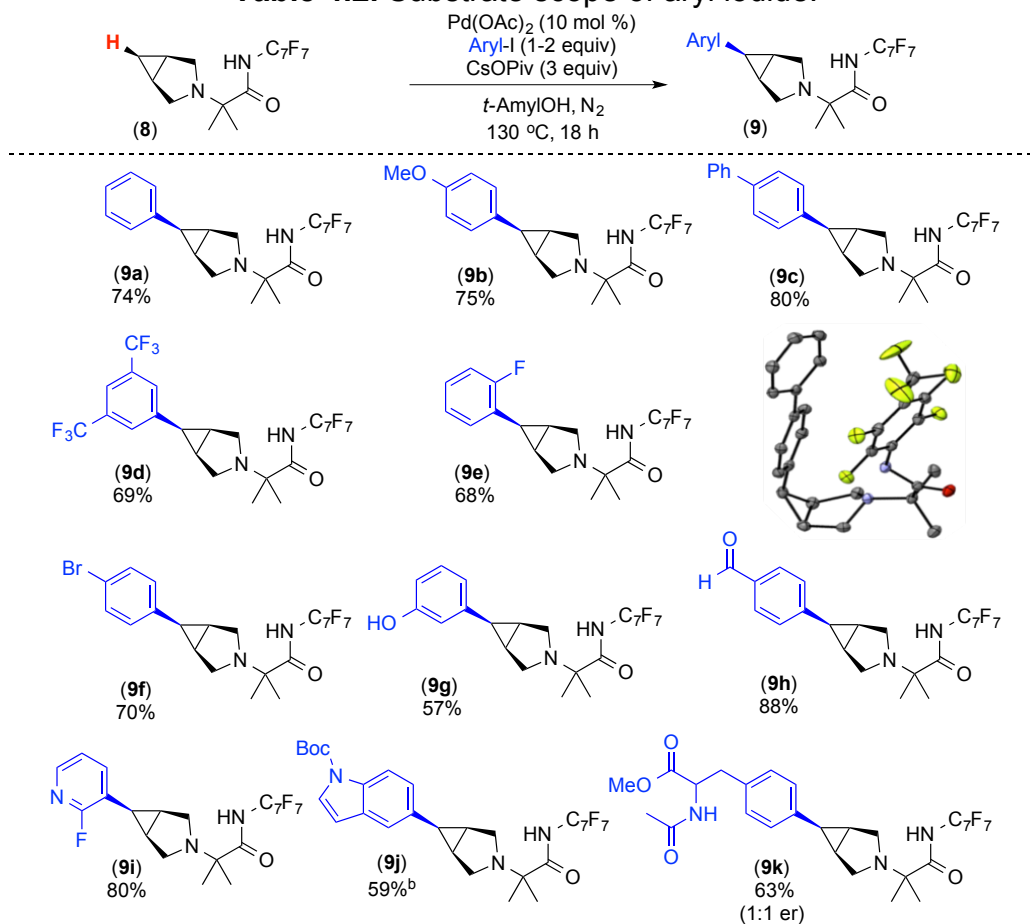
^a Conditions: **8** (1 equiv), Pd(OAc)₂ (20-10 mol %), Ag salt (3 equiv), base (3 equiv), PhI (20 equiv), 100-130 °C, ambient conditions. ^b Under N₂-atmosphere and dry *t*AmylOH. ^c PhI (1 equiv), N₂-atmosphere, dry *t*AmylOH.

As shown in entry 10, control experiments in the absence of Pd demonstrated that Ag promotes amination formation. We propose that Ag oxidizes the amine in **8** to an α -amino radical intermediate that can undergo a subsequent oxidation to the iminium ion. The pendant fluoroamide then attacks the iminium ion, affording the bicyclic amination (Figure 4.12).³²

Figure 4.12. Proposed mechanism for amination formation.

Literature reports in related C–H arylation reactions indicate that the role of Ag is to regenerate the Pd carboxylate catalyst by abstracting the halide from the Pd center.³³ Thus, we hypothesized that replacing Ag with a non-oxidizing alkali metal carboxylate could regenerate the Pd catalyst and suppress amination. Indeed, KOPiv was able to provide 43% of **9a** and traces of amination **10** in the absence of Ag (entry 11). To our delight, CsOPiv afforded 93% yield of product, while minimizing amination (entry 12). Further optimization revealed that reducing iodobenzene to 1 equivalent maintained excellent yield of **9a** (entry 13).

We next evaluated the scope of aryl iodides in the reaction. As shown in Table 4.2 several aryl iodides with electron-neutral (**9a**, **9c**), electron-donating (**9b**) and electron-withdrawing (**9d**, **9e**) substituents provided excellent yields of product. The solid-state structure of **9c** demonstrates that C–H activation occurs at the concave face of the molecule, further verifying the proposed transannular C–H activation pathway. We were particularly pleased to observe that important functional groups such as bromo (**9f**), alcohol (**9g**) and aldehyde (**9h**) were compatible with the reaction conditions. These provide excellent functional group handles for subsequent reactions that can increase molecular complexity. Furthermore, we were pleased to observe that the reaction was amenable to iodo-heteroarenes. For example, the electron-deficient 2-fluoro-pyridine was successfully installed in 80% yield (**9i**). In addition, electron-donating heteroarenes such as the boc-protected indole underwent productive arylation in 59% yield (**9j**). Finally, a phenylalanine derivative underwent C–H arylation with **8** affording 63% yield of the desired product **9k**.

Table 4.2. Substrate scope of aryl iodide.

^aConditions: **8** (1 equiv), Pd(OAc)₂ (10 mol %), CsOPiv (3 equiv), aryl iodide (1-2 equiv), tAmylOH (0.12 M), N₂, 130 °C, 18 h. ^b**8** (1 equiv), Pd(OAc)₂ (30 mol %), AgOAc (1.1 equiv), KOPiv (3 equiv), aryl iodide (1 equiv), tAmylOH, 100 °C, air, 18 hours.

Investigation on the aryl electrophile showed that phenyl triflate or chloride does not generate product **9a** (Table 4.3, entries 1 and 2), as only aminor byproduct **10** was observed. Interestingly, phenyl bromide is compatible with our reaction conditions, albeit in low yield (Table 4.3, entry 3).

Table 4.3. Scope of aryl electrophile.

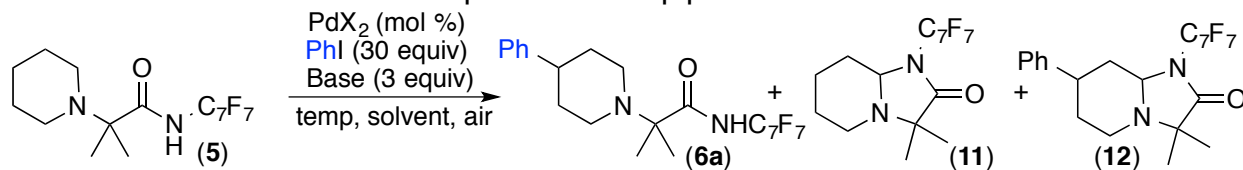
Entry	Ph-X (equiv)	Conversion	Yield 9a ^a	Yield 10
1	Chlorobenzene (20)	26%	nd	14%
2	Phenyl triflate (20)	17%	nd	8%
3	Bromobenzene (20)	43%	14%	17%
4	Bromobenzene (2)	43%	<2%	13%
5	Bromobenzene (1)	47%	<2%	13%

^aConditions: **8** (1 equiv), Pd(OAc)₂ (10 mol %), CsOPiv (3 equiv), Aryl electrophile (1-20 equiv), tAmylOH (0.12 M), N₂, 130 °C, 18 hours. All yields determined by gas chromatography (GC). nd = not detected.

C–H Arylation of Piperidine

We next sought to expand the scope in alicyclic amines. We began our studies with the piperidine substrate **5**. Under the optimized conditions for the 3-azabicyclo[3.1.0]hexane **8**, we observed 12% yield of product **6a** (Table 4.4, entry 1). We reasoned that the low yield is a consequence of the energetically unfavorable chair-to-boat interconversion that increases the activation barrier by at least 6 kcal/mol relative to **8**.³⁴ As such, we evaluated different reaction conditions to increase the yield of **6a**. We rationalized that increasing temperature would be beneficial as a higher activation energy for the substrate was expected. Indeed increasing the temperature to 140 °C provided 23% yield of **6a** (entry 2). At this higher temperature, 14% yield of amination **11** and traces of **12** were observed (entry 2). This competing amination formation is proposed to be promoted by the Pd-catalyst. Encouraged by this result, we explored other known C–H activation solvents. The use of hexafluoro isopropanol (HFIP, entry 3) and trifluoroethanol (TFE, entry 4) did not result in improved reactivity. Interestingly, *t*BuOH afforded an improved 30% yield of **6a** (entry 5). Reports by Daugulis in C–H arylation reactions have shown that neat aryl iodide could also be a suitable solvent for this transformation.²⁹ To our delight, use of neat iodobenzene resulted in 44% yield of **6a** and 6% of arylated amination **12**.

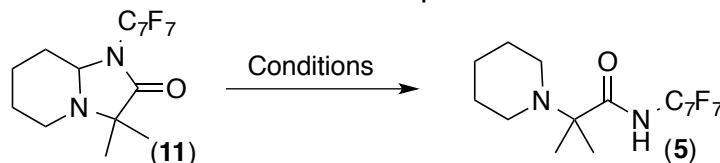
Notably, evaluation of other Cs salts drastically diminished the yield of arylated piperidine (entries 7-9). This indicates that pivalate is essential for the reaction to proceed. We proposed that the steric bulk of pivalate could prevent formation of off-cycle Pd intermediates or to lower the energy of activation in the system as proposed in related C–H activation methods.³⁵ Increasing the temperature to 150 °C afforded a combined 55% yield of arylated piperidine (sum of **6a** and **12**). Evaluation of catalyst loading showed that 5 or 20 mol % of Pd provided improved yield of product (entries 11-12). Finally, evaluation of other Pd sources did not lead to further reaction improvement (entries 13-15).

Table 4.4. Optimization of piperidine substrate **5**.

Entry	Temp.	Base (3 equiv)	Pd (mol %)	Solvent	Conv.	Yield 6a	Yield 11	Yield 12
1	130 °C	CsOPiv	Pd(OAc) ₂ (10 mol %)	<i>t</i> AmylOH	40%	12%	3%	nd
2	140 °C	CsOPiv	Pd(OAc) ₂ (10 mol %)	<i>t</i> AmylOH	54%	22%	18%	6%
3	140 °C	CsOPiv	Pd(OAc) ₂ (10 mol %)	HFIP	86%	44%	16%	6%
4	140 °C	CsOPiv	Pd(OAc) ₂ (10 mol %)	TFE	79%	3%	26%	2%
5	140 °C	CsOPiv	Pd(OAc) ₂ (10 mol %)	<i>t</i>BuOH	63%	30%	13%	2%
6	140 °C	CsOPiv	Pd(OAc) ₂ (10 mol %)	neat	77%	44%	16%	6%
7	140 °C	CsOAc	Pd(OAc) ₂ (10 mol %)	neat	35%	4%	nd	17%
8	140 °C	CsTFA	Pd(OAc) ₂ (10 mol %)	neat	78%	nd	nd	40%
9	140 °C	Cs₂CO₃	Pd(OAc) ₂ (10 mol %)	neat	81%	nd	nd	21%
10	150 °C	CsOPiv	Pd(OAc)₂ (10 mol %)	neat	93%	44%	28%	11%
11	150 °C	CsOPiv	Pd(OAc) ₂ (5 mol %)	neat	82%	35%	24%	9%
12	150 °C	CsOPiv	Pd(OAc) ₂ (20 mol %)	neat	96%	46%	17%	13%
13	150 °C	CsOPiv	Pd(OPiv)₂ (10 mol %)	neat	76%	44%	15%	6%
14	150 °C	CsOPiv	Pd(TFA)₂ (10 mol %)	neat	74%	41%	14%	5%
15	150 °C	CsOPiv	Pd(Cl)₂ (10 mol %)	neat	60%	29%	14%	3%

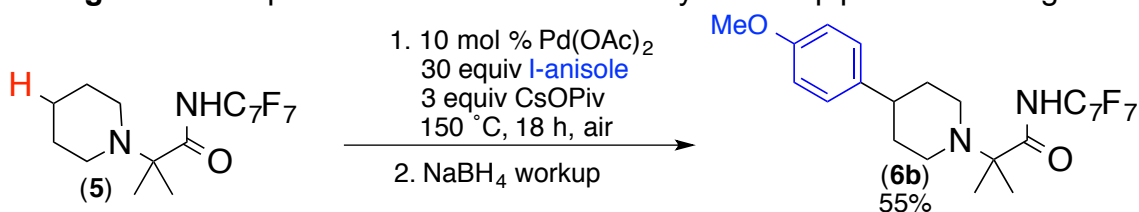
^aConditions: **5** (1 equiv), Pd(OAc)₂ (X mol %), base (3 equiv), iodobenzene (30 equiv), solvent (0.12 M), air, temp, 18 hours. All yields determined by gas chromatography (GC). nd = not detected.

Isolation of **6a** under the identified conditions (entry 10, Table 4.4) revealed that separation of product from aminals and remaining starting material was difficult. As such, we next looked at the conversion of aminal byproducts to starting material or product by ring-opening the aminal. Based on literature reports, we hypothesized that ring opening the bicyclic aminal can be done under reducing conditions.³⁶ As shown in Table 4.5, several reducing conditions were successful at cleaving the C–N bond of the aminal; however, it was found that sodium borohydride in methanol quantitatively converted aminal **11** to amine **5** (entry 4). With the two-step procedure, we were pleased to obtain a 55% yield of the arylated piperidine (**6b**, Figure 4.13).

Table 4.5. Aminoal reduction optimization conditions.

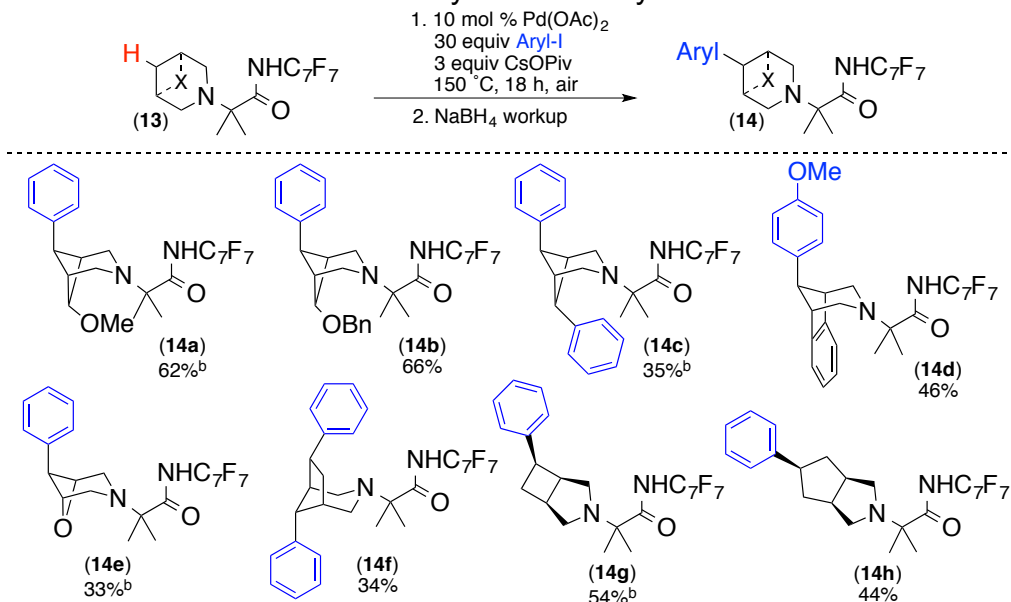
Entry	Conditions	Time	Temperature	Yield 5 ^a
1	5% Pd/C, H ₂	12 h	RT	34%
2	Zn/AcOH	12 h	80 °C	70%
3	NaBH ₄ in THF	12 h	RT	50%
4	NaBH ₄ in MeOH	12 h	RT	99% ^a

^a Conditions: **11** (0.04 mmol), NaBH₄ (5 equiv), MeOH (0.2 M). GC yields.

Figure 4.13. Optimized conditions for C4-Arylation of piperidine analog **5**.

Scope of Alicyclic Amines:

Subsequently, we explored the scope of alicyclic amines. Several bicyclic amines were tolerated under the optimized reaction conditions affording modest to good yields (**14a-14h**, Table 4.6). Azabicyclo[3.1.1]heptanes bearing a methoxy (**14a**) and benzyl protected alcohol (**14b**) were arylated in good yields. Interestingly, the bicyclo[3.1.1]heptane (**14c**) with two available C–H bonds underwent diarylation in 35% yield. Furthermore, other bicyclic scaffolds with an embedded morpholine ring provided 33% yield of product (**14e**). In addition, larger ring sizes such as the azabicyclo[3.2.1]octane (**14d** and **14f**) prove successful under the reaction conditions. Finally, substrates derived from pyrrolidine with a cyclobutane and cyclopentane ring afforded arylated products in decent yields (54% of **14g** and 44% of **14h**).

Table 4.6. C–H arylation of alicyclic amines.^a

^aConditions: 13 (0.25 mmol, 1 equiv), Pd(OAc)₂ (10 mol %), CsOPiv (3 equiv), Aryl iodide (30 equiv), 150 °C, air, 18 hours. ^b Step 3 (NaBH₄ reduction) was not performed as a minimal was not observed by GC.

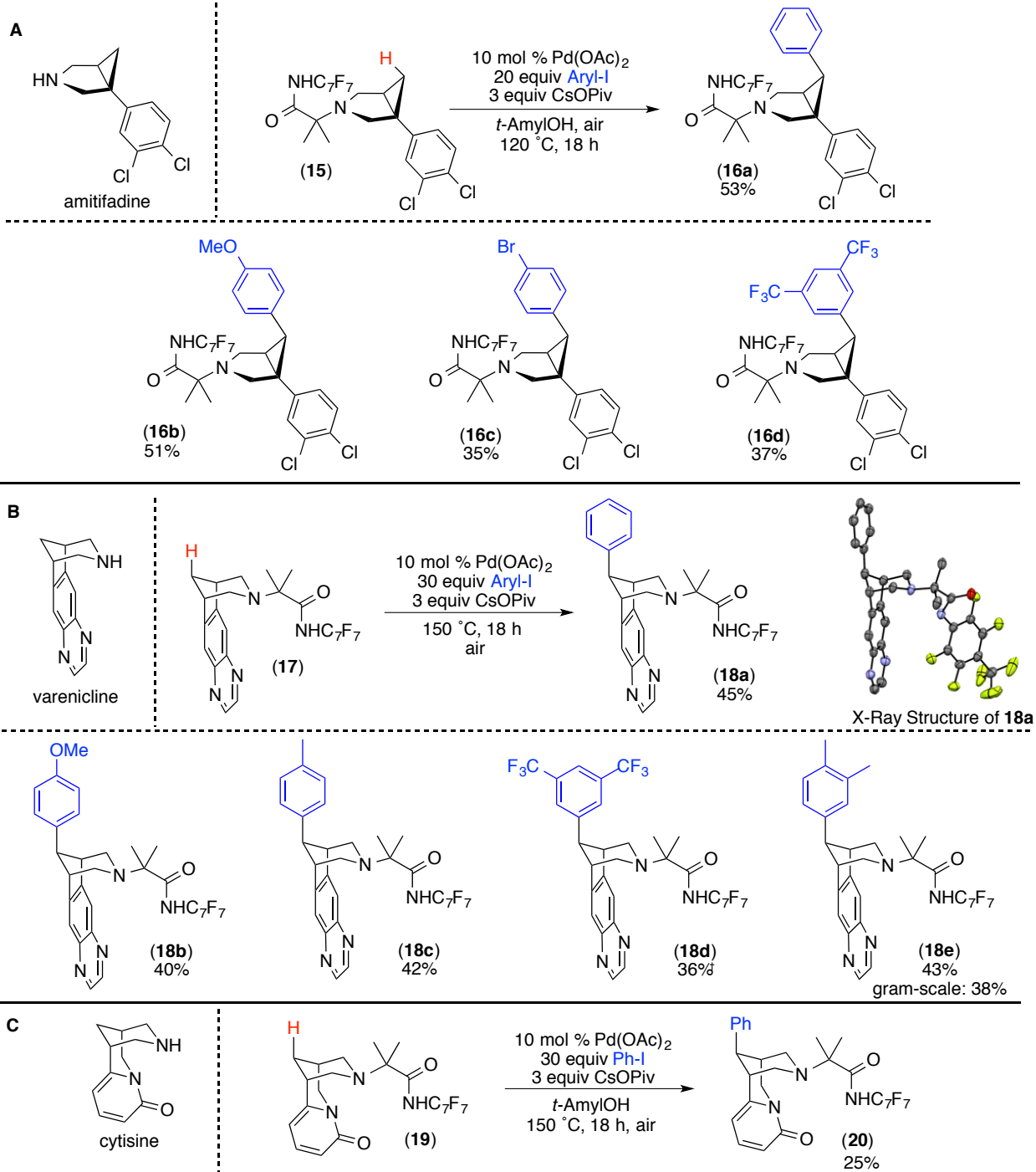
The importance of this transformation is demonstrated by the arylation of several bioactive molecules (Figure 4.14). First, we demonstrated that amitifadine, a serotonin–noradrenaline–dopamine reuptake inhibitor with a bicyclo[3.1.0] scaffold, was successfully arylated (Figure 4.14 A). A variety of aryl groups containing electron-neutral, donating and withdrawing substituents (**16a** to **16d**) delivered new amitifadine derivatives.

Furthermore, incorporation of the directing group to varenicline (**17**), Pfizer's billion-dollar anti-smoking drug, afforded a variety of arylated products in modest yields (Figure 4.14 B, **18a–18e**). Products derived from this reaction show that the aryl group was installed at the axial position of the piperidine-unit as shown in the crystal structure of **18a**. Synthesis of this stereoisomer by other methods would be challenging. We were pleased to observe that the reaction is also scalable as the isolated yield of **18e** at 0.25 mmol and 4 mmol was similar (43% and 38%, respectively).

Finally, the natural product and anti-smoking medicine, cytisine, was subjected to our reaction conditions and provided 25% yield of phenyl-cytisine derivative (**20**, Figure 4.14 C). Again, this substrate incorporated the aryl group at the axial position of the substrate. Our method represents a practical way to obtain a variety of arylated

products with added molecular complexity that otherwise would require multiple steps of synthesis by traditional routes. Additionally, this rapid analog derivatization offers new opportunities for structure-activity relationship studies in pharmaceutical candidates. Overall, our method highlights the importance of developing late-stage C–H functionalization strategies. We hope that this approach could find use in the synthesis of new alicyclic amines and in the development of new pharmaceuticals.

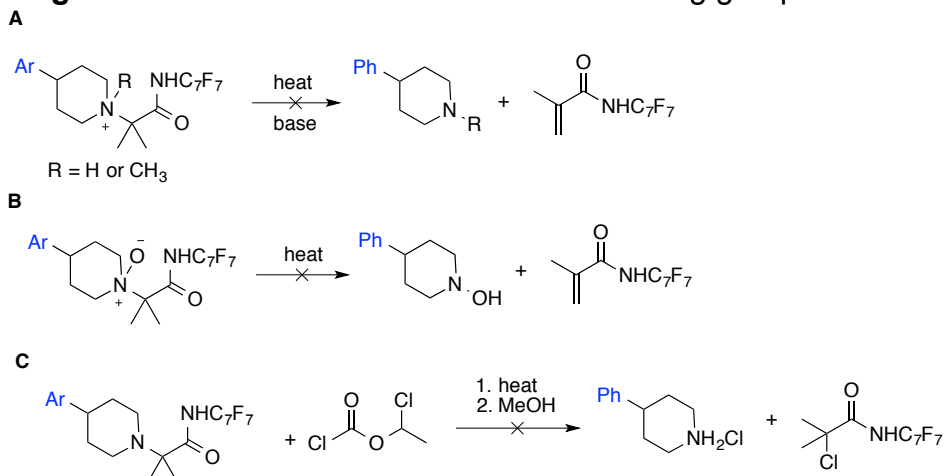
Figure 4.14. C–H arylation of bioactive bicyclic amines.



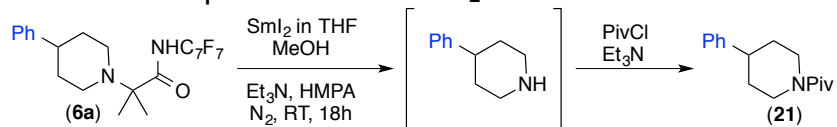
An important aspect of the method is to provide the free amine by removing the directing group. Traditional routes to cleave C(sp³)–N bonds such as Hoffman elimination of the quaternary ammonium salt of the substrate, Cope elimination from the

N-oxide of the substrate or chloroformate de-alkylation led to low yields of the free amine (Figure 4.15).

Figure 4.15. Unsuccessful methods for directing group removal.



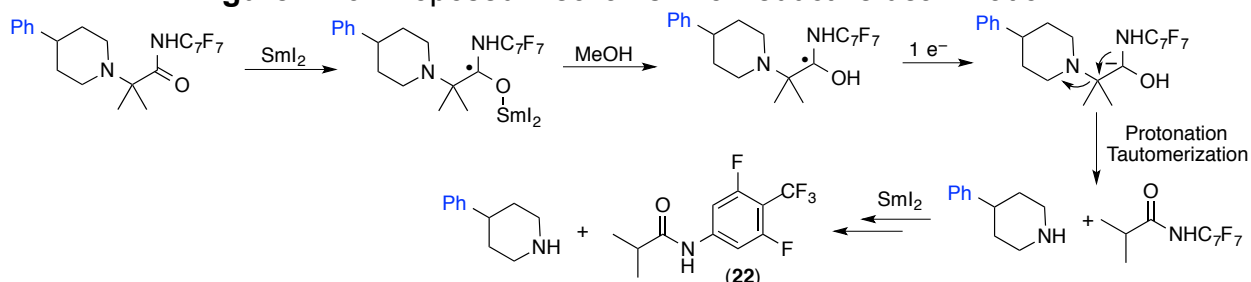
Thus, we next explored methods to reductively cleave the C–N bond. Our initial trials with outer sphere reductants such as strongly reducing photoredox catalysts led to decomposition products attributed to the reduction of the perfluoroarene (C₇F₇) in the substrate. Inspired by the work of Honda and co-workers in the inner sphere SmI₂ reductive cleavage of C–N bonds, we began optimizing reaction conditions to cleave the directing group employing SmI₂ (Table 4.7).³⁷ We found that using a mixture of methanol and triethylamine provided traces of the desired pivalated amine (**21**, entry 1). Further increasing the amount of MeOH and Et₃N afforded higher yields of **21** (entries 2-3). Optimal conditions for the reaction included addition of hexamethylphosphoramide (HMPA) to provide 95% yield of **21** (entry 4).

Table 4.7. Optimization for Sml₂ reductive deamination.^a

Entry	Sml ₂ (equiv)	MeOH (equiv)	Triethylamine (equiv)	Conversion	Yield
1	5	5	5	<10%	< 10%
2	10	15	15	74%	39%
3	10	50	50	94%	62%
4 ^b	10	50	50	100%	95%

^aConditions: **6a** (0.018 mmol, 1 equiv), Sml₂ (5-10 equiv, 0.1 M in THF), MeOH (5-50 equiv), triethylamine (5-50 equiv), THF (0.09 M in **6a**), N₂, RT, 18 hours. After 18 h, quench with PivCl (3 equiv), triethylamine (5 equiv). ^b Hexamethylphosphoramide was added (8 equiv). Calibrated GC yields.

Under the reductive deamination conditions, pivalated phenyl piperidine (**21**) was isolated in 74% yield. We proposed that Sml₂ chelates to the carbonyl group and undergoes two consecutive inner sphere 1 e⁻ reductions to release the free amine and perfluorinated isobutyramide (Figure 4.16). Due to the highly electrophilic perfluorinated amide, the directing group undergoes an *ortho*-defluorination reaction affording **22** as byproduct.

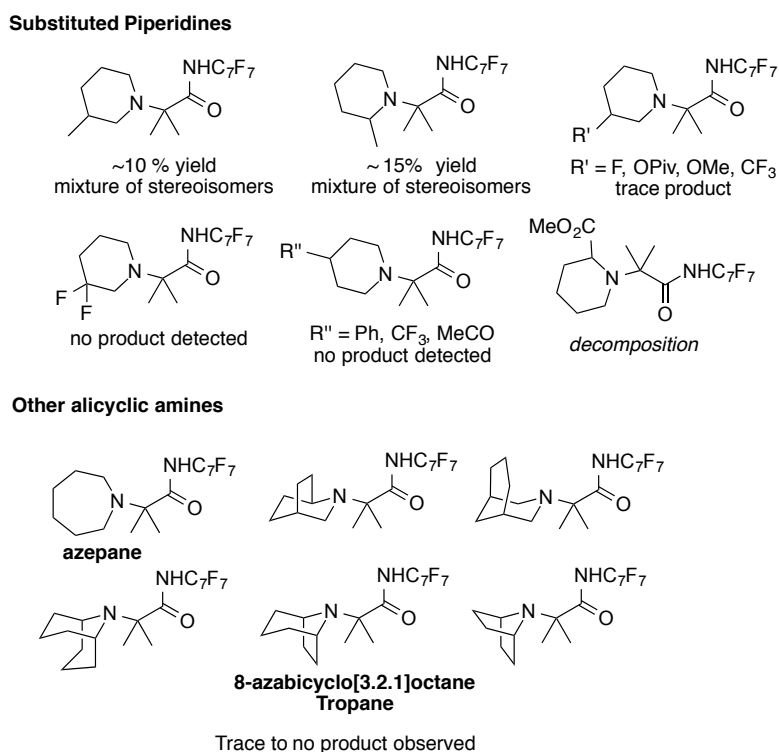
Figure 4.16. Proposed mechanism for reductive deamination.

Unsuccessful Substrates:

Several substituted piperidines and other bicyclic amines failed to generate C–H arylated products (all substrates in Figure 4.17 were analyzed by GC or GCMS). Although some substrates such as 3-methyl and 2-methyl piperidine showed product formation, the presence of stereoisomers and low yields (10% and 15%, respectively) afforded a complex mixture of isolated products. Larger ring sizes such as the 7-

member azepane did not provide the desired arylated product. Additionally, several other important bicyclic amines with adjacent substituents to the nitrogen atom such as 8-azabicyclo[3.2.1]octane core of tropane (prevalent in FDA approved drugs³⁸) only afforded traces of product. We proposed that accessing the high-energy boat conformer species in these amines is more difficult due to the presence of ring substituents that increase axial-axial interactions. In addition, adjacent substituents to the nitrogen atom can prevent favorable coordination to Pd. The exploration of these more challenging amines is described in chapter 5.

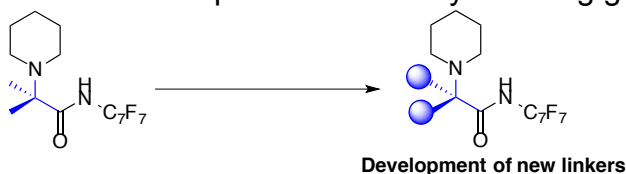
Figure 4.17. Unsuccessful amines for transannular C–H arylation.



Development of New Directing Groups:

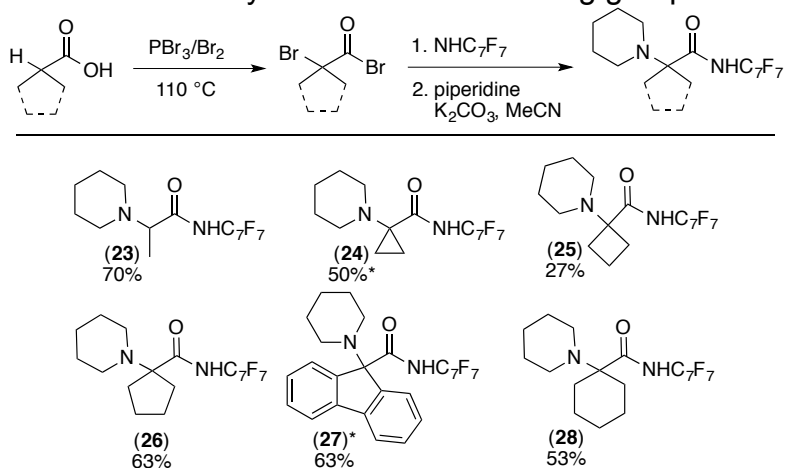
We decided to investigate the effect of substitution on the α -carbon that connects the alicyclic amine and the fluoroamide (Figure 4.18). We reasoned that the steric contribution of these substituents would modify the natural bite angle of the substrate and in turn influence reactivity upon coordination to the Pd catalyst.³⁹

Figure 4.18. Development of auxiliary directing groups.



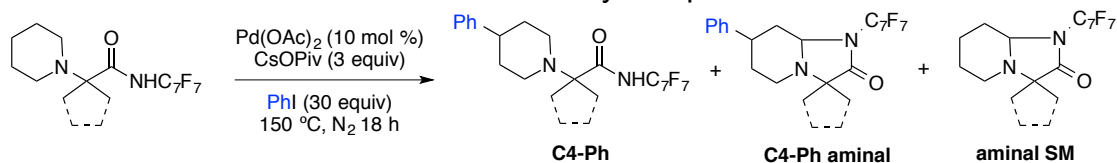
We sought out to develop a variety of new substrates with varying steric properties on the α -carbon. As shown in Table 4.8, substrates with varying substituents were synthesized including: methyl (**23**), cyclopropyl (**24**), cyclobutyl (**25**), cyclopentyl (**26**), fluorene (**27**) and cyclohexyl (**28**) linkers.

Table 4.8. Synthesis of new directing groups.^a



^a Yields shown correspond to the final amination step. * Synthesized by different synthetic route (see experimental section).

These compounds were reacted under a variety of reaction conditions and analyzed using a calibration curve for product **6a**. Table 4.9 shows a reactivity comparison of these substrates under the optimized conditions for piperidine substrate bearing a *gem*-dimethyl substituent (**5**). We noticed that most of these substrates were unstable at 150 °C as determined by the high starting material conversion but poor reactivity. Only substrate **26** afforded good mass balance with 31% of the arylated product.

Table 4.9. Substrates reactivity comparison at 150 °C.^a

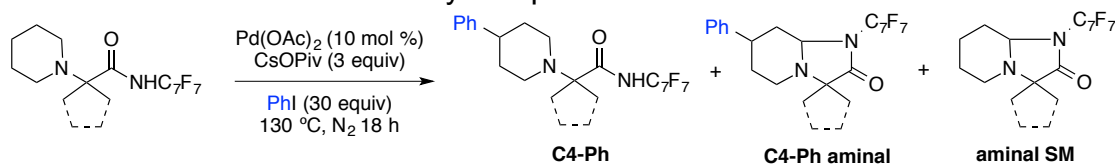
Entry	Substrate	Conversion	C4-Ph	C4-Ph aminor	Aminor SM
1	5	93%	44%	11%	28%
2	23	75%	15%	< 2%	9%
3	24	100%	nd	nd	nd
4	25	100%	nd	nd	nd
5	26	92%	31%	13%	26%
7	28	93%	4%	7%	< 2%

^aConditions: substrate (0.03 mmol, 1 equiv), $\text{Pd}(\text{OAc})_2$ (10 mol %), CsOPiv (3 equiv), iodobenzene (30 equiv), N_2 , 150 °C, 18 hours. All yields determined by gas chromatography (GC) with a calibration curve for **6a**. nd = not detected.

As such, we decided to lower the reaction temperature to 130 °C (Table 4.10). Under these reaction conditions, substrate **23** bearing a methyl substituent did not provide detectable amounts of arylated product and mostly unreacted starting material was observed (10% conversion, entry 2). In contrast, substrates **24** and **25** bearing the cyclopropyl and cyclobutyl substituents, respectively, led to unidentified decomposition products (entries 3 and 4). To our delight, substrate **26** (cyclopentyl substituent) and **28** (cyclohexyl substituent) resulted in comparable reactivity to substrate **5** (19%, 24% respectively, versus 30%, entries 5, 6 versus entry 1). However, we noticed that aminor formation from starting material with these substrates (**26** and **28**) was higher than that for substrate **5**. Given the possibility of substrate **28** to undergo arylation at the cyclohexyl ring instead of the piperidine ring, we synthesized an authentic sample of the phenyl arylated product using 4-phenyl piperidine. We were unable to fully purify the authentic product away from starting material, but analysis by GC confirmed that the arylated product from C–H activation is functionalizing the piperidine ring. With the promising reactivity of substrate **28** (38% yield of arylated products), we conducted further reaction optimization with this substrate. Despite our efforts to minimize

competing aminal formation and increase the yield of arylated product with **28**, no significant improvement was observed.

Table 4.10. Reactivity comparison of substrates at 130 °C.

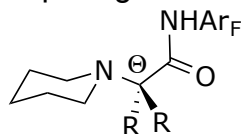


entry	substrate	conversion	C4-Ph	C4-Ph aminal	aminal SM
1	5	63%	30%	< 2%	8%
2	23	10%	nd	nd	nd
3	24	100%	nd	nd	nd
4	25	not determined	nd	nd	nd
5	26	58%	19%	< 2%	23%
6	28	86%	24%	14%	31%

^aConditions: substrate (0.03 mmol, 1 equiv), Pd(OAc)₂ (10 mol%), CsOPiv (3 equiv), iodobenzene (30 equiv), N₂, 130 °C, 18 hours. All yields determined by gas chromatography (GC) with a calibration curve for **6a**. nd = not detected.

Overall, we were able to show that substituents at the linker carbon have drastic effects on reactivity. We observed that the best reaction yields are obtained for substrates with large substituents in the order cyclohexyl > *gem*-dimethyl > cyclopentyl >>> methyl, cyclobutyl and cyclopropyl (at 130 °C). These results indicate that compression of the internal angle N_{piperidine}-C-C_{carbonyl} (θ) is important for reactivity (Figure 4.19). However, aminal byproduct formation increases in a similar order of reactivity. This is attributed to the increased Thorpe-Ingold effect (*gem*-dimethyl effect).⁴⁰ Several cyclization reactions analogous to the proposed aminal formation have shown that as the angle between the nucleophile and electrophile is compressed, reactivity increases.

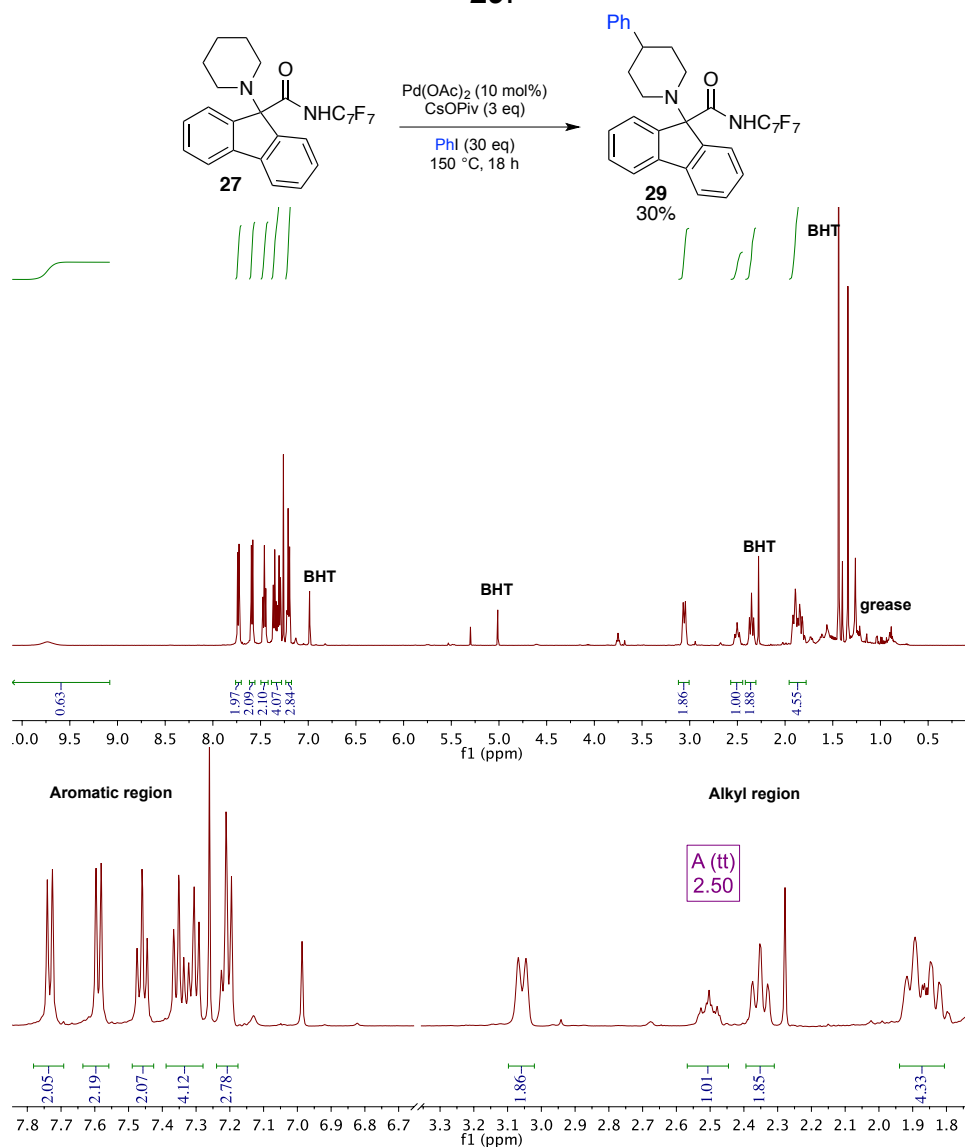
Figure 4.19. Thorpe-Ingold Effect in substrates.



Finally, reactions with substrate **27** were difficult to analyze by GC. However, product from substrate **27** was isolated in 30% yield. As shown in Figure 4.20, the ^1H NMR of the isolated product **29** indicates that arylation occurred at the C4 position of piperidine. This is consistent with the diagnostic triplet of triplets resonance of the benzylic C–H bond at 2.5 ppm of the alkyl region. This is remarkable as nearby reactive $\text{C}(\text{sp}^2)\text{--H}$ bonds were not functionalized.⁴¹ Signals corresponding to BHT (stabilizer for THF) and grease show up in the spectrum as 10% THF in hexanes was used for isolation.

Compound **27** has very attractive characteristics due to the presence of a benzylic alicyclic amine. This offers opportunities to cleave the directing group using alternative routes such as Pd/C hydrogenations. Unfortunately, **27** was very insoluble which made substrate synthesis and product isolation difficult.

Figure 4.20. C–H Arylation of substrate **27** and ^1H NMR spectrum of isolated product **29**.



4.3 Conclusions

In summary, we have developed a protocol for the transannular C–H functionalization of a wide range of alicyclic amines. We demonstrated that the native nitrogen atom in these amines serve as a coordination point to direct Pd to the ring and undergoes C–H activation from the boat conformer. The reaction exhibits high compatibility with a wide range of aryl iodides in the diversification of 3-azabicyclo[3.1.0]hexane. We demonstrated that several bicyclic amine scaffolds

undergo mono- or di-arylation reactions with modest to good yields. The utility of the methodology was demonstrated with the synthesis and isolation of several arylated analogs of amitifadine, varenicline and cytisine. Several cyclic and bicyclic amines are not compatible with our system, presumably due to the difficulty in accessing boat conformer species and/or steric hindrance of the amine by α -substituents. The exploration of these more challenging amines is described in the next chapter. Finally, several auxiliary directing groups were synthesized which showed a wide range of reactivity toward the C4–H functionalization of piperidine.

4.4 Experimental

General Procedures, Materials, and Methods for Synthesis and C–H Activation

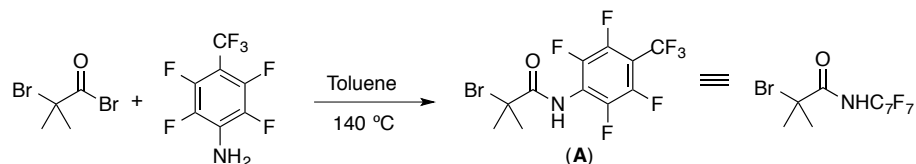
Instrumental Information. NMR spectra were obtained on Varian 400 MHz, Varian 500 MHz, or Varian 700 MHz NMR spectrometers. ^1H and ^{13}C NMR chemical shifts are reported in parts per million relative to TMS with the residual solvent peak (most commonly CDCl_3) used as an internal reference (δ 7.26 for ^1H NMR and δ 77.2 for ^{13}C NMR for CDCl_3). ^{19}F NMR spectra were referenced to the solvent lock. ^1H and ^{19}F multiplicities are reported as follows: singlet (s), doublet (d), triplet (t), quartet (q), and multiplet (m). High resolution mass spectra were obtained at the University of Michigan core facility. Flash chromatography was conducted on a Biotage Isolera One auto chromatography system using preloaded high performance silica gel columns (10 g, 25 g, 50 g, or 100 g as appropriate). GC-FID was conducted on a Shimadzu CG-17A system. Melting points were obtained on a OptiMelt automated melting point system. IR spectra were obtained on an FT Perkin Elmer instrument via thin film deposition.

Materials. All reagents were obtained from a commercial vendor (Aldrich, CombiBlocks, Oakwood, AstaTech, Synthonix, Enamine, Manchester Organics, Carbosynth, Pressure Chemicals, Matrix, SantaCruz Biotech, or Ontario Chemicals) and were used without further purification unless otherwise stated. Reagents were stored under ambient conditions unless otherwise stated. The solvent *tert*-amyl alcohol was stored over

activated molecular sieves. Solutions of SmI_2 were stored and used inside of a nitrogen-filled glovebox.

General Methods. The manipulation of solid reagents was conducted on the bench top unless otherwise stated. Reactions were conducted under an ambient atmosphere unless otherwise stated. Reaction vessels were sealed with either a septum (flask) or a Teflon-lined cap (4 mL or 20 mL vial). Reactions conducted at elevated temperatures were heated on a hot plate using an aluminum block. Temperatures were regulated using an external thermocouple. For reactions that were heated in excess of the ambient boiling point of the solvent (e.g. *tert*-amyl alcohol heated to 140 °C), electrical tape was wrapped around the cap of the sealed vial prior to heating. For TLC analysis, R_f values are reported based on normal phase silica plates with fluorescent indicator, and sample detection was conducted based on quenched fluorescence at 254 nm.

Synthesis and Characterization:



Compound A. A round bottom flask was charged with 2,3,5,6-tetrafluoro-4-(trifluoromethyl)aniline (7.01 g, 30.1 mmol, 1 equiv) and toluene (30 mL). To this solution, 2-bromoisobutyryl bromide (4 mL, 32.3 mmol, 1.1 equiv) was added. The flask was fitted with a reflux condenser topped with a drying tube that was packed with K_2CO_3 (5 g). The reaction was heated to an external temperature of 140 °C. After 18 h, the reaction mixture was cooled to room temperature and concentrated under vacuum. The solid residue was redissolved in a minimum amount of hexanes and heated to reflux. Upon slow cooling, a crystalline solid precipitated from solution. The solid was collected and rinsed with cold hexanes (3 x 5 mL). The solid was then dried under vacuum to afford product **A** as white needles (10.9 g, 95% yield).

MP 125-126 °C

IR (thin film): 1685 cm^{-1}

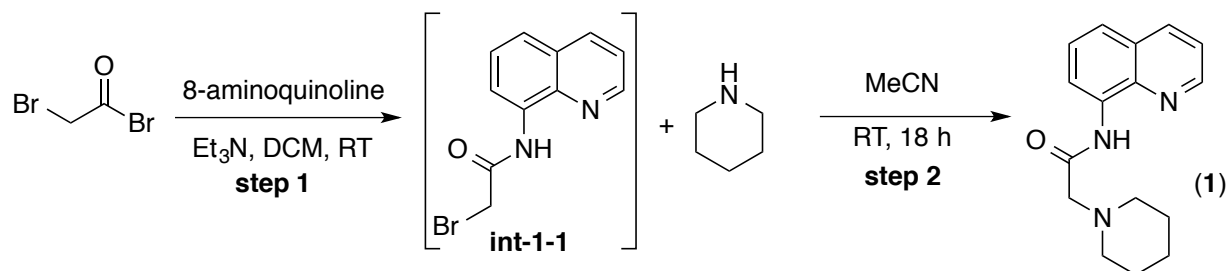
^1H NMR (700 MHz, CDCl_3) δ 8.19 (s, 1H), 2.06 (s, 6H).

^{19}F NMR (377 MHz, CDCl_3) δ -56.0 (t, J = 21.7 Hz, 3F), -141.2 (m, 2F), -144.2 (m, 2F). The carbon resonances corresponding to the perfluoroarene (C_7F_7) in this compound appear as a complex series of multiplets between 105 ppm to 155 ppm as a result of $^{13}\text{C}/^{19}\text{F}$ coupling. Due to the complexities of the system, the peaks are not listed. ^{19}F NMR and HRMS were used to confirm the presence of this ring system.

^{13}C NMR (176 MHz, CDCl_3) δ 170.2, 60.7, 32.2.

HRMS (ESI $^+$) $[\text{M}+\text{H}]^+$ Calcd for $\text{C}_{11}\text{H}_8\text{BrF}_7\text{NO}^+$: 381.9677; Found: 381.9668.

R_f = 0.55 in 20% EtOAc in hexanes.



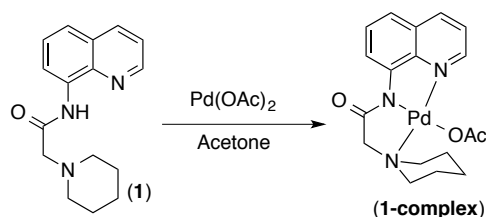
Substrate 1. Step 1. 8-aminoquinoline (500 mg, 3.5 mmol, 1 equiv) was dissolved in DCM (17.5 mL, 0.2 M) followed by addition of Et_3N (0.5 mL, 3.5 mmol, 1 equiv). To this solution, 2-bromoacetyl bromide (0.35 mL, 4 mmol, 1.1 equiv) was added. The mixture was stirred for 45 minutes at room temperature. After consumption of the starting reagents, based on TLC monitoring, the solution was concentrated. Purification of the crude product via column chromatography (100% DCM) provided 2-bromo-*N*-(quinolin-8-yl)acetamide intermediate (**int-1-1**) and was subsequently used in the next step.

Step 2. Int-1-1 (400 mg, 1.5 mmol, 1 equiv) was dissolved in acetonitrile (7.5 mL, 0.2 M), followed by addition of piperidine (0.45 mL, 4.5 mmol, 3 equiv). This mixture was stirred overnight at room temperature. The volatiles were removed and the crude product was purified via column chromatography (25% EtOAc in hexanes) affording 72% yield of desired product.

^1H NMR (CDCl_3 , 700 MHz): δ 11.51 (br s, 1H), 8.82 (dd, J = 4.1, 1.7 Hz, 1H), 8.77 (m, 1H), 8.08 (dd, J = 8.2, 1.7 Hz, 1H), 7.49 (m, 1H), 7.44 (m, 1H), 7.38 (dd, J = 8.2, 4.1 Hz, 1H), 3.23 (s, 2 H), 2.57 (br s, 4H), 1.74 (m, 4 H), 1.50 (br s, 2 H).

^{13}C NMR (CDCl_3 , 175.95 MHz): δ 169.82, 148.44, 139.01, 136.00, 134.52, 127.98, 127.21, 121.51, 121.46, 116.38, 63.32, 54.94, 26.31, 23.91.

HRMS (ESI $^+$) $[\text{M}+\text{H}]^+$ calcd for $\text{C}_{16}\text{H}_{20}\text{N}_3\text{O}$: 270.1601; found: 270.1601.

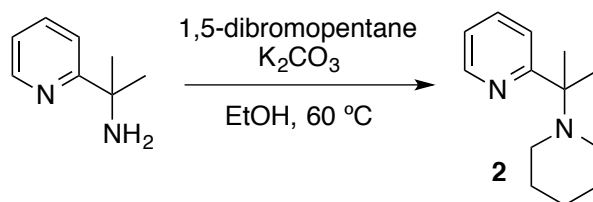


1-complex. A 20-mL vial was charged with **1** (60 mg, 0.22 mmol, 1 equiv), Pd(OAc)₂ (51 mg, 0.22 mmol, 1 equiv) in acetone (1 mL, 0.2 M). The mixture was stirred at room temperature until a yellow precipitate formed. Then, the yellow colored product was collected via filtration and washed with Et₂O (10 mL) affording 91% yield of **1-complex**.

¹H NMR (CDCl₃, 700 MHz) δ 8.62 (app. d, *J* = 7.9 Hz, 1H), 8.24 (dd, *J* = 8.3, 1.4 Hz, 1H), 8.16 (dd, *J* = 5.0, 1.4 Hz, 1H), 7.48 (t, *J* = 7.9 Hz, 1H), 7.37 (dd, *J* = 8.3, 5.0 Hz, 1H), 7.32 (app. d, *J* = 8.0 Hz, 1H), 3.95 (s, 2H), 3.62–3.46 (m, 2H), 3.33 (m, 2H), 2.15 (s, 3H), 1.86–1.65 (m, 3H), 1.63–1.40 (m, 3H).

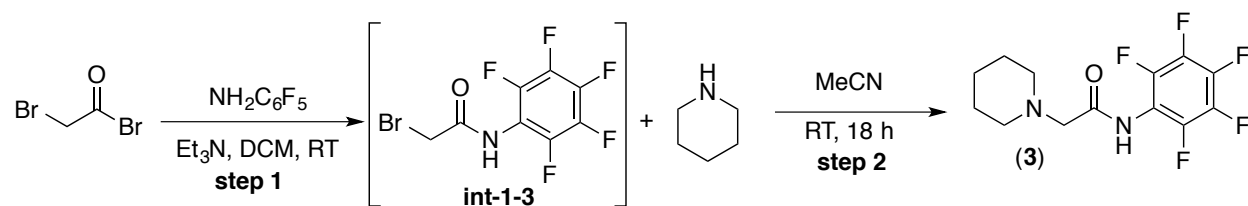
¹³C NMR (CDCl₃, 176 MHz) δ 178.21, 174.10, 148.65, 146.48, 144.93, 138.99, 129.70, 129.38, 121.02, 120.66, 120.09, 66.94, 59.20, 24.28, 23.10, 20.51.

HRMS (ESI⁺) [M–OAc]⁺ calcd for C₁₆H₁₈N₃OPd: 374.0485; found: 374.0489.



Compound 2. A 20-mL vial was charged with 2-(pyridin-2-yl)propan-2-amine (0.25 g, 1.84 mmol, 1 equiv), K₂CO₃ (0.25 g, 1.84 mmol, 1 equiv) and EtOH (0.7 mL). To this solution, 1,5-dibromopentane (0.3 mL, 2.2 mmol, 1.2 equiv) was added. The reaction mixture was heated to 60 °C for 2 days. After, the reaction was dissolved in DCM (15 mL) and washed with 10% KOH (3 x 5 mL). The organics were dried over Na₂SO₄, decanted, and concentrated via rotary evaporation. The residue was purified via column chromatography (100% DCM to 3:2:1 v/v DCM:Et₂O:Et₃N) to afford **2** in 65% yield.

¹H NMR (CDCl₃, 500 MHz) δ 8.51 (m, 1H), 7.76 (app. d, *J* = 8.1 Hz, 1H), 7.61 (td, *J* = 7.7, 1.8 Hz, 1H), 7.08 (m, 1H), 2.41 (br s, 4H), 1.54 (p, *J* = 5.6 Hz, 4H), 1.43 (m, 2H), 1.35 (s, 6H).



Substrate 3. Step 1. A 20-mL vial was charged with pentafluoroaniline (500 mg, 2.7 mmol, 1 equiv), Et_3N (0.38 mL, 2.7 mmol, 1 equiv) and DCM (13.5 mL, 0.2 M). 2-bromoacetyl bromide (0.30 mL, 3.24 mmol, 1.2 equiv) was added dropwise. The reaction was stirred for 30 minutes at room temperature. After, the volatiles were concentrated via rotary evaporation, and purification of the crude product by column chromatography (20% EtOAc in hexanes) afforded 76% yield of 2-bromo-N-(perfluorophenyl)acetamide intermediate (**int-1-3**), which was subsequently used in the next step.

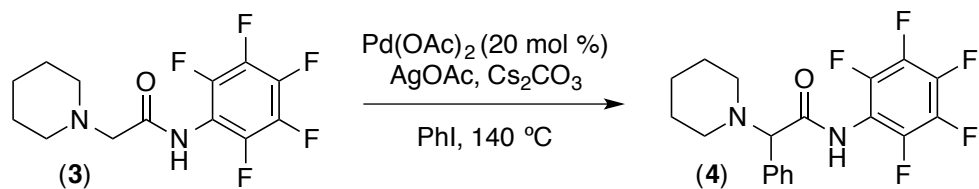
Step 2. A 20-mL vial was charged with **int-1-3** (228 mg, 0.75 mmol, 1 equiv), MeCN (5 mL, 0.15 M) and piperidine (0.22 mL, 2.25 mmol, 3 equiv). The reaction mixture was stirred at room temperature for 3 hours. The mixture was passed through a short silica plug and the volatiles were concentrated via rotary evaporation. The residue was dissolved in DCM (10 mL) and washed with water (3 x 5 mL). The organics were dried over Na_2SO_4 , filtered and concentrated to afford pure product **3** in 91% yield.

^1H NMR (CDCl_3 , 500 MHz) δ 8.95 (br s, 1 H), 3.16 (s, 2 H), 2.58 (app. s, 4 H), 1.65 (m, 4 H), 1.49 (app. s, 2H).

^{13}C NMR (CDCl_3 , 175 MHz) δ 169.8, 62.3, 55.1, 26.3, 23.7.

Note: The carbon resonances corresponding to the perfluoroarene (C_6F_5) in this compound appear as a complex series of multiplets between 110 ppm to 150 ppm as a result of $^{13}\text{C}/^{19}\text{F}$ coupling. Due to the complexities of the system, the peaks are not listed.

HRMS (ESI⁺) $[\text{M}+\text{H}]^+$ calcd for $\text{C}_{13}\text{H}_{14}\text{F}_5\text{N}_2\text{O}$: 309.1021; found: 309.1024.

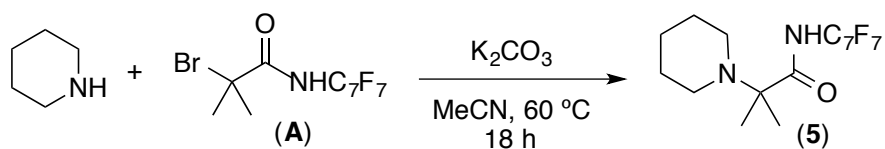


Compound 4. A 4-mL vial was charged with **3** (120 mg, 0.39 mmol, 1 equiv), Pd(OAc)₂ (17 mg, 0.078 mmol, 20 mol %), AgOAc (260 mg, 1.6 mmol, 4 equiv), Cs₂CO₃ (152 mg, 0.47 mmol, 1.2 equiv) and iodobenzene (1 mL). The mixture was heated to 140 °C for 18 hours. After, the crude product was purified by column chromatography (15% EtOAc in hexanes) affording 20% yield of **4**.

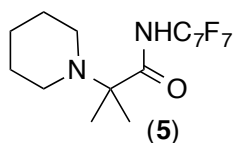
¹H NMR (CDCl₃, 400 MHz) δ 7.42–7.29 (multiple peaks, 5H), 4.12 (s, 1H), 2.49 (m, 4H), 1.64 (m, 4H), 1.46 (m, 2H). Note: N–H not observed.

GCMS [M– C₇H₂F₅NO] calcd for C₁₂H₁₆N: 174.1277; found: 174.15.

Synthesis of amine starting materials



A 20-mL scintillation vial was charged with piperidine (86 mg, 1.01 mmol, 1 equiv), α-bromo methylpropanamide **A** (430 mg, 1.1 mmol, 1.1 equiv), and K₂CO₃ (280 mg, 2.02 mmol, 2 equiv). To the solids, anhydrous acetonitrile (5 mL) was added. The vial was sealed, and the reaction was heated to an external temperature of 60 °C. After 18 h, the reaction was cooled to room temperature, diluted with EtOAc (~5 mL), and filtered through Celite. The filtrate was concentrated under reduced pressure. Final purification via column chromatography (gradient elution from 0% to 20% EtOAc in hexanes) afforded product **5** (328 mg, 84% yield) as a white solid. Other amine derivatives were prepared in an analogous manner by using the appropriate amine starting material. When an amine hydrochloride was used, 3.2 equiv of K₂CO₃ were used. When the amine free base was used, 2 equiv of K₂CO₃ were used. See substrate specific notes below.



MP 72-74 °C

IR (thin film): 1707 (br) cm^{-1}

^1H NMR (700 MHz, CDCl_3) δ 9.50 (br s, 1H), 2.50 (br s, 4H), 1.66 (br s, 4H), 1.51 (br s, 2H), 1.29 (s, 6H).

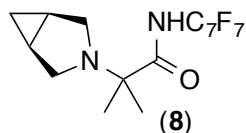
^{19}F NMR (377 MHz, CDCl_3) δ -56.0 (t, $J = 21.7$ Hz, 3F), -141.2 (m, 2F), -144.2 (m, 2F).

The carbon resonances corresponding to the perfluoroarene (C_7F_7) in this compound appear as a complex series of multiplets between 105 ppm to 155 ppm as a result of $^{13}\text{C}/^{19}\text{F}$ coupling. Due to the complexities of the system, the peaks are not listed. ^{19}F NMR and HRMS were used to confirm the presence of this ring system.

^{13}C NMR (176 MHz, CDCl_3) δ 175.9, 64.9, 48.0, 26.7, 24.5, 20.5.

HRMS (ESI⁺) $[\text{M}+\text{H}]^+$ Calcd for $\text{C}_{16}\text{H}_{18}\text{F}_7\text{N}_2\text{O}^+$: 387.1307; Found: 387.1304.

$R_f = 0.60$ in 20% EtOAc in hexanes



Compound **8** was isolated in 81% yield as a white solid using standard conditions above.

MP 114-116 °C

IR (thin film): 1700 cm^{-1}

^1H NMR (700 MHz, CDCl_3) δ 9.02 (s, 1H), 2.88 (d, $J = 8.5$ Hz, 2H), 2.69 (dt, $J = 8.5, 1.6$ Hz, 2H), 1.43 (m, 2H), 1.31 (s, 6H), 0.63 (q, $J = 4.2$ Hz, 1H), 0.48 (td, $J = 7.7, 4.3$ Hz, 1H).

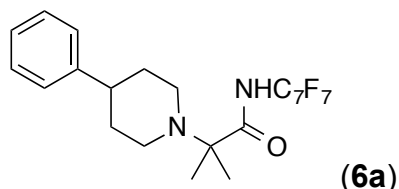
^{19}F NMR (377 MHz, CDCl_3) δ -56.0 (t, $J = 21.7$ Hz, 3F), -141.2 (m, 2F), -144.2 (m, 2F).

The carbon resonances corresponding to the perfluoroarene (C_7F_7) in this compound appear as a complex series of multiplets between 105 ppm to 155 ppm as a result of $^{13}\text{C}/^{19}\text{F}$ coupling. Due to the complexities of the system, the peaks are not listed. ^{19}F NMR and HRMS were used to confirm the presence of this ring system.

^{13}C NMR (176 MHz, CDCl_3) δ 175.1, 61.1, 47.6, 21.0, 14.5, 6.5.

HRMS (ESI⁺) [M+H]⁺ Calcd for C₁₆H₁₆F₇N₂O⁺: 385.1151; Found: 385.1145.

R_f = 0.60 in 20% EtOAc in hexanes



Authentic sample of compound **6a** was isolated in 80% yield as a white solid using the standard conditions.

MP 138-141 °C

IR (thin film): 1717 (br) cm⁻¹

¹H NMR (700 MHz, CDCl₃) δ 9.45 (s, 1H), 7.32 (t, *J* = 7.5 Hz, 2H), 7.25-7.20 (multiple peaks, 3H), 2.99 (d, *J* = 11.2 Hz, 2H), 2.58 (tt, *J* = 12.4, 3.9 Hz, 1H), 2.40 (td, *J* = 11.5, 2.1 Hz, 2H), 1.99 (dt, *J* = 12.7, 2.9 Hz, 2H), 1.79 (m, 2H), 1.36 (s, 6H).

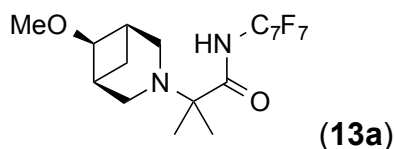
¹⁹F NMR (471 MHz, CDCl₃) δ -56.0 (t, *J* = 21.7 Hz, 3F), -141.0 (m, 2F), -144.1 (m, 2F).

The carbon resonances corresponding to the perfluoroarene (C₇F₇) in this compound appear as a complex series of multiplets between 105 ppm to 155 ppm as a result of ¹³C/¹⁹F coupling. Due to the complexities of the system, the peaks are not listed. ¹⁹F NMR and HRMS were used to confirm the presence of this ring system.

¹³C NMR (176 MHz, CDCl₃) δ 175.7, 145.6, 128.5, 126.7, 126.4, 64.8, 47.8, 42.6, 34.0, 20.5.

HRMS (ESI⁺) [M+H]⁺ Calcd for C₂₂H₂₂F₇N₂O⁺: 463.1620; Found: 463.1621.

R_f = 0.60 in 20% EtOAc in hexanes



Note: The trifluoroacetate salt of the amine was used as the precursor. Preparative TLC (10 % EtOAc in hexanes) was used for isolation of the substrate.

Compound **13a** was isolated in 33% yield as a white solid using the standard conditions.

MP 89-91 °C

IR (thin film): 1700 cm^{-1}

^1H NMR (500 MHz, CDCl_3) δ 9.67 (s, 1H), 3.57 (t, $J = 5$ Hz, 1H), 3.29 (s, 3H), 3.14 – 3.06 (multiple peaks, 4H), 2.65 (br s, 2H), 1.59 (d, $J = 10$ Hz, 1H), 1.50 (m, 1H), 1.43 (s, 6H).

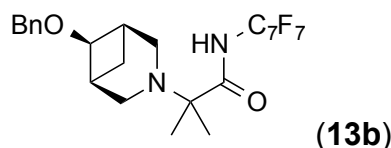
^{19}F NMR (377 MHz, CDCl_3) δ -56.1 (t, $J = 18.9$ Hz, 3F), -141.4 (m, 2F), -143.7 (m, 2F).

The carbon resonances corresponding to the perfluoroarene (C_7F_7) in this compound appear as a complex series of multiplets between 105 ppm to 155 ppm as a result of $^{13}\text{C}/^{19}\text{F}$ coupling. Due to the complexities of the system, the peaks are not listed. ^{19}F NMR and HRMS were used to confirm the presence of this ring system.

^{13}C NMR (126 MHz, CDCl_3) δ 176.4, 75.3, 63.4, 56.5, 44.7, 37.6, 22.8, 22.5.

HRMS (ESI⁺) $[\text{M}+\text{H}]^+$ Calcd for $\text{C}_{18}\text{H}_{20}\text{F}_7\text{N}_2\text{O}_2$: 429.1408 ; Found: 429.1411.

$R_f = 0.27$ in 10% EtOAc in hexanes



Note: The hydrochloric salt of the amine was used as the precursor.

Compound **13b** was isolated in 51% yield as a white solid using the standard conditions.

MP 111-113 $^{\circ}\text{C}$

IR (thin film): 1693 cm^{-1}

^1H NMR (700 MHz, CDCl_3) δ 9.60 (br s, 1H), 7.22 (d, $J = 7$ Hz, 2H), 7.14 (t, $J = 7$ Hz, 2H), 7.08 (t, $J = 7$ Hz, 1H), 4.47 (s, 2H), 3.87 (t, $J = 9.1$ Hz, 1H), 3.25 (d, $J = 14$ Hz, 2H), 3.15 (d, $J = 9.1$ Hz, 2H), 2.73 (t, $J = 4.9$ Hz, 2H), 1.57 (m, 1H), 1.46 (app d, $J = 9.1$ Hz, 1H), 1.42 (s, 6H).

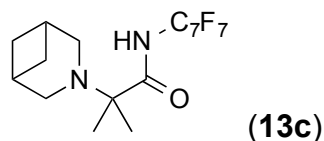
^{19}F NMR (377 MHz, CDCl_3) δ -56.20 (t, $J = 21.5$ Hz, 3F), -142.31 (m, 2F), -143.57 (m, 2F).

The carbon resonances corresponding to the perfluoroarene (C_7F_7) in this compound appear as a complex series of multiplets between 105 ppm to 155 ppm as a result of $^{13}\text{C}/^{19}\text{F}$ coupling. Due to the complexities of the system, the peaks are not listed. ^{19}F NMR and HRMS were used to confirm the presence of this ring system.

^{13}C NMR (176 MHz, CDCl_3) δ 176.8, 137.2, 128.2, 128.1, 128.0, 74.5, 72.1, 63.1, 45.7, 38.2, 24.2, 23.2.

HRMS (ESI⁺) $[\text{M}+\text{H}]^+$ Calcd for $\text{C}_{24}\text{H}_{23}\text{F}_7\text{N}_2\text{O}_2$: 505.1721; Found: 505.1721.

R_f = 0.19 in 10% EtOAc in hexanes



Compound **13c** was isolated in 56% yield as a white solid using the standard conditions.

MP 91-93 °C

IR (thin film): 1701 cm^{-1}

^1H NMR (700 MHz, CDCl_3) δ 9.22 (br s, 1H), 2.95 (s, 4H), 2.41 (tt, J = 5.9, 1.6 Hz, 2H), 2.05 (m, 2H), 1.49 (m, 2H), 1.38 (s, 6H).

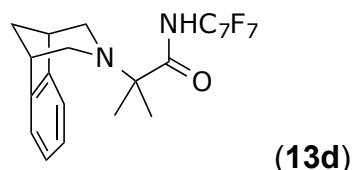
^{19}F NMR (377 MHz, CDCl_3) δ -56.0 (t, J = 21.7 Hz, 3F), -141.2 (m, 2F), -144.3 (m, 2F).

The carbon resonances corresponding to the perfluoroarene (C_7F_7) in this compound appear as a complex series of multiplets between 105 ppm to 155 ppm as a result of $^{13}\text{C}/^{19}\text{F}$ coupling. Due to the complexities of the system, the peaks are not listed. ^{19}F NMR and HRMS were used to confirm the presence of this ring system.

^{13}C NMR (176 MHz, CDCl_3) δ 175.5, 63.2, 49.9, 33.2, 32.6, 20.7.

HRMS (ESI⁺) $[\text{M}+\text{H}]^+$ Calcd for $\text{C}_{17}\text{H}_{18}\text{F}_7\text{N}_2\text{O}^+$: 399.1307; Found: 399.1300.

R_f = 0.60 in 20% EtOAc in hexanes



Compound **13d** was isolated in 86% yield as a white solid using the standard conditions.

MP 121-123 °C

IR (thin film): 1712 cm^{-1}

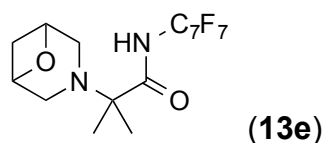
^1H NMR (700 MHz, CDCl_3) δ 7.49 (br s, 1H), 7.16 (dd, J = 5.3, 3.2 Hz, 2H), 7.06 (dd, J = 5.3, 3.1 Hz, 2H), 3.21 (t, J = 4.2 Hz, 2H), 2.70 (m, 2H), 2.69 (d, J = 10.4 Hz, 2H), 2.31 (dt, J = 10.3, 3.6 Hz, 1H), 1.74 (d, J = 10.4 Hz, 1H), 1.20 (s, 6H).

^{19}F NMR (377 MHz, CDCl_3) δ -56.0 (t, J = 21.8 Hz, 3F), -141.5 (m, 2F), -143.0 (m, 2F). The carbon resonances corresponding to the perfluoroarene (C_7F_7) in this compound appear as a complex series of multiplets between 105 ppm to 155 ppm as a result of $^{13}\text{C}/^{19}\text{F}$ coupling. Due to the complexities of the system, the peaks are not listed. ^{19}F NMR and HRMS were used to confirm the presence of this ring system.

^{13}C NMR (176 MHz, CDCl_3) δ 176.2, 145.5, 126.7, 121.6, 63.7, 50.5, 43.6, 41.0, 21.6.

HRMS (ESI⁺) $[\text{M}+\text{H}]^+$ Calcd for $\text{C}_{22}\text{H}_{20}\text{F}_7\text{N}_2\text{O}^+$: 461.1464; Found: 461.1469.

R_f = 0.55 in 20% EtOAc in hexanes



Note: The tosylate salt of the amine was used as the precursor.

Compound **13e** was isolated in 59% yield as an oil using the standard conditions.

IR (thin film): 1702 (br) cm^{-1}

^1H NMR (700 MHz, CDCl_3) δ 8.97 (s, 1H), 4.58 (m, 2H), 3.12 – 3.03 (multiple peaks, 3H), 2.96 (dt, J = 11.5, 2.0 Hz, 2H), 2.26 (d, J = 8.3 Hz, 1H), 1.39 (s, 6H).

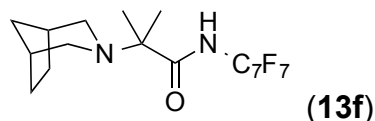
^{19}F NMR (377 MHz, CDCl_3) δ -56.3 (t, J = 21.7 Hz, 3F), -141.4 (m, 2F), -144.5 (m, 2F).

The carbon resonances corresponding to the perfluoroarene (C_7F_7) in this compound appear as a complex series of multiplets between 105 ppm to 155 ppm as a result of $^{13}\text{C}/^{19}\text{F}$ coupling. Due to the complexities of the system, the peaks are not listed. ^{19}F NMR and HRMS were used to confirm the presence of this ring system.

^{13}C NMR (176 MHz, CDCl_3) δ 174.6, 79.1, 63.3, 48.8, 30.0, 20.6.

HRMS (ESI⁺) $[\text{M}+\text{H}]^+$ Calcd for $\text{C}_{16}\text{H}_{16}\text{F}_7\text{N}_2\text{O}_2^+$: 401.1100; Found: 401.1095.

R_f = 0.30 in 35% EtOAc in hexanes



Compound **13f** was isolated in 93% yield as a white solid using standard conditions, except that purification was conducted via column chromatography, followed by recrystallization of the substrate from hot hexanes.

MP 121-123 °C

IR (thin film): 1699 cm⁻¹

¹H NMR (500 MHz, CDCl₃) δ 9.24 (s, 1H), 2.61 (dd, *J* = 4, 11 Hz, 2H), 2.37 (d, *J* = 11 Hz, 2H), 2.23 (br s, 2H), 1.66 (m, 4 H), 1.50 (m, 1H), 1.39 (d, *J* = 11 Hz, 1H), 1.26 (s, 6H).

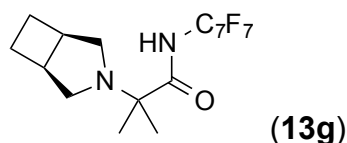
¹⁹F NMR (471 MHz, CDCl₃): -56.3 (t, *J* = 23.6 Hz, 3F), -141.7 (m, 2F), -143.7 (m, 2F)

The carbon resonances corresponding to the perfluoroarene (C₇F₇) in this compound appear as a complex series of multiplets between 105 ppm to 155 ppm as a result of ¹³C/¹⁹F coupling. Due to the complexities of the system, the peaks are not listed. ¹⁹F NMR and HRMS were used to confirm the presence of this ring system.

¹³C NMR (176 MHz, CDCl₃) δ 176.0, 64.2, 53.3, 37.5, 35.2, 28.2, 20.8.

HRMS (ESI⁺) [M+H]⁺ Calcd for C₁₈H₂₀F₇N₂O: 413.1458 ; Found: 413.1460.

R_f = 0.29 in 5% EtOAc in hexanes



Note: The hydrochloric salt of the amine was used as the precursor.

Compound **13g** was isolated in 40% yield as a white solid using the standard conditions.

MP 84-86 °C

IR (thin film): 1700 cm⁻¹

¹H NMR (500 MHz, CDCl₃) δ 9.64 (br s, 1H), 2.86 (m, 2H), 2.75 (d, *J* = 9.5 Hz, 2H), 2.46 (dd, *J* = 9.5, 5 Hz, 2H), 2.25 (s, *J* = 6.5 Hz, 2H), 1.72 (m, 2H), 1.39 (s, 6H).

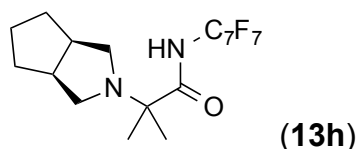
¹⁹F NMR (471 MHz, CDCl₃) δ -56.0 (t, *J* = 23.6 Hz, 3F), -141.2 (m, 2F), -143.7 (m, 2F).

The carbon resonances corresponding to the perfluoroarene (C₇F₇) in this compound appear as a complex series of multiplets between 105 ppm to 155 ppm as a result of ¹³C/¹⁹F coupling. Due to the complexities of the system, the peaks are not listed. ¹⁹F NMR and HRMS were used to confirm the presence of this ring system.

¹³C NMR (126 MHz, CDCl₃) δ 175.7, 61.7, 53.7, 36.5, 24.4, 21.2.

HRMS (ESI⁺) [M+H]⁺ Calcd for C₁₇H₁₈F₇N₂O: 399.1302; Found: 399.1299.

R_f = 0.33 in 10% EtOAc in hexanes



Note: The hydrochloric salt of the amine was used as the precursor.

Compound **13h** was isolated in 45% yield as a white solid using the standard conditions.

MP 68-70 °C

IR (thin film): 1698 cm^{-1}

^1H NMR (700 MHz, CDCl_3) δ 9.38 (br s, 1H), 2.75 (app t, $J = 7.7$ Hz, 2H), 2.58 (m, 2H), 2.37 (app d, $J = 7.7$ Hz, 2H), 1.81 (app sextet, $J = 7$ Hz, 2H), 1.65 (septet, $J = 7$ Hz, 1H), 1.52 (septet, $J = 7$ Hz, 1H), 1.39 (m, 2H), 1.32 (s, 6H).

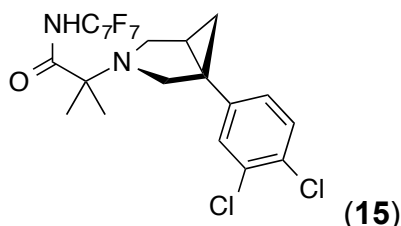
^{19}F NMR (377 MHz, CDCl_3) δ -56.04 (t, $J = 21.9$ Hz, 3F), -141.24 (m, 2F), -143.95 (m, 2F).

The carbon resonances corresponding to the perfluoroarene (C_6F_5) in this compound appear as a complex series of multiplets between 105 ppm to 155 ppm as a result of $^{13}\text{C}/^{19}\text{F}$ coupling. Due to the complexities of the system, the peaks are not listed. ^{19}F NMR and HRMS were used to confirm the presence of this ring system.

^{13}C NMR (176 MHz, CDCl_3) δ 175.5, 61.7, 54.0, 41.8, 33.6, 26.8, 20.9.

HRMS (ESI⁺) $[\text{M}+\text{H}]^+$ Calcd for $\text{C}_{18}\text{H}_{19}\text{F}_7\text{N}_2\text{O}$: 413.1458; Found: 413.1458.

$R_f = 0.23$ in 10% EtOAc in hexanes



Compound **15** was isolated in 87% yield as a white solid using standard conditions above.

MP 75-77 °C

IR (thin film): 1716 (br) cm^{-1}

^1H NMR (700 MHz, CDCl_3) δ 8.93 (s, 1H), 7.34 (d, $J = 8.3$ Hz, 1H), 7.23 (d, $J = 2.2$ Hz, 1H), 6.99 (dd, $J = 8.3, 2.2$ Hz, 1H), 3.22 (d, $J = 8.5$ Hz, 1H), 3.02 (d, $J = 8.6$ Hz, 1H),

2.95-2.88 (multiple peaks, 2H), 1.82 (dt, $J = 7.9, 3.9$ Hz, 1H), 1.41 – 1.38 (multiple peaks, 4H), 1.37 (s, 3H), 0.93 (dd, $J = 8.0, 4.8$ Hz, 1H).

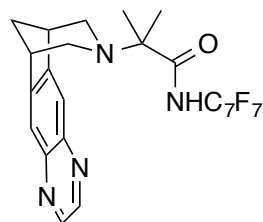
^{19}F NMR (377 MHz, CDCl_3) δ -56.0 (t, $J = 21.7$ Hz, 3F), -141.0 (dd, $J = 21.7, 11.7$ Hz, 2F), -144.1 (m, 2F).

The carbon resonances corresponding to the perfluoroarene (C_7F_7) in this compound appear as a complex series of multiplets between 105 ppm to 155 ppm as a result of $^{13}\text{C}/^{19}\text{F}$ coupling. Due to the complexities of the system, the peaks are not listed. ^{19}F NMR and HRMS were used to confirm the presence of this ring system.

^{13}C NMR (176 MHz, CDCl_3) δ 174.5, 142.3, 132.3, 130.2, 130.0, 128.5, 125.9, 61.3, 51.5, 47.9, 29.3, 23.8, 21.2, 20.7, 16.6.

HRMS (ESI⁺) $[\text{M}+\text{H}]^+$ Calcd for $\text{C}_{22}\text{H}_{18}\text{F}_7\text{N}_2\text{O}^+$: 529.0684; Found: 529.0679.

$R_f = 0.60$ in 20% EtOAc in hexanes



Note: the tartrate salt of the amine was used as the precursor

Compound **17** was isolated in 81% yield as a white solid using standard conditions.

MP 153-155 °C

IR (thin film): 1718 cm^{-1}

^1H NMR (700 MHz, CDCl_3) δ 8.67 (s, 2H), 7.76 (s, 2H), 7.37 (s, 1H), 3.46 (t, $J = 4.5$ Hz, 2H), 2.96 (dd, $J = 11.0, 4.3$ Hz, 2H), 2.83 (d, $J = 10.8$ Hz, 2H), 2.38 (dt, $J = 11.0, 4.5$ Hz, 1H), 1.92 (d, $J = 10.9$ Hz, 1H), 1.16 (s, 6H).

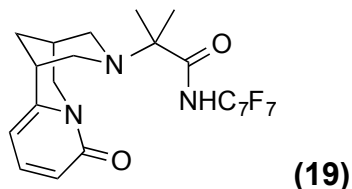
^{19}F NMR (377 MHz, CDCl_3) δ -56.1 (t, $J = 21.7$ Hz, 3F), -141.4 (m, 2F), -144.3 (m, 2F).

The carbon resonances corresponding to the perfluoroarene (C_7F_7) in this compound appear as a complex series of multiplets between 105 ppm to 155 ppm as a result of $^{13}\text{C}/^{19}\text{F}$ coupling. Due to the complexities of the system, the peaks are not listed. ^{19}F NMR and HRMS were used to confirm the presence of this ring system.

^{13}C NMR (176 MHz, CDCl_3) δ 174.9, 149.6, 143.9, 143.1, 120.9, 63.8, 51.7, 42.8, 40.9, 21.3.

HRMS (ESI⁺) [M+H]⁺ Calcd for $\text{C}_{24}\text{H}_{20}\text{F}_7\text{N}_4\text{O}^+$: 513.1525; Found: 513.1519.

R_f = 0.50 in 50% EtOAc in hexanes



Note: Sodium iodide (1 equiv) was added to the reaction mixture.

Compound **19** was isolated in 85% yield as light yellow solid using standard conditions.

MP 65-67 °C

IR (thin film): 1700, 1653 cm^{-1}

^1H NMR (500 MHz, CDCl_3) δ 7.72 (s, 1H), 7.02 (dd, J = 6.5, 9 Hz, 1H), 6.28 (app d, J = 9 Hz, 1H), 5.94 (app d, J = 6.5 Hz, 1H), 4.18 (d, J = 15.5 Hz, 1H), 3.87 (dd, J = 6 Hz, 15.5 Hz, 1H), 3.10-3.07 (multiple peaks, 2H), 2.87 (m, 1H), 2.66-2.56 (multiple peaks, 3H), 1.98 (m, 1H), 1.86 (m, 1H), 1.29 (s, 3H), 1.19 (s, 3H).

^{19}F NMR (377 MHz, CDCl_3) δ -56.1 (t, J = 22.6 Hz, 3F), -141.0 (m, 2F), -142.8 (m, 2F).

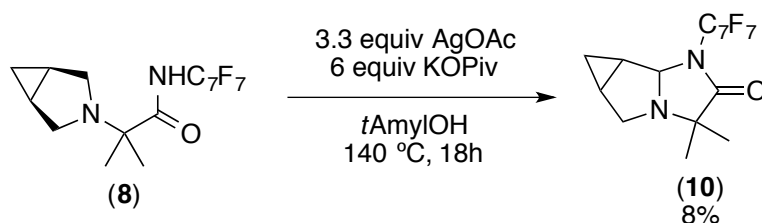
The carbon resonances corresponding to the perfluoroarene (C_7F_7) in this compound appear as a complex series of multiplets between 105 ppm to 155 ppm as a result of $^{13}\text{C}/^{19}\text{F}$ coupling. Due to the complexities of the system, the peaks are not listed. ^{19}F NMR and HRMS were used to confirm the presence of this ring system.

^{13}C NMR (126 MHz, CDCl_3) δ 174.9, 163.0, 150.3, 138.3, 116.9, 104.8, 64.5, 55.7, 53.0, 49.9, 35.5, 28.0, 26.1, 23.5, 17.7.

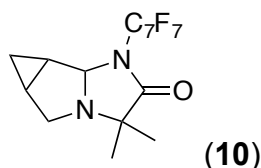
HRMS (ESI⁺) [M+H]⁺ Calcd for $\text{C}_{22}\text{H}_{21}\text{F}_7\text{N}_3\text{O}_2$: 492.1517; Found: 492.1517.

R_f = 0.09 in 60% EtOAc in hexanes

Isolation of Amino Products



Under ambient conditions, a 4 mL scintillation vial was charged with amine **8** (45 mg, 0.12 mmol, 1 equiv), AgOAc (65 mg, 0.39 mmol, 3.3 equiv), and KO piv (94 mg, 0.67 mmol, 6 equiv). To the solids, *tert*-amyl alcohol (0.8 mL) was added. The vial was sealed with a Teflon-lined cap, wrapped in electrical tape, and heated to an external temperature of 140 °C. After 18 h, the reaction was removed from the heat source, diluted with EtOAc, and filtered through a plug of Celite. The filtrate was concentrated under reduced pressure. Final purification by column chromatography (10 g cartridge, gradient elution from 0% to 20% EtOAc in hexanes) afforded amino **10** (26 mg, 58% yield) as a yellow oil.



IR (thin film): 1728 (br) cm^{-1}

^1H NMR (700 MHz, CDCl_3) δ 5.29 (s, 1H), 3.10 – 3.03 (multiple peaks, 2H), 1.60 (m, 1H), 1.43 (ddd, J = 9.2, 6.2, 3.5 Hz, 1H), 1.38 (s, 3H), 1.37 (s, 3H), 0.82 (q, J = 4.3, Hz, 1H), 0.58 (td, J = 8.1, 4.9 Hz, 1H).

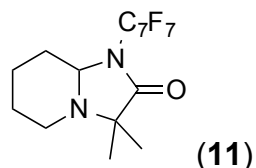
^{19}F NMR (377 MHz, CDCl_3) δ -56.2 (t, J = 21.8 Hz, 3F), -139.5 (br s, 1F), -140.2 (br s, 1F), -140.6 (m, 1F), -144.5 (m, 1F).

The carbon resonances corresponding to the perfluoroarene (C_7F_7) in this compound appear as a complex series of multiplets between 105 ppm to 155 ppm as a result of $^{13}\text{C}/^{19}\text{F}$ coupling. Due to the complexities of the system, the peaks are not listed. ^{19}F NMR and HRMS were used to confirm the presence of this ring system.

^{13}C NMR (176 MHz, CDCl_3) δ 177.4, 79.9, 63.7, 49.8, 24.9, 19.4, 17.5, 16.6, 6.0.

HRMS (ESI⁺) $[\text{M}+\text{H}]^+$ Calcd for $\text{C}_{16}\text{H}_{14}\text{F}_7\text{N}_2\text{O}^+$: 383.0994; Found: 383.0992.

$R_f = 0.30$ in 20% EtOAc in hexanes



Note: No KO₂Piv was used; instead 20 mol% Pd(OAc)₂ was added.

Compound **11** was isolated as faintly yellow solid in 47% yield.

MP 83 °C

IR (thin film): 1736 cm⁻¹

¹H NMR (700 MHz, CDCl₃) δ 4.25 (d, $J = 8.3$ Hz, 1H), 2.90 (m, 1H), 2.44 (td, $J = 11.4, 2.7$ Hz, 1H), 1.90 (m, 1H), 1.74-1.69 (m, 2H), 1.63 (m, 1H), 1.40 (t, $J = 4.5$ Hz, 2H), 1.36 (s, 3H), 1.16 (s, 3H).

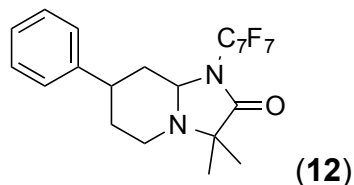
¹⁹F NMR (377 MHz, CDCl₃) δ -56.2 (t, $J = 21.7$ Hz, 3F), -139.1 (dd, $J = 22.0, 11.1$ Hz, 1F), -139.5 (m, 1F), -140.8 (m, 1F), -143.7 (dd, $J = 21.9, 10.3$ Hz, 1F).

The carbon resonances corresponding to the perfluoroarene (C₇F₇) in this compound appear as a complex series of multiplets between 105 ppm to 155 ppm as a result of ¹³C/¹⁹F coupling. Due to the complexities of the system, the peaks are not listed. ¹⁹F NMR and HRMS were used to confirm the presence of this ring system.

¹³C NMR (176 MHz, CDCl₃) δ 175.9, 74.7, 61.0, 42.8, 29.4, 25.1, 23.0, 22.6, 14.6.

HRMS (ESI⁺) [M+H]⁺ Calcd for C₁₆H₁₆F₇N₂O⁺: 385.1151; Found: 385.1145.

$R_f = 0.35$ in 20% EtOAc in hexanes



Compound **12** was isolated as a yellow oil in 30% yield.

IR (thin film): 1741 (br) cm⁻¹

¹H NMR (700 MHz, CDCl₃) δ 7.30 (dd, $J = 8.7, 6.7$ Hz, 2H), 7.27 – 7.19 (multiple peaks, 3H), 4.45 (dd, $J = 10.2, 2.4$ Hz, 1H), 3.07 (dd, $J = 11.2, 4.6$ Hz, 1H), 2.72 (tt, $J = 12.3,$

3.9 Hz, 1H), 2.63 (td, $J = 11.3, 2.9$ Hz, 1H), 1.97 (m, 1H), 1.89 (m, 2H), 1.65 (q, $J = 11.2$ Hz, 1H), 1.43 (s, 3H), 1.23 (s, 3H).

^{19}F NMR (377 MHz, CDCl_3) δ -56.3 (t, $J = 21.7$ Hz, 3F), -139.0 (dd, $J = 22.1, 10.7$ Hz, 1F), -139.3 (m, 1F), -140.6 (m, 1F), -143.8 (dd, $J = 22.1, 10.6$ Hz, 1F).

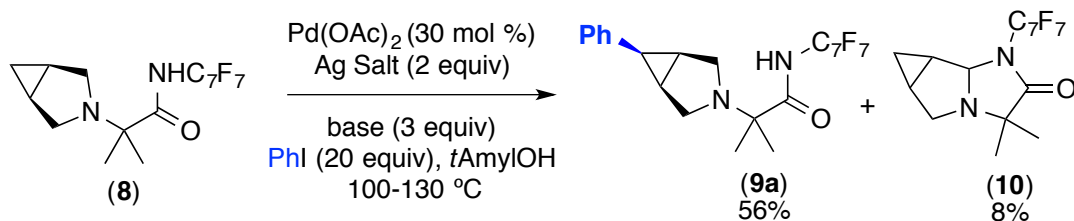
The carbon resonances corresponding to the perfluoroarene (C_7F_7) in this compound appear as a complex series of multiplets between 105 ppm to 155 ppm as a result of $^{13}\text{C}/^{19}\text{F}$ coupling. Due to the complexities of the system, the peaks are not listed. ^{19}F NMR and HRMS were used to confirm the presence of this ring system.

^{13}C NMR (176 MHz, CDCl_3) δ 175.8, 144.2, 128.6, 126.8, 126.7, 74.30, 60.9, 42.3, 41.4, 36.7, 32.9, 23.1, 14.7.

HRMS (ESI $^+$) $[\text{M}+\text{H}]^+$ Calcd for $\text{C}_{22}\text{H}_{20}\text{F}_7\text{N}_2\text{O}^+$: 461.1464; Found: 461.1458.

$R_f = 0.55$ in 20% EtOAc in hexanes

Optimization of C–H Arylation of Azabicyclo[3.1.0]hexane **8**



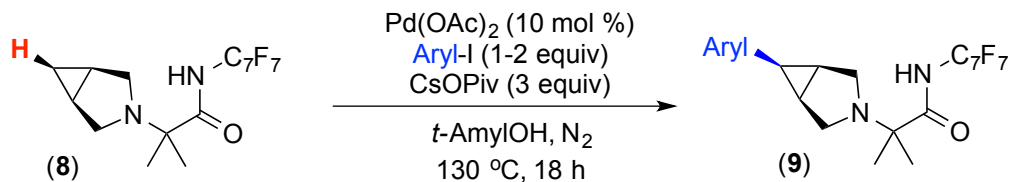
Under ambient conditions, a stock solution of $\text{Pd}(\text{OAc})_2$ (21 mg, 0.09 mmol) was prepared in dichloromethane (2 mL). An aliquot of this solution was transferred to a 4 mL vial (200 μL , 0.009 mmol Pd, 30 mol %). The dichloromethane was removed by heating the open vial to 100 °C for approximately 20 s. To the concentrated $\text{Pd}(\text{OAc})_2$, solid AgX (2 equiv) and/or base (3 equiv) were added.

A separate vial was charged with substrate **8** (120 mg, 0.31 mmol). A mixture of PhI (710 μL , 6.2 mmol, 20 equiv) and *tert*-amyl alcohol (2.8 mL) was gently heated (at ~60 °C) to form a homogeneous solution. An aliquot (370 μL , 0.031 mmol substrate) of this solution was transferred to the vial containing $\text{Pd}(\text{OAc})_2$, AgX, and/or base (prepared as described above). The vial was sealed with a Teflon-lined cap, wrapped in electrical tape, and heated to the designated temperature on an aluminum heating block. After 18

h, the reaction was removed from the heat source and hydrazine (28 μL , 35% in H_2O , 0.3 mmol, 10 equiv) was added to the warm solution. The addition of hydrazine resulted in the immediate precipitation of a black solid (presumably Pd^0). A solution of internal standard (1,3,5-trimethoxybenzene, 168 mg in 5 mL of DCM) was prepared, and an aliquot (150 μL) of the stock standard solution was added to the reaction vial. The reaction solution was then diluted with EtOAc to an approximate total volume of 2 mL. The solution was then filtered through a pipette packed with Celite and was analyzed by GC-FID. The average value of duplicate GC injections was used to determine the GC yield based on a linear calibration curve (minimum 5 points) with 1,3,5-trimethoxybenzene.

Variations of this procedure were used in all optimization reactions (Table 4.1) where the yield was determined by GC-FID. For instance, the impact of the mol % of $\text{Pd}(\text{OAc})_2$ was determined by following the same procedure outlined above except that different volumes of the $\text{Pd}(\text{OAc})_2$ stock solution were transferred to each vial.

Scope of Ar-I for C–H Arylation of **8**

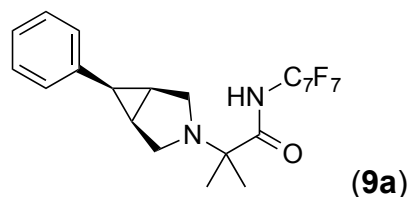


Standard conditions A: Under ambient conditions, a 20 mL scintillation vial was charged with solid substrate **8** (100 mg, 0.26 mmol, 1 equiv), $\text{Pd}(\text{OAc})_2$ (6 mg, 0.03 mmol, 10 mol %) and iodoarene (when solid, 1-2 equiv). The vial was then brought inside of a glove box. To these solids, iodoarene (when liquid, 1-20 equiv), cesium pivalate (182 mg, 0.78 mmol, 3 equiv), and *tert*-amyl alcohol (2.4 mL) were added. The vial was sealed with a Teflon-lined cap, wrapped in electrical tape, removed from the glove box, and heated to an external temperature of 130 $^\circ\text{C}$. After 18 h, the reaction was removed from the heat source, and hydrazine (250 μL , 35% in H_2O , 2.7 mmol, 10 equiv) was added to the warm solution. The mixture was then allowed to stir for 10 to 30 min at 60 $^\circ\text{C}$ to remove ligated Pd from the product. The resulting solution was diluted with EtOAc (~5 mL) and filtered through a layered plug of Celite and basic alumina. The

plug was rinsed with additional EtOAc, and the resulting solution was concentrated under reduced pressure. Purification by column chromatography (25 g cartridge, gradient elution from 0% to 20% EtOAc in hexanes) afforded the desired product.

The use of a glove box was not necessary to obtain reliable conversion in the C–H activation reaction. In general, the yield using a glove box was 10-15% higher than when conducted under ambient atmosphere with reagents stored under ambient conditions. This observation was unique to the azabicyclo[3.1.0]hexane system (substrate **8**).

Note: Reaction with compound **9j** was done by a modified procedure. Under ambient conditions, a 20 mL scintillation vial was charged with solid substrate (100 mg, 0.26 mmol, 1 equiv), Pd(OAc)₂ (18 mg, 0.08 mmol, 30 mol %), AgOAc (52 mg, 0.31 mmol, 1.2 equiv), and KO_iPiv (109 mg, 0.78 mmol, 3 equiv). To these solids, PhI (590 μ L, 5.2 mmol, 20 equiv) and *tert*-amyl alcohol (2.4 mL) were added. The vial was sealed with a Teflon-lined cap and heated to an external temperature of 100 °C for 18 hours. Work up procedure is similar to the standard conditions above.



Isolated yield using standard conditions A (using 1 equiv of Aryl-I): 74% yield

MP 83-85 °C (white solid)

IR (thin film): 1711 cm^{-1}

¹H NMR (700 MHz, CDCl₃) δ 7.30 (d, *J* = 7.5 Hz, 2H), 7.08 (t, *J* = 7.6 Hz, 2H), 6.93 (t, *J* = 7.4 Hz, 1H), 6.34 (s, 1H), 2.95 (d, *J* = 9.1 Hz, 2H), 2.85 (dt, *J* = 9.1, 2.0 Hz, 2H), 2.08 (t, *J* = 8.1 Hz, 1H), 1.86 (dt, *J* = 8.4, 1.8 Hz, 2H), 1.11 (s, 6H).

¹⁹F NMR (471 MHz, CDCl₃) δ -56.0 (t, *J* = 21.7 Hz, 3F), -141.5 (m, 2F), -144.6 (m, 2F).

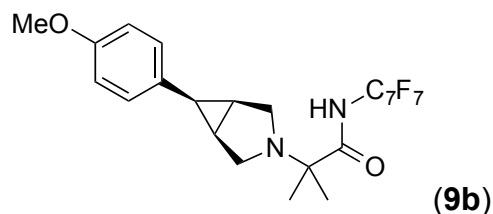
The carbon resonances corresponding to the perfluoroarene (C₇F₇) in this compound appear as a complex series of multiplets between 105 ppm to 155 ppm as a result of ¹³C/¹⁹F coupling. Due to the complexities of the system, the peaks are not listed. ¹⁹F NMR and HRMS were used to confirm the presence of this ring system.

^{13}C NMR (176 MHz, CDCl_3) δ 175.9, 138.0, 128.1, 128.0, 125.9, 60.9, 45.0, 22.8, 20.8, 19.9.

HRMS (ESI⁺) [M+H]⁺ Calcd for $\text{C}_{22}\text{H}_{20}\text{F}_7\text{N}_2\text{O}^+$: 461.1464; Found: 461.1458.

Anal. Calc for $\text{C}_{22}\text{H}_{19}\text{F}_7\text{N}_2\text{O}$: C, 57.39; H, 4.16. Found C, 57.14; H, 3.99. Found C, 57.12; H, 4.03.

R_f = 0.67 in 20% EtOAc in hexanes



Isolated yield using standard conditions A (using 1 equiv of Aryl-I): 75% yield

MP 75-77 °C (white solid)

IR (thin film): 1711 cm^{-1}

^1H NMR (700 MHz, CDCl_3) δ 7.20 (d, J = 8.4 Hz, 2H), 6.56 (d, J = 8.4 Hz, 2H), 6.51 (s, 1H), 3.53 (s, 3H), 2.94 (d, J = 9.1 Hz, 2H), 2.87 (ddd, J = 9.1, 2.6, 1.4 Hz, 2H), 1.99 (t, J = 8.0 Hz, 1H), 1.81 (ddd, J = 8.0, 2.6, 1.3 Hz, 2H), 1.14 (s, 6H).

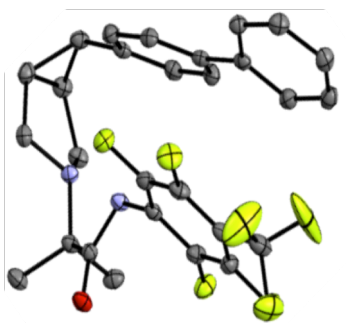
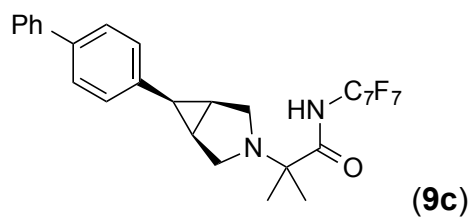
^{19}F NMR (377 MHz, CDCl_3) δ -56.1 (t, J = 21.8 Hz, 3F), -141.4 (m, 2F), -143.1 (m, 2F).

The carbon resonances corresponding to the perfluoroarene (C_7F_7) in this compound appear as a complex series of multiplets between 105 ppm to 155 ppm as a result of $^{13}\text{C}/^{19}\text{F}$ coupling. Due to the complexities of the system, the peaks are not listed. ^{19}F NMR and HRMS were used to confirm the presence of this ring system.

^{13}C NMR (176 MHz, CDCl_3) δ 176.1, 157.5, 129.7, 128.9, 113.4, 60.9, 54.6, 45.1, 22.8, 20.9, 20.0.

HRMS (ESI⁺) [M+H]⁺ Calcd for $\text{C}_{23}\text{H}_{22}\text{F}_7\text{N}_2\text{O}_2^+$: 491.1570; Found: 491.1560.

R_f = 0.50 in 20% EtOAc in hexanes



Isolated yield using standard conditions A (using 1 equiv of Aryl-I): 80% yield

MP 116-118 °C (white solid)

IR (thin film): 1705 (br) cm^{-1}

^1H NMR (700 MHz, CDCl_3) δ 7.43-7.36 (multiple peaks, 4H), 7.34-7.21 (multiple peaks, 5H), 6.37 (s, 1H), 3.01 (d, $J = 9.2$ Hz, 2H), 2.90 (dt, $J = 9.2, 1.7$ Hz, 2H), 2.13 (t, $J = 8.1$ Hz, 1H), 1.89 (dt, $J = 8.2, 1.6$ Hz, 2H), 1.16 (s, 6H).

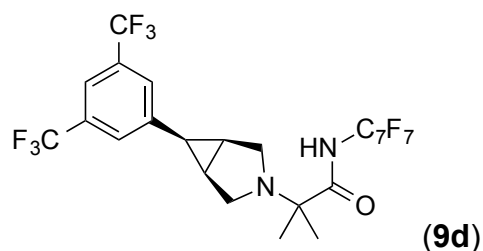
^{19}F NMR (377 MHz, CDCl_3) δ -56.2 (t, $J = 21.7$ Hz, 3F), -141.4 (m, 2F), -143.0 (m, 2F).

The carbon resonances corresponding to the perfluoroarene (C_6F_5) in this compound appear as a complex series of multiplets between 105 ppm to 155 ppm as a result of $^{13}\text{C}/^{19}\text{F}$ coupling. Due to the complexities of the system, the peaks are not listed. ^{19}F NMR and HRMS were used to confirm the presence of this ring system.

^{13}C NMR (176 MHz, CDCl_3) δ 176.4, 138.9, 137.9, 137.1, 128.8, 128.7, 127.5, 126.3, 125.4, 61.04, 45.2, 22.4, 21.1, 20.1.

HRMS (ESI $^+$) $[\text{M}+\text{H}]^+$ Calcd for $\text{C}_{28}\text{H}_{24}\text{F}_7\text{N}_2\text{O}^+$: 537.1777; Found: 537.1773.

$R_f = 0.55$ in 20% EtOAc in hexanes



Isolated yield using standard conditions A (using 1 equiv of Aryl-I): 69% yield

MP 116-118 °C (white solid)

^1H NMR (700 MHz, CDCl_3) δ 7.77 (s, 2H), 7.56 (s, 1H), 6.09 (s, 1H), 2.97 (d, $J = 9.7$ Hz, 2H), 2.93 (ddd, $J = 9.7, 2.5, 1.4$ Hz, 2H), 2.15 (t, $J = 8.0$ Hz, 1H), 2.00 (ddd, $J = 8.0, 2.5, 1.3$ Hz, 2H), 1.14 (s, 6H).

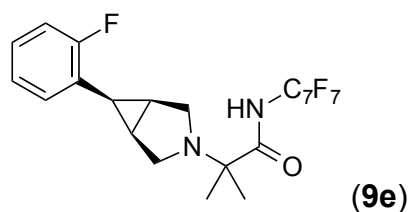
^{19}F NMR (377 MHz, CDCl_3) δ -56.3 (t, $J = 21.8$ Hz, 3F), -63.5 (s, 6F), -141.3 (m, 2F), -143.7 (m, 2F).

The carbon resonances corresponding to the perfluoroarene (C_7F_7) in this compound appear as a complex series of multiplets between 105 ppm to 155 ppm as a result of $^{13}\text{C}/^{19}\text{F}$ coupling. Due to the complexities of the system, the peaks are not listed. ^{19}F NMR and HRMS were used to confirm the presence of this ring system.

^{13}C NMR (176 MHz, CDCl_3) δ 174.6, 141.0, 131.5 (q, $J_{\text{C-F}} = 33.9$ Hz), 128.5 (q, $J_{\text{C-F}} = 3.1$ Hz), 122.9 (q, $J_{\text{C-F}} = 271$ Hz), 119.7 (q, $J_{\text{C-F}} = 3.9$ Hz), 61.2, 45.0, 22.5, 20.6, 20.5.

HRMS (ESI $^+$) $[\text{M}+\text{H}]^+$ Calcd for $\text{C}_{24}\text{H}_{18}\text{F}_{13}\text{N}_2\text{O}^+$: 597.1212; Found: 597.1206.

$R_f = 0.67$ in 20% EtOAc in hexanes



Isolated yield using standard conditions A (using 2 equiv of Aryl-I): 68% yield

MP 60-65 °C (white solid)

IR (thin film): 1712 (br) cm^{-1}

^1H NMR (700 MHz, CDCl_3) δ 7.33 (td, $J = 7.4, 1.6$ Hz, 1H), 6.93 (m, 1H), 6.89-6.81 (multiple peaks, 2H), 6.48 (s, 1H), 3.00 (d, $J = 9.3$ Hz, 2H), 2.84 (dt, $J = 9.3, 1.7$ Hz, 2H), 1.94 (multiple peaks, 3H), 1.13 (s, 6H).

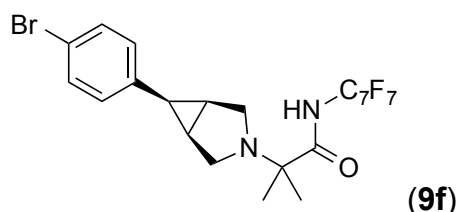
^{19}F NMR (471 MHz, CDCl_3) δ -56.1 (t, J = 21.8 Hz, 3F), -116.1 (q, J = 7.4 Hz, 1F), -141.5 (m, 2F), -143.5 (m, 2F).

The carbon resonances corresponding to the perfluoroarene (C_7F_7) in this compound appear as a complex series of multiplets between 105 ppm to 155 ppm as a result of $^{13}\text{C}/^{19}\text{F}$ coupling. Due to the complexities of the system, the peaks are not listed. ^{19}F NMR and HRMS were used to confirm the presence of this ring system.

^{13}C NMR (176 MHz, CDCl_3) δ 175.64, 161.2 (d, $J_{\text{C-F}}$ = 247 Hz), 130.4 (d, $J_{\text{C-F}}$ = 4.5 Hz), 127.5 (d, $J_{\text{C-F}}$ = 7.7 Hz), 125.5 (d, $J_{\text{C-F}}$ = 16.1 Hz), 123.3 (d, $J_{\text{C-F}}$ = 3.1 Hz), 115.2 (d, $J_{\text{C-F}}$ = 22.2 Hz), 61.10, 45.6, 20.7, 19.9, 18.1.

HRMS (ESI⁺) $[\text{M}+\text{H}]^+$ Calcd for $\text{C}_{22}\text{H}_{19}\text{F}_8\text{N}_2\text{O}^+$: 479.1370; Found: 479.1364.

R_f = 0.67 in 20% EtOAc in hexanes



Isolated yield using standard conditions A (using 2 equiv of Aryl-I): 70% yield

MP 105-108 °C (white solid)

IR (thin film): 1712 cm^{-1}

^1H NMR (700 MHz, CDCl_3) δ 7.22 – 7.15 (multiple peaks, 4H), 6.39 (s, 1H), 2.93 (d, J = 9.3 Hz, 2H), 2.88 (ddd, J = 9.2, 2.6, 1.4 Hz, 2H), 2.00 (t, J = 8.0 Hz, 1H), 1.87 (ddd, J = 8.0, 2.6, 1.3 Hz, 2H), 1.14 (s, 6H).

^{19}F NMR (471 MHz, CDCl_3) δ -56.2 (t, J = 21.7 Hz, 3F), -141.1 (m, 2F), -143.0 (m, 2F).

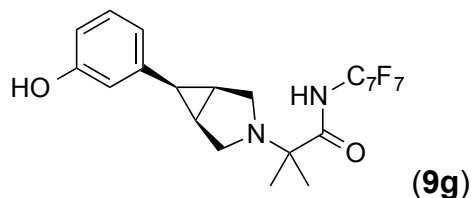
The carbon resonances corresponding to the perfluoroarene (C_7F_7) in this compound appear as a complex series of multiplets between 105 ppm to 155 ppm as a result of $^{13}\text{C}/^{19}\text{F}$ coupling. Due to the complexities of the system, the peaks are not listed. ^{19}F NMR and HRMS were used to confirm the presence of this ring system.

^{13}C NMR (176 MHz, CDCl_3) δ 175.9, 137.0, 131.3, 129.9, 119.9, 61.0, 45.0, 22.3, 21.0, 20.0.

HRMS (ESI⁺) $[\text{M}+\text{H}]^+$ Calcd for $\text{C}_{22}\text{H}_{17}\text{BrF}_7\text{N}_2\text{O}^+$: 539.0569; Found: 539.0561.

Anal. Calc for $C_{22}H_{16}BrF_7N_2O$: C, 49.00; H, 3.36. Found C, 48.93; H, 3.40. Found C, 49.10; H, 3.33.

$R_f = 0.50$ in 20% EtOAc in hexanes



NOTE: chromatography gradient was 0% to 30% EtOAc in hexanes

Isolated yield using standard conditions A (using 2 equiv of Aryl-I): 57% yield

MP 200-203 °C (white solid)

IR (thin film): 1684 cm^{-1}

^1H NMR (700 MHz, CD_3OD) δ 6.97 (t, $J = 7.8$ Hz, 1H), 6.82 (dd, $J = 7.8, 1.2$ Hz, 1H), 6.68 (dd, $J = 2.6, 1.4$ Hz, 1H), 6.27 (dd, $J = 8.0, 2.4$ Hz, 1H), 3.00 (d, $J = 9.0$ Hz, 2H), 2.86 (ddd, $J = 9.0, 2.5, 1.4$ Hz, 2H), 2.00 (t, $J = 8.0$ Hz, 1H), 1.83 (ddd, $J = 8.0, 2.6, 1.2$ Hz, 2H), 1.11 (s, 6H).

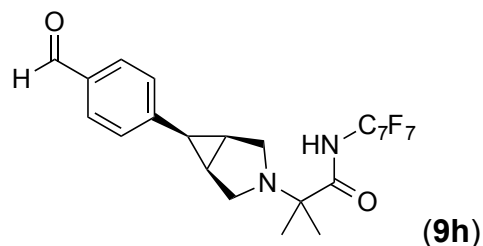
^{19}F NMR (377 MHz, CD_3OD) δ -56.9 (t, $J = 21.2$ Hz, 3F), -144.1 (multiple peaks, 4F).

The carbon resonances corresponding to the perfluoroarene (C_7F_7) in this compound appear as a complex series of multiplets between 105 ppm to 155 ppm as a result of $^{13}\text{C}/^{19}\text{F}$ coupling. Due to the complexities of the system, the peaks are not listed. ^{19}F NMR and HRMS were used to confirm the presence of this ring system.

^{13}C NMR (176 MHz, CD_3OD) δ 177.3, 157.0, 139.5, 128.9, 118.8, 114.5, 112.4, 60.6, 44.5, 22.4, 19.9, 19.4.

HRMS (ESI⁺) $[\text{M}+\text{H}]^+$ Calcd for $\text{C}_{22}\text{H}_{20}\text{F}_7\text{N}_2\text{O}_2^+$: 477.1413; Found: 477.1408.

$R_f = 0.40$ in 20% EtOAc in hexanes



NOTE: Due to the rapid formation of a hydrazone, hydrazine was not used in the isolation of this aldehyde. Instead, the reaction was diluted with MeOH (0.2 mL) and heated at 60 °C for 4 h prior to filtration.

Isolated yield using standard conditions A (using 1 equiv of Aryl-I): 88% yield

MP 116 °C (white solid)

IR (thin film): 1704, 1700 cm^{-1}

^1H NMR (700 MHz, CDCl_3) δ 9.77 (s, 1H), 7.61 (m, 2H), 7.46 (m, 2H), 6.19 (s, 1H), 2.95 (d, J = 9.5 Hz, 2H), 2.88 (ddd, J = 9.4, 2.4, 1.3 Hz, 2H), 2.13 (t, J = 8.0 Hz, 1H), 1.94 (ddd, J = 8.1, 2.6, 1.3 Hz, 2H), 1.11 (s, 6H).

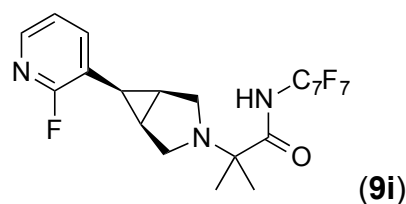
^{19}F NMR (377 MHz, CDCl_3) δ -56.2 (t, J = 21.7 Hz, 3F), -140.9 (m, 2F), -143.0 (m, 2F).

The carbon resonances corresponding to the perfluoroarene (C_7F_7) in this compound appear as a complex series of multiplets between 105 ppm to 155 ppm as a result of $^{13}\text{C}/^{19}\text{F}$ coupling. Due to the complexities of the system, the peaks are not listed. ^{19}F NMR and HRMS were used to confirm the presence of this ring system.

^{13}C NMR (176 MHz, CDCl_3) δ 190.6, 175.3, 145.3, 134.5, 129.2, 128.7, 61.0, 45.0, 23.0, 20.8, 20.2.

HRMS (ESI $^+$) $[\text{M}+\text{H}]^+$ Calcd for $\text{C}_{23}\text{H}_{20}\text{F}_7\text{N}_2\text{O}_2^+$: 489.1413; Found: 489.1407.

R_f = 0.45 in 20% EtOAc in hexanes



NOTE: chromatography gradient was 0% to 40% EtOAc in hexanes.

Isolated yield using standard conditions A (using 2 equiv of Aryl-I): 80% yield

MP 118-120 °C (white solid)

IR (thin film): 1710 cm^{-1}

^1H NMR (700 MHz, CDCl_3) δ 7.90 (d, $J = 4.4$ Hz, 1H), 7.78 (t, $J = 8.4$ Hz, 1H), 6.99 (ddd, $J = 6.9, 4.8, 1.7$ Hz, 1H), 6.46 (s, 1H), 2.98 (d, $J = 9.5$ Hz, 2H), 2.86 (dt, $J = 9.6, 1.7$ Hz, 2H), 2.01 – 1.93 (m, 3H), 1.13 (s, 6H).

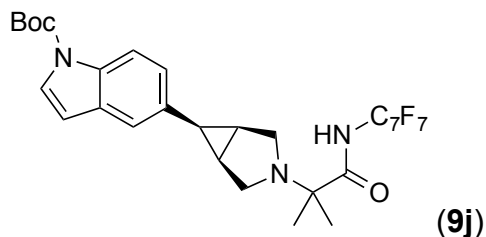
^{19}F NMR (471 MHz, CDCl_3) δ -56.1 (t, $J = 21.8$ Hz, 3F), -70.1 (d, $J = 9.1$ Hz, 1F), -141.1 (m, 2F), -142.8 (m, 2F).

The carbon resonances corresponding to the perfluoroarene (C_7F_7) in this compound appear as a complex series of multiplets between 105 ppm to 155 ppm as a result of $^{13}\text{C}/^{19}\text{F}$ coupling. Due to the complexities of the system, the peaks are not listed. ^{19}F NMR and HRMS were used to confirm the presence of this ring system.

^{13}C NMR (176 MHz, CDCl_3) δ 174.86, 162.6 (d, $J_{\text{C-F}} = 241$ Hz), 145.2 (d, $J_{\text{C-F}} = 13.8$ Hz), 140.5 (d, $J_{\text{C-F}} = 5.5$ Hz), 120.6 (d, $J_{\text{C-F}} = 4.3$ Hz), 120.5 (d, $J_{\text{C-F}} = 30.7$ Hz), 61.3, 45.5, 20.6, 20.1, 17.5 (d, $J_{\text{C-F}} = 3.2$ Hz).

HRMS (ESI⁺) $[\text{M}+\text{H}]^+$ Calcd for $\text{C}_{21}\text{H}_{18}\text{F}_8\text{N}_3\text{O}^+$: 480.1322; Found: 480.1318.

$R_f = 0.80$ in 50% EtOAc in hexanes



Isolated yield using modified standard conditions A (using 2 equiv of Aryl-I): 59% yield

MP 158-161 $^{\circ}\text{C}$ (white solid)

IR (thin film): 1733, 1701 cm^{-1}

^1H NMR (700 MHz, CDCl_3) δ 8.05 (d, $J = 8.5$ Hz, 1H), 7.40 (s, 1H), 7.30 (m, 1H), 7.17 (d, $J = 3.8$ Hz, 1H), 6.15 – 6.10 (multiple peaks, 2H), 3.00 (d, $J = 9.1$ Hz, 2H), 2.88 (dt, $J = 9.2, 1.9$ Hz, 2H), 2.14 (t, $J = 8.1$ Hz, 1H), 1.86 (dt, $J = 8.1, 1.9$ Hz, 2H), 1.64 (s, 9H), 1.11 (s, 6H).

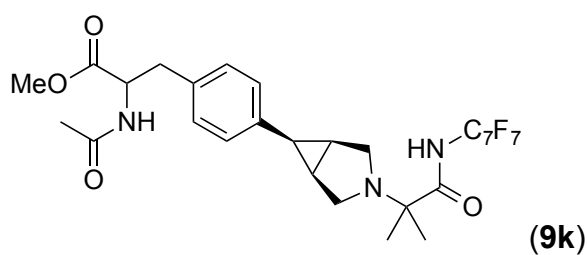
^{19}F NMR (377 MHz, CDCl_3) δ -56.2 (t, $J = 21.7$ Hz, 3F), -142.0 (m, 7.4 Hz, 2F), -143.9 (m, 2F).

The carbon resonances corresponding to the perfluoroarene (C₇F₇) in this compound appear as a complex series of multiplets between 105 ppm to 155 ppm as a result of ¹³C/¹⁹F coupling. Due to the complexities of the system, the peaks are not listed. ¹⁹F NMR and HRMS were used to confirm the presence of this ring system.

¹³C NMR (176 MHz, CDCl₃) δ 176.2, 149.0, 132.12, 130.1, 125.6, 124.3, 119.9, 115.0, 112.9, 105.8, 83.9, 60.76, 45.04, 27.89, 22.70, 21.4 (br s), 20.07.

HRMS (ESI⁺) [M+H]⁺ Calcd for C₂₉H₂₉F₇N₃O₃⁺: 600.2097; Found: 600.2091.

R_f = 0.60 in 20% EtOAc in hexanes



NOTE: Due to the rapid N-deacylation of the product, hydrazine was not used in the isolation of this substrate. Instead, the reaction was diluted with MeOH (0.4 mL) and heated at 60 °C for 4 h prior to filtration. Chromatography gradient was 0% to 60% EtOAc in hexanes.

Isolated yield using standard conditions A (using 1.5 equiv of Aryl-I): 63% yield

MP 112-115 °C (white solid)

IR (thin film): 1700 (br) cm⁻¹

¹H NMR (700 MHz, CDCl₃) δ 7.22 (d, *J* = 7.9 Hz, 2H), 6.82 (d, *J* = 7.9 Hz, 2H), 6.42 (s, 1H), 5.78 (d, *J* = 7.8 Hz, 1H), 4.65 (dt, *J* = 7.9, 5.9 Hz, 1H), 3.68 (s, 3H), 2.94 (dd, *J* = 9.2, 6.7 Hz, 2H), 2.84 (dd, *J* = 9.3, 2.9 Hz, 2H), 2.74 (dd, *J* = 13.9, 6.1 Hz, 1H), 2.63 (dd, *J* = 13.9, 5.8 Hz, 1H), 2.02 (t, *J* = 8.0 Hz, 1H), 1.93 (s, 3H), 1.88-1.81 (multiple peaks, 2H), 1.11 (s, 3H), 1.10 (s, 3H).

¹⁹F NMR (377 MHz, CDCl₃) δ -56.1 (t, *J* = 21.8 Hz, 3F), -141.4 (m, 2F), -142.6 (m, 2F).

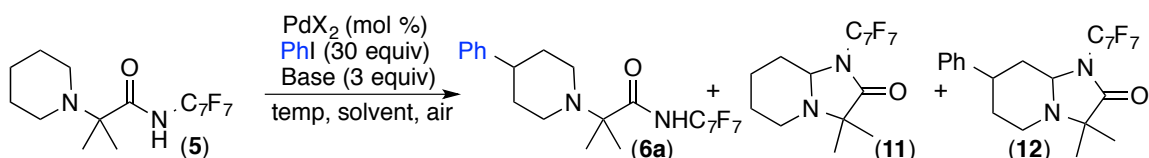
The carbon resonances corresponding to the perfluoroarene (C₇F₇) in this compound appear as a complex series of multiplets between 105 ppm to 155 ppm as a result of ¹³C/¹⁹F coupling. Due to the complexities of the system, the peaks are not listed. ¹⁹F NMR and HRMS were used to confirm the presence of this ring system.

^{13}C NMR (176 MHz, CDCl_3) δ 175.8, 171.9, 169.3, 136.8, 133.8, 128.8, 128.3, 61.0, 52.9, 52.2, 45.1, 45.0, 37.2, 22.9, 22.4, 21.0, 20.6, 19.9, 19.8

HRMS (ESI⁺) $[\text{M}+\text{H}]^+$ Calcd for $\text{C}_{28}\text{H}_{29}\text{F}_7\text{N}_3\text{O}_4^+$: 604.2046; Found: 604.2038.

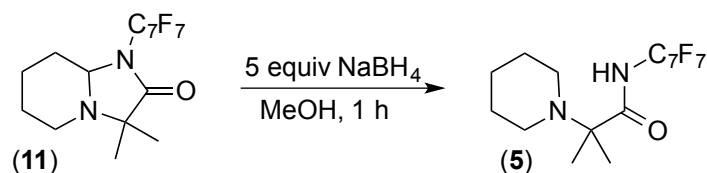
R_f = 0.30 in 50% EtOAc in hexanes

Optimization of C–H Arylation of piperidine substrate 5



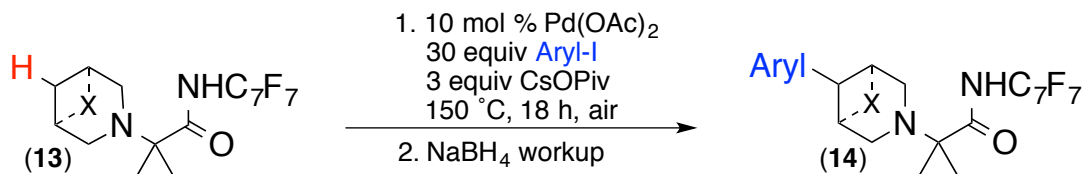
A stock solution of $\text{Pd}(\text{OAc})_2$ was prepared by dissolving 22.5 mg of $\text{Pd}(\text{OAc})_2$ in 5 mL of dichloromethane (0.02 M solution of $\text{Pd}(\text{OAc})_2$). To a 4-mL vial a 150 μL aliquot of the Pd stock solution was added (0.7mg, 0.003 mmol, 10 mol %). The solvent was removed by heating the vial gently to 40 $^\circ\text{C}$. After, substrate **5** (12 mg, 0.03 mmol, 1 equiv), CsOPiv (21 mg, 0.09 mmol, 3 equiv) and iodoarene (30 equiv) were added to the vial containing Pd. Finally, solvent was added if shown in entry of Table 4.4 (0.12 M). The vial was sealed with a Teflon-lined cap and heated to the corresponding temperature for 18 hours. After, the reaction mixture was removed from the heat source and hydrazine (50 μL , 65% in H_2O , 0.6 mmol, 20 equiv) was added to the warm solution. The addition of hydrazine resulted in the precipitation of a black solid. A solution of internal standard (1,3,5-trimethoxybenzene, 168 mg in 5 mL of DCM) was prepared, and an aliquot (150 μL , 0.03 mmol) of the stock standard solution was added to the reaction vial. The reaction solution was then diluted with DCM to an approximate total volume of 4 mL. The solution was then filtered through a pipette packed with Celite and was analyzed by GC-FID. The average value of duplicate GC injections was used to determine the GC yield based on a linear calibration curve with 1,3,5-trimethoxybenzene. Results are shown in Table 4.4.

Work-up to Effect Reduction of Aminoal Products



A solution of aminoal (**11**) (15 mg, 0.04 mmol, 1 equiv) in MeOH (0.2 mL) was pre-cooled in an ice bath, and solid NaBH₄ (7.5 mg, 0.2 mmol, 5 equiv) was added in one portion. The solution was allowed to gradually warm to room temperature. After 1 h, the reaction was poured into water, the resulting mixture was extracted with CH₂Cl₂ (3 x ~10 mL), and the organic extracts were dried over Na₂SO₄, filtered, and concentrated under reduced pressure. Analysis of the crude oil by ¹H NMR, ¹⁹F NMR, and GC-FID indicated full conversion of the aminoal **11** to the piperidine **5**.

Standard Conditions for C-H Arylation of Alicyclic Amines



Standard conditions B: Under ambient conditions, a 20 mL scintillation vial was charged with solid substrate **13** (0.25 mmol, 1 equiv), Pd(OAc)₂ (5.6 mg, 0.0325 mmol, 10 mol %), cesium pivalate (176 mg, 0.75 mmol, 3 equiv), and iodoarene (30 equiv). The vial was sealed with a Teflon-lined cap and heated to an external temperature of 150 °C. After 18 h, the reaction was removed from the heat source and diluted with hexanes (5 mL). Hydrazine (250 μL, 35% in H₂O, 2.6 mmol, 10 equiv) was added to the warm solution. The mixture was allowed to stir for 30 min at 60 °C to remove Pd from the product.

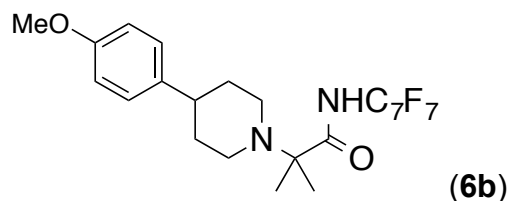
Isolation Procedure A: If aminoal (such as **11**) is not formed during the reaction.

The mixture was filtered through a small plug of silica gel with 100% EtOAc. The resulting solution was concentrated under vacuum. Purification by column chromatography (25 g cartridge, gradient elution using Hex, EtOAc and/or THF) or

preparative TLC afforded the desired product. Modifications to the procedure and chromatography conditions are noted under each substrate.

Isolation Procedure B: If aminal (such as **11**) is formed during the reaction.

The mixture was loaded onto a small plug of silica gel over which hexanes (150 mL) was passed to remove iodoarene. The plug of silica was then rinsed with EtOAc (150 mL) to elute the products, and this solution was concentrated under reduced pressure. The mixture of products was dissolved in MeOH (2 mL), and cooled in an ice bath to 0 °C. NaBH₄ (total 100 mg, 2.6 mmol, 20 equiv) was added portion-wise over 30 min. [*Caution: gas evolution occurs!*] The solution was allowed to warm to room temperature. After stirring for 12 h, the reaction was diluted with water and the resulting solution was extracted with CH₂Cl₂, dried (Na₂SO₄), and concentrated under reduced pressure. Purification by column chromatography (25 g cartridge, gradient elution using Hex, EtOAc and/or THF) or preparative TLC afforded the desired product. Modifications to the procedure and chromatography conditions are noted under each substrate.



NOTE: Aminal formation was observed. NaBH₄ reduction was required on this substrate following **Isolation Procedure B**.

Isolated yield using standard conditions B: 57%, 52%; 55% average yield

Isolated yield when calculated based on recovered starting material: 67%, 62%; 65% average yield

MP 121 °C (white solid)

IR (thin film): 1715 (br) cm⁻¹

¹H NMR (700 MHz, CDCl₃) δ 9.45 (br s, 1H), 7.15 (m, 2H), 6.87 (m, 2H), 3.79 (s, 3H), 2.97 (dt, *J* = 11.3, 2.1 Hz, 2H), 2.53 (tt, *J* = 12.3, 3.8 Hz, 1H), 2.39 (td, *J* = 11.6, 2.2 Hz, 2H), 1.96 (d, *J* = 12.5 Hz, 2H), 1.75 (qd, *J* = 12.5, 3.6 Hz, 2H), 1.35 (s, 6H).

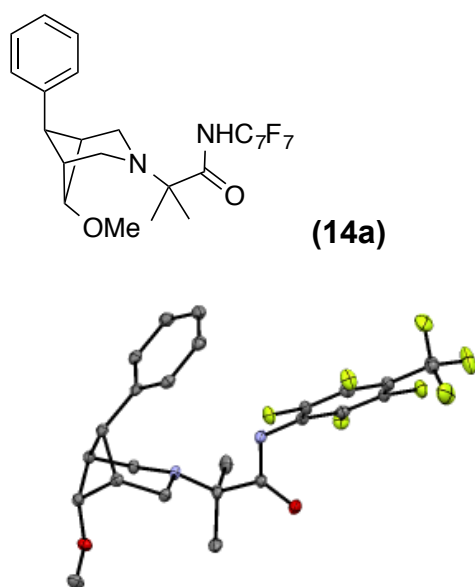
¹⁹F NMR (377 MHz, CDCl₃) δ -56.0 (t, *J* = 21.8 Hz, 3F), -141.2 (m, 2F), -144.1 (m, 2F).

The carbon resonances corresponding to the perfluoroarene (C_7F_7) in this compound appear as a complex series of multiplets between 105 ppm to 155 ppm as a result of $^{13}C/^{19}F$ coupling. Due to the complexities of the system, the peaks are not listed. ^{19}F NMR and HRMS were used to confirm the presence of this ring system.

^{13}C NMR (176 MHz, $CDCl_3$) δ 175.6, 158.0, 137.7, 127.5, 113.8, 64.8, 55.2, 47.8, 41.7, 34.3, 20.5.

HRMS (ESI⁺) $[M+H]^+$ Calcd for $C_{23}H_{24}F_7N_2O_2^+$: 493.1726; Found: 493.1718.

R_f = 0.50 in 20% EtOAc in hexanes



NOTE: The arylation reaction was conducted at 100 °C for 16 h. Aminoal was not observed, thus purification was performed following **Isolation Procedure A**.

A mixture of starting material and product were isolated from the initial column chromatography (10% THF in hexanes). The mixture of product and recovered starting material were subjected to a preparative TLC (5% THF in hexanes, plate was run four times).

Isolated yield using standard conditions B: 62% yield.

MP 101-103 °C (white solid)

IR (thin film): 1712 cm^{-1}

^1H NMR (500 MHz, CDCl_3) δ 7.23 (d, $J = 7.5$ Hz, 2H), 7.12 (t, $J = 7.5$ Hz, 2H), 6.96 (t, $J = 7.5$ Hz, 1H), 6.75 (s, 1H), 3.60 (t, $J = 5.5$ Hz, 1H), 3.38 (s, 3H), 3.08-2.96 (multiple peaks, 7H), 1.19 (s, 6H).

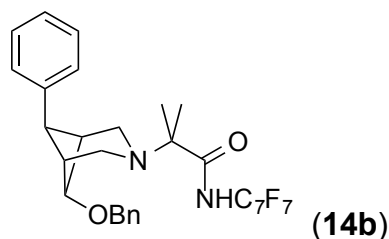
^{19}F NMR (471 MHz, CDCl_3) δ -56.1 (t, $J = 23.6$ Hz, 3F), -141.8 (m, 2F), -142.3 (m, 2F).

The carbon resonances corresponding to the perfluoroarene (C_7F_7) in this compound appear as a complex series of multiplets between 105 ppm to 155 ppm as a result of $^{13}\text{C}/^{19}\text{F}$ coupling. Due to the complexities of the system, the peaks are not listed. ^{19}F NMR and HRMS were used to confirm the presence of this ring system.

^{13}C NMR (126 MHz, CDCl_3) δ 176.3, 140.9, 128.2, 125.5, 125.1, 72.9, 63.2, 55.8, 39.8, 39.6, 34.7, 21.1.

HRMS (ESI $^+$) $[\text{M}+\text{H}]^+$ Calcd for $\text{C}_{24}\text{H}_{24}\text{F}_7\text{N}_2\text{O}_2$: 505.1721; Found: 505.1721.

$R_f = 0.12$ in 5% THF in hexanes



NOTE: The arylation reaction was conducted at 120 °C for 16 h. Aminal formation was observed. NaBH_4 reduction was required on this substrate following **Isolation Procedure B**. Purification via column chromatography (10 g cartridge, gradient elution from 0% to 5% THF in hexanes) afforded a colorless oil. This oil was diluted with a small amount of methanol (~0.3 mL). Slow evaporation at RT of the methanol to about 0.15 mL yielded pure product as a white solid. The supernatant was removed by decantation.

Isolated yield using standard conditions B: 66% yield.

MP 114-116 °C (white solid)

IR (thin film): 1690 cm^{-1}

^1H NMR (700 MHz, CDCl_3) δ 7.37 (app d, $J = 7.7$ Hz, 2H), 7.34 (t, $J = 7.7$ Hz, 2H), 7.28 (t, $J = 7.7$ Hz, 1H), 7.22 (app d, $J = 7.7$ Hz, 2H), 7.14 (t, $J = 7.7$ Hz, 2H), 6.99 (t, $J = 7$

Hz, 1H), 6.90 (br s, 1H), 4.57 (s, 2H), 3.83 (t, $J = 5.6$ Hz, 1H), 3.16 (d, $J = 9.8$ Hz, 2H), 3.10 (m, 2H), 3.04 (app d, $J = 9.1$ Hz, 2H), 2.99 (t, $J = 5.6$ Hz, 1H), 1.16 (s, 6H).

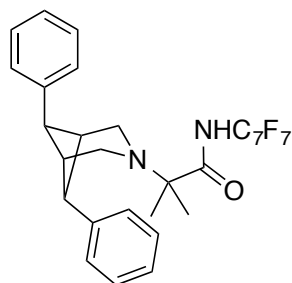
^{19}F NMR (377 MHz, CDCl_3) δ -56.11 (t, $J = 21.5$ Hz, 3F), -141.87 (m, 2F), -142.38 (m, 2F).

The carbon resonances corresponding to the perfluoroarene (C_7F_7) in this compound appear as a complex series of multiplets between 105 ppm to 155 ppm as a result of $^{13}\text{C}/^{19}\text{F}$ coupling. Due to the complexities of the system, the peaks are not listed. ^{19}F NMR and HRMS were used to confirm the presence of this ring system.

^{13}C NMR (176 MHz, CDCl_3) δ 176.4, 140.6, 137.8, 128.6, 128.2, 128.0, 127.9, 125.6, 125.2, 71.6, 70.8, 63.2, 40.12, 40.11, 34.9, 21.5

HRMS (ESI $^+$) $[\text{M}+\text{H}]^+$ Calcd for $\text{C}_{30}\text{H}_{28}\text{F}_7\text{N}_2\text{O}_2$: 581.2034; Found: 581.2034.

$R_f = 0.19$ in 5% THF in hexanes



(14c)

NOTE: The arylation reaction was conducted at 100 °C. Aminoal was not observed, thus purification was performed following **Isolation Procedure A**. No starting material was recovered from this reaction.

Isolated yield using standard conditions B: 35%, 34%; 35% average yield

MP 152-156 °C (white solid)

IR (thin film): 1715 cm^{-1}

^1H NMR (700 MHz, CDCl_3) δ 7.27 (m, 4H), 7.20 (d, $J = 7.4$ Hz, 4H), 7.10 (t, $J = 7.4$ Hz, 2H), 6.48 (s, 1H), 3.48 (m, 2H), 3.40 (m, 2H), 3.11 (m, 4H), 0.76 (s, 6H).

^{19}F NMR (377 MHz, CDCl_3) δ -56.1 (t, $J = 21.8$ Hz, 3F), -141.8 (m, 2F), -142.5 (m, 2F).

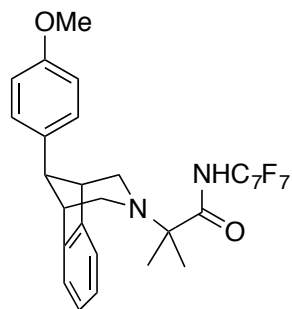
The carbon resonances corresponding to the perfluoroarene (C_7F_7) in this compound appear as a complex series of multiplets between 105 ppm to 155 ppm as a result of

$^{13}\text{C}/^{19}\text{F}$ coupling. Due to the complexities of the system, the peaks are not listed. ^{19}F NMR and HRMS were used to confirm the presence of this ring system.

^{13}C NMR (176 MHz, CDCl_3) δ 175.7, 128.3, 128.3, 126.3, 125.6, 62.9, 40.9, 40.1, 38.0, 20.2.

HRMS (ESI⁺) [M+H]⁺ Calcd for $\text{C}_{29}\text{H}_{26}\text{F}_7\text{N}_2\text{O}^+$: 551.1933; Found: 551.1926.

R_f = 0.80 in 20% EtOAc in hexanes



NOTE: Aminal formation was observed. NaBH_4 reduction was required on this substrate following **Isolation Procedure B**.

Isolated yield using standard conditions B: 47%, 45%; 46% average yield

Isolated yield when based on recovered starting material: 66%, 75%; 71% average yield

MP 161-164 °C (white solid)

IR (thin film): 1713 cm^{-1}

^1H NMR (700 MHz, CDCl_3) δ 7.47 (br s, 1H), 7.31-7.22 (multiple peaks, 4H), 7.13 (dd, J = 5.3, 3.1 Hz, 2H), 6.96 (m, 2H), 3.84 (s, 3H), 3.69 (t, J = 4.2 Hz, 2H), 3.58 (t, J = 4.4 Hz, 1H), 3.01 (d, J = 10.8 Hz, 2H), 2.56 (dd, J = 11.0, 4.2 Hz, 2H), 1.04 (s, 6H).

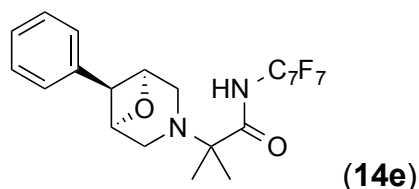
^{19}F NMR (377 MHz, CDCl_3) δ -56.0 (t, J = 21.8 Hz, 3F), -141.5 (m, 2F), -142.9 (m, 2F).

The carbon resonances corresponding to the perfluoroarene (C_7F_7) in this compound appear as a complex series of multiplets between 105 ppm to 155 ppm as a result of $^{13}\text{C}/^{19}\text{F}$ coupling. Due to the complexities of the system, the peaks are not listed. ^{19}F NMR and HRMS were used to confirm the presence of this ring system.

^{13}C NMR (176 MHz, CDCl_3) δ 176.0, 157.6, 146.2, 130.8, 129.2, 126.7, 121.7, 114.2, 63.5, 55.2, 51.0, 43.6, 42.6, 21.4.

HRMS (ESI⁺) [M+H]⁺ Calcd for $\text{C}_{27}\text{H}_{26}\text{F}_7\text{N}_2\text{O}_2^+$: 567.1882; Found: 567.1874.

R_f = 0.50 in 20% EtOAc in hexanes



Note: The arylation reaction was conducted at 95 °C. Aminal was not observed, thus purification was performed following **Isolation Procedure A**.

Isolated yield using standard conditions B: 32%, 34%; 33% average yield

Isolated yield when calculated based on recovered starting material: 69%, 74%; 72% average yield

MP 202 °C (white solid)

IR (thin film): 1713 cm^{-1}

^1H NMR (700 MHz, CDCl_3) δ 7.12 (t, $J = 7.7$ Hz, 2H), 7.05 (d, $J = 7.7$ Hz, 2H), 7.00 (t, $J = 7.7$ Hz, 1H), 6.42 (s, 1H), 4.95 (d, $J = 6.1$ Hz, 2H), 4.60 (t, $J = 6.3$ Hz, 1H), 3.19 (d, $J = 11.6$ Hz, 2H), 3.09 (d, 11.4 Hz, 2H), 1.23 (s, 6H).

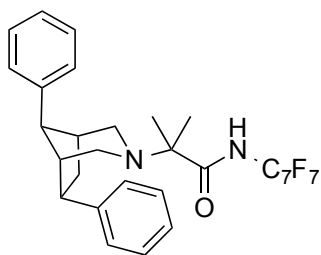
^{19}F NMR (377 MHz, CDCl_3) δ -56.1 (t, $J = 21.8$ Hz, 3F), -141.4 (m, 2F), -142.5 (m, 2F).

The carbon resonances corresponding to the perfluoroarene (C_7F_7) in this compound appear as a complex series of multiplets between 105 ppm to 155 ppm as a result of $^{13}\text{C}/^{19}\text{F}$ coupling. Due to the complexities of the system, the peaks are not listed. ^{19}F NMR and HRMS were used to confirm the presence of this ring system.

^{13}C NMR (176 MHz, CDCl_3) δ 175.2, 139.2, 128.3, 126.1, 123.8, 81.4, 63.0, 45.8, 44.7, 20.5.

HRMS (ESI $^+$) $[\text{M}+\text{H}]^+$ Calcd for $\text{C}_{22}\text{H}_{20}\text{F}_7\text{N}_2\text{O}_2^+$: 477.1413; Found: 477.1505.

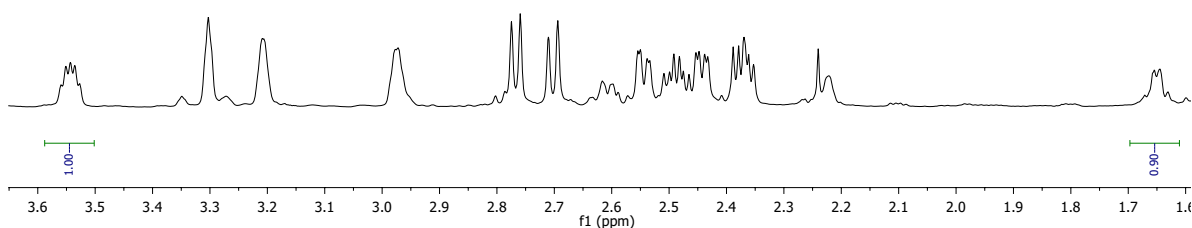
$R_f = 0.38$ in 35% EtOAc in hexanes



(14f)

NOTE: The reaction was performed at a larger scale (0.4 mmol of substrate), and was conducted at 145 °C in *t*-amyIOH (0.13 M in substrate). Amino formation was observed. NaBH₄ reduction was required on this substrate following a modified **Isolation Procedure B** where iodobenzene was removed under vacuum instead of via filtration through silica gel plug.

The yield for compound **14f** was determined by isolating a mixture of recovered starting material **13f** and compound **14f** via column chromatography (2% THF in hexanes). The mixture was analyzed by ¹H NMR spectroscopy to determine the ratio of **13f**:**14f** (ca. 0.23:1). This ratio, in combination with the isolated mass of the mixture and the respective molecular masses, was used to determine a yield of **14f** based on the mixture. Pure **14f** was obtained after repeated chromatography (2% THF in hexanes). An excerpt of the NMR used to determine the ratio is below:



Yield using standard conditions B: 34% yield

MP 142-144 °C (white solid)

IR (thin film): 1716 cm⁻¹

¹H NMR (700 MHz, CDCl₃) δ 7.83 (s, 1H), 7.41-7.38 (multiple peaks, 4H), 7.34 (app d, *J* = 8.4 Hz, 2H), 7.23 (t, *J* = 7.7 Hz, 1 H), 7.16 (t, *J* = 7.7 Hz, 2H), 6.75 (t, *J* = 7.7 Hz, 1H), 3.58 (quintet, *J* = 5.6 Hz, 1H), 3.34 (br s, 1H), 3.25 (br s, 1H), 3.01 (m, 1H), 2.80 (d, *J* = 10.5 Hz, 1H), 2.73 (d, *J* = 12.6 Hz, 1H), 2.58 (dd, *J* = 3.5, 11.2 Hz, 1 H), 2.53 (m, 1H), 2.48 (dd, *J* = 4.2, 11.2 Hz, 1H), 2.41 (dd, *J* = 7, 5.6 Hz, 1H), 1.01 (s, 3H), 0.77 (s, 3H).

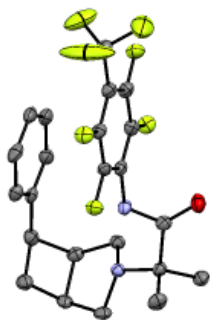
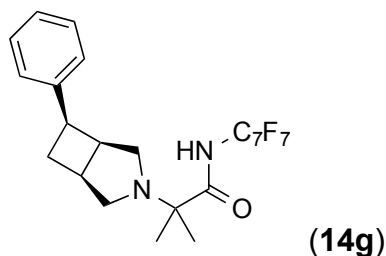
^{19}F NMR (377 MHz, CDCl_3) δ -56.0 (t, J = 22.6 Hz, 3F), -142.1 (m, 2H), -143.2 (m, 2H).

The carbon resonances corresponding to the perfluoroarene (C_7F_7) in this compound appear as a complex series of multiplets between 105 ppm to 155 ppm as a result of $^{13}\text{C}/^{19}\text{F}$ coupling. Due to the complexities of the system, the peaks are not listed. ^{19}F NMR and HRMS were used to confirm the presence of this ring system.

^{13}C NMR (176 MHz, CDCl_3) δ 175.3, 143.4, 139.6, 128.92, 128.86, 128.6, 127.2, 126.0, 125.1, 63.9, 47.6, 46.9, 44.9, 41.5, 40.0, 36.4, 32.4, 22.5, 18.3.

HRMS (ESI $^+$) $[\text{M}+\text{H}]^+$ Calcd for $\text{C}_{30}\text{H}_{28}\text{F}_7\text{N}_2\text{O}$: 565.2084; Found: 565.2089.

R_f = 0.10 in 2% THF in hexanes



NOTE: The arylation reaction was conducted at 130 °C in *t*-AmylOH (0.12 M in substrate). Aminal was not observed, thus purification was performed following **Isolation Procedure A**.

Isolated yield using standard conditions B: 54% yield

Isolated yield when calculated based on recovered starting material: 57% yield

MP 138-140 °C (white solid)

IR (thin film): 1708 cm^{-1}

^1H NMR (500 MHz, CDCl_3) δ 8.28 (br s, 1H), 7.08 (multiple peaks, 4H), 6.64 (m, 1H), 3.79 (q, J = 9.5 Hz, 1H), 3.26 (q, J = 8 Hz, 1H), 2.97 (m, 1H), 2.76 (dd, J = 15, 10 Hz,

2H), 2.61 (m, 1H), 2.42 (dd, $J = 9, 5.5$ Hz, 1H), 2.35 (dd, $J = 10, 7$ Hz, 1H), 2.25 (m, 1H), 1.31 (s, 3H), 1.14 (s, 3H).

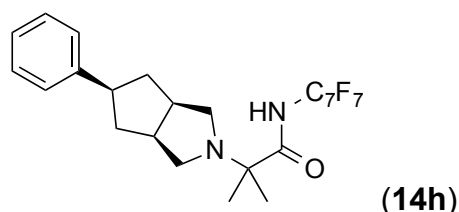
^{19}F NMR (471 MHz, CDCl_3) δ -56.0 (t, $J = 22.1$ Hz, 3F), -142.1 (m, 2F), -143.5 (m, 2F).

The carbon resonances corresponding to the perfluoroarene (C_7F_7) in this compound appear as a complex series of multiplets between 105 ppm to 155 ppm as a result of $^{13}\text{C}/^{19}\text{F}$ coupling. Due to the complexities of the system, the peaks are not listed. ^{19}F NMR and HRMS were used to confirm the presence of this ring system.

^{13}C NMR (126 MHz, CDCl_3) δ 175.3, 142.3, 128.1, 126.7, 124.8, 61.3, 53.0, 48.0, 41.5, 36.5, 32.9, 28.9, 25.1, 16.8.

HRMS (ESI⁺) $[\text{M}+\text{H}]^+$ Calcd for $\text{C}_{23}\text{H}_{22}\text{F}_7\text{N}_2\text{O}$: 475.1615; Found: 475.1612.

$R_f = 0.21$ in 5% THF in hexanes



NOTE: Aminal formation was observed. NaBH_4 reduction was required on this substrate following **Isolation Procedure B**. Purification via preparative TLC (5% THF in hexanes). Isolated yield using standard conditions B: 44% yield.

MP 93-95 °C (white solid)

IR (thin film): 1722 cm^{-1}

^1H NMR (500 MHz, CDCl_3) δ 9.36 (br s, 1H), 7.31-7.18 (multiple peaks, 5H), 3.01 (app septet, $J = 5.5$ Hz, 1 H), 2.71-2.59 (multiple peaks, 6H), 2.42 (m, 2H), 1.49 (m, 2H), 1.37 (s, 6H).

^{19}F NMR (471 MHz, CDCl_3) δ -56.02 (t, $J = 18.8$ Hz, 3F), -141.10 (m, 2F), -143.77 (m, 2F).

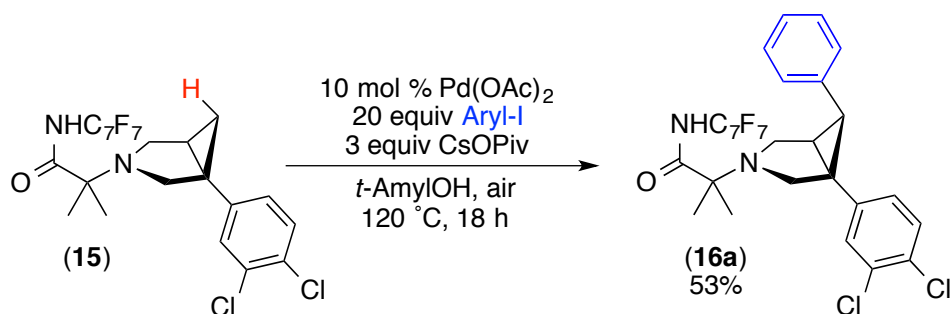
The carbon resonances corresponding to the perfluoroarene (C_7F_7) in this compound appear as a complex series of multiplets between 105 ppm to 155 ppm as a result of $^{13}\text{C}/^{19}\text{F}$ coupling. Due to the complexities of the system, the peaks are not listed. ^{19}F NMR and HRMS were used to confirm the presence of this ring system.

^{13}C NMR (126 MHz, CDCl_3) δ 175.3, 143.8, 128.5, 127.0, 126.3, 61.7, 53.2, 46.9, 41.7, 41.5, 21.1.

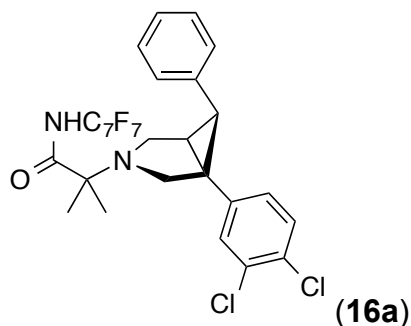
HRMS (ESI $^+$) $[\text{M}+\text{H}]^+$ Calcd for $\text{C}_{24}\text{H}_{24}\text{F}_7\text{N}_2\text{O}$: 489.1771; Found: 489.1772.

R_f = 0.13 in 5% THF in hexanes

Scope of Ar-I for C–H Arylation of **15**



Standard conditions C: Under ambient conditions, a 20 mL scintillation vial was charged with solid substrate **15** (137.6 mg, 0.26 mmol, 1 equiv), $\text{Pd}(\text{OAc})_2$ (6 mg, 0.03 mmol, 10 mol %) and iodoarene (when solid, 20 equiv). To these solids, iodoarene (when liquid, 1-20 equiv), cesium pivalate (182 mg, 0.78 mmol, 3 equiv), and *tert*-amyl alcohol (2.4 mL) were added. The vial was sealed with a Teflon-lined cap, wrapped in electrical tape and heated to an external temperature of 120 °C. After 18 h, the reaction was removed from the heat source, and hydrazine (250 μL , 35% in H_2O , 2.7 mmol, 10 equiv) was added to the warm solution. The mixture was then allowed to stir for 10 to 30 min at 60 °C to remove ligated Pd from the product. The resulting solution was diluted with EtOAc (~5 mL) and filtered through a layered plug of Celite and basic alumina. The plug was rinsed with additional EtOAc, and the resulting solution was concentrated under reduced pressure. Purification by column chromatography (25 g cartridge, gradient elution from 0% to 20% EtOAc in hexanes) afforded the desired product.



NOTE: NaBH₄ reduction was required on this substrate following the **Isolation Procedure B** found in the **Standard Conditions for C-H Arylation of Alicyclic Amines** section.

Isolated as a colorless oil.

Isolated yield using modified standard conditions C: 52%, 54%; 53% average yield

Isolated yield when based on recovered starting material: 61%, 59%; 60% average yield

IR (thin film): 1710 (br) cm⁻¹

¹H NMR (700 MHz, CDCl₃) δ 7.43 (d, *J* = 8.4 Hz, 1H), 7.39 (d, *J* = 2.0 Hz, 1H), 7.35 (d, *J* = 7.2 Hz, 2H), 7.17 – 7.08 (multiple peaks, 3H), 7.00 (t, *J* = 7.4 Hz, 1H), 6.25 (s, 1H), 3.28 (d, *J* = 9.2 Hz, 1H), 3.15 (d, *J* = 9.6 Hz, 1H), 3.10 (dd, *J* = 9.6, 3.9 Hz, 1H), 3.04 (d, *J* = 9.2 Hz, 1H), 2.42 (d, *J* = 8.5 Hz, 1H), 2.21 (dd, *J* = 8.5, 3.7 Hz, 1H), 1.16 (s, 3H), 1.10 (s, 3H).

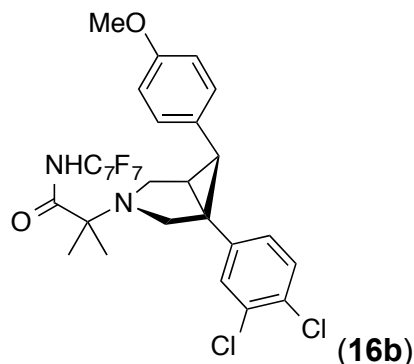
¹⁹F NMR (377 MHz, CDCl₃) δ -56.0 (t, *J* = 21.8 Hz, 3F), -141.4 (m, 2F), -142.3 (m, 2F).

The carbon resonances corresponding to the perfluoroarene (C₇F₇) in this compound appear as a complex series of multiplets between 105 ppm to 155 ppm as a result of ¹³C/¹⁹F coupling. Due to the complexities of the system, the peaks are not listed. ¹⁹F NMR and HRMS were used to confirm the presence of this ring system.

¹³C NMR (176 MHz, CDCl₃) δ 175.2, 142.4, 137.0, 132.6, 130.5, 130.5, 129.0, 128.2, 127.6, 126.4, 126.3, 61.2, 49.8, 45.5, 35.0, 32.5, 28.1, 20.8, 20.6.

HRMS (ESI⁺) [M+H]⁺ Calcd for C₂₈H₂₂Cl₂F₇N₂O⁺: 605.0997; Found: 605.0996.

*R*_f = 0.60 in 20% EtOAc in hexanes



Isolated yield using modified standard conditions C (using 1 equiv of Aryl-I): 40% yield

Isolated yield using modified standard conditions C (using 20 equiv of Aryl-I): 50%, 51%; 51% average yield

Isolated yield when based on recovered starting material (using 20 equiv of Aryl-I): 77%, 69%; 73% average yield

MP 140-143 °C (white solid)

IR (thin film): 1707 cm^{-1}

^1H NMR (700 MHz, CDCl_3) δ 7.41 (d, J = 8.3 Hz, 1H), 7.36 (d, J = 2.1 Hz, 1H), 7.25 (d, J = 8.4 Hz, 2H), 7.12 (dd, J = 8.3, 2.2 Hz, 1H), 6.61 (d, J = 8.4 Hz, 2H), 6.43 (s, 1H), 3.56 (s, 3H), 3.26 (d, J = 9.1 Hz, 1H), 3.16 – 3.09 (multiple peaks, 2H), 3.05 (d, J = 9.1 Hz, 1H), 2.36 (d, J = 8.4 Hz, 1H), 2.18 (dd, J = 8.5, 3.8 Hz, 1H), 1.20 (s, 3H), 1.18 (s, 3H).

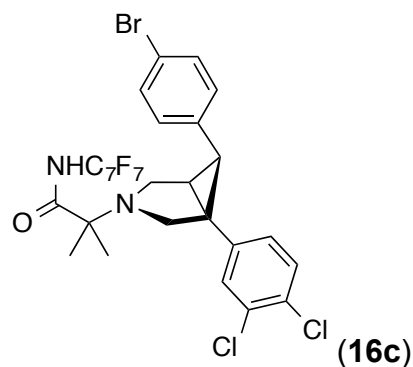
^{19}F NMR (377 MHz, CDCl_3) δ -56.1 (t, J = 21 Hz, 3F), -141.4 (m, 2F), -143.0 (m, 2F).

The carbon resonances corresponding to the perfluoroarene (C_7F_7) in this compound appear as a complex series of multiplets between 105 ppm to 155 ppm as a result of $^{13}\text{C}/^{19}\text{F}$ coupling. Due to the complexities of the system, the peaks are not listed. ^{19}F NMR and HRMS were used to confirm the presence of this ring system.

^{13}C NMR (176 MHz, CDCl_3) δ 175.4, 157.8, 142.6, 132.6, 130.5, 130.4, 128.9, 128.6, 128.5, 126.2, 113.6, 61.2, 54.6, 49.8, 45.6, 35.0, 32.0, 28.2, 21.4, 20.4.

HRMS (ESI $^+$) $[\text{M}+\text{H}]^+$ Calcd for $\text{C}_{29}\text{H}_{24}\text{Cl}_2\text{F}_7\text{N}_2\text{O}^+$: 635.1103; Found: 635.1098.

R_f = 0.60 in 20% EtOAc in hexanes



Isolated yield using modified standard conditions C: 44%, 24%; 35% average yield

Isolated yield when based on recovered starting material: 54%, 27%; 41% average yield

MP 162-165 °C (white solid)

IR (thin film): 1709 cm^{-1}

^1H NMR (700 MHz, CDCl_3) δ 7.43 (d, $J = 8.3$ Hz, 1H), 7.36 (d, $J = 2.2$ Hz, 1H), 7.27 (d, $J = 8.4$ Hz, 2H), 7.24 (d, $J = 8.4$ Hz, 2H), 7.12 (dd, $J = 8.3, 2.2$ Hz, 1H), 6.30 (s, 1H), 3.25 (d, $J = 9.3$ Hz, 1H), 3.12 (m, 2H), 3.06 (d, $J = 9.3$ Hz, 1H), 2.35 (d, $J = 8.4$ Hz, 1H), 2.25 (dd, $J = 8.5, 3.8$ Hz, 1H), 1.20 (s, 3H), 1.19 (s, 3H).

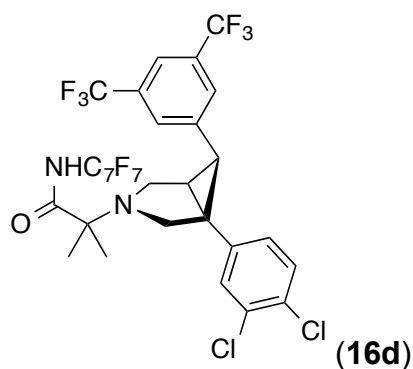
^{19}F NMR (377 MHz, CDCl_3) δ -56.2 (t, $J = 21.8$ Hz, 3F), -140.8 (m, 2F), -142.9 (dt, $J = 13.7, 8.8$ Hz, 2F).

The carbon resonances corresponding to the perfluoroarene (C_7F_7) in this compound appear as a complex series of multiplets between 105 ppm to 155 ppm as a result of $^{13}\text{C}/^{19}\text{F}$ coupling. Due to the complexities of the system, the peaks are not listed. ^{19}F NMR and HRMS were used to confirm the presence of this ring system.

^{13}C NMR (176 MHz, CDCl_3) δ 175.2, 141.9, 135.9, 132.7, 131.5, 130.7, 130.6, 129.4, 128.9, 126.2, 120.4, 61.2, 49.8, 45.6, 35.1, 32.0, 28.0, 21.4, 20.5.

HRMS (ESI⁺) $[\text{M}+\text{H}]^+$ Calcd for $\text{C}_{28}\text{H}_{21}\text{BrCl}_2\text{F}_7\text{N}_2\text{O}^+$: 683.0103; Found: 683.0093.

$R_f = 0.52$ in 20% EtOAc in hexanes



NaBH₄ reduction was required on this substrate following the **Isolation Procedure B** found in the **Standard Conditions for C-H Arylation of Alicyclic Amines** section. Isolated as colorless oil.

Isolated yield using modified standard conditions C: 33%, 34%, 46%, 33%; 37% average yield

Isolated yield when based on recovered starting material: 55%, 46%, 54%, 37%; 49% average yield

IR (thin film): 1717 cm⁻¹

¹H NMR (700 MHz, CDCl₃) δ 7.80 (s, 2H), 7.63 (s, 1H), 7.46 (d, *J* = 8.3 Hz, 1H), 7.38 (d, *J* = 2.2 Hz, 1H), 7.15 (dd, *J* = 8.3, 2.2 Hz, 1H), 6.01 (s, 1H), 3.28 (d, *J* = 9.7 Hz, 1H), 3.19-3.09 (multiple peaks, 3H), 2.49 (d, *J* = 8.4 Hz, 1H), 2.35 (dd, *J* = 8.5, 3.7 Hz, 1H), 1.20 (s, 3H), 1.19 (s, 3H).

¹⁹F NMR (377 MHz, CDCl₃) δ -56.2 (t, *J* = 21 Hz, 3F), -63.5 (s, 6F), -141.2 (m, 2F), -143.5 (m, 2F).

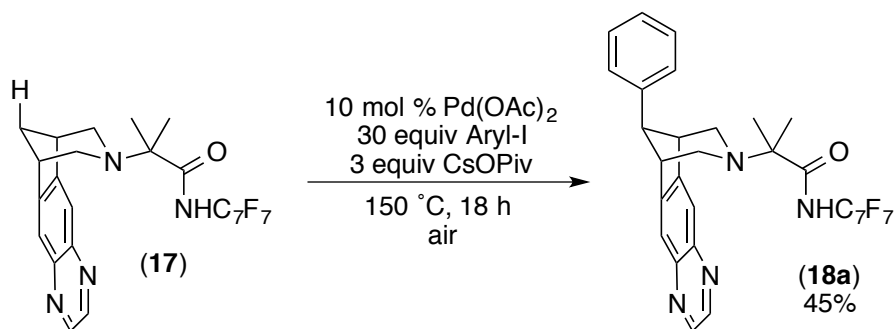
The carbon resonances corresponding to the perfluoroarene (C₇F₇) in this compound appear as a complex series of multiplets between 105 ppm to 155 ppm as a result of ¹³C/¹⁹F coupling. Due to the complexities of the system, the peaks are not listed. ¹⁹F NMR and HRMS were used to confirm the presence of this ring system.

¹³C NMR (176 MHz, CDCl₃) δ 174.0, 140.9, 140.0, 132.9, 131.9 (q, *J*_{C-F} = 33 Hz), 131.2, 130.7, 128.8, 127.9, 126.2, 122.8 (q, *J*_{C-F} = 273 Hz), 120.2 (q, *J*_{C-F} = 3.9 Hz), 61.4, 49.8, 45.5, 35.5, 31.7, 28.2, 20.8, 20.4.

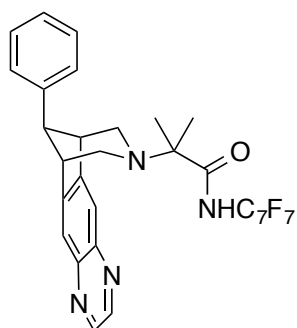
HRMS (ESI⁺) [M+H]⁺ Calcd for C₃₀H₂₀Cl₂F₁₃N₂O⁺: 741.0745; Found: 741.0744.

*R*_f = 0.60 in 20% EtOAc in hexanes

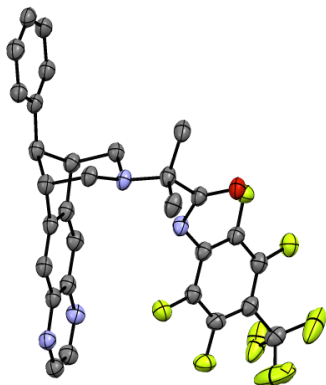
Diversification of varenicline and cytisine core via transannular C–H arylation



Standard conditions D. Example given for Aryl-I = PhI: Under ambient conditions, a 20 mL scintillation vial was charged with solid substrate **17** (77 mg, 0.15 mmol, 1 equiv), Pd(OAc)₂ (3.5 mg, 0.01 mmol, 10 mol %), cesium pivalate (105 mg, 0.45 mmol, 3 equiv), and iodobenzene (0.55 mL, 5.3 mmol 30 equiv). The vial was sealed with a Teflon-lined cap and heated to an external temperature of 150 °C. After 24 h, the reaction was removed from the heat source and diluted with hexanes (5 mL). Hydrazine (300 μL, 35% in H₂O, 1.5 mmol, 20 equiv) was added to the warm solution. The mixture was allowed to stir for 60 min at 60 °C to remove Pd from the product. This solution was loaded onto a small plug of silica gel over which hexanes (150 mL) was passed to remove iodoarene. The plug of silica was then rinsed with EtOAc (150 mL) to elute the product, and this solution was concentrated under reduced pressure. Purification by column chromatography (25 g cartridge, gradient elution from 0% to 40% EtOAc in hexanes) afforded recovered starting material (26 mg) along with the desired product **18a** (40 mg, 45%).



(18a)



Isolated yield using standard conditions D: 41%, 55%, 45%; 45% average yield

Isolated yield when calculated based on recovered starting material: 63%, 77%, 61%;
67% average yield

MP 203-205 °C (white solid)

IR (thin film): 1721 cm^{-1}

^1H NMR (700 MHz, CDCl_3) δ 8.76 (s, 2H), 7.93 (s, 2H), 7.46 (t, $J = 7.6$ Hz, 2H), 7.40-7.35 (multiple peaks, 3H), 7.30 (m, 1H), 4.03 (t, $J = 4.3$ Hz, 2H), 3.77 (m, 1H), 3.17 (d, $J = 11.0$ Hz, 2H), 2.76 (dd, $J = 11.2, 4.2$ Hz, 2H), 1.02 (s, 6H).

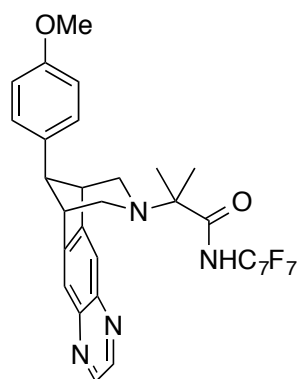
^{19}F NMR (377 MHz, CDCl_3) δ -56.0 (t, $J = 21.6$ Hz, 3F), -141.4 (m, 2F), -144.4 (m, 2F).

The carbon resonances corresponding to the perfluoroarene (C_7F_7) in this compound appear as a complex series of multiplets between 105 ppm to 155 ppm as a result of $^{13}\text{C}/^{19}\text{F}$ coupling. Due to the complexities of the system, the peaks are not listed. ^{19}F NMR and HRMS were used to confirm the presence of this ring system.

^{13}C NMR (176 MHz, CDCl_3) δ 174.8, 149.9, 144.1, 143.0, 138.0, 129.1, 128.2, 126.5, 121.1, 63.8, 51.4, 44.9, 42.5, 21.2.

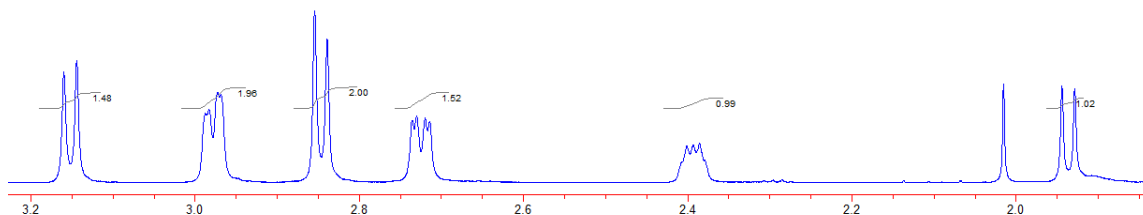
HRMS (ESI $^+$) $[\text{M}+\text{H}]^+$ Calcd for $\text{C}_{30}\text{H}_{24}\text{F}_7\text{N}_4\text{O}^+$: 589.1838; Found: 589.1830.

$R_f = 0.60$ in 50% EtOAc in hexanes



(18b)

The yield for compound **18b** was determined by isolating a mixture of recovered starting material **17** and compound **18b** from the column chromatography. The mixture was analyzed by ^1H NMR spectroscopy to determine the ratio of **17:18b** (ca. 2:1.6 depending on sample). This ratio, in combination with the isolated mass of the mixture and the respective molecular masses, was used to determine a yield of **18b** based on the mixture. Pure **18b** was isolated after repeated chromatography. An excerpt of the NMR spectrum used to determine the ratio is below:



Yield using standard conditions D: 41%, 38%; 40% average yield

Yield calculated based on recovered starting material: 80%, 70%; 75% average yield

MP 161-164 °C (white solid)

^1H NMR (700 MHz, CDCl_3) δ 8.75 (s, 2H), 7.91 (s, 2H), 7.36 (s, 1H), 7.28 (m, 2H), 6.99 (m, 2H), 3.97 (t, $J = 4.2$ Hz, 2H), 3.86 (s, 3H), 3.71 (m, 1H), 3.17 (d, $J = 11.0$ Hz, 2H), 2.74 (dd, $J = 11.1, 4.1$ Hz, 2H), 1.03 (s, 6H).

^{19}F NMR (377 MHz, CDCl_3) δ -56.1 (t, $J = 21.7$ Hz, 3F), -141.4 (qd, $J = 21.7, 12.6$ Hz, 2F), -144.3 (m, 2F).

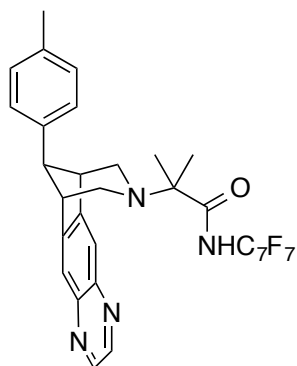
The carbon resonances corresponding to the perfluoroarene (C_7F_7) in this compound appear as a complex series of multiplets between 105 ppm to 155 ppm as a result of

$^{13}\text{C}/^{19}\text{F}$ coupling. Due to the complexities of the system, the peaks are not listed. ^{19}F NMR and HRMS were used to confirm the presence of this ring system.

^{13}C NMR (176 MHz, CDCl_3) δ 174.8, 157.9, 150.0, 144.0, 143.1, 129.9, 129.2, 121.1, 114.5, 63.8, 55.2, 50.7, 44.8, 42.7, 21.2.

HRMS (ESI⁺) [M+H]⁺ Calcd for $\text{C}_{31}\text{H}_{26}\text{F}_7\text{N}_4\text{O}_2^+$: 619.1944; Found: 619.1936.

R_f = 0.50 in 50% EtOAc in hexanes



(18c)

Isolated yield using standard conditions D: 41%, 43%; 42% average yield

Isolated yield when calculated based on recovered starting material: 55%, 53%; 54% average yield

MP 239-244 °C (light brown solid)

IR (thin film): 1721 cm^{-1}

^1H NMR (700 MHz, CDCl_3) δ 8.75 (s, 2H), 7.91 (s, 2H), 7.37 (s, 1H), 7.26 (s, 4H), 3.99 (t, J = 4.3 Hz, 2H), 3.72 (t, J = 4.3 Hz, 1H), 3.17 (d, J = 11.0 Hz, 2H), 2.75 (dd, J = 11.2, 4.2 Hz, 2H), 2.39 (s, 3H), 1.03 (s, 6H).

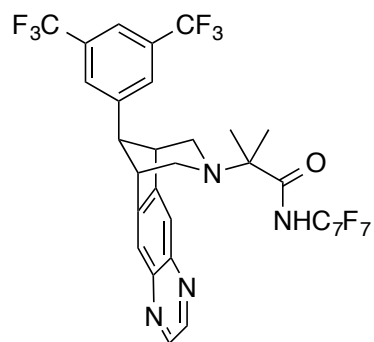
^{19}F NMR (377 MHz, CDCl_3) δ -56.1 (t, J = 21.6 Hz, 3F), -141.4 (m, 2F), -144.3 (m, 2F).

The carbon resonances corresponding to the perfluoroarene (C_7F_7) in this compound appear as a complex series of multiplets between 105 ppm to 155 ppm as a result of $^{13}\text{C}/^{19}\text{F}$ coupling. Due to the complexities of the system, the peaks are not listed. ^{19}F NMR and HRMS were used to confirm the presence of this ring system.

^{13}C NMR (176 MHz, CDCl_3) δ 174.9, 150.0, 144.0, 143.0, 136.0, 134.8, 129.7, 128.0, 121.1, 63.8, 51.1, 44.8, 42.6, 21.2, 21.0.

HRMS (ESI⁺) [M+H]⁺ Calcd for $\text{C}_{31}\text{H}_{26}\text{F}_7\text{N}_4\text{O}^+$: 603.1995; Found: 603.1989.

R_f = 0.65 in 50% EtOAc in hexanes



(18d)

NOTE: This reaction was conducted at 140 °C using 20 mol % Pd(OAc)₂, 3 equiv AgOAc, and 3 equiv KOⁱPiv analogous conditions in the standard conditions of azabicyclo[3.1.0]hexane system **8** for isolation of **9j**.

Isolated yield using modified standard conditions: 36%, 39%, 34%; 36% average yield

Isolated yield when calculated based on recovered starting material: 51%, 46%, 53%; 50% average yield

MP >250 °C (dec.) (white solid)

IR (thin film): 1715 cm⁻¹

¹H NMR (700 MHz, CDCl₃) δ 8.77 (s, 2H), 7.96 (s, 2H), 7.86 (s, 1H), 7.84 (s, 2H), 7.18 (s, 1H), 4.13 (t, *J* = 4.2 Hz, 2H), 3.85 (bs, 1H), 3.02 (d, *J* = 11.4 Hz, 2H), 2.87 (dd, *J* = 11.6, 4.2 Hz, 2H), 1.05 (s, 6H).

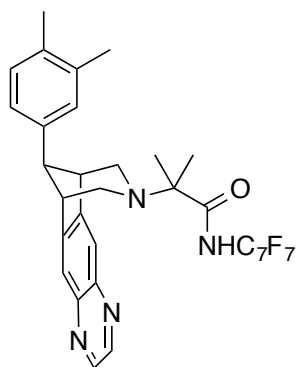
¹⁹F NMR (377 MHz, CDCl₃) δ -56.1 (t, *J* = 21.7 Hz, 3F), -62.8 (s, 6F), -141.2 (m, 2F), -144.4 (m, 2F).

The carbon resonances corresponding to the perfluoroarene (C₇F₇) in this compound appear as a complex series of multiplets between 105 ppm to 155 ppm as a result of ¹³C/¹⁹F coupling. Due to the complexities of the system, the peaks are not listed. ¹⁹F NMR and HRMS were used to confirm the presence of this ring system.

¹³C NMR (176 MHz, CDCl₃) δ 174.3, 148.5, 144.4, 143.1, 140.9, 132.5 (q, *J*_{C-F} = 33 Hz), 128.6 (q, *J*_{C-F} = 4.0 Hz), 123.1 (q, *J*_{C-F} = 273 Hz), 121.5, 120.7 (q, *J*_{C-F} = 4.0 Hz), 63.8, 51.1, 44.8, 42.3, 21.1.

HRMS (ESI⁺) [M+H]⁺ Calcd for C₃₂H₂₂F₁₃N₄O⁺: 725.1586; Found: 725.1575.

*R*_f = 0.70 in 50% EtOAc in hexanes



(18e)

Isolated yield using standard conditions D: 44%, 42%; 43% average yield

Isolated yield when calculated based on recovered starting material: 78%, 74%; 76% average yield

MP 228-231 °C (brown solid)

IR (thin film): 1714 cm^{-1}

^1H NMR (700 MHz, CDCl_3) δ 8.75 (s, 2H), 7.91 (s, 2H), 7.37 (s, 1H), 7.20 (d, $J = 7.7$ Hz, 1H), 7.13 (s, 1H), 7.09 (d, $J = 7.7$ Hz, 1H), 4.00 (t, $J = 4.3$ Hz, 2H), 3.70 (m, 1H), 3.18 (d, $J = 10.9$ Hz, 2H), 2.75 (dd, $J = 11.1, 4.2$ Hz, 2H), 2.33 (s, 3H), 2.30 (s, 3H), 1.04 (s, 6H).

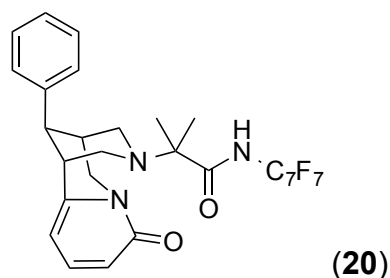
^{19}F NMR (377 MHz, CDCl_3) δ -56.1 (t, $J = 21.7$ Hz, 3F), -141.4 (m, 2F), -144.4 (m, 2F).

The carbon resonances corresponding to the perfluoroarene (C_7F_7) in this compound appear as a complex series of multiplets between 105 ppm to 155 ppm as a result of $^{13}\text{C}/^{19}\text{F}$ coupling. Due to the complexities of the system, the peaks are not listed. ^{19}F NMR and HRMS were used to confirm the presence of this ring system.

^{13}C NMR (176 MHz, CDCl_3) δ 174.9, 150.1, 144.0, 143.1, 137.2, 135.3, 134.6, 130.2, 129.3, 125.5, 121.0, 63.8, 51.1, 44.9, 42.5, 21.2, 20.0, 19.3.

HRMS (ESI $^+$) $[\text{M}+\text{H}]^+$ Calcd for $\text{C}_{32}\text{H}_{28}\text{F}_7\text{N}_4\text{O}^+$: 617.2151; Found: 617.2145.

$R_f = 0.70$ in 50% EtOAc in hexanes



NOTE: The arylation reaction was conducted in *t*AmylOH (0.13 M in substrate).

Isolated yield using standard conditions D: 25% yield (yellow oil).

Isolated yield when calculated based on recovered starting material: 32%

IR (thin film): 1717, 1653 cm^{-1}

^1H NMR (700 MHz, CDCl_3) δ 7.68 (s, 1H), 7.44 (t, $J = 14$ Hz, 2H), 7.38 (d, $J = 14$ Hz, 2H), 7.31 (t, $J = 14$ Hz, 1H), 7.09 (dd, $J = 7, 0.7$ Hz, 1H), 6.38 (app d, $J = 10.5$ Hz, 1H), 6.09 (app d, $J = 7$ Hz, 1H), 4.45 (d, $J = 15.4$ Hz, 1H), 4.15 (dd, $J = 6.3, 15.4$ Hz, 1H), 3.65 (br s, 1H), 3.38 (br s, 1H), 3.18 (br s, 1H), 2.95 (m, 1H), 2.89 (m, 1H), 2.82 (d, $J = 11.9$ Hz, 1H), 2.65 (app d, $J = 11.9$ Hz, 1H), 1.24 (s, 3H), 1.08 (s, 3H).

^{19}F NMR (377 MHz, CDCl_3) δ -56.1 (t, $J = 21.9$ Hz, 3F), -140.9 (m, 2F), -142.9 (m, 2F).

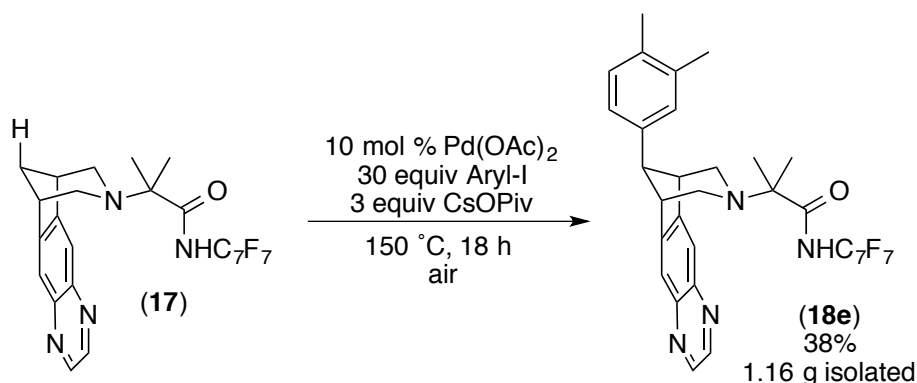
The carbon resonances corresponding to the perfluoroarene (C_7F_7) in this compound appear as a complex series of multiplets between 105 ppm to 155 ppm as a result of $^{13}\text{C}/^{19}\text{F}$ coupling. Due to the complexities of the system, the peaks are not listed. ^{19}F NMR and HRMS were used to confirm the presence of this ring system.

^{13}C NMR (176 MHz, CDCl_3) δ 174.8, 163.1, 150.9, 138.6, 137.7, 129.3, 127.3, 127.1, 117.5, 105.0, 64.6, 52.6, 50.0, 48.0, 39.7, 36.1, 31.1, 23.7, 17.8.

HRMS (ESI $^+$) $[\text{M}+\text{H}]^+$ Calcd for $\text{C}_{28}\text{H}_{25}\text{F}_7\text{N}_3\text{O}_2$: 568.1830; Found: 568.1829.

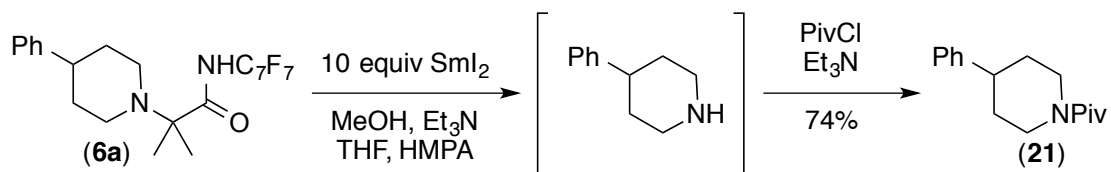
$R_f = 0.25$ in 60% EtOAc in hexanes

Gram scale C–H arylation reaction:



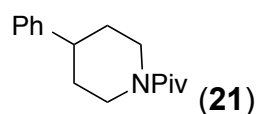
Under ambient conditions, a 50 mL round bottom flask was charge with substrate **17** (2.51 g, 4.0 mmol, 1 equiv), Pd(OAc)₂ (110 mg, 0.49 mmol, 10 mol %), cesium pivalate (3.45 g, 14.7 mmol, 3 equiv) and 4-iodo-*o*-xylene (20.9 mL, 147 mmol, 30 equiv). The flask was sealed with a glass stopper, and heated to an external temperature of 150 °C. After reaching the appropriate temperature, excess pressure was vented from the flask, and it was resealed. After 24 h, the reaction was removed from the heat source, and hydrazine (3 mL, 65% in H₂O, 40 mmol, 8 equiv) and hexanes (5 mL) were added to the warm solution. The mixture was then allowed to stir for 1 h at 60 °C to remove Pd from the product. This solution was loaded onto a large plug of silica gel over which hexanes (1.5 L) was passed to remove iodoarene. The plug of silica was then rinsed with EtOAc (1 L) to elute the product, and this solution was concentrated under reduced pressure. Purification by column chromatography (100 g cartridge, gradient elution from 0% to 40% EtOAc in hexanes) afforded the desired product **18e** as a brown solid (1.16 g, 38% yield).

Directing group cleavage by Sml₂ reductive deamination



In a glove box, a vial was charged with solid amine **6a** (66 mg, 0.14 mmol, 1 equiv) to which a solution of Sml₂ (15 mL, 0.1M in THF, 1.5 mmol, 10 equiv) was added. To this solution, MeOH (0.3 mL, 7.5 mmol, 53 equiv), HMPA (0.2 mL, 1.12 mmol, 8 equiv) and

Et₃N (1.0 mL, 14 mmol, 100 equiv) were added. The vial was then sealed with a Teflon-lined cap and removed from the glove box. The solution was allowed to stand at room temperature for 18 h, after which the reaction was quenched by dropwise addition of pivaloyl chloride (1.0 mL, 8.1 mmol, 58 equiv) followed by the addition of additional TEA (1.0 mL, 14 mmol, 100 equiv). The resulting solution was allowed to remain at room temperature for 90 min, after which it was poured onto 2M HCl. The mixture was extracted with EtOAc. The combined organic phases were washed with brine, dried (Na₂SO₄), filtered, and concentrated under reduced pressure. Purification by column chromatography (25 g cartridge, gradient elution from 0% to 40% EtOAc in hexanes) afforded amide **21** (29 mg, 78% yield) and reduced fluoroamide (**22**) in 40% yield.



Isolated yield: 78%, 70%; 74% average yield

MP 87 °C (off white solid)

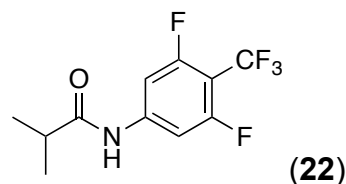
IR (thin film): 1617 cm⁻¹

¹H NMR (700 MHz, CDCl₃) δ 7.31 (m, 2H), 7.23-7.19 (multiple peaks, 3H), 4.58 (d, *J* = 12.2 Hz, 2H), 2.87 (t, *J* = 12.9 Hz, 2H), 2.76 (tt, *J* = 12.2, 4.1 Hz, 1H), 1.90 (d, *J* = 13.1 Hz, 2H), 1.63 (qd, *J* = 12.6, 4.1 Hz, 2H), 1.31 (s, 9H).

¹³C NMR (176 MHz, CDCl₃) δ 176.1, 145.3, 128.5, 126.7, 126.4, 45.8, 42.8, 38.7, 33.5, 28.4.

HRMS (ESI⁺) [M+H]⁺ Calcd for C₁₆H₂₄NO⁺: 246.1858; Found: 246.1852.

*R*_f = 0.40 in 20% EtOAc in hexanes



Isolated yield: 41%, 40%; 41% average yield

MP 140 °C (white solid)

IR (thin film): 1683 cm⁻¹

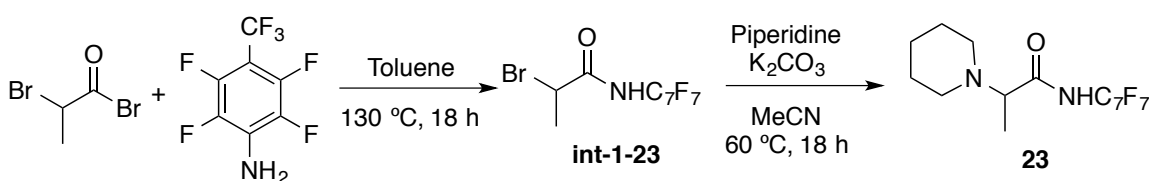
^1H NMR (700 MHz, CDCl_3) δ 7.41 (br s, 1H), 7.29 (d, $J = 11.5$ Hz, 2H), 2.52 (septet, $J = 7.0$ Hz, 1H), 1.25 (d, $J = 7.0$ Hz, 6H).

^{19}F NMR (377 MHz, CDCl_3) δ -56.0 (t, $J = 21.3$ Hz, 3F), -108.8 (qd, $J = 21.3, 11.2$ Hz, 2F).

^{13}C NMR (176 MHz, CDCl_3) δ 175.7, 160 (m), 142.9 (t, $J_{\text{C-F}} = 13.4$ Hz) 121.6 (q, $J_{\text{C-F}} = 272$ Hz), 103.1 (dd, $J_{\text{C-F}} = 26.6, 3.7$ Hz), 102.7 (m), 36.8, 19.3.

HRMS (ESI $^+$) $[\text{M}+\text{H}]^+$ Calcd for $\text{C}_{11}\text{H}_{11}\text{F}_5\text{NO}^+$: 268.0761; Found: 268.0751.

$R_f = 0.38$ in 20% EtOAc in hexanes



Compound 23. Step 1: 2-bromopropanoyl bromide (0.55 mL, 5.25 mmol, 1 equiv) and 2,3,5,6-tetrafluoro-4-(trifluoromethyl)aniline (0.74 mL, 5.25 mmol, 1 equiv) were dissolved in toluene (20 mL, 0.25 M) and heated to reflux for 18 hours. The reflux condenser was equipped with a drying tube that was packed with K_2CO_3 (5 g). After cooling to room temperature, the volatiles were removed via rotary evaporation. The crude product was recrystallized from hexanes affording 93% yield of **int-1-23**.

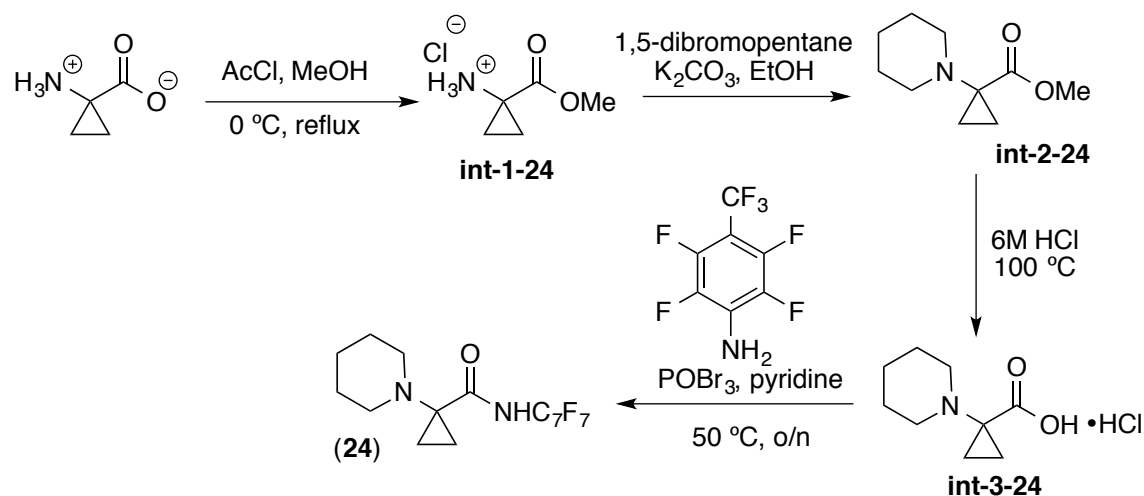
^1H NMR (CDCl_3 , 401 MHz) δ 7.84 (s, 1H), 4.63 (q, $J = 7.0$ Hz, 1H), 2.00 (d, $J = 7.0$ Hz, 4H).

^{19}F NMR (CDCl_3 , 377 MHz) δ -56.16 (t, $J = 21.7$ Hz, 3F), -140.17 (m, 2F), -142.82 (m, 2F).

Step 2: **int-1-23** (0.9 g, 2.45 mmol, 1 equiv), piperidine (0.49 mL, 4.9 mmol, 2 equiv), K_2CO_3 (1.01 g, 7.35 mmol, 3 equiv) were mixed in acetonitrile (9.8 mL, 0.25 M). The reaction mixture was heated to 60 °C for 18 h. The mixture was filtered through a silica plug (100% EtOAc) and the volatiles were removed via rotary evaporation. The residue was purified via column chromatography (5% to 20% EtOAc in hexanes) to afford 70% yield of **23**.

^1H NMR (CDCl_3 , 500 MHz) δ 9.53 (s, 1H), 3.35 (q, $J = 7.0$ Hz, 1H), 2.68–2.43 (multiple peaks, 4H), 1.78–1.58 (m, 4H), 1.51 (m, 2H), 1.30 (t, $J = 7.0$, 3H).

^{19}F NMR (CDCl_3 , 471 MHz) δ -56.02 (t, $J = 21.8$ Hz), -141.07 (m, 2F), -143.97 (m, 2F).



Compound 24.

Step 1: 1-aminocyclopropane-1-carboxylic acid (1g, 9.89, 1 equiv) was mixed with acetyl chloride (1.5 mL, 19.8 mmol, 2 equiv) and methanol (5 mL) at 0 °C under N_2 . The mixture was heated to reflux overnight. The volatiles were removed via rotary evaporation affording quantitative yield of **int-1-24**.

^1H NMR (500 MHz, Methanol- d_4) δ 3.81 (s, 3H), 1.57 (m, 2H), 1.37 (m, 2H).

Step 2: **int-1-24** (90 mg, 0.66 mmol, 1 equiv), 1,5-dibromopentane (90 μL , 0.66 mmol, 1 equiv), K_2CO_3 (100 mg, 0.66 mmol, 1 equiv) were dissolved in ethanol (0.2 mL). The reaction was heated to 60 °C for two days. The reaction mixture was diluted in DCM (10 mL) and washed with aqueous K_2CO_3 (4 X 5 mL). The organics were dried over Na_2SO_4 , decanted and concentrated. The crude product was purified via column chromatography (4 : 1 v/v DCM : Et_2O) affording 89% of **int-2-24**.

^1H NMR (CDCl_3 , 500 MHz) δ 3.62 (s, 3H), 2.86 (app. br s, 4H), 1.48–1.34 (multiple peaks, 6H), 1.23 (m, 2H), 0.88 (m, 2H).

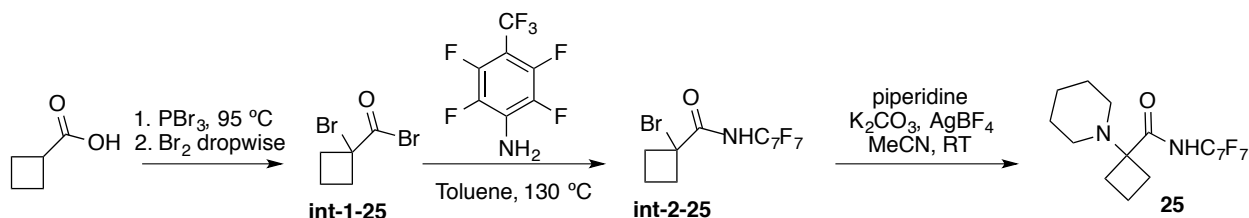
Step 3: **int-2-24** (400 mg, 2.2 mmol, 1 equiv) was dissolved in 6 M HCl (42 mL) and was heated to 105 °C for 2 days. The water was removed by rotary evaporation. The crude product (**int-3-24**) was dried in high vacuum and used without further purification.

^1H NMR (700 MHz, Deuterium Oxide) δ 3.35 (br s, 4H), 1.79 (m, 2H), 1.70 – 1.53 (multiple peaks, 3H), 1.47 (m, 2H), 1.37 (m, 2H), 1.32 (m, 1H).

Step 4: A round-bottom flask was charged with **int-3-24** (500 mg, 2.43 mmol, 1 equiv) and POBr_3 (1.39 g, 4.86 mmol, 2 equiv) and cooled to $-78\text{ }^\circ\text{C}$. Pyridine (9.5 mL) was slowly added, followed by 2,3,5,6-tetrafluoro-4-(trifluoromethyl)aniline (0.75 mL, 5.35 mmol, 2.2 equiv). The reaction was slowly brought to room temperature and then heated to $50\text{ }^\circ\text{C}$ for 24 hours. The reaction was diluted with DCM (10 mL) and triethylamine was added (1 mL, 7.3 mmol, 3 equiv). The mixture was filtered through a plug of celite and the volatiles were removed via rotary evaporation. The residue was purified via column chromatography (20% DCM in hexanes to 100% DCM) to give **24** in 50% yield.

^1H NMR (400 MHz, Methanol- d_4) δ 2.51 (br s, 4H), 1.72 (p, $J = 5.7\text{ Hz}$, 4H), 1.47 (m, 2H), 1.30 (m, 2H), 1.21 (m, 2H). Note: N–H not observed.

^{19}F NMR (376 MHz, Methanol- d_4) δ -57.62 (t, $J = 21.9\text{ Hz}$, 3F), -144.72 (m, 2F), -145.61 (m, 2F).



Compound 25.

Step 1: A round-bottom flask was charged with cyclobutanecarboxylic acid (1.2 mL, 11.9 mmol, 1 equiv) and PBr_3 (0.46 mL, 4.7 mmol, 0.4 equiv). A rubber septum was fitted to the flask and the reaction was placed under a N_2 atmosphere. The mixture was heated to $95\text{ }^\circ\text{C}$ for 5 minutes. Subsequently, Br_2 (1.54 mL, 29.8 mmol, 2.5 equiv) was added dropwise over 2 hours [*Caution: Evolution of gas*]. A needle was used to puncture the septum to vent the system into a saturated solution of sodium thiosulfate. After 4 hours, additional Br_2 (0.5 mL, 9.7 mmol, 0.8 equiv) was added to the reaction mixture. After 12 hours, additional Br_2 (0.5 mL, 9.7 mmol, 0.8 equiv) was added to the reaction mixture. Next, the reaction was cooled to room temperature and the crude product was placed under high vacuum for 5 minutes, followed by purification of the viscous residue via Kugelrohr ($50\text{ }^\circ\text{C}$, 50 mTorr) to afford 93% yield of **int-1-25** in 80% purity as determined by ^1H NMR.

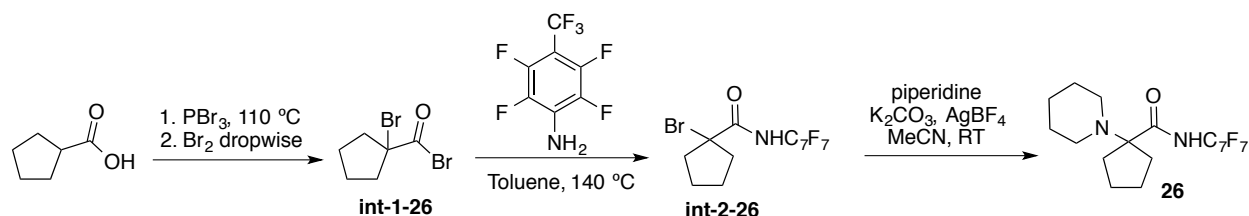
^1H NMR (CDCl_3 , 400 MHz) δ 2.96 (m, 2H), 2.61 (m, 2H), 2.29 (m, 1H), 1.89 (m, 1H).

Step 2: A dry round bottom flask was charged with 2,3,5,6-tetrafluoro-4-(trifluoromethyl)aniline (0.6 mL, 4.01 mmol, 1 equiv) and toluene (19 mL). To this solution, **int-1-25** (0.97 g, 4.01 mmol, 1 equiv) was added. The flask was fitted with a reflux condenser topped with a drying tube that was packed with K_2CO_3 (5 g). The reaction was heated to an external temperature of 130 °C. After 18 h, the reaction mixture was cooled to room temperature and concentrated under vacuum. The solid residue was recrystallized from hot hexanes. The solid was then dried under vacuum to afford **int-2-25** and was used in the next step without further purification.

Step 3: Inside a N_2 glovebox, a dry round-bottom flask was charged with **int-2-25** (1.6 g, 4 mmol, 1 equiv), K_2CO_3 (0.56 g, 4 mmol, 1 equiv), $AgBF_4$ (0.79 g, 4 mmol, 1 equiv) and acetonitrile (20 mL). To this solution, piperidine (1.5 mL, 15.2 mmol, 3.8 equiv) was added. The reaction was stirred at room temperature outside of the glovebox. After 18 hours, the mixture was filtered through celite and the volatiles were removed under vacuum. The residue was purified via column chromatography (0% to 10% THF in hexanes) to afford product **25** in 27% yield.

1H NMR (401 MHz, Methanol- d_4) δ 2.54 (app. t, $J = 5.6$ Hz, 4H), 2.43 (m, 2H), 2.29 (m, 2H), 1.93–1.74 (multiple peaks, 2H), 1.68 (app. p, $J = 5.6$ Hz, 4H), 1.52 (m, 2H). Note: N–H not observed.

^{19}F NMR (377 MHz, Methanol- d_4) δ –57.63 (t, $J = 22.0$ Hz, 3F), –144.61 (m, 2F), –145.46 (m, 2F).



Compound 26.

Step 1: A round-bottom flask was charged with cyclopentanecarboxylic acid (1 mL, 9.23 mmol, 1 equiv) and PBr_3 (0.35 mL, 3.7 mmol, 0.4 equiv). A rubber septum was fitted to the flask and the reaction was placed under a N_2 atmosphere. The mixture was heated to 110 °C for 5 minutes. Subsequently, Br_2 (0.71 mL, 13.8 mmol, 1.5 equiv) was added dropwise over 1 hour, until the solution retained the brown color of bromine [*Caution:*

Evolution of gas]. A needle was used to puncture the septum to vent the system into a saturated solution of sodium thiosulfate. The reaction was cooled to room temperature and the crude product was placed under high vacuum for 10 minutes, followed by purification of the viscous residue via Kugelrohr (50 °C, 50 mTorr) to afford 78% yield of **int-1-26** as a colorless oil.

^1H NMR (CDCl_3 , 400 MHz) δ 2.37 (m, 4H), 2.04 (m, 2H), 1.88 (m, 2H).

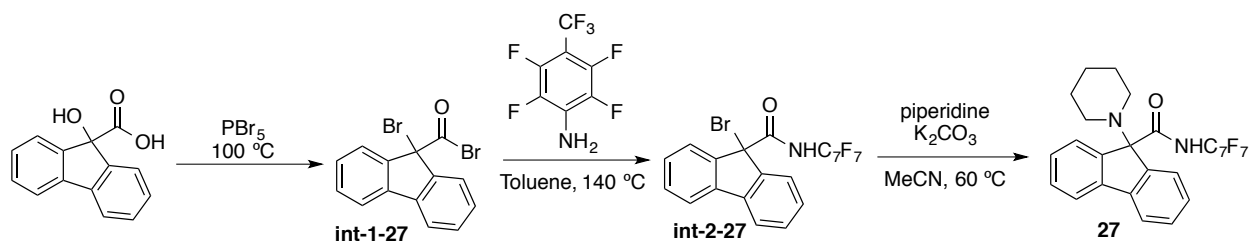
Step 2: A round bottom flask was charged with 2,3,5,6-tetrafluoro-4-(trifluoromethyl)aniline (1 mL, 7.2 mmol, 1 equiv) and toluene (30 mL). To this solution, **int-1-26** (1.84 g, 7.2 mmol, 1 equiv) was added. The flask was fitted with a reflux condenser topped with a drying tube that was packed with K_2CO_3 (5 g). The reaction was heated to an external temperature of 140 °C. After 18 h, the reaction mixture was cooled to room temperature and concentrated under vacuum. The solid residue was recrystallized from hot hexanes. The solid was then dried under vacuum to afford product **int-2-26** in 79% yield.

^1H NMR (CDCl_3 , 401 MHz) δ 8.22 (s, 1H), 2.62–2.47 (multiple peaks, 2H), 2.44–2.33 (multiple peaks, 2H), 2.13–1.89 (multiple peaks, 4H).

Step 3: Inside a N_2 glovebox, a 20-mL vial was charged with **int-2-26** (1.15 g, 2.83 mmol, 1 equiv), K_2CO_3 (0.39 g, 2.83 mmol, 1 equiv), AgBF_4 (0.55g, 2.83 mmol, 1 equiv) and acetonitrile (14 mL). To this solution, piperidine (1.07 mL, 10.8 mmol, 3.8 equiv) was added. The reaction was stirred at room temperature outside of the glovebox. After 18 hours, the mixture was filtered through celite and the volatiles were removed under vacuum. The residue was purified via column chromatography (0% to 5% THF in hexanes) to afford product **26** in 63% yield.

^1H NMR (400 MHz, Methanol- d_4) δ 2.51 (app. s, 4H), 1.97 (m, 4H), 1.77–1.59 (multiple peaks, 8H), 1.53 (m, 2H). Note: N–H not observed.

^{19}F NMR (376 MHz, Methanol- d_4) δ –57.61 (t, J = 21.9 Hz, 3F), –144.73 (m, 2F), –146.02 (m, 2F).



Compound 27.

Step 1: A round-bottom flask was charged with 9-hydroxy-9H-fluorene-9-carboxylic acid (0.5 g, 2.21 mmol, 1 equiv) and PBr₅ (1.9 g, 4.42 mmol, 2 equiv). The neat mixture was heated to 100 °C for 2 hours. After cooling to room temperature, the reaction mixture was dissolved in chloroform (15 mL) and passed through a small silica gel plug (100% EtOAc). The solvent was removed via rotary evaporation and dried under high vacuum to afford **int-1-27**. The product was used in the next step without further purification or characterization.

HRMS EI+ [M⁺] Calcd for C₁₄H₈Br₂O: 349.8942, found: 349.8929.

Step 2: A dry round bottom flask was charged with 2,3,5,6-tetrafluoro-4-(trifluoromethyl)aniline (0.31 mL, 2.21 mmol, 1 equiv) and toluene (10 mL). To this solution, **int-1-27** (0.78 g, 2.21 mmol, 1 equiv) was added. The flask was fitted with a reflux condenser topped with a drying tube that was packed with K₂CO₃ (5 g). The reaction was heated to an external temperature of 140 °C. After 18 h, the reaction mixture was cooled to room temperature and concentrated via rotary evaporation. The residue was purified via column chromatography (10% EtOAc in hexanes) to give 34% yield of **int-2-27**.

¹H NMR (CDCl₃, 401 MHz) δ 7.79 (d, *J* = 7.6 Hz, 2H), 7.74 (d, *J* = 7.6 Hz, 2H), 7.51 (t, *J* = 7.4 Hz, 2H), 7.48–7.40 (multiple peaks, 3H).

¹⁹F NMR (CDCl₃, 377 MHz) δ –56.18 (t, *J* = 21.7 Hz, 3F), –140.33 (m, 2F), –142.68 (m, 2F).

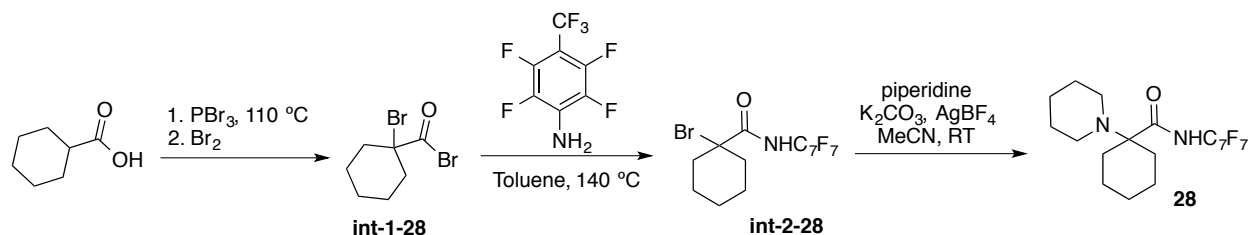
HRMS ESI+ [M+H]⁺ calcd. for C₂₁H₁₀BrF₇NO: 503.9829; found: 503.9820.

Step 3: A 4-mL vial was charged with **int-2-27** (150 mg, 0.3 mmol, 1 equiv), K₂CO₃ (83 mg, 0.6 mmol, 2 equiv) and acetonitrile (1.5 mL). To this solution, piperidine (89 μL, 0.9 mmol, 3 equiv) was added. The reaction mixture was heated to 60 °C for 18 h. After, the mixture was filtered through a silica plug (100% EtOAc) and the volatiles were removed

via rotary evaporation. The residue was purified via column chromatography (5% THF in hexanes) to afford 63% yield of **27**.

^1H NMR (CDCl_3 , 401 MHz) δ 7.71 (d, $J = 7.6$ Hz, 2H), 7.54 (d, $J = 7.6$ Hz, 2H), 7.43 (t, $J = 7.5$ Hz, 2H), 7.32 (t, $J = 7.5$ Hz, 2H), 2.53 (br s, 4H), 1.63 (m, 4H), 1.46 (br s, 2H).

^{19}F NMR (CDCl_3 , 471 MHz) δ -56.03 (t, $J = 21.8$ Hz, 3F), -140.96 (m, 2F), -143.55 (m, 2F). Note: N-H not observed.



Compound 28.

Step 1: Step one was done following a literature procedure affording **int-1-28**.⁴²

Step 2: A dry round bottom flask was charged with 2,3,5,6-tetrafluoro-4-(trifluoromethyl)aniline (0.52 mL, 3.7 mmol, 1 equiv) and toluene (14 mL). To this solution, **int-1-28** (1 g, 3.7 mmol, 1 equiv) was added. The flask was fitted with a reflux condenser topped with a drying tube that was packed with K_2CO_3 (5 g). The reaction was heated to an external temperature of $140\text{ }^\circ\text{C}$. After 18 h, the reaction mixture was cooled to room temperature and concentrated via rotary evaporation. The solid residue was recrystallized from hot hexanes to give **int-2-28** as a white solid in 83% yield.

^1H NMR (CDCl_3 , 400 MHz) δ 8.09 (s, 1H), 2.21 (m, 4H), 1.87–1.66 (multiple peaks, 5H), 1.40 (m, 1H).

^{19}F NMR (CDCl_3 , 376 MHz) δ -56.12 (t, $J = 21.8$ Hz, 3F), -140.51 (m, 2F), -143.05 (m, 2F).

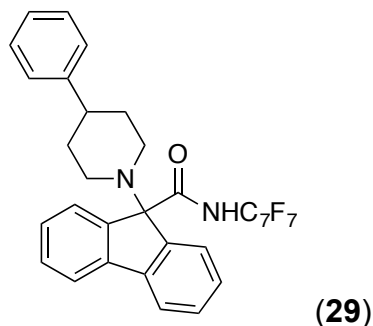
HRMS ESI⁺ $[\text{M}+\text{H}]^+$ calcd for $\text{C}_{14}\text{H}_{11}\text{BrF}_7\text{NO}$: 421.9985; found 421.9979.

Step 3: Inside a N_2 glovebox, a 20-mL vial was charged with **int-2-28** (0.45 g, 1.07 mmol, 1 equiv), K_2CO_3 (0.15 g, 1.07 mmol, 1 equiv), AgBF_4 (0.21 g, 1.07 mmol, 1 equiv) and acetonitrile (9 mL). To this solution, piperidine (0.4 mL, 4.1 mmol, 3.8 equiv) was added. The reaction was stirred at room temperature outside of the glovebox. After 18 hours, the mixture was filtered through celite and the volatiles were removed under

vacuum. The residue was purified via column chromatography (0% to 10% THF in hexanes) to afford product **28** in 53% yield.

^1H NMR (CDCl_3 , 400 MHz) δ 2.57 (m, 4H), 1.99–1.39 (m, 15H), 1.15 (m, 1H). Note: N–H not observed.

^{19}F NMR (CDCl_3 , 376 MHz) δ –55.96 (t, J = 21.7 Hz, 3F), –141.41 (m, 2H), –144.28 (m, 2H)



NOTE: Aminal formation was not observed. This substrate was isolated following **Isolation Procedure A** of the **Standard Conditions for C-H Arylation of Alicyclic Amines**. Purification via column chromatography (0% to 10% THF in hexanes).

Isolated yield using standard conditions B: 30% yield

^1H NMR (CDCl_3 , 500 MHz) δ 9.73 (br s, 1H), 7.73 (d, J = 7.6 Hz, 2H), 7.59 (d, J = 7.6 Hz, 2H), 7.46 (app. t, J = 7.4 Hz, 2H), 7.38–7.28 (multiple peaks, 4H), 7.21 (m, 3H), 3.06 (d, J = 11.4 Hz, 2H), 2.50 (tt, J = 11.8, 4.1 Hz, 1H), 2.35 (app. t, J = 11.0 Hz, 2H), 1.94–1.77 (multiple peaks, 4H).

^{19}F NMR (CDCl_3 , 471 MHz) δ –56.03 (t, J = 21.6 Hz, 3F), –140.81 (m, 2F), –143.45 (m, 2F).

4.5 References

(1) This chapter is adapted with permission from: Topczewski, J. T., Cabrera, P. J., Saper, N. I.; Sanford, M. S. *Nature* **2016**, 531, 220.

(2) Taylor, R. D.; MacCoss, M.; Lawson, A. D. G. *J. Med. Chem.* **2014**, 57, 5845.

(3) Vitaku, E.; Smith, D. T.; Njardarson, J. T. *J. Med. Chem.* **2014**, 57, 10257.

- (4) (a) Wang, C.-L.; Wuonola, M. A. *Org. Prep. Proc. Int.* **1992**, *24*, 583. (b) Weintraub, P. M.; Sabol, J. S.; Kane, J. M.; Borchering, D. R. *Tetrahedron* **2003**, *58*, 2953. (c) Buffat, M. G. P. *Tetrahedron* **2004**, *60*, 1701. (d) Duttwyler, S.; Chen, S.; Takase, M. K.; Wiberg, K. B.; Bergman, R. G.; Ellman, J. A. *Science* **2013**, *339*, 678.
- (5) (a) Christensen, J. A.; Squires, R. F. (Ferrosan A/S, Denmark). 4-Phenylpiperidine Compounds. U.S. Patent 3,912,743. (b) Christensen, J. A.; Squires, R. F. (Ferrosan A/S, Denmark). 4-Phenylpiperidine Compounds. U.S. Patent 4,007,196. (c) Mathis, C. A.; Gerdes, J. M.; Enas, J. D.; Whitney, J. M.; Taylor, S. E.; Zhang, Y.; McKenna, D. J.; Havlik, S.; Peroutka, S. J. *J. Pharm. Pharmacol.* **1992**, *44*, 801.
- (6) Cernak, T.; Dykstra, K. D.; Tyagarajan, S.; Vachal, P.; Krska, S. W. *Chem. Soc. Rev.* **2016**, *45*, 546.
- (7) Mitchell, E. A.; Peschiulli, A.; Lefevre, N.; Meerpoel, L.; Maes, B. U. W. *Chem. Eur. J.* **2012**, *18*, 10092.
- (8) (a) Davies, H. M. L.; Antoulinakis, E. G. *J. Organomet. Chem.* **2001**, *617-618*, 47. (b) Davies, H. M. L.; Venkataramani, C.; Hansen, T.; Hopper, D. W. *J. Am. Chem. Soc.* **2003**, *125*, 6462.
- (9) (a) Shaw, M. H.; Shurtleff, V. W.; Terrett, J. A.; Cuthbertson, J. D.; MacMillan, D. W. C. *Science* **2016**, *352*, 1304. (b) Shi, L.; Xia, W. *Chem. Soc. Rev.* **2012**, *41*, 7687.
- (10) Campos, K. R.; Klapars, A.; Waldman, J. H.; Dormer, P. G.; Chen, C.-Y. *J. Am. Chem. Soc.* **2006**, *128*, 3538.
- (11) (a) Spangler, J. E.; Kobayashi, Y.; Verma, P.; Wang, D.-H.; Yu, J.-Q. *J. Am. Chem. Soc.* **2015**, *137*, 11876. (b) Pastine, S. J.; Gribkov, D. V.; Sames, D. *J. Am. Chem. Soc.* **2006**, *128*, 14220.
- (12) Asensio, G.; *et al.* *J. Am. Chem. Soc.* **1993**, *115*, 7250.
- (13) (a) Affron, D. P.; Davis, O. A.; Bull, J. A. *Org. Lett.* **2014**, *16*, 4956. (b) Ye, S.; Yang, W.; Coon, T.; Fanning, D.; Neubert, T.; Stamos, D.; Yu, J.-Q. *Chem. Eur. J.* **2016**, *22*, 4748.
- (14) (a) Ryabov, A. D.; Sakodinskaya, I. K.; Dvoryantsev, S. N.; Eliseev, A. V.; Yatsimirsky, A. K. *Tetrahedron Lett.* **1986**, *27*, 2169. (b) Tsuji, J. *Acc. Chem. Res.* **1969**, *2*, 144. (c) Vicente, J.; Saura-Llamas, I.; Garcia-Lopez, J.-A. *Organometallics*, **2010**, *29*, 4320.
- (15) (a) Orito, K.; Horibata, A.; Nakamura, T.; Ushito, H.; Nagasaki, H.; Yuguchi, M.; Yamashita, S.; Tokuda, M. *J. Am. Chem. Soc.*, **2004**, *126*, 14342. (b) Cai, G.; Fu, Y.; Li, Y.; Wan, X.; Shi, Z. *J. Am. Chem. Soc.*, **2007**, *129*, 7666.
- (16) (a) McNally, A.; Haffemayer, B.; Collins, B. S. L.; Gaunt, M. J. *Nature* **2014**, *510*, 129. (b) Smalley, A. P.; Gaunt, M. J. *J. Am. Chem. Soc.* **2015**, *137*, 10632. (c) He, C.; Gaunt, M. J. *Angew. Chem. Int. Ed.* **2015**, *54*, 15840. (d) Calleja, J.; Pla, D.; Gorman, T. W.; Domingo, V.; Haffemayer, B.; Gaunt, M. J. *Nat. Chem.* **2015**, *7*, 1009.
- (17) Bercaw, J. E.; Day, M. W.; Golisz, S. R.; Hazari, N.; Henling, L. M.; Labinger, J. A.; Schofer, S. J.; Virgil, S. *Organometallics* **2009**, *28*, 5017.
- (18) Ryabov, A. D.; Sakodinskaya, I. K.; Yatsimirsky, A. K. *J. Chem. Soc., Dalton Trans.* **1985**, 2629.
- (19) Legacy, C. J.; Wang, A.; O'Day, B. J.; Emmert, M. H. *Angew. Chem. Int. Ed.* **2015**, *54*, 14907.
- (20) Muci, A.R.; Buchwald, S.L. *Top. Curr. Chem.* **2002**, *219*, 131.
- (21) Anet, F. A. L.; Yavari, I. *J. Am. Chem. Soc.*, **1977**, *99*, 2794.

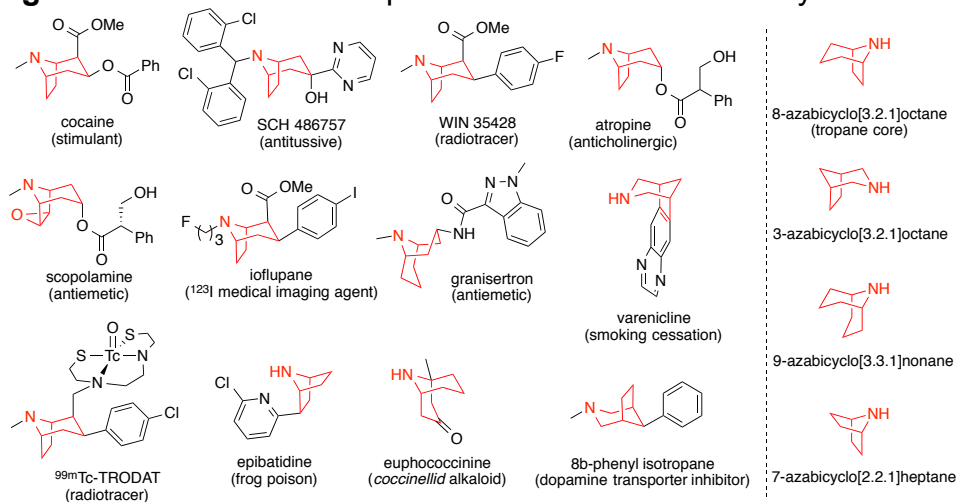
- (22) Shabashov, D.; Daugulis, O. *Org. Lett.*, **2005**, *7*, 3657.
- (23) Gigant, N.; Chausset-Boissarie, L.; Gillaizeau, I. *Org. Lett.* **2013**, *15*, 816.
- (24) Shabashov, D.; Daugulis, O. *J. Am. Chem. Soc.*, **2010**, *132*, 3965.
- (25) Lyons, T. W.; Sanford, M. S. *Chem. Rev.* **2010**, *110*, 1147.
- (26) Desai, L. V.; Hull, K. L.; Sanford, M. S. *J. Am. Chem. Soc.* **2004**, *126*, 9542.
- (27) (a) Wasa, M.; Engle, K. M.; Yu, J.-Q. *J. Am. Chem. Soc.* **2009**, *131*, 9886. (b) He, J.; Li, S.; Deng, Y.; Fu, H.; Laforteza, B. N.; Spangler, J. E.; Homs, A.; Yu, J.-Q. *Science* **2014**, *343*, 1216.
- (28) Cheong, C. L.; Wakefield, B. J. *J. Chem. Soc., Perkin Transactions 1: Organic and Bio-Organic Chemistry*, **1988**, *12*, 3301.
- (29) Zaitsev, V. G., Shabashov, D. & Daugulis, O. *J. Am. Chem. Soc.* **2005**, *127*, 13154.
- (30) Zhu, R.-Y.; He, J.; Wang, X.-C.; Yu, J.-Q. *J. Am. Chem. Soc.* **2014**, *136*, 13194.
- (31) Giri, R., Chen, X. & Yu, J.-Q. *Angew. Chem. Int. Ed.* **2005**, *44*, 2112.
- (32) (a) Lee, J.B.; Parkin, C.; Shaw, M.J. *Tetrahedron*, **1973**, *29*, 751. (b) Hampson, N. A.; Lee, J.B.; Morley, J. R.; Scanlon, B. *Canad. J. Chem.* **1969**, *47*, 3729.
- (33) (a) Nadres, E. T., Santos, G. I. F., Shabashov, S. & Daugulis, O. *J. Org. Chem.* **2013**, *78*, 9689. (b) Lafrance, M. & Fagnou, K. *J. Am. Chem. Soc.* **2006**, *128*, 16496.
- (34) Juaristi, E. *Conformational Behavior of Six-Membered Rings: Analysis, Dynamics, and Stereoelectronic Effects*; 1st ed.; Wiley-VCH; **1995**.
- (35) (a) Lafrance, M.; Fagnou, K. *J. Am. Chem. Soc.* **2006**, *128*, 16496. (b) Lafrance, M.; Gorelsky, S. I.; Fagnou, K. *J. Am. Chem. Soc.* **2007**, *129*, 14570.
- (36) (a) Beke, D.; Toke, L. *Chemische Berichte*, **1962**, *95*, 2122. (b) Solovjova, J.; Martynaitis, V.; Holzer, W.; Mangelinckx, S.; Kimpe, N. D.; Šačkus, A. *ARKIVOC*, **2009**, *6*, 48.
- (37) Honda, T.; Ishikawa, F. *Chem. Comm.* **1999**, *12*, 1065.
- (38) Vitaku, E.; Smith, D. T.; Njardarson, J. T. *J. Med. Chem.*, **2014**, *57*, 10257.
- (39) (a) Casey, C. P.; Whiteker, G. T. *Isr. J. Chem.* **1990**, *30*, 299. (b) Kamer, P. C. J.; van-Leeuwen, P. W. N. M.; Reek, J. N. H. *Acc. Chem. Res.*, **2001**, *34*, 895.
- (40) Jung, M. E.; Piizi, G. *Chem. Rev.*, **2005**, *105*, 1735.
- (41) Jones, W. D.; Feher, F. *Acc. Chem. Res.* **1989**, *22*, 91.
- (42) Richmond, E.; Duguet, N.; Slawin, A. M. Z.; Lébl, T.; Smith, A. D. *Org. Lett.* **2012**, *14*, 2762.

Chapter 5. Ligand Effects on the Pd-Catalyzed Transannular C–H Functionalization of Azabicycloalkanes

5.1 Introduction

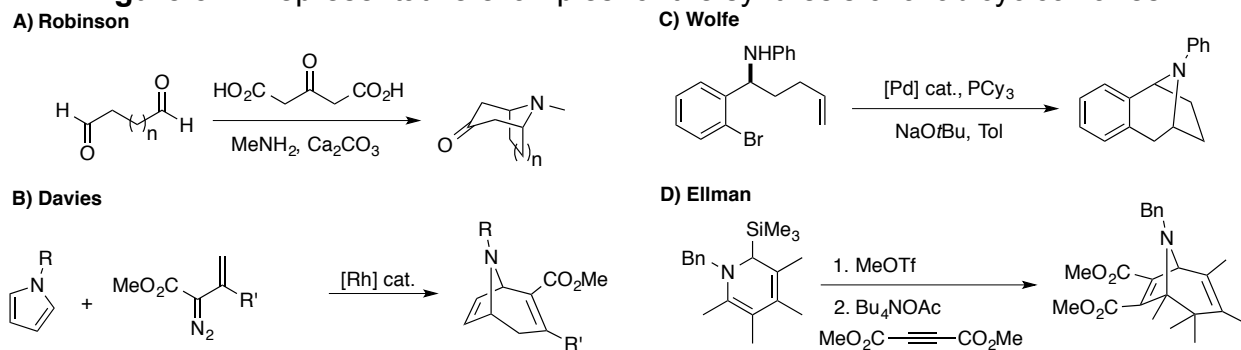
Naturally occurring alkaloids have long inspired the development of pharmaceutical agents with 59% of U.S. FDA approved drugs containing a nitrogen heterocycle.¹ Bicyclic alkaloids are especially notable and are featured in several biologically active molecules (Figure 5.1). For example, 8-azabicyclo[3.2.1]octane (tropane) is the second most prevalent bicyclic nitrogen heterocycle among U.S. FDA approved drugs.¹ The tropane core is present in several bioactive natural products such as cocaine (stimulant), atropine (anticholinergic), and scopolamine (antiemetic; Figure 5.1).^{1,2} Furthermore, other azabicycloalkanes with the [3.2.1]-, [3.3.1]- and [2.2.1]-bridged systems appear in several natural products (epibatidine, euphococcinine) and pharmaceutical agents (varenicline, granisertron; Figure 5.1).

Figure 5.1. Relevance of representative bioactive azabicycloalkanes.



Despite this pervasiveness, the synthesis and derivatization of bicyclic alkaloids rely on the use of *de novo* synthetic routes to construct the bridged bicyclic core.³ For example, Robinson's double Mannich reaction allows for a one-pot synthesis of tropinone but with limited functional group tolerance (Figure 5.2 A).⁴ This strategy has also been employed to synthesize several bicyclic systems with bridgehead-carbons adjacent to the nitrogen atom. Metal-catalyzed strategies have been used to construct highly functionalized bicyclic amines (Figure 5.2 B-C). For example, Professor Huw Davies at Emory University developed the synthesis of functionalized [3.2.1]-bridged frameworks via a Rh-catalyzed tandem cyclopropanation/Cope rearrangement strategy between vinyldiazoacetates and pyrroles (Figure 5.2 B).⁵ Additionally, a Pd-catalyzed alkene carboamination strategy has been explored for the intramolecular synthesis of benzo-tropanes by Professor John Wolfe at University of Michigan (Figure 5.2 C).⁶ Furthermore, Professor Jonathan A. Ellman at Yale University reported on a [3+2] cycloaddition of unstabilized azomethine ylides and alkynes to provide functionalized tropane structures (Figure 5.2 D).⁷

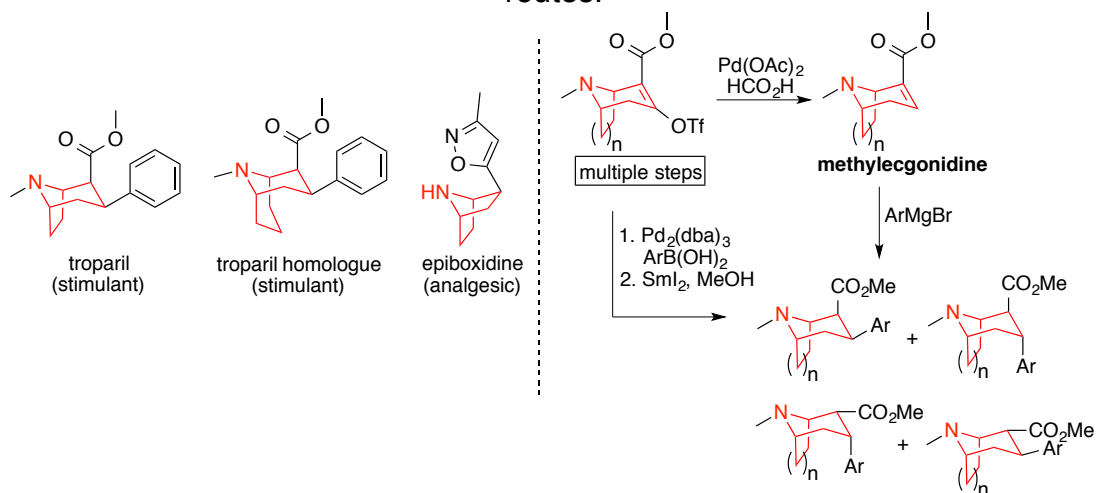
Figure 5.2. Representative examples for the synthesis of azabicycloalkanes.



One important subclass of azabicycloalkanes contains an aromatic functional group on the core structure (Figure 5.3, left). These arylated azabicycloalkanes are known for their potent pharmacological properties related to central nervous system cognitive, anticholinergic and motor activities.^{3a,8} Furthermore, several aryltropanes have been synthesized to understand the biochemical mechanisms associated with cocaine effects in order to design and develop novel pharmacotherapies for cocaine addiction.⁹ Structure-activity-relationship (SAR) studies revealed that the nature of the

aryl group has a strong correlation to the binding affinity and transporter selectivity on these molecules making the rapid synthesis and development of these arylated derivatives critically important. Common synthetic routes for aryl azabicycloalkanes require multi-step synthetic sequences and many of them employ methylecgonidine derivatives as reactive intermediates to afford racemic *cis/trans*-isomeric mixtures of aryltropanes (Figure 5.3, right).^{8a} Although these methods allow access to valuable bicyclic cores (*vide supra*), all of them represent an iterative and resource-intensive strategy to prepare functionalized azabicycles.

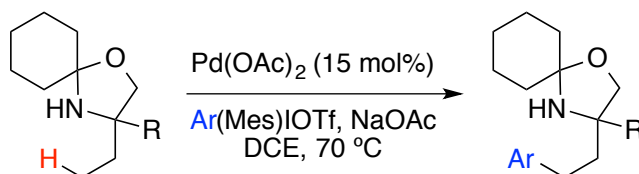
Figure 5.3. Representative examples of arylated azabicycloalkanes and synthetic routes.



A complementary and more efficient approach is the direct C–H functionalization of the azabicyclic core. Although, C–H functionalization has become an increasingly relevant synthetic strategy for the rapid derivatization of organic molecules¹⁰, methods to C–H functionalize azabicyclic systems are currently limited¹¹ with most methods involving the functionalization of $\text{C}(\text{sp}^2)\text{--H}$ sites or tandem deprotonation/functionalization of acidic $\text{C}(\text{sp}^3)\text{--H}$ sites.^{12, 13, 14, 15} Additionally, C–H functionalization strategies have been employed to construct azabicyclic cores.¹⁶ However, metal catalyzed methods for the direct C–H functionalization of tropane and related bicyclic alkaloids are rare (see Chapter 4).¹⁷

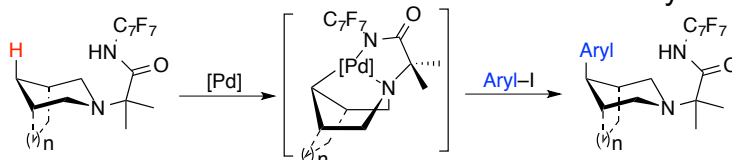
Recently, the use of sp^3 -nitrogen atoms as directing groups to transition metals has enabled the site-selective $C(sp^3)\text{--}H$ functionalization of aliphatic amines. Professor Matthew Gaunt at the University of Cambridge employed this strategy for the $C\text{--}H$ functionalization of pendant alkyl chains in nitrogen heterocycles (Figure 5.4).¹⁸

Figure 5.4. Gaunt's $C\text{--}H$ arylation of alkylamines.^{18b}
Gaunt



We have also reported on the remote $C\text{--}H$ functionalization of aliphatic cyclic amines (alicyclic amines, Figure 5.5).¹⁷ Our transannular $C\text{--}H$ functionalization protocol leverages the strongly coordinating ability of the nitrogen atom of alicyclic amines to guide the Pd-catalyst to distal $C\text{--}H$ bonds from the boat conformer (Figure 5.5).¹⁷ Using this strategy, a variety of alicyclic amines were functionalized affording arylated products with added molecular complexity (full details in chapter 4). However, the reaction conditions for most azabicycles (other than 3-azabicyclo[3.1.0]hexane) afforded modest yields of arylated products (25–60%) with remaining starting material. Furthermore, bioactive scaffolds such as tropane and related azabicycloalkanes with substituents adjacent to the nitrogen-atom led to trace arylated products and poor mass balance.

Figure 5.5. Transannular $C\text{--}H$ functionalization of alicyclic amines.



Given the importance of functionalized bicyclic aliphatic amines, we sought to advance the transannular $C\text{--}H$ activation strategy through a combination of reaction optimizations and mechanistic studies to enable the functionalization of diverse

bioactive azabicycloalkanes. We envisioned utilizing ligand additives to improve reactivity. Ligands in Pd(II)-catalyzed C–H functionalization reactions are known to modulate the catalyst reactivity to enhance site-, stereo- and chemo-selectivity.¹⁹ Additives, such as pyridines or quinolines, in Pd catalysis have enabled the development of new C–H functionalization reactions by 1) lowering activation barriers,^{20,21} or 2) preventing catalyst decomposition^{18c,22} or inhibition.^{23,24} As a result, we hypothesized that identification of suitable ligands could allow for the expansion of our method to the C–H functionalization of challenging azabicycloalkanes.

This chapter describes the use of 2-picolinic acid or 2-quinaldic acid for the transannular Pd-catalyzed C–H activation of aliphatic azabicycles. We demonstrate that the addition of these ligands can dramatically increase the yields of remotely functionalized azabicyclic products. Furthermore, a combination of kinetic experiments (initial rates, KIEs, catalyst inhibition and recovery studies) suggests that the role of the ligand is to recover deactivated Pd species. Finally, the use of these ligand additives enable the C–H functionalization of tropane and related azabicycloalkaloids.

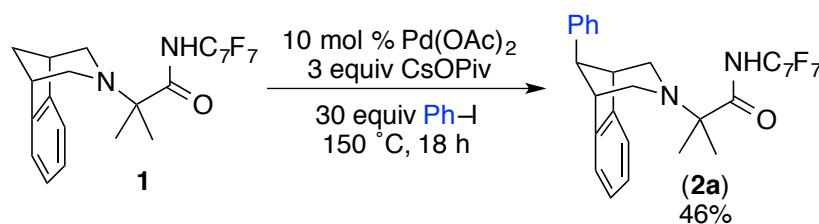
The work described in this chapter has been done in collaboration with my colleague Melissa Lee.

5.2 Results and Discussion

Ligand identification

Initial studies focused on utilizing a model bicyclic system with modest reactivity to identify ligand-induced reactivity trends. We began our investigation using the benzo-fused 3-azabicyclo[3.2.1]octane substrate (**1**). Under our previously reported reaction conditions this substrate afforded 46% yield of the C4-arylated product **2a** (Figure 5.6 and Chapter 4).¹⁷ This important bicyclic core (**1**) is present in several bioactive molecules such as varenicline (Pfizer's smoking cessation drug) and other isotropane alkaloids²⁵ (Figure 5.1). Therefore, **1** provides an opportunity for significant yield improvement via the use of ligands.

Figure 5.6. Ligand-less reactivity of benzo-isotropane substrate **1**.

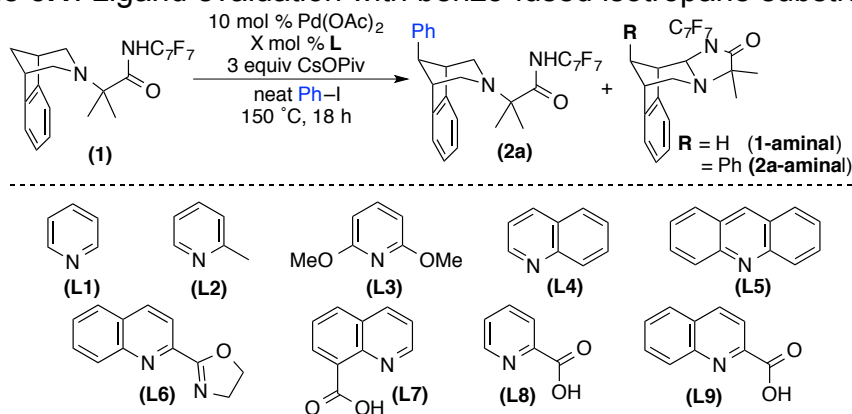


As shown in Table 5.1, we explored a series of pyridine-based ligands based on their use in related Pd-catalyzed C–H activation reactions.^{18c,19-26} We first investigated pyridine ligands with varied steric bulk around the nitrogen (**L1-L3**). Addition of these monodentate ligands to the reaction afforded yields similar to the ligandless reaction (43-47% yield, entries 3-4 versus entry 1). Similarly, bulky π -systems such as quinoline (**L4**) and acridine (**L5**) led to no improvements in yield (40% and 46%, respectively, entries 5-6). Additionally, ligands **L1-L5** did not change the conversion of **1** leaving approximately 25% of unaccounted mass balance (entries 2-6). Importantly, the conversion of starting material does not account for aminor byproduct (**1-aminal**); however, **1-aminal** formation was negligible across ligands (< 4%). Overall, the use of monodentate pyridine ligands at 5 mol % loading resulted in minimal change to the reaction outcome for **1**. This result suggested that monodentate ligands might be too labile to coordinate the Pd center in the presence of the strongly coordinating bidentate substrate **1**.

Based on these results, we next explored bidentate ligands that could more strongly coordinate to the Pd catalyst. Gratifyingly, the addition of bidentate ligands (**L6-L9**) resulted in an increase in reactivity. The quinolinyl-oxazoline ligand (**L6**) demonstrated slight improvement in yield of **2a** compared to the reaction in the absence of ligand (56% versus 46%, respectively; entry 7 versus entry 1). Furthermore, the use of X,L-type ligands bearing an anionic carboxylate group, recently used in Pd C–H activation,²⁷ led to a favorable increase in reactivity. The addition of ligand **L7** increased the yield of the C–H arylated product **2a** to 68% with 96% conversion (entry 8), indicating that the ligand shut down the undesired side reactions. Further evaluation revealed that 2-picolinic acid (**L8**) and 2-quinaldic acid (**L9**) afforded high yields of **2a** in 80% and 77%, respectively (entries 9 and 12). Evaluation of the ligand loading showed

that beyond 20 mol % of picolinic acid the reaction was drastically inhibited with only 26% conversion of starting substrate **1** (entry 11). In contrast, addition of varying amounts of quinaldic acid had minimal impact on the yield (77-85%, entries 12-14) and conversion of **1** (> 99%). Furthermore, **2a** was isolated in 82% yield with addition of 20 mol % of quinaldic acid, which represents an almost 2-fold yield improvement from the ligandless reaction (entry 14).

Table 5.1. Ligand evaluation with benzo-fused isotropane substrate **1**.



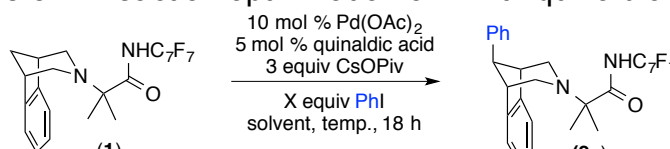
Entry	L	L (mol%)	Yield 2a ^a	Conversion ^b
1	---	---	46%	68%
2	L1	5	44%	68%
3	L2	5	47%	73%
4	L3	5	43%	68%
5	L4	5	40%	68%
6	L5	5	46%	75%
7	L6	5	56%	80%
8	L7	5	68%	96%
9	L8	5	80%	> 99%
10	L8	10	78%	> 99%
11	L8	20	24%	26%
12	L9	5	77%	> 99%
13	L9	10	77%	> 99%
14	L9	20	85% (82% ^c)	> 99%

^a Conditions: **1** (0.03 mmol, 1 equiv), Pd(OAc)₂ (10 mol %), ligand **L** (5 - 20 mol %) CsOPiv (3 equiv), PhI (30 equiv), 150 °C. Calibrated GC yields are a sum of products **2a** and **2a-aminal**. ^b For entries 1-7, **1-aminal** detected below < 4%; entries 8-14 **1-aminal** not detected. ^c Isolated yield of **2a** (0.3 mmol scale).

We continued the reaction optimization with quinaldic acid (5 mol %). Table 5.2 shows that the reaction could be performed at lower temperatures and in the presence of solvent while maintaining good yield of **2a** (entries 2-10). Optimal conditions were found at 100 °C with 3 equiv of PhI in *tert*-amyl alcohol, which generated 84% yield of

2a and 95% conversion of **1** (entry 8). Similarly, replacement of ligand with picolinic acid (5 mol %) afforded 85% yield of **2a** (entry 9). Notably, the reaction in the absence of ligand only afforded 29% yield of **2a** (entry 10), which highlights the importance of the ligand to the reaction.

Table 5.2. Reaction optimization of **1** with quinaldic acid.^a



Entry	Temp.	Solvent	Ph-I (equiv)	Yield 2a	Conversion
1	150 °C	neat	30	77%	> 99%
2	120 °C	neat	30	60%	74%
3	120 °C	<i>t</i> AmylOH	30	87%	> 99%
4	120 °C	<i>t</i> AmylOH	15	85%	> 99%
5	120 °C	<i>t</i> AmylOH	3	87%	> 99%
6	120 °C	<i>t</i> AmylOH	1	79%	95%
7	110 °C	<i>t</i> AmylOH	3	86%	> 98%
8	100 °C	<i>t</i> AmylOH	3	84%	95%
9 ^b	100 °C	<i>t</i> AmylOH	3	85%	96%
10 ^c	100 °C	<i>t</i> AmylOH	3	29%	42%

^a Conditions: **1** (0.03 mmol, 1 equiv), Pd(OAc)₂ (10 mol %), quinaldic acid (5 mol %), CsOPiv (3 equiv), PhI (1-30 equiv), 100-150 °C. Calibrated GC yields for **2a**. ^b Ligand: picolinic acid (5 mol %). ^c No ligand additive.

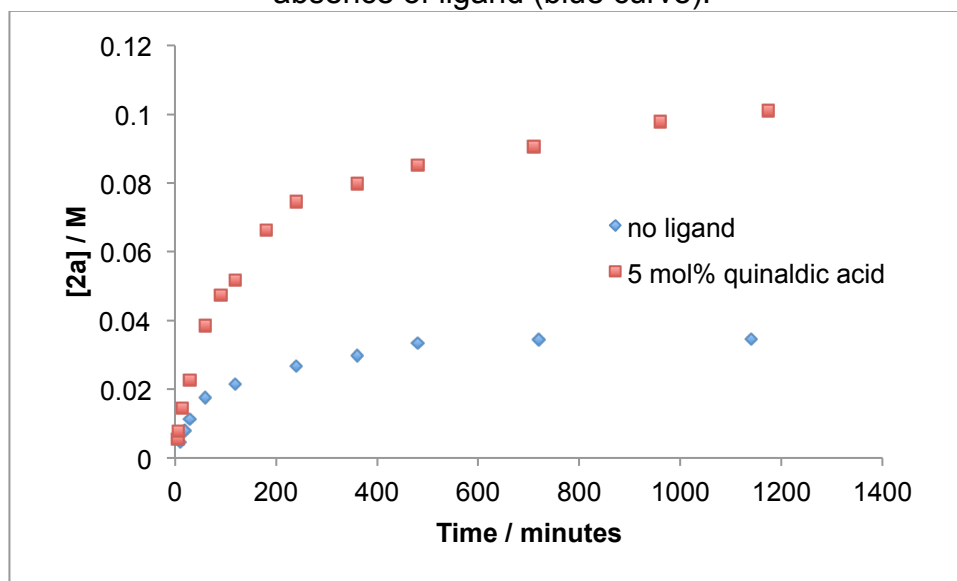
Reaction Rate Profile

Ligands in other Pd catalyzed C–H activation reactions have enabled the development of challenging transformations by enhancing catalyst activity (i.e. lowering activation barrier) or preventing catalyst deactivation or product inhibition pathways.¹⁹ Given the positive results with these pyridinecarboxylate ligands we decided to investigate the role of the ligand in the reaction.²⁷

We began our investigation by assessing the reaction rate profile of **1** with and without ligand (Figure 5.7). The reaction progress was monitored via gas chromatography (GC) by measuring the concentration of starting material (**1**) and product (**2a**) over time. Each time-point represents an independent vial reaction. As shown in Figure 5.7, the concentration of **2a** versus time plots show that both reactions (with and without ligand) start with comparably fast initial rates. However, the reaction in the absence of ligand plateaus after 60 minutes and completely stalls after 480 minutes

(8 hours) to a maximum concentration of 0.035 M **2a** (blue curve). In contrast, the reaction with quinaldic acid after 60 minutes has reached a product concentration of 0.039 M, which is a 2.2-fold increase in [**2a**] from the ligandless reaction (0.018 M). The quinaldic acid reaction continues to produce product and finally plateaus to a concentration of ~ 0.1 M.

Figure 5.7. Rate profile of **2a** in the presence of 5 mol% quinaldic acid (red curve) and absence of ligand (blue curve).



Conditions red curve: **1** (0.03 mmol, 1 equiv, 0.12 M), Pd(OAc)₂ (0.012 M), CsOPiv (0.36 M), PhI (0.36 M), quinaldic acid (0.006 M), 0.25 mL *t*AmylOH, 100 °C. Conditions blue curve: **1** (0.03 mmol, 1 equiv, 0.12 M), Pd(OAc)₂ (0.012 M), CsOPiv (0.36 M), PhI (0.36 M), 0.25 mL *t*AmylOH, 100 °C.

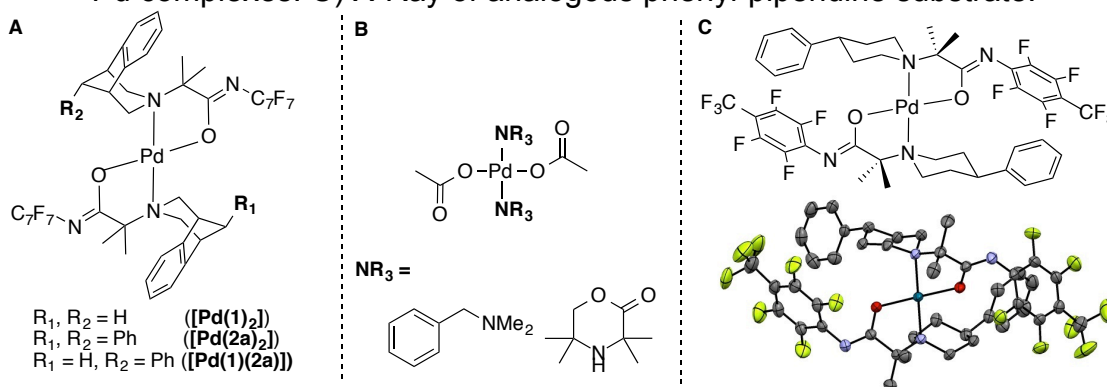
Analysis of the ligandless reaction profile suggests that product formation might inhibit Pd-catalyst turnover (product inhibition). The increase in product concentration over time could be preventing the coordination of substrate **1** to the Pd-catalyst, thus leading to the observed low yield of **2a**. It seems plausible that the role of the ligand is to serve as a transient coordinating group to promote catalyst turnover and prevent product inhibition.²⁴

Catalyst Inhibition Studies

Previous reports suggest that a vacant coordination site at the Pd center is required for C–H bond cleavage to occur.^{26a,28,29} Due to the bidentate coordination of

the substrate and product, we hypothesized that formation of square planar off-cycle $[\text{Pd}(\mathbf{1})_2]$, $[\text{Pd}(\mathbf{2a})_2]$ or $[\text{Pd}(\mathbf{1})(\mathbf{2a})]$ complexes in solution could be leading to product/substrate inhibition (Figure 5.8 A). Analogous structures have been observed when strongly coordinating sp^3 -amines bind to Pd(II) centers (Figure 5.8 B).^{29,30}

Figure 5.8. A) Plausible off-cycle Pd species. B) Literature sp^3 -hybridized amine bound Pd complexes. C) X-Ray of analogous phenyl-piperidine substrate.

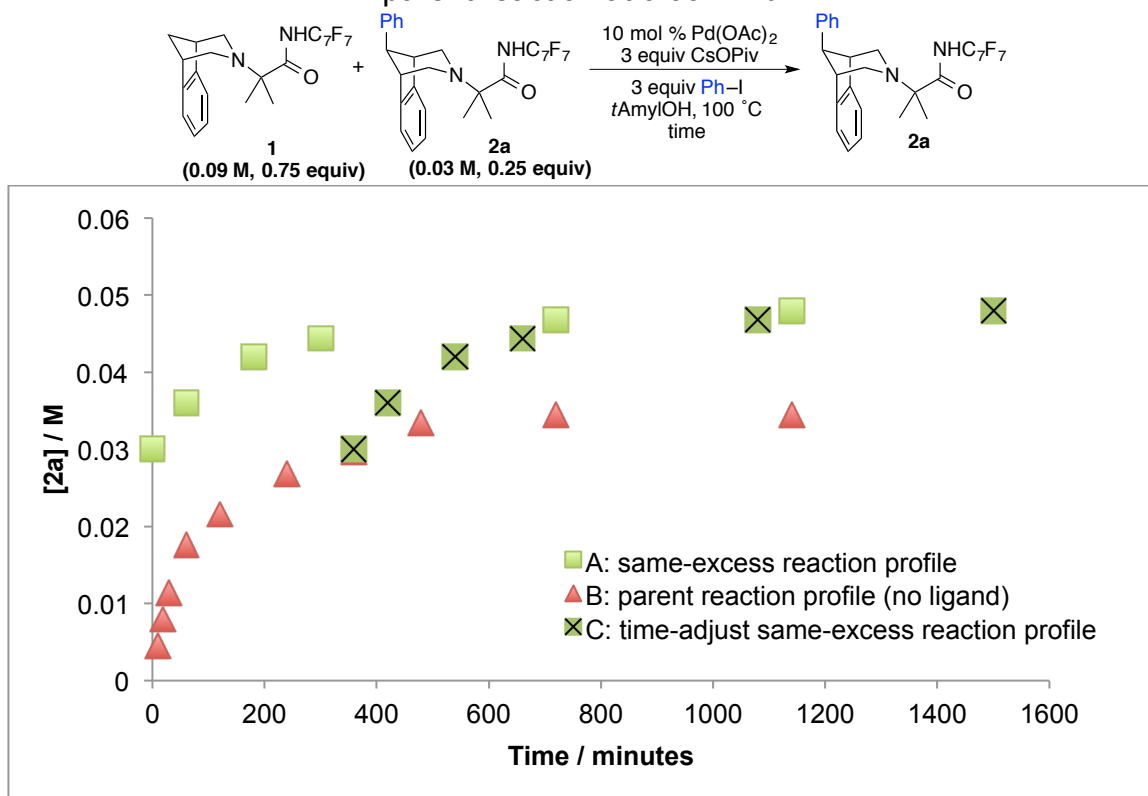


Attempts to observe or isolate these Pd species with **1** or **2a** were difficult as complex mixtures were obtained, presumably due to the formation of monomeric and dimeric Pd species. However, an analogous solid-state crystal structure of two arylated piperidine molecules bound to palladium suggests that these off-cycle species could form in solution (Figure 5.8 C).

To investigate the possibility of product inhibition, we employed the same-excess protocol by Donna Blackmond at The Scripps Research Institute.³¹ This experiment allows access to different starting points of a reaction by adjusting the concentrations of reactants and product. We proceeded to conduct the same-excess reaction profile with added 0.03 M of **2a** at the reaction onset (reaction conditions equivalent to 25% yield of **2a** and 75% conversion of **1**, Figure 5.9 curve A).³² We reasoned that if product is inhibiting the catalyst and no other catalyst deactivation paths are operating, we should expect little to no product forming during the course of the reaction (as observed in the parent reaction profile Figure 5.9 curve B). As shown in Figure 5.9 curve A, we observed that product proceeds to form in the first 3 hours (180 minutes) and plateaus to a concentration of 0.048 M (40% yield of **2a**) after 19 hours. This is in stark contrast to the observed reactivity of the parent reaction (curve B).

Employing the time-adjustment protocol,²⁴ the same-excess reaction profile can be time-shifted to match concentration profile of the parent reaction at the time point where [2a] is ~ 0.03M (360 minutes, Figure 5.9 curve C). The frame-shifted curve from the same-excess product-added reaction profile shows a visualization of the significant rate difference between curves. The lack of overlay cannot fully rule out product inhibition, but it does indicate that other catalyst deactivation pathways are operating.

Figure 5.9. Curve A: same-excess product-added reaction profile. Curve B: Ligand-less C–H arylation of **1** (parent reaction profile). Curve C: Time-shifted curve A to match parent reaction at 0.03 M **2a**.



Conditions curve A: **1** (0.0225 mmol, 0.75 equiv, 0.09 M), **2a** (0.0075 mmol, 0.25 equiv, 0.03 M) Pd(OAc)₂ (0.012 M), CsOPiv (0.36 M), PhI (0.36 M), 0.25 mL *t*AmylOH, 100 °C. Conditions curve B: **1** (0.03 mmol, 1 equiv, 0.12 M), Pd(OAc)₂ (0.012 M), CsOPiv (0.36 M), PhI (0.36 M), 0.25 mL *t*AmylOH, 100 °C.

To probe product inhibition, we added varying amounts of product to the reaction onset. This method has been previously used to demonstrate product inhibition in related Pd catalyzed C–H activation reactions.²³ If product hampers reactivity, we expect that the excess product would impact the catalyst's reactivity by competing with starting material **1** to coordinate to the Pd center. This in turn would change the reaction

rate and **[2a]** over the course of the reaction and we would expect to see drastic differences in the yield of **2a** as a function of product loading.

We chose to add varying amounts of the anisole derived product **2b** to accurately determine product formation solely from iodobenzene in the reaction. Addition of different amounts of **2b** from 0.012 M to 0.09 M to the ligandless reaction shows that all reactions provided the same amount of product **2a** after 45 minutes (Table 5.3, column 4). Furthermore, experiments in the presence of quinaldic acid also resulted in similar yield of **2a** irrespective of product loading (Table 5.3, column 5). This result provides evidence that 1) product is not interacting with the active catalyst to inhibit turnover and 2) the ligand is not preventing product from deactivating the Pd-catalyst.

Table 5.3. Addition of **2b** to the C–H arylation of **1**.

Entry	[2b] (M)	2b (equiv)	Yield 2a (no ligand) ^a	Yield 2a (5 mol % QA) ^b
1	0	0	13%	28%
2	0.012	0.1	13%	29%
3	0.03	0.25	13%	30%
4	0.06	0.50	13%	28%
5	0.09	0.75	11%	28%

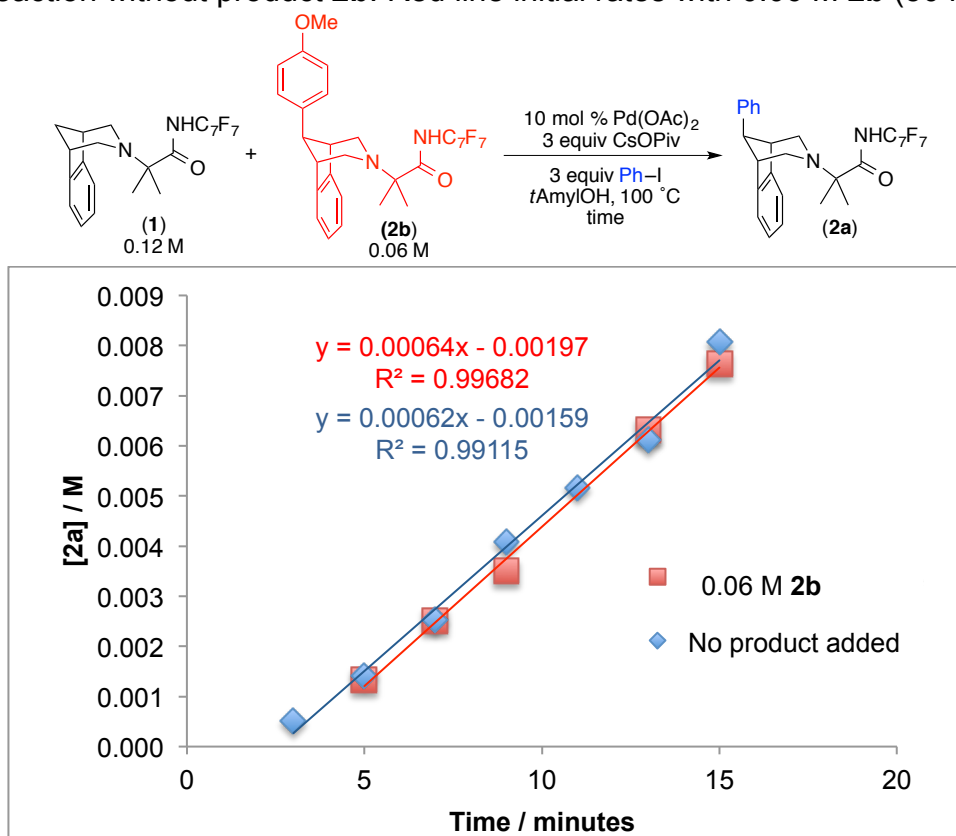
^a Conditions: **1** (0.03 mmol, 1 equiv, 0.12 M), **2b** (0, 0.012, 0.03, 0.06 or 0.09 M), Pd(OAc)₂ (0.012 M), CsOPiv (0.36 M), PhI (0.36 M), 0.25 mL *t*AmylOH, 100 °C. ^b Reaction with quinaldic acid (0.006 M).

Following our previous results with addition of excess product, we investigated initial reaction rates in the presence and absence of product. The initial rates method avoids the need to address problems associated with possible catalyst deactivation; thus, decoupling catalyst deactivation from product inhibition. If product inhibition is occurring, we hypothesized that addition of **2b** to the reaction would slow down the initial rate of the reaction in the absence of ligand. If the role of the ligand is to prevent product inhibition, addition of **2b** to the reaction in the presence of ligand should not affect the initial rate of the reaction. As shown in Figure 5.10, we conducted initial rates of the reaction with and without added product **2b** (0.06 M **2b**, 50 mol %). Plotting **[2a]**

versus time profiles of the reaction without product (blue line) and the reaction with added product (red line) shows superimposable lines. This suggests that product is not affecting the turnover of the Pd-catalyst.

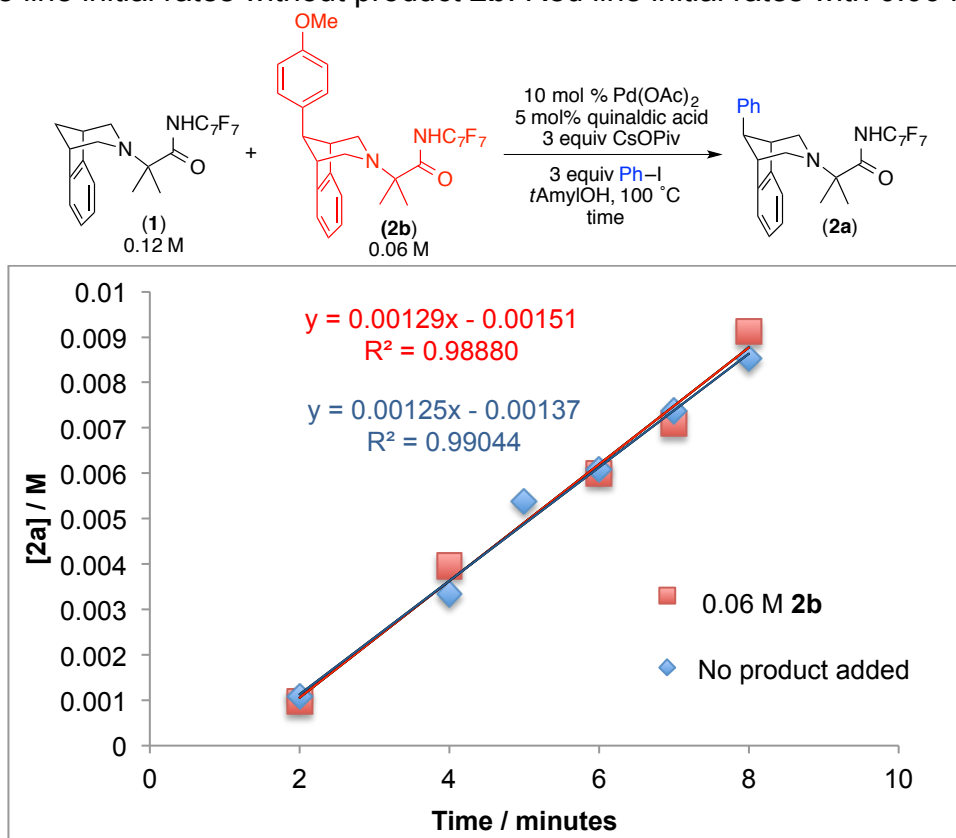
Similarly, the superimposable initial rate profiles between the quinaldic acid reactions with or without 50 mol % **2b** (Figure 5.11) indicates that ligand's role is not to prevent product inhibition. However, we noticed a 2-fold increase in rate between the quinaldic acid reaction and the ligandless reaction (compare initial rates of Figure 5.11 versus Figure 5.10). This enhanced reaction rate prompted us to further investigate the role of the ligand additive in the turnover-limiting step.²¹

Figure 5.10. Ligand-less reaction initial rates comparison of [2a] versus time plots. Blue line reaction without product **2b**. Red line initial rates with 0.06 M **2b** (50 mol %).



Conditions: **1** (0.03 mmol, 0.12 M), **2b** (0.06 M), Pd(OAc)₂ (0.012 M), CsOPiv (0.36 M), PhI (0.36 M), 0.25 mL tAmylOH, 100 °C. **2b** was not added in blue line initial rates

Figure 5.11. Ligand-added reaction initial rates comparison of [2a] versus time plots. Blue line initial rates without product **2b**. Red line initial rates with 0.06 M **2b**.



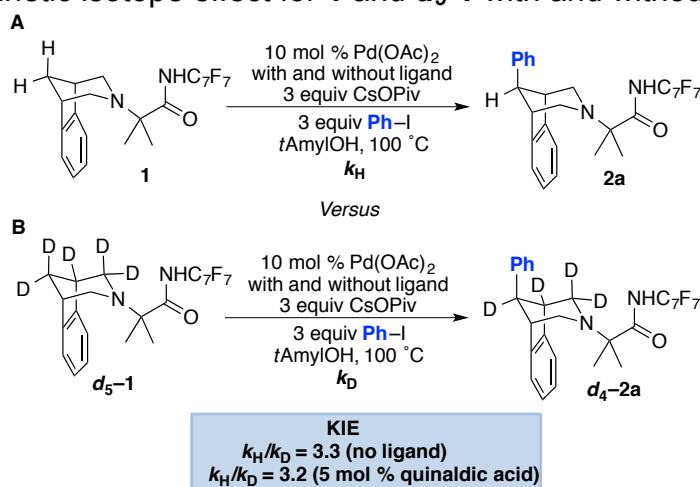
Conditions: **1** (0.03 mmol, 0.12 M), **2b** (0.06 M), Pd(OAc)₂ (0.012 M), CsOPiv (0.36 M), PhI (0.36 M), quinaldic acid (0.006 M), 0.25 mL tAmylOH, 100 °C. **2b** was not added in blue line initial rates

Kinetic Isotope Effect (KIE)

Given the ligand-induced rate acceleration (Figure 5.11), we next investigated the involvement of the ligand in the turnover-limiting step (TOLS) of the reaction. Isotope effects are a commonly used tool when determining if C–H bond cleavage occurs during the TOLS of a catalytic reaction or rate-determining step of a stoichiometric reaction.³³ In order to measure the KIE (k_H/k_D) of C(sp³)–H activation under our reaction conditions, we synthesized the deuterio-benzoazabicycloalkane **d₅-1** (Figure 5.12) by designing a new synthetic route to introduce deuterium in the amine scaffold (see experimental section for details). In separate KIE experiments without ligand additive, a primary isotope effect of 3.3 was observed, suggesting that C–H activation occurs in the TOLS. If the ligand is involved in the TOLS, we expect to observe an isotope effect dependence on ligand additive. However, two parallel reactions (**1** vs **d₅-1**) with quinaldic acid led to a primary isotope effect of 3.2. The similar KIE values with and

without ligand suggest that ligand is not involved in the TOLS and that the TOLS of the reaction is not changing as a function of ligand. Furthermore, the bidentate nature of the pyridinecarboxylate ligand would prevent vacant sites at Pd(II) center necessary for C–H activation. This result differs from other Pd-catalyzed C–H activation reactions where large differences in KIE values are observed as a function of ligand, and the authors suggest that ligand is involved in the transition-state of the C–H activation step.^{20a,21}

Figure 5.12. Kinetic isotope effect for **1** and **d₅-1** with and without quinaldic acid.



Conditions: **1** or **d₅-1** (0.03 mmol, 0.12 M), Pd(OAc)₂ (0.012 M), CsOPiv (0.36 M), PhI (0.36 M), 0.25 mL tAmylOH, 100 °C, with and without quinaldic acid (0.006 M).

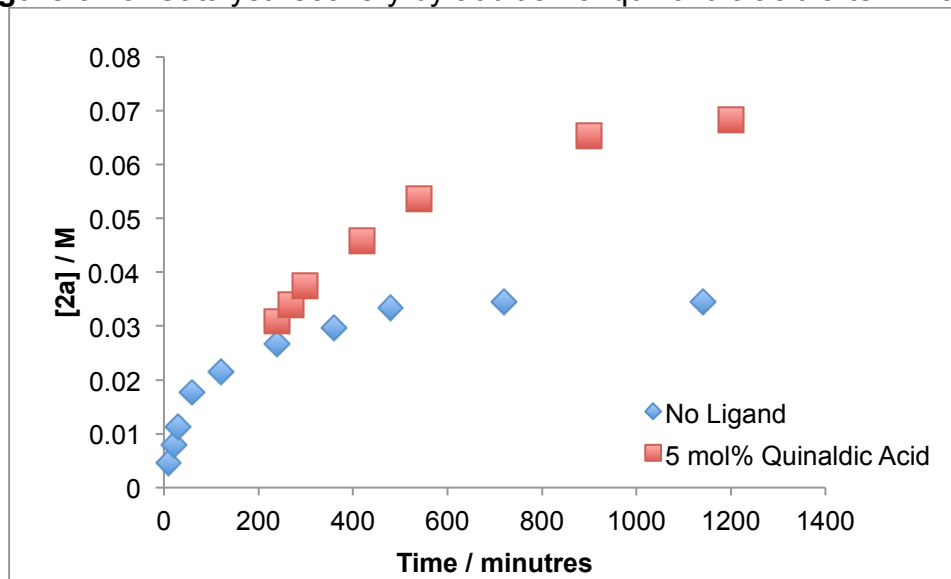
Catalyst Deactivation

We next investigated if the ligand could be preventing catalyst decomposition pathways. This could occur through either an irreversible Pd-catalyst decomposition²² or a reversible Pd-catalyst off-cycle pathway.^{24,34} If the Pd-catalyst is deactivated, we hypothesized that addition of the ligand at the time point where the ligandless reaction stalls would provide an increase in catalyst turnover (catalyst recovery by ligand). In contrast, if most of the catalyst has irreversibly decomposed (*i.e.* Pd black), we would expect minor increase in product concentration upon addition of ligand.

We conducted the C–H arylation reaction of **1** under the ligandless conditions for 240 minutes, which is the time-point where reaction begins to stall (see Figure 5.7, blue curve). At this point, the reaction mixture was charged with 5 mol % of quinaldic acid and heated back to 100 °C. Remarkably, the reaction recommenced to produce **2a** (Figure 5.13) and after 20 hours (1200 minutes) the reaction has doubled the

concentration of **2a** compared to the ligandless reaction. This result suggests that the Pd-catalyst undergoes a deactivation mechanism that ligand additives are able to reverse, regenerating an active catalyst.

Figure 5.13. Catalyst recovery by addition of quinaldic acid after 4 hours.



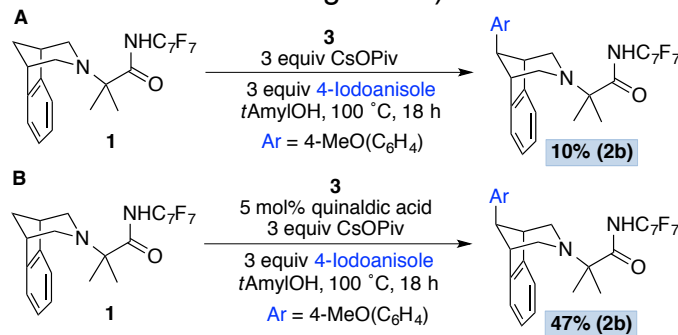
Conditions: **1** (0.03 mmol, 0.12 M), Pd(OAc)₂ (0.012 M), CsOPiv (0.36 M), PhI (0.36 M), 0.25 mL *t*AmylOH, 100 °C, 4 hours. Then, add quinaldic acid (0.006 M) and heat to 100 °C.

The rate profile upon addition of ligand completes fewer turnovers than the reaction with ligand added at the reaction onset (see Figure 5.7 red curve). This result indicates that some portion of the catalyst has undergone irreversible decomposition. This is further supported by performing a similar catalyst-recovery experiment, except that quinaldic acid was added after 12 hours, where **[2a]** was 0.034 M. Results demonstrate that addition of ligand to the reaction provided a slight increase in **[2a]** after an additional 12 hours up to 0.047 M.

We observed that over the course of the reaction, the reaction mixture changed from a bright yellow homogeneous solution to a black heterogeneous mixture. We hypothesized that insoluble Pd species were forming, thus hindering reactivity. An initial isolation and analysis by ICP of the heterogeneous black species indicated the presence of Pd.³⁵ This result led us to conduct a series of experiments where the black insoluble species (**3**) formed after 90 minutes of a ligand-less reaction were isolated by centrifugation and used as catalyst for subsequent reactions.

We conducted the C–H arylation reaction of **1** without ligand, employing **3** as catalyst (no Pd(OAc)₂ added). We chose 4-iodoanisole as the aryl iodide coupling partner in order to confirm that product formation was catalyzed by **3**. As shown in Figure 5.14 A, 10% yield of **2b** was formed after 18 hours. In contrast, when **3** was used in combination with quinaldic acid, we obtained a 47% yield of **2b** (Figure 5.14 B). A similar experiment was conducted with the supernatant post-removal of **3**. The reaction without ligand afforded 41% yield of **2a** after 18 h. In contrast, the addition of quinaldic acid to the supernatant furnished 73% yield of **2a** (see experimental section for details). Collectively, these results indicate that the Pd catalyst undergoes a deactivation mechanism that decreases the total Pd concentration in solution via precipitation. Although, we recognize that the role of the ligand involves multiple factors, we have demonstrated that a major role of quinaldic acid (or picolinic acid, see experimental section) in the reaction with **1** is to rescue insoluble Pd species.

Figure 5.14. A) Reaction of **3** without ligand. B) Reaction of **3** with quinaldic acid.



Conditions: **1** (0.03 mmol), black precipitate (**3**), CsOPiv (0.09 mmol), with or without quinaldic acid (0.0015 mmol), PhI (0.09 mmol), 0.25 mL *t*AmylOH, 100 °C, 18 hours.

Ligand effects in other azabicycloalkanes

The studies on the C–H arylation of the benzo-fused isotropane substrate (**1**) demonstrated that ligand additives provide improved reactivity by preventing catalyst deactivation and regenerating active Pd species. This led us to investigate the use of ligands in the C–H functionalization of challenging substrates that afforded only trace product under our previous reaction conditions. We began our studies with 8-azabicyclo[3.2.1]octane substrate (tropane core, **4**). Gratifyingly, the addition of ligand (quinaldic or picolinic acid) increased the yield of arylated tropane product (**5**, Figure

5.15). Further reaction optimization showed that picolinic acid was a more suitable ligand for the C–H arylation of **4** (see experimental section for optimization details).

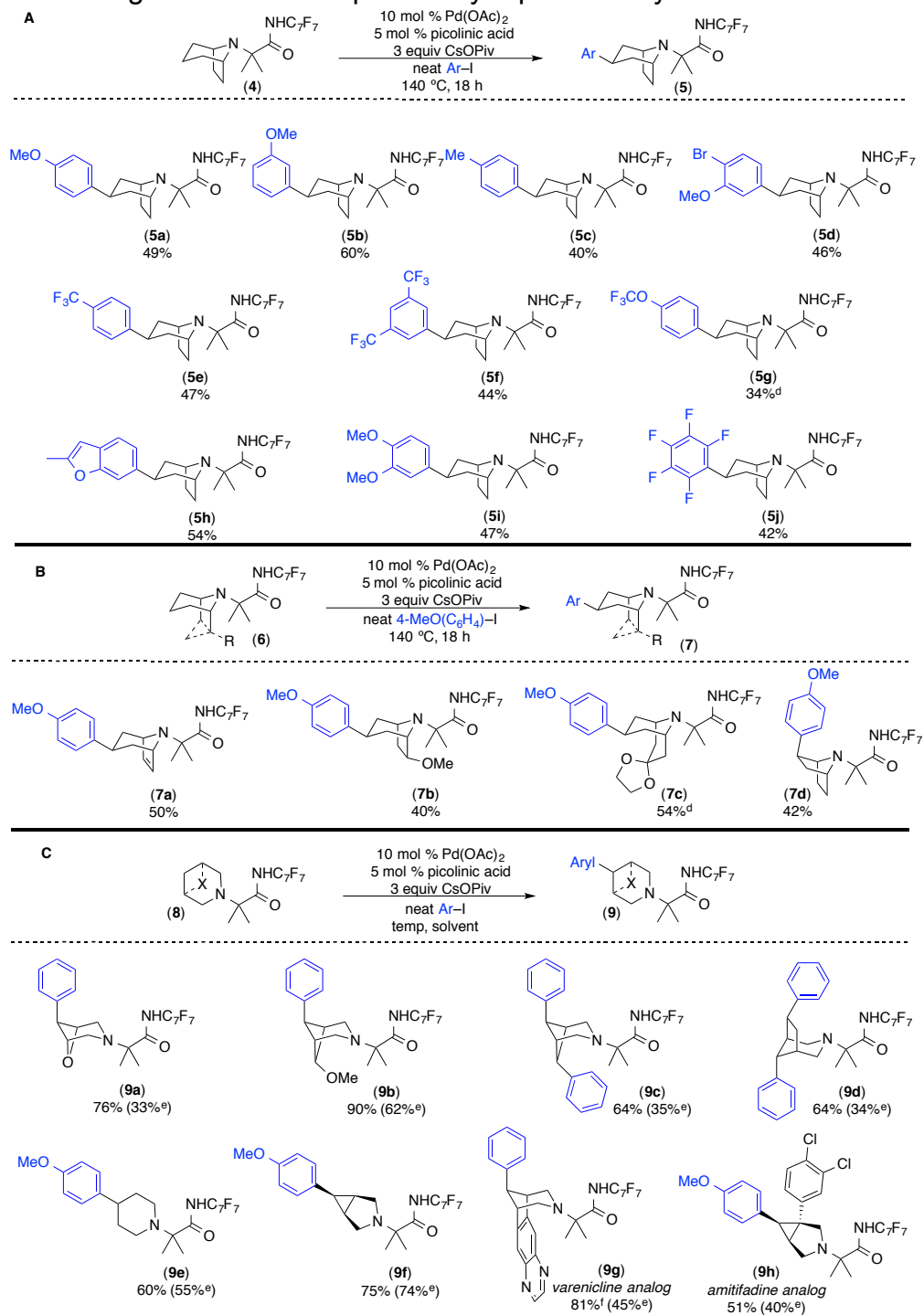
With the optimized conditions, we explored the scope in aryl iodide. As shown in Figure 5.15 A, a wide range of aryl iodides with varying steric and electronic properties were compatible in the C–H functionalization of **4**. Electron-rich aryl iodides bearing methoxy- and methyl-substituents afforded good yields of the C–H arylated products (40–60%, **5a-5d**). The reaction also tolerated other halides. For example, product **5d** provides a bromide handle that can be used in subsequent cross-coupling reactions. In addition, electron-deficient aryl iodides furnished good yields of the desired arylated product (**5e-5g**). Given the importance of the trifluoromethoxy group in agrochemical and pharmaceutical agents,³⁶ we were pleased to observe the incorporation of the trifluoroanisole ring in reasonable yields (34%, **5g**). Finally, other important aromatic scaffolds were amenable to the reaction conditions affording arylated tropane analogs bearing the benzofuran (**5h**), veratrole (**5i**) and perfluorobenzene (**5j**) moieties.

We then explored the functionalization of other bicycloalkanes (Figure 5.15 B). The tropane derivative containing a bridged-alkene functionality (**7a**) afforded 50% yield of the desired arylated product. Furthermore, the functionalized alkoxy-tropane was arylated in good yield (**7b**). C–H functionalization of other bicycles demonstrated that the tropane homologue ketal-protected azabicyclo[3.3.1]nonanone provided a 54% yield of arylated product **7c**. Finally, the ring-contracted 7-aza-norbornane substrate afforded 42% yield of **7d**.

The generality of the new reaction conditions was tested with a selection of previously reported amine substrates (Figure 5.15 C).¹⁷ Addition of ligand significantly increased the yield of several arylated azabicycloalkanes products (**9a-9d**). In other alicyclic amines the yield was only slightly improved as in the case of piperidine (**9e**) and 3-azabicyclo[3.1.0]hexane (**9f**). Notably, none of the tested amines resulted in lower yields in the presence of ligand additives. Finally, we were pleased to see that bioactive molecules were compatible with the ligand conditions. For example, Pfizer's anti-smoking drug varenicline improved the yield by almost 2-fold (85% yield versus 45% yield **9g**) and the drug candidate amitifadine also improved the isolated yield of the

arylated analog **9h**. Overall, this method provides an improved method for the C–H arylation of several bioactive azabicycloalkane scaffolds.

Figure 5.15. A) Scope in aryl iodide for tropane **4**.^a B) Scope in azabicycloalkanes.^b C) Ligand addition on previously reported alicyclic amines.^c

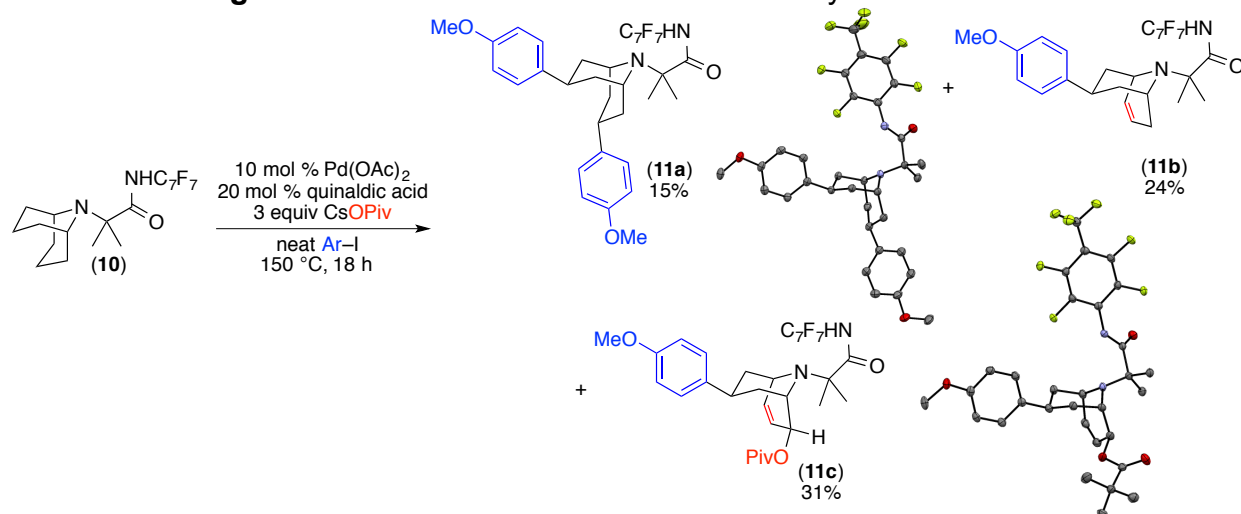


^a Conditions for part A: **4** (0.1 mmol, 1 equiv), Pd(OAc)₂ (0.01 mmol, 10 mol %), CsOPiv (0.3 mmol, 3 equiv), picolinic acid (0.005 mmol, 5 mol%), neat Ar–I, 140 °C, 18 h. Isolated yields. See details in experimental section. ^b Conditions for part B: **6** (0.1 mmol, 1 equiv), Pd(OAc)₂ (0.01 mmol, 10 mol %),

CsOPiv (0.3 mmol, 3 equiv), picolinic acid (0.005 mmol, 5 mol%), neat 4-iodoanisole, 140 °C, 18 h. Isolated yields. See details in experimental section.^c Reaction conditions for part C were analogous to reported conditions (Ref X) except that ligand (5 mol %) was added. Isolated yields. ^d 20 mol % Pd(OAc)₂. ^e Previously reported yield in Ref. 17. ^f 20 mol % quinaldic acid.

Independent optimization of the azabicyclo[3.3.1]nonane substrate (**10**) showed that quinaldic acid was a suitable ligand for the C–H arylation reaction (Figure 5.16). Subjecting **10** to the reaction conditions furnished three different C–H functionalized products (combined 70% yield, **11a-11c**). The first product underwent a transannular C–H di-arylation reaction providing **11a** in 15% yield. The structure of **11a** was confirmed via X-ray crystallography. The second product underwent two distinct C–H functionalization reactions (arylation and dehydrogenation) affording **11b** in 24% yield. Finally, the third C–H functionalized product was isolated in 31% yield (**11c**). The structure of **11c** was confirmed via a combination of NMR spectroscopy and X-ray crystallography. The bicyclic amine underwent three C–H functionalization reactions to yield **11c** (C–H arylation, dehydrogenation, and C–H oxygenation). Furthermore, we hypothesized that **11b** is an intermediate to **11c** via a Pd-catalyzed allylic C–H oxygenation reaction.³⁷ To test this hypothesis, we re-subjected **11b** under the C–H arylation conditions. Indeed, ¹H NMR analysis indicated that **11c** formed in 30% yield. The synthesis of these highly functionalized products (**11a-11c**) by traditional synthetic routes would require parallel multistep sequences. This preliminary result with substrate **10** demonstrates the potential of our Pd C–H activation protocol to incorporate diverse functional groups in azabicycloalkanes. As such, we hope this methodology can be useful for the rapid screening of bioactive alkaloids in the context of medicinal chemistry. Ongoing work in our lab is focused on exploring these opportunities.

Figure 5.16. C–H functionalization of azabicyclo-nonane **10**.



5.3 Conclusions

In summary, this chapter has focused on the development of a transannular Pd-catalyzed C–H functionalization of azabicycloalkanes. The addition of ligands (2-picolinic acid or 2-quinaldic acid) was found to dramatically improve reactivity. Mechanistic studies with the benzo-isotropane substrate **1** demonstrated that catalyst deactivation leads to low yields of arylated product. Furthermore, these studies led to the discovery of the unusual role of the ligand, which seems to regenerate active catalyst from insoluble Pd species during the reaction.

Finally, the ligand additives promoted the challenging distal C–H functionalization of several bioactive cores such as 8-azabicyclo[3.2.1]octane (tropane core) and related azabicyclic bridged-analogs. Interestingly, the 9-azabicyclo[3.3.1]nonane core underwent an unusual one-pot multi-C–H functionalization reaction furnishing highly functionalized products.

5.4 Perspective and Outlook

The transannular C–H functionalization of alicyclic amines has enabled the synthesis of value-added amines. This transformation has permitted the rapid diversification of pharmaceutical agents such as varenicline, amitifidine and cytosine

(chapter 4). Furthermore, the use of ligands has allowed for the increase in reaction yields and the expansion of the substrate scope to diverse alkaloids such as tropane, azabicyclo-nonane and azabicyclo-norbornane. However, there are several remaining opportunities in this area:

1) The development of new directing groups that can promote the transformation, but are easily removed and recycled (see Chapter 4).

2) The exploration of reaction conditions, oxidants, and ligands to promote other C–H functionalization reactions. Initial efforts with substrate **10** have demonstrated that C–H oxygenation and dehydrogenation reactions are feasible and may provide important synthetic methodologies.

3) Stoichiometric studies with these alicyclic amines could provide invaluable insights into the C–H activation mechanism. Although C–H activation could occur at Pd(II) through a cyclometallation-deprotonation mechanism,³⁸ there is a possibility that C–H activation might be occurring at Pd(IV). Additionally, isolation of the boat-conformer C–H activated palladacycle would validate the proposed mechanism and increase the understanding of its reactivity. This would be a significant step forward, as studies in Pd-alkyl amine complexes are limited. As such, our work presents an excellent opportunity to understand and further explore Pd-catalyzed sp³-amine directed C–H activation transformations.

Finally, we hope that the improvement of the transannular C–H functionalization strategy will enable the synthesis of highly valuable products for development of new pharmaceutical and agrochemical agents.

5.5 Experimental

Materials and Methods

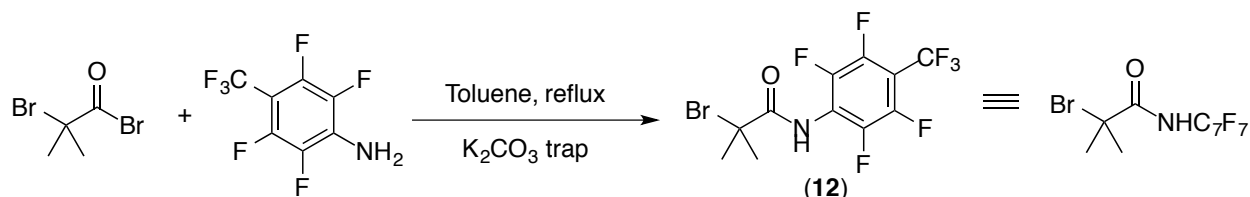
All reagents were obtained from a commercial vendor (Aldrich, CombiBlocks, Oakwood, AstaTech, Synthonix, Enamine, Manchester Organics, Carbosynth, Pressure Chemicals, Matrix, SantaCruz Biotech, PharmaBlock, Ark Pharm, or Ontario Chemicals) and were used without further purification unless otherwise stated. Reagents were stored under ambient conditions unless otherwise stated. The solvent *tert*-amyl alcohol was stored over activated molecular sieves.

The manipulation of solid reagents was conducted on the bench top unless otherwise stated. Reactions were conducted under an ambient atmosphere unless otherwise stated. Reaction vessels were sealed with either a septum (flask) or a Teflon-lined screw cap (4-mL or 20-mL vial). Reactions conducted at elevated temperatures were heated on a hot plate using an aluminum block. Temperatures were regulated using an external thermocouple. For reactions that were heated in excess of the ambient boiling point of the solvent (*i.e.* *tert*-amyl alcohol heated to 140 °C), the cap of the sealed vial was re-tightened after 5 minutes of heating. For TLC analysis, R_f values are reported based on normal phase silica plates with fluorescent indicator, and sample detection was conducted based on quenched fluorescence at 254 nm or KMNO₄ stain.

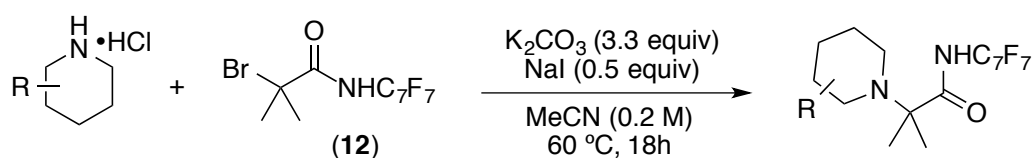
Instrumental Information

NMR spectra were obtained on Varian 400 MHz, Varian 500 MHz, or Varian 700 MHz NMR spectrometers. ¹H, ²H and ¹³C NMR chemical shifts are reported in parts per million relative to TMS with the residual solvent peak (most commonly CDCl₃) used as an internal reference (δ 7.26 for ¹H, ²H NMR and δ 77.16 for ¹³C NMR for CDCl₃). ¹⁹F NMR spectra were referenced to the solvent lock. ¹H and ¹⁹F multiplicities are reported as follows: singlet (s), doublet (d), triplet (t), quartet (q), double of doublets (dd), double of triplet (dt), and multiplet (m). High-resolution mass spectra were obtained at the University of Michigan core facility. Flash chromatography was conducted on a Biotage Isolera One auto chromatography system using preloaded high performance silica gel columns (10 g, 25 g, 50 g, or 100 g as appropriate). GC-FID was conducted on a Shimadzu 17A using a Restek Rtx®-5 (Crossbond 5% diphenyl/95% dimethyl polysiloxane; 15 m, 0.25 mm ID, 0.25 μ m df) column. All stock solutions were made using volumetric glassware. Melting points were obtained on a OptiMelt automated melting point system.

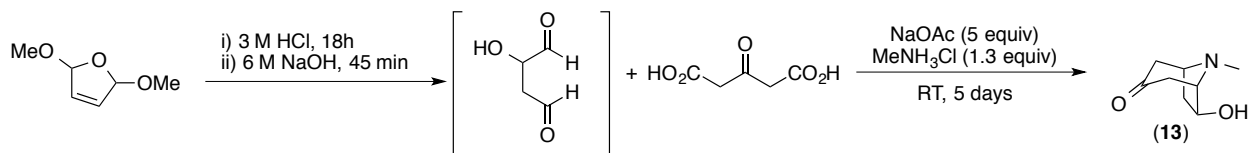
Synthesis of Starting Materials:



Compound 12. **12** was synthesized using 2,3,5,6-tetrafluoro-4-(trifluoromethyl)aniline and 2-bromoisobutyryl bromide following a literature procedure.¹⁷

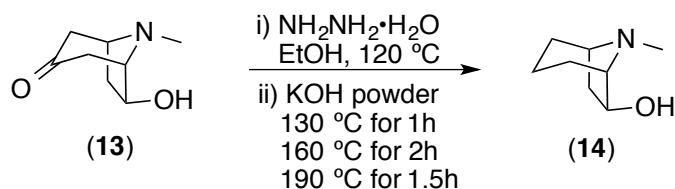


General Procedure A: Synthesis of starting materials. A 20 mL scintillation vial was charged with the corresponding hydrochloride salt of the saturated nitrogen heterocycle (2.5 mmol, 1 equiv), α -bromo methylpropanamide **12** (955 mg, 2.50 mmol, 1 equiv), K_2CO_3 (1.1 g, 8.25 mmol, 3.3 equiv) and NaI (188 mg, 1.25 mmol, 0.5 equiv). To the solids, anhydrous acetonitrile (12 mL, 0.2 M) was added. The vial was equipped with a stirbar, sealed with a Teflon-lined screw cap and heated to 60 °C. After 18 h, the reaction was cooled to room temperature, diluted with EtOAc (~5 mL), and filtered through a pad of silica gel using 100% EtOAc (~50 mL). The filtrate was concentrated under reduced pressure. Final purification via column chromatography (gradient elution from 0% to 20% EtOAc in hexanes) afforded product. See each substrate for specific details.



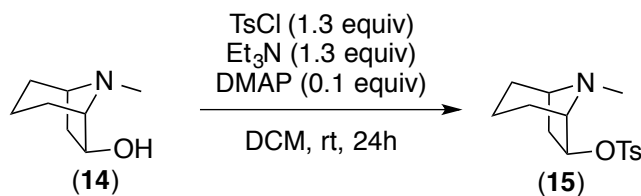
Synthesis of 6-hydroxytropolone (13). **13** was prepared by a modified literature procedure.³⁹ In a 100-mL round-bottom flask 2,5-dimethoxy-2,5-dihydrofuran (mixture of cis and trans) (2.6 g, 2.5 mL, 20 mmol, 1 equiv) was added to a 3 M aqueous HCl solution (36 mL). The mixture was stirred overnight (~12 h). The solution was

neutralized (pH 7-8) with 6 M aqueous NaOH (~18 mL) and stirred for 45 minutes. During this time, the pH dropped to 5; as such, dropwise addition of 6 M aq. NaOH brought the pH back to 7. This solution was added to a 500-mL round-bottom flask containing a solution of NaOAc·3H₂O (13.6 g, 100 mmol, 5 equiv), methylamine hydrochloride (1.75 g, 26 mmol, 1.3 equiv) and 1,3 acetonedicarboxylic acid (3.8 g, 26 mmol, 1.3 equiv) in H₂O (150 mL). The reaction mixture was stirred at room temperature for 5 days. Solid K₂CO₃ (15 g) and NaCl (15 g) were added to the brown solution and stirred for 30 minutes. The solution was extracted with CHCl₃ (15 × 75 mL) and EtOAc:Acetone (9:1; 4 × 75 mL). The combined organics were dried over Na₂SO₄, decanted, and volatiles removed via rotary evaporation. The crude product was purified via column chromatography (silica gel; 0% to 10% MeOH in DCM) using a Biotage column (50-g column) affording a 36% yield of **13** as a brown solid. NMR characterization of product matches the literature report.³⁹



Synthesis of 14. **14** was prepared following a modified literature procedure.⁴⁰ In a 50-mL round bottom flask, **13** (0.6 g, 3.87 mmol, 1 equiv) was dissolved in absolute ethanol (8 mL, 0.5 M), followed by addition of hydrazine monohydrate (1.9 mL, 38.7 mmol, 10 equiv). The reaction mixture was refluxed to 120 °C for 2 hours. The reflux condenser was replaced with a short-path distillation apparatus and the temperature increased to 130 °C allowing the solvent to gradually distill over 1 hour. After the solvent was distilled, KOH powder (2g, 34.8 mmol, 9 equiv) was added to the oily residue in one portion. The reflux condenser (no water flowing) was fitted to the flask and the mixture was heated to 130 °C for 1 hour, then at 160 °C for 2 hours and finally to 190 °C for 1.5 hours (Caution: Fumes evolve). After cooling to room temperature, the residue was dissolved in water (20 mL) and extracted with Et₂O (5 × 30 mL), DCM (5 × 30 mL) and EtOAc:Acetone (9:1; 1 × 30 mL). The combined organic extracts were dried over Na₂SO₄, decanted and volatiles removed via rotary evaporation. The product was

obtained in 56% yield as a brown semi-solid, and it was utilized without further purification. NMR characterization matches the literature report.⁴⁰



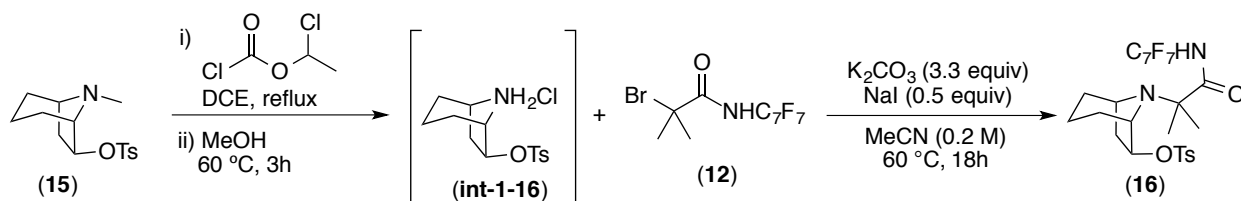
Synthesis of 15. A 50-mL round bottom flask was charged with **14** (298 mg, 2.11 mmol, 1 equiv), Et₃N (0.4 mL, 2.87 mmol, 1.3 equiv), 4-dimethylaminopyridine (27 mg, 0.21 mmol, 0.1 equiv), *p*-toluenesulfonyl chloride (0.55 g, 2.87 mmol, 1.3 equiv) and DCM (9.6 mL, 0.23 M). The mixture was stirred at room temperature for 24 hours. The reaction mixture was diluted with water (10 mL) and the product was extracted with DCM (5 × 10 mL). The combined organic extracts were dried over Na₂SO₄, decanted and volatiles removed via rotary evaporation. The crude product was purified via column chromatography (silica gel, hexanes:EtOAc:Et₃N 3:2:0.5) affording 61% yield of **15** as a yellow oil.

R_f: 0.2 (Hex:EtOAc:Et₃N ratio of 3:2:0.5)

¹H NMR (500 MHz, Chloroform-*d*) δ 7.79 (d, *J* = 8.0 Hz, 2H), 7.34 (d, *J* = 8.0 Hz, 2H), 4.96 (app. dd, *J* = 7.8, 3.0 Hz, 1H), 3.29 (m, 1H), 3.16 (m, 1H), 2.45 (s, 3H), 2.41 (s, 3H), 2.21 (m, 1H), 1.98 (m, 1H), 1.77–1.68 (multiple peaks, 2H), 1.50 (m, 1H), 1.37 (m, 1H), 1.26–1.11 (multiple peaks, 2H).

¹³C NMR (176 MHz, Chloroform-*d*) δ 144.80, 134.38, 129.99, 127.89, 86.45, 67.23, 61.99, 40.32, 36.11, 28.64, 27.30, 21.82, 16.96.

HRMS (ESI⁺) [M+H]⁺ Calcd for C₁₅H₂₂NO₃S: 296.1315; Found: 296.1316.



Synthesis of 16. A Schlenk flask was charged with compound **15** (0.379 g, 1.28 mmol, 1 equiv) and anhydrous 1,2-dichloroethane (4.7 mL, 0.4 M) under a N₂ atmosphere. To

this mixture, 1-chloroethyl chloroformate (0.28 mL, 2.57 mmol, 2 equiv) was added dropwise via syringe. The mixture was heated to reflux for 5 hours. After cooling to room temperature, the reaction was concentrated via rotary evaporation and placed under high vacuum for 1 hour. The remaining brown oil was dissolved in methanol (5 mL) and heated to 60 °C for 3 hours under a N₂ atmosphere. After, the reaction mixture was transferred to a 20-mL scintillation vial and solvent was removed via rotary evaporation. The crude hydrochloride salt of the amine intermediate **int-1-16** was dried under high vacuum for 2 hours. After, **int-1-16** was mixed with α -bromo 2-methylpropanamide **12** (0.489 g, 1.28 mmol, 1 equiv), K₂CO₃ (0.584 g, 4.22 mmol, 3.3 equiv) and NaI (96 mg, 0.64 mmol, 0.5 equiv) in MeCN (6.4 mL, 0.2 M) and heated to 60 °C. After 18 h, the reaction was cooled to room temperature, diluted with EtOAc (~5 mL), and filtered through a pad of silica gel using 100% EtOAc (~50 mL). The filtrate was concentrated under reduced pressure. Final purification via column chromatography (gradient elution from 0% to 10% EtOAc in hexanes) afforded product **16** in 60% yield as a white solid.

MP: 95-97 °C

R_f: 0.1 (10% EtOAc in Hexanes)

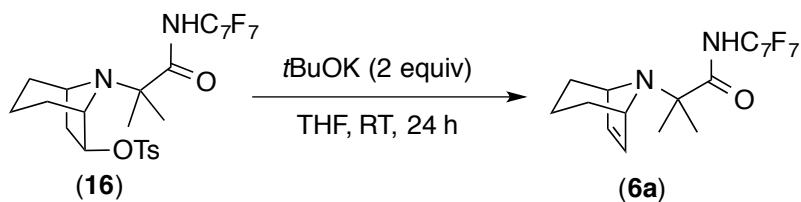
¹H NMR (700 MHz, Chloroform-*d*) δ 9.56 (s, 1H), 7.78 (d, *J* = 7.8 Hz, 2H), 7.36 (d, *J* = 7.8 Hz, 2H), 5.03 (app. t, *J* = 5.6 Hz, 1H), 3.75 (m, 1H), 3.51 (m, 1H), 2.46 (s, 3H), 2.04 (m, 2H), 1.77–1.61 (multiple peaks, 4H), 1.44 (m, 1H), 1.47–1.35 (multiple peaks, 8H).

¹³C NMR (176 MHz, Chloroform-*d*) δ 176.05, 145.23, 133.98, 130.12, 127.79, 85.81, 63.60, 61.35, 58.26, 38.33, 31.73, 31.49, 26.73, 21.81, 21.61, 17.53.

The carbon resonances corresponding to the perfluoroarene (C₇F₇) in this compound appear as a complex series of multiplets between 105 ppm to 155 ppm as a result of ¹³C/¹⁹F coupling. Due to the complexities of the system, the peaks are not listed. ¹⁹F NMR and HRMS were used to confirm the presence of this ring system.

¹⁹F NMR (377 MHz, Chloroform-*d*) δ -56.03 (t, *J* = 21.7 Hz, 3F), -140.36 (m, 2F), -143.57 (m, 2F).

HRMS (ESI⁺) [M+H]⁺ Calcd for C₂₅H₂₆F₇N₂O₄S: 583.1496 ; Found: 583.1503 .



Synthesis of 6a. Inside a N₂ glove box a 20-mL vial was charged with **16** (0.414 g, 0.71 mmol, 1 equiv), *t*BuOK (0.16 g, 1.4 mmol, 2 equiv) and THF (7 mL, 0.1 M). The reaction mixture was stirred at room temperature for 24 hours (Caution: excess *t*BuOK leads to S_nAr in the perfluorinated ring). The reaction was mixed with water (1 mL) and stirred for 10 minutes. The solution was filtered through a silica gel plug with 100% EtOAc (~10 mL). The volatiles were removed via rotary evaporation and the crude product was purified by column chromatography (silica gel, 0% to 10% EtOAc in Hexanes) affording 45% yield of **6a** as a white solid (90% yield based on recovered starting material).

MP: 111-113 °C

R_f: 0.3 (10% EtOAc in Hexanes)

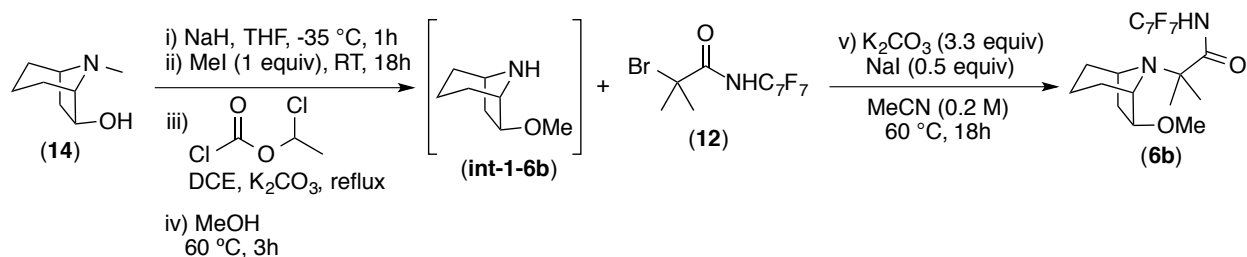
¹H NMR (700 MHz, Chloroform-*d*) δ 5.94 (s, 2H), 3.73 (s, 2H), 1.76–1.69 (multiple peaks, 2H), 1.61 (m, 1H), 1.53–1.43 (multiple peaks, 3H), 1.24 (s, 6H).

¹³C NMR (176 MHz, Chloroform-*d*) δ 175.84, 130.23, 64.13, 61.57, 27.35, 24.03, 16.98.

The carbon resonances corresponding to the perfluoroarene (C₇F₇) in this compound appear as a complex series of multiplets between 105 ppm to 155 ppm as a result of ¹³C/¹⁹F coupling. Due to the complexities of the system, the peaks are not listed. ¹⁹F NMR and HRMS were used to confirm the presence of this ring system.

¹⁹F NMR (377 MHz, Chloroform-*d*) δ -56.04 (t, *J* = 21.7 Hz, 3F), -141.3 (m, 2F), -143.49 (m, 2F).

HRMS (ESI⁺) [M+H]⁺ Calcd for C₁₈H₁₈F₇N₂O: 411.1302; Found: 411.1304.



Synthesis of 6b. Steps i and ii: Inside of a N_2 glovebox, a dry 50-mL round-bottom flask was charged with **14** (0.6 g, 4.25 mmol, 1 equiv) and THF (15 mL, 0.2 M). The mixture was cooled inside a freezer ($-35\text{ }^{\circ}\text{C}$) for 10 minutes, and then NaH (0.11g, 4.5 mmol, 1.05 equiv) was added to the mixture. The suspension was brought out of the glovebox and placed under a N_2 atmosphere in the fume hood. After 30 minutes, methyl iodide (0.28 mL, 4.5 mmol, 1.05 equiv) was added via syringe at room temperature. The mixture was stirred vigorously overnight. The white suspension was filtered through a pad of celite and washed with DCM. The volatiles were removed by rotary evaporation. **Steps iii and iv:** The concentrated crude mixture was transferred to a Schlenk flask using anhydrous DCE (10 mL, 0.4 M). To this solution K_2CO_3 (587 mg, 4.25 mmol, 1 equiv) was added, followed by dropwise addition of 1-chloroethylchloroformate (1.38 mL, 12.75 mmol, 3 equiv). The reaction mixture was refluxed for 5 hours under N_2 atmosphere. After cooling to room temperature, the solution was concentrated via rotary evaporation and placed under high vacuum for 1 hour. The residue was dissolved in methanol (10 mL) and heated to $60\text{ }^{\circ}\text{C}$ overnight under a N_2 atmosphere. After, the reaction mixture was transferred to a 20-mL scintillation vial and the solvent was removed via rotary evaporation to afford crude **int-1-6b**. **Step v:** The crude **int-1-6b** was mixed with α -bromo 2-methylpropanamide **12** (1.6 g, 4.25 mmol, 1 equiv), K_2CO_3 (1.9 g, 14 mmol, 3.3 equiv) and NaI (0.32 g, 2.12 mmol, 0.5 equiv) in MeCN (18 mL) and heated to $60\text{ }^{\circ}\text{C}$ for 18 hours. The reaction was cooled to room temperature, diluted with EtOAc (~ 5 mL), and filtered through a pad of silica gel using 100% EtOAc (~ 80 mL). The filtrate was concentrated under reduced pressure. Purification via column chromatography (gradient elution from 0% to 10% THF in hexanes). Collection of fractions containing product showed minor impurities by NMR and the product was further purified by a subsequent column chromatography (0% to 80% THF in DCM) to afford product **6b** in 5% overall yield as a white solid.

MP: 67-69 °C

R_f: 0.3 (10% THF in hexanes)

¹H NMR (700 MHz, Chloroform-*d*) δ 9.96 (s, 1H), 3.86 (m, 1H), 3.59 (m, 1H), 3.55 (m, 1H), 3.27 (s, 3H), 2.02–1.86 (multiple peaks, 2H), 1.76–1.38 (multiple peaks, 12H).

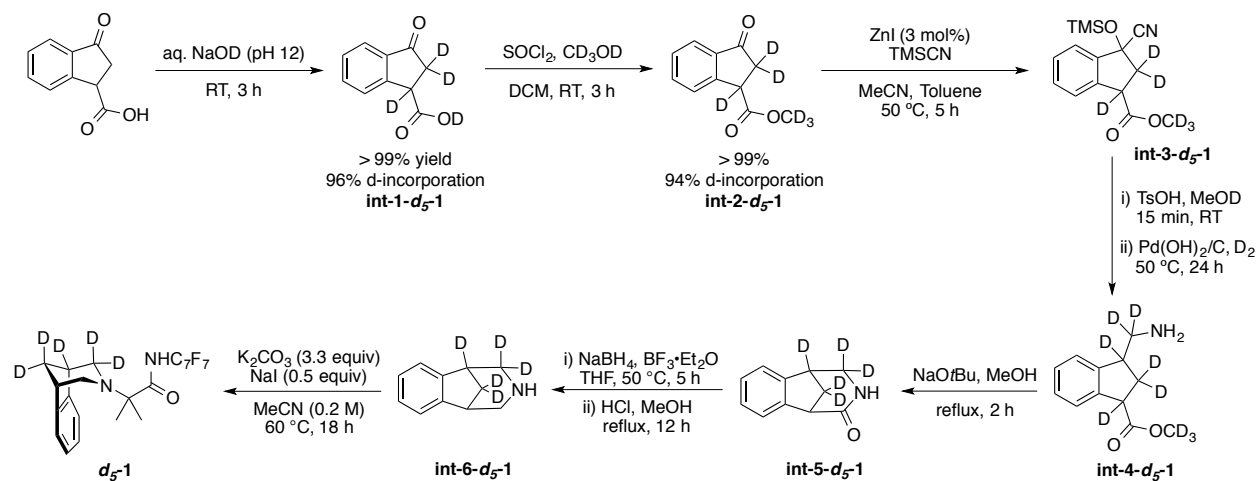
¹³C NMR (176 MHz, Chloroform-*d*) δ 176.98, 85.87, 63.17, 59.62, 57.44, 56.28, 37.47, 31.54, 30.89, 26.87, 22.31, 17.57.

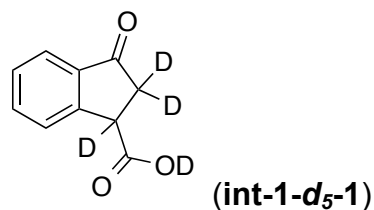
The carbon resonances corresponding to the perfluoroarene (C₇F₇) in this compound appear as a complex series of multiplets between 105 ppm to 155 ppm as a result of ¹³C/¹⁹F coupling. Due to the complexities of the system, the peaks are not listed. ¹⁹F NMR and HRMS were used to confirm the presence of this ring system.

¹⁹F NMR (377 MHz, Chloroform-*d*) δ -56.02 (t, *J* = 21.7 Hz, 3F), -141.46 (m, 2F), -143.58 (m, 2F).

HRMS (ESI⁺) [M+H]⁺ Calcd for C₁₉H₂₂F₇N₂O₂: 443.1564; Found: 443.1564.

Synthesis of *d*₅-1





A 20-mL scintillation vial was charged with solid 3-oxo-2,3-dihydro-1*H*-indene-1-carboxylic acid (500 mg, 2.83 mmol) and D₂O (10 mL). To this solution, dropwise NaOD (30% in D₂O) was added at 0 °C to a pH 12-13. The reaction was warmed to room temperature and allowed to stir for 3 hours. The reaction was quenched with dropwise addition of D₂SO₄ at 0 °C to a pH 2-3. The reaction mixture was extracted with DCM (3 x 75 mL), dried over Na₂SO₄, decanted, and the volatiles were removed by rotary evaporation, affording compound **int-1-d₅-1** in >99% yield as an off-white solid that was used without further purification (96% deuterium incorporation by ¹H NMR).

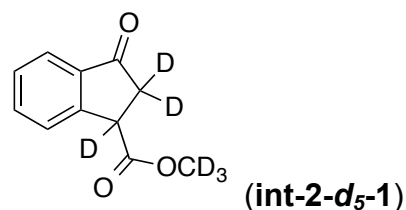
¹H NMR (700 MHz, Chloroform-*d*) δ 7.79 (d, *J* = 7.7, 1H), 7.76 (d, *J* = 7.7, 1H), 7.66 (t, *J* = 7.7, 1H), 7.48 (t, *J* = 7.7, 1H).

²H NMR (700 MHz, Chloroform-*d*) δ 4.34 (br s, 1D), 3.13 (br s, 1D), 2.90 (br s, 1D).

¹³C NMR (176 MHz, Chloroform-*d*) δ 204.1, 177.5, 150.5, 136.5, 135.3, 129.2, 126.8, 124.2, 43.1, 38.7.

Note: *J*_{C-D} were not assigned, the incorporation of deuterium was confirmed by ²H NMR and HRMS.

HRMS (ESI⁺) [M-D] Calcd for C₁₀H₃D₄O₃: 178.0589; found:178.0588.



A 20-mL scintillation vial was charged with solid **int-1-d₅-1** (485 mg, 2.69 mmol) and DCM (27 mL). To this solution, thionyl chloride (0.39 mL, 5.38 mmol) was added dropwise at 0 °C followed by *d*₄-MeOD (1.09 mL, 26.9 mmol) and warmed to room temperature. The reaction was allowed to stir for 3 hours at room temperature. After, the volatiles were removed, leading to quantitative conversion to compound **int-2-d₅-1** as a

yellow oil. The intermediate was used without further purification (94% deuterium incorporation by ^1H NMR).

^1H NMR (700 MHz, Chloroform-*d*) δ 7.78 (d, $J = 7.7$, 1H), 7.70 (d, $J = 7.7$, 1H), 7.64 (t, $J = 7.7$, 1H), 7.46 (t, $J = 7.7$, 1H).

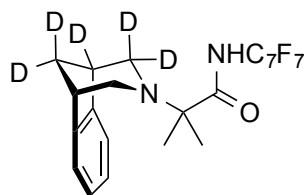
^2H NMR (700 MHz, Chloroform-*d*) δ 4.30 (br s, 1D), 3.77 (br s, 3D), 3.13 (br s, 1D), 2.87 (br s, 1D).

^{13}C NMR (176 MHz, Chloroform-*d*) δ 204.3, 172.4, 151.2, 136.6, 135.1, 129.0, 126.6, 124.1, 52.1, 43.3, 39.0.

Note: $J_{\text{C-D}}$ were not assigned, the incorporation of deuterium was confirmed by ^2H NMR and HRMS.

HRMS (ESI $^+$) $[\text{M}+\text{H}]^+$ Calcd for $\text{C}_{11}\text{H}_4\text{D}_6\text{O}_3$: 197.1079; found:197.1076.

Compounds int-3-*d*₅-1 to int-6-*d*₅-1: Intermediates **int-3-*d*₅-1** to **int-6-*d*₅-1** were prepared following a reported literature procedure.⁴¹ Note: For the synthesis of **int-4-*d*₅-1** (hydrogenation step), D₂ gas (3.6 bar) was employed instead of H₂.



(***d*₅-1**)

Compound ***d*₅-1** was isolated in 54% yield (over seven steps) as a white solid using **general procedure A** (90% deuterium incorporation by ^1H NMR) and purified by column chromatography (silica gel; 0% EtOAc to 20% EtOAc in hexanes). Collection of fractions containing product showed minor impurities by NMR and the product was further purified by subsequent column chromatography (0% to 5% THF in hexanes).

MP: 118.9-120.0 °C

R_f: 0.24 (5% THF in hexanes)

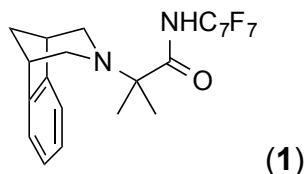
^1H NMR (700 MHz, Chloroform-*d*) δ 7.49 (br s, 1H), 7.16 (multiple peaks, 2H), 7.07 (multiple peaks, 2H), 3.21 (m, 1H), 2.79 (m, 1H), 2.69 (m, 1H), 1.21 (s, 6H),

^2H NMR (700 MHz, Chloroform-*d*) δ 3.21 (br s, 1D), 2.79 (br s, 1D), 2.69 (br s, 1D), 2.30 (br s, 1D), 1.73 (br s, 1D).

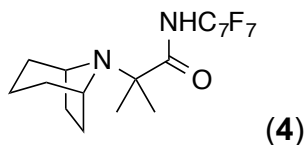
^{13}C NMR chemical shifts were not assigned due to complex $J_{\text{C-D}}$ and $J_{\text{C-F}}$ splitting.

^{19}F NMR (377 MHz, Chloroform-*d*) δ -56.07 (t, J = 21.9 Hz, 3F), -141.57 (m, 2F), -142.99 (m, 2F).

HRMS (ESI⁺) $[M+H]^+$ Calcd for $\text{C}_{22}\text{H}_{14}\text{D}_5\text{F}_7\text{N}_2\text{O}$: 466.1772; found: 466.1758.



Compound **1** was isolated in 85% yield as a white solid following **general procedure A**. Product characterization matches with previous literature report.¹⁷



Compound **4** was isolated in 69% yield as a white solid following **general procedure A**.

MP: 81-83 °C

R_f: 0.23 (10% EtOAc in hexanes)

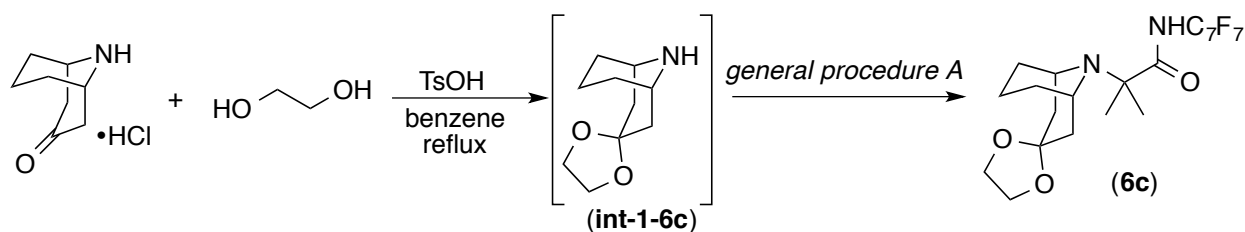
^1H NMR (401 MHz, Chloroform-*d*) δ 9.86 (s, 1H), 3.45 (m, 2H), 1.89–1.51 (multiple peaks, 10H), 1.33 (s, 6H).

^{13}C NMR (176 MHz, Chloroform-*d*) δ 176.40, 63.97, 57.20, 34.87, 29.81, 23.75, 17.27.

The carbon resonances corresponding to the perfluoroarene (C_7F_7) in this compound appear as a complex series of multiplets between 105 ppm to 155 ppm as a result of $^{13}\text{C}/^{19}\text{F}$ coupling. Due to the complexities of the system, the peaks are not listed. ^{19}F NMR and HRMS were used to confirm the presence of this ring system.

^{19}F NMR (377 MHz, Chloroform-*d*) δ -56.03 (t, J = 21.7 Hz, 3F), -141.36 (m, 2F), -143.57 (m, 2F).

HRMS (ESI⁺) $[M+H]^+$ Calcd for $\text{C}_{18}\text{H}_{20}\text{F}_7\text{N}_2\text{O}$: 413.1458; Found: 413.1461.



Step 1: A round-bottom flask was charged with 9-azabicyclo[3.3.1]nonan-3-one hydrochloride (500 mg, 2.84 mmol, 1 equiv), toluene sulfonic acid (594 mg, 3.12 mmol, 1.1 equiv), ethylene glycol (1.7 mL, 28.4 mmol, 10 equiv) and benzene (14 mL, 0.2 M). The flask was equipped with a Dean-Stark trap and heated to 110 °C overnight. The reaction was allowed to cool to room temperature, followed by addition of Na₂CO₃ (1.18 g) and brine (26 mL). The aqueous layer was extracted with chloroform (3 x 75 mL). The organic layer was dried over Na₂SO₄, decanted and concentrated via rotary evaporation. Intermediate **int-1-6c** was carried forward without analysis or purification.

Step 2: **Int-1-6c** was used as starting amine reagent following **general procedure A** to isolate compound **6c** in 15% yield as a white solid over the two steps.

MP: 93.3-94.9 °C

R_f: 0.13 (5% EtOAc in hexanes)

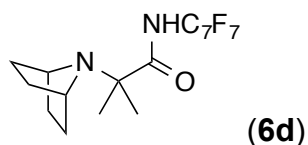
¹H NMR (700 MHz, Chloroform-*d*) δ 10.87 (s, 1H), 3.89 (m, 4H), 3.46 (d, *J* = 10.5 Hz, 2H), 2.34 (t, *J* = 12.6 Hz, 2H), 2.07 (m, 1H), 1.85–1.77 (multiple peaks, 4H), 1.66 (app. d, *J* = 14.7 Hz, 2H), 1.49 (s, 6H), 1.30 (d, *J* = 13.3 Hz).

¹³C NMR (176 MHz, Chloroform-*d*) δ 178.1, 108.9, 64.7, 64.0, 45.8, 38.4, 29.5, 26.7, 14.3.

The carbon resonances corresponding to the perfluoroarene (C₇F₇) in this compound appear as a complex series of multiplets between 105 ppm to 155 ppm as a result of ¹³C/¹⁹F coupling. Due to the complexities of the system, the peaks are not listed. ¹⁹F NMR and HRMS were used to confirm the presence of this ring system.

¹⁹F NMR (377 MHz, Chloroform-*d*) δ -56.03 (t, *J* = 21.8 Hz, 3F), -141.69 (m, 2F), -143.87 (m, 2F).

HRMS (ESI⁺) [M+H]⁺ Calcd for C₂₁H₂₄F₇N₂O₃: 485.1670; Found: 485.1671.



Compound **6d** was isolated in 50% yield as a pale yellow solid following **general procedure A**.

MP: 75-77 °C

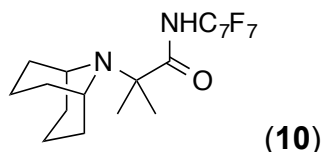
R_f: 0.29 (10% EtOAc in Hexanes).

¹H NMR (700 MHz, Chloroform-*d*) δ 10.21 (s, 1H), 3.61 (m, 2H), 1.74 (m, 4H), 1.45 - 1.39 (multiple peaks, 10H).

¹³C NMR (176 MHz, Chloroform-*d*) δ 176.58, 61.23, 56.78, 30.94, 24.43.

¹⁹F NMR (376 MHz, Chloroform-*d*) δ -56.01 (t, *J* = 21.7 Hz, 3F), -141.35 (m, 2F), -144.17 (m, 2F)

HRMS (ESI⁺) [M+H]⁺ Calcd for C₁₇H₁₈F₇N₂O: 399.1302; Found: 399.1304.



Compound **10** was isolated in 75% yield as a white solid following **general procedure A**.

MP: 118-120 °C

R_f: 0.42 (10% EtOAc in hexanes)

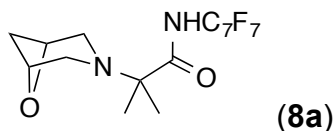
¹H NMR (700 MHz, Chloroform-*d*) δ 9.73 (s, 1H), 3.15 (m, 2H), 2.14 (m, 2H), 1.96 (m, 4H), 1.71 (m, 2H), 1.64 (m, 4H), 1.47 (s, 6H).

¹³C NMR (176 MHz, Chloroform-*d*) δ 177.26, 65.21, 48.13, 30.09, 25.62, 20.54.

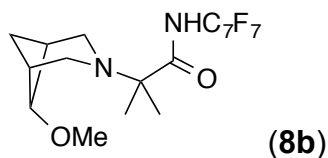
The carbon resonances corresponding to the perfluoroarene (C₇F₇) in this compound appear as a complex series of multiplets between 105 ppm to 155 ppm as a result of ¹³C/¹⁹F coupling. Due to the complexities of the system, the peaks are not listed. ¹⁹F NMR and HRMS were used to confirm the presence of this ring system.

¹⁹F NMR (377 MHz, Chloroform-*d*) δ -56.25 (t, *J* = 21.7 Hz, 3F), -141.76 (m, 2F), -143.73 (m, 2F).

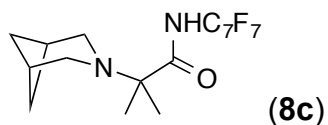
HRMS (ESI⁺) [M+H]⁺ Calcd for C₁₉H₂₂F₇N₂O: 427.1615; Found: 427.1619.



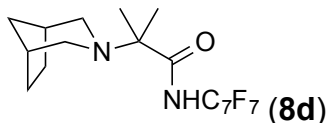
Compound **8a** was isolated in 59% yield following a previous literature report.¹⁷



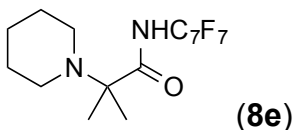
Compound **8b** was isolated in 33% yield following a previous literature report.¹⁷



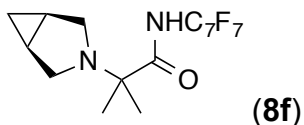
Note: Reaction was heated to 75 °C for 6 hours. Compound **8c** was isolated in 31% yield as a white solid following **general procedure A**. Product characterization matches with previous literature report.¹⁷



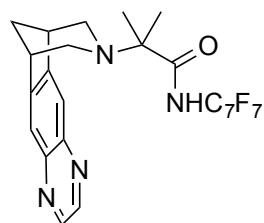
Compound **8d** was isolated in 93% yield following a previous literature report.¹⁷



Compound **8e** was isolated in 84% yield following a previous literature report.¹⁷

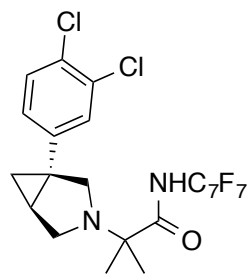


Compound **8f** was isolated in 81% yield following a previous literature report.¹⁷



(8g)

Compound **8g** was isolated in 81% yield following a previous literature report.¹⁷



(8h)

Compound **8h** was isolated in 87% yield following a previous literature report.¹⁷

Optimization of 2,3,4,5-tetrahydro-1*H*-1,5-methanobenzo[*d*]azepine **1**:

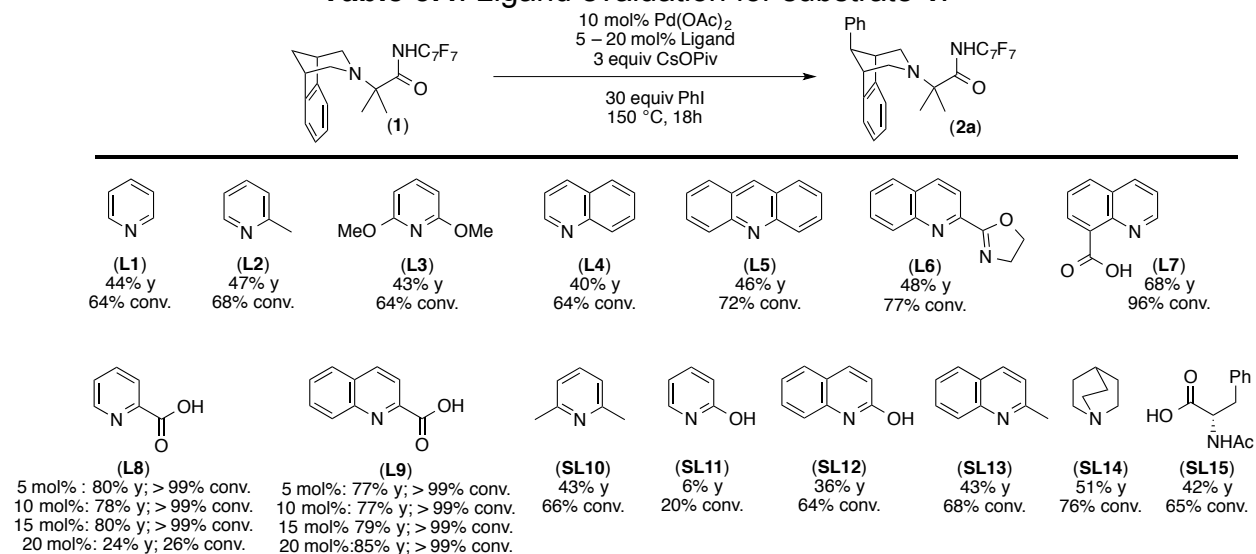
Ligand Evaluation with azabicycloalkane **1**:

General Procedure B: Ligand evaluation reaction conditions. Under ambient conditions, a 0.02 M stock solution of Pd(OAc)₂ (23 mg Pd(OAc)₂, 0.10 mmol) dissolved in dichloromethane (5 mL) was prepared. An aliquot of this solution was transferred to a vial (4 mL capacity, 150 μL, 0.003 mmol Pd, 10 mol %). DCM was removed by gently heating the open vial to 45 °C for 5 minutes. To the concentrated Pd(OAc)₂, the appropriate ligand (0.0015 mmol, 5 mol%) was added (ligand was weighed on a Sartorius ME36S microgram analytical balance). Solid substrate **1** (13.8 mg, 0.03 mmol, 1 equiv) and CsOPiv (21.1 mg, 0.09 mmol, 3 equiv) were added. To this mixture, PhI (0.1 mL, 0.9 mmol, 30 equiv) was added via plastic syringe. The vial was equipped with a stirbar, sealed with a Telfon-lined cap and heated to an external temperature of 150 °C in a preheated aluminum block. After 18 hours, the reaction was cooled to room temperature and diluted with DCM (2.5 mL). Hydrazine monohydrate (50 μL) was added and the solution was vigorously stirred for 15 minutes. A 0.2 M stock solution of 1,3,5-trimethoxybenzene (168 mg, 1 mmol) dissolved in DCM (5 mL) was prepared. An

aliquot of this solution (150 μ L, 0.03 mmol) was added to the reaction as the GC internal standard. The reaction solution was then filtered through a pipette packed with Celite and was analyzed by GC-FID. Yield of **2a** was determined based on a 10-point calibration curve.

Variations of this procedure were used in all optimization reactions (Table 5.1, 5.4) where the yield was determined by GC-FID. For instance, the effect of ligand loading (5 to 20 mol%) was determined by following the same procedure outlined above except that the amount of ligand was varied.

Table 5.4. Ligand evaluation for substrate **1**.



Conditions following **general procedure B**.

Reaction optimization for C–H arylation of **1**

General Procedure C: Reaction optimization of Table 5.2. Under ambient conditions, a 0.02 M stock solution of Pd(OAc)₂ (23 mg Pd(OAc)₂ dissolved in DCM (5 mL) was prepared. An aliquot of this solution was transferred to a vial (4 mL capacity, 150 μ L, 0.003 mmol Pd, 10 mol %). To the Pd(OAc)₂ solution, a quinaldic acid aliquot (75 μ L, 0.0015 mmol, 5 mol %) from a 0.02 M stock solution (17.3 mg of quinaldic acid in 5 mL of DCM) was added. DCM was removed by gently heating the open vial to 45 °C for 5 minutes. To the concentrated reaction mixture, solid substrate **1** (13.8 mg, 0.03 mmol, 1 equiv), CsOPiv (21.1 mg, 0.09 mmol, 3 equiv) and PhI (1 – 30 equiv) were added. The reaction mixture was then diluted with *t*AmylOH (0.25 mL, if indicated in Table 5.2). The

vial was equipped with a stirbar, sealed with a Teflon-lined cap and heated to the indicated temperature in Table 5.2 in a preheated aluminum block. After 18 hours, the reaction was cooled to room temperature and diluted with DCM (2.5 mL). Hydrazine monohydrate (50 μ L) was added and the solution was vigorously stirred for 15 minutes. A 0.2 M stock solution of 1,3,5-trimethoxybenzene (168 mg, 1 mmol) dissolved in DCM (5 mL) was prepared. An aliquot of this solution (150 μ L, 0.03 mmol) was added to the reaction as the GC internal standard. The reaction solution was then filtered through a pipette packed with Celite and was analyzed by GC-FID. Yield of **2a** was determined based on a 10-point calibration curve.

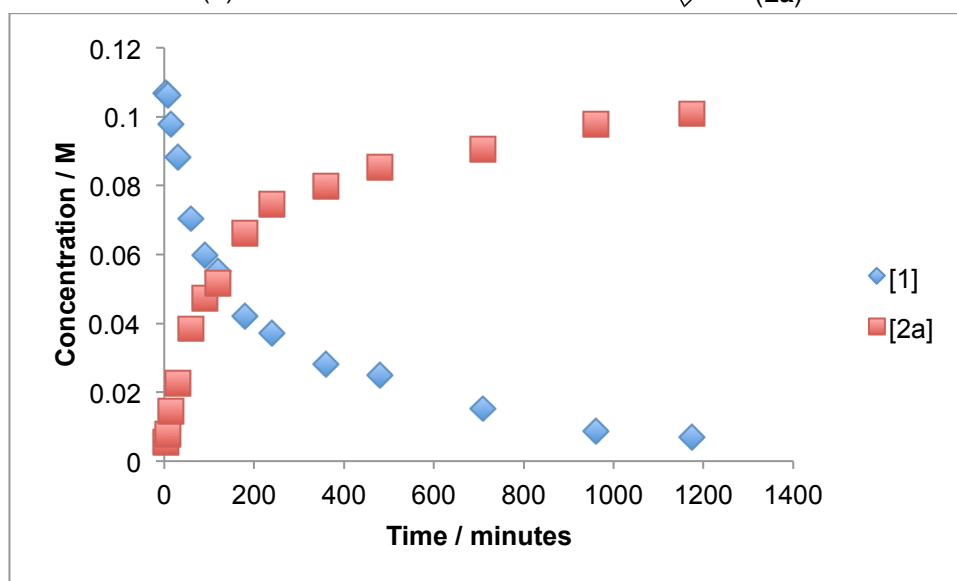
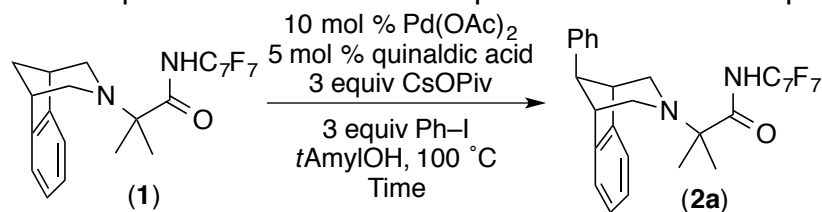
Kinetic Analysis of azabicycloalkane 1:

General Procedure D: Reaction conditions for kinetic studies. Under ambient conditions, if ligand was used, a 0.02 M stock solution of picolinic acid (12.3 mg picolinic acid dissolved in 5 mL of MeOH) or quinaldic acid (17.3 mg quinaldic acid dissolved in 5 mL of DCM) was prepared. An aliquot of this solution was transferred to a vial (4 mL capacity, 75 μ L, 0.0015 mmol ligand, 5 mol %). MeOH was removed by heating the open vial to 68 $^{\circ}$ C for 10 minutes or DCM was removed by heating the open vial to 45 $^{\circ}$ C for 5 minutes. To the concentrated carboxylate ligand, a Pd(OAc)₂ aliquot (150 μ L, 0.003 mmol Pd, 10 mol %) of a 0.02 M stock solution (23 mg Pd(OAc)₂ in 5 mL of DCM) was added. DCM was removed by gently heating the open vial to 45 $^{\circ}$ C for 5 minutes. To the vial containing the resulting solid, substrate **1** (13.8 mg, 0.03 mmol, 1 equiv) and CsOPiv (21.1 mg, 0.09 mmol, 3 equiv) were added, followed by PhI (10 μ L, 0.09 mmol, 3 equiv) and *t*AmyOH (0.25 mL). The vial was equipped with a stirbar, tightly sealed with a Teflon-lined screw cap and heated to 100 $^{\circ}$ C in a preheated aluminum block. At the desired reaction time (measured by a stopwatch), the reaction was flash-cooled in a liquid nitrogen bath until frozen solid (35 seconds). The reaction was then allowed to warm up to room temperature and diluted with DCM (2.5 mL). Hydrazine monohydrate (50 μ L) was added and the solution was vigorously stirred for 15 minutes. A 0.2 M stock solution of 1,3,5-trimethoxybenzene (168 mg, 1 mmol) dissolved in DCM (5 mL) was prepared. An aliquot of this solution (150 μ L, 0.03 mmol) was added to the reaction as the GC internal standard. The reaction solution was then filtered through a pipette

packed with Celite and was analyzed by GC-FID. Yields and concentrations of **1** and **2a** were used to obtain reaction rate profiles and initial rates.

Rate profile of **1** with 5 mol % quinaldic acid

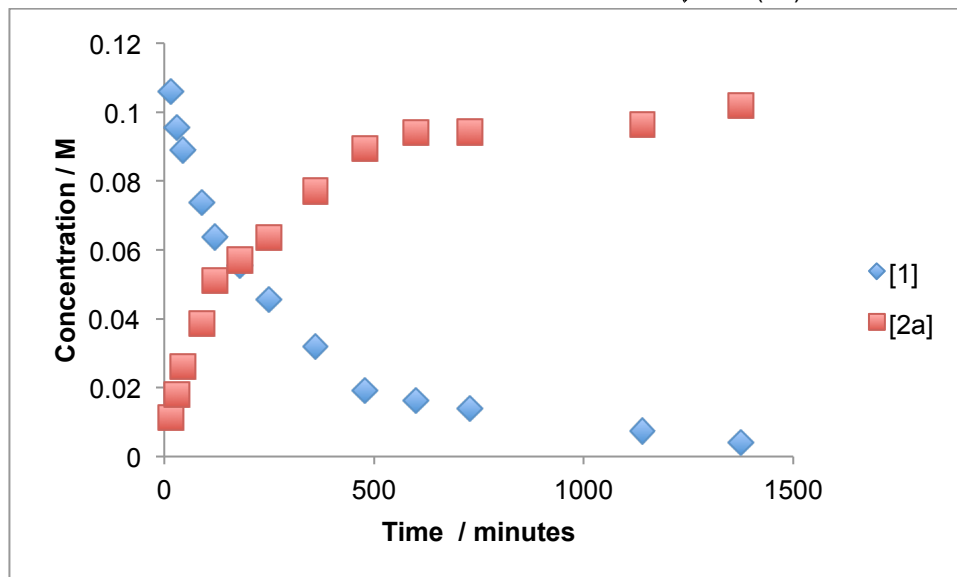
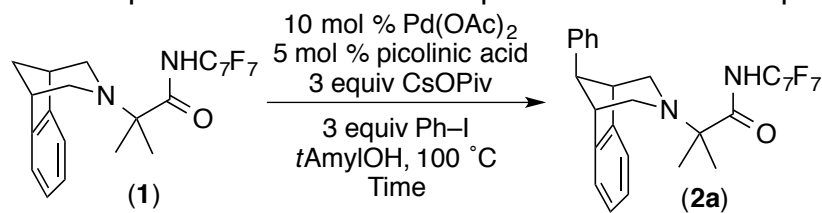
Figure 5.17. Rate profile of **1** and **2a** in the presence of 5 mol % quinaldic acid.



Conditions: **1** (0.12 M), Pd(OAc)₂ (0.012 M), CsOPiv (0.36 M), PhI (0.36 M), quinaldic acid (0.006 M), 0.25 mL *t*AmyIOH, 100 °C.

Rate profile of **1** with 5 mol % picolinic acid

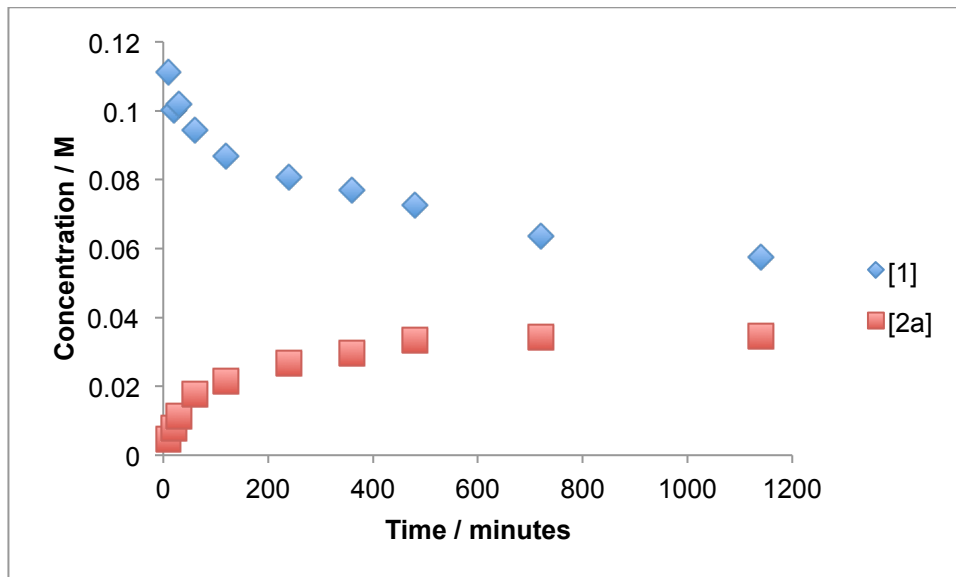
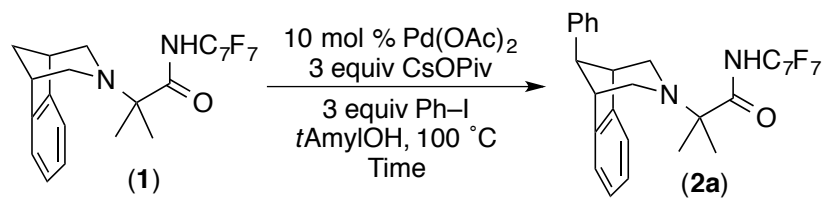
Figure 5.18. Rate profile of **1** and **2a** in the presence of 5 mol % picolinic acid.



Conditions: **1** (0.12 M), Pd(OAc)₂ (0.012 M), CsOPiv (0.36 M), PhI (0.36 M), picolinic acid (0.006 M), 0.25 mL *t*AmylOH, 100 °C.

Rate profile of **1** without ligand additive

Figure 5.19. Rate profile of **1** and **2a** without ligand.

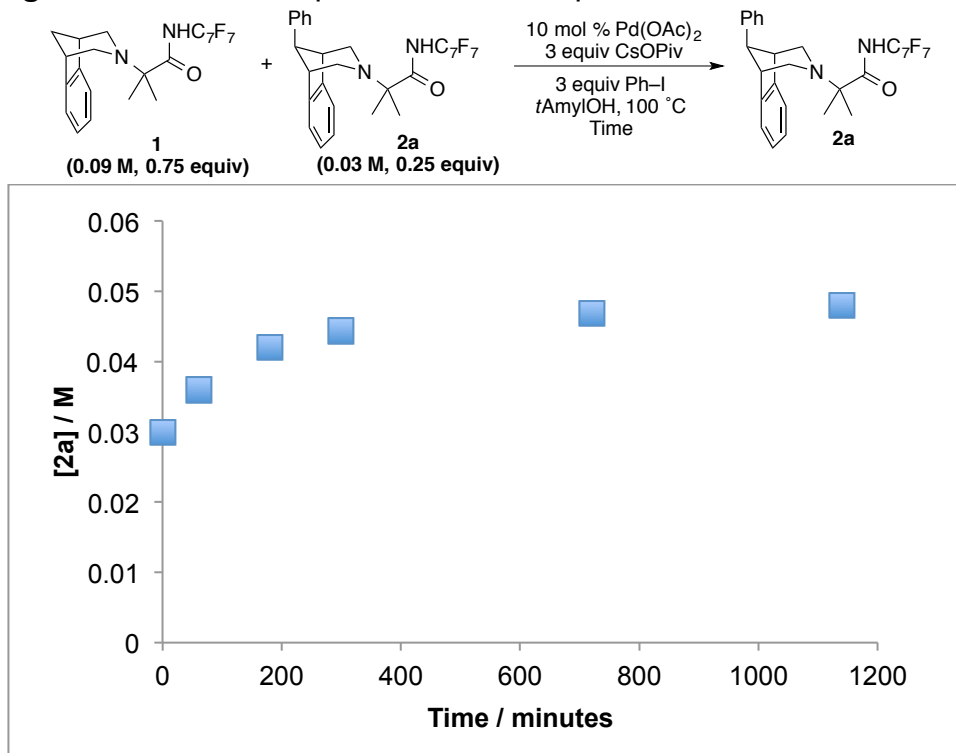


Conditions: **1** (0.12 M), Pd(OAc)₂ (0.012 M), CsOPiv (0.36 M), PhI (0.36 M), 0.25 mL tAmylOH, 100 °C.

Product addition at the reaction onset

General Procedure D was used with the following modifications/details: To each vial, **1** (10.4 mg, 0.0225 mmol, 0.75 equiv, 0.9 M) and **2a** (4 mg, 0.0075 mmol, 0.25 equiv, 0.03 M) were added.

Figure 5.20. Reaction profile with added product at the reaction onset.



Conditions: **1** (0.09 M), **2a** (0.03 M), Pd(OAc)₂ (0.012 M), CsOPiv (0.36 M), PhI (0.36 M), 0.25 mL *t*AmylOH, 100 °C.

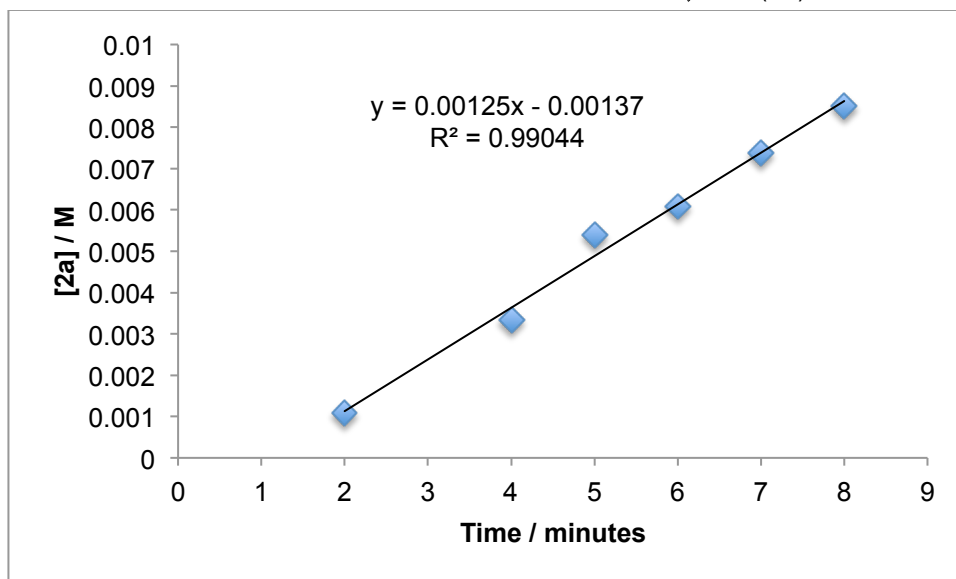
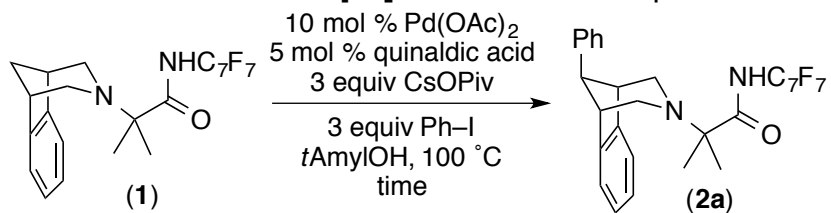
Addition of **2b** to the reaction onset

General Procedure D was used with the following modifications/details: To each vial, a varying amount of **2b** was added (1.7 mg–12.8 mg, 0.003–0.0225 mmol, 0.1–0.75 equiv, 0.012–0.09 M). The amount of **2b** is indicated in each entry of Table 5.3. Reactions were stopped after 45 minutes and immediately flash-cooled in a liquid nitrogen bath until frozen solid (35 seconds).

Initial rate with 5 mol% quinaldic acid

General Procedure D was used with quinaldic acid as the ligand.

Figure 5.21. Plot of initial rate of [2a] versus time with quinaldic acid additive.

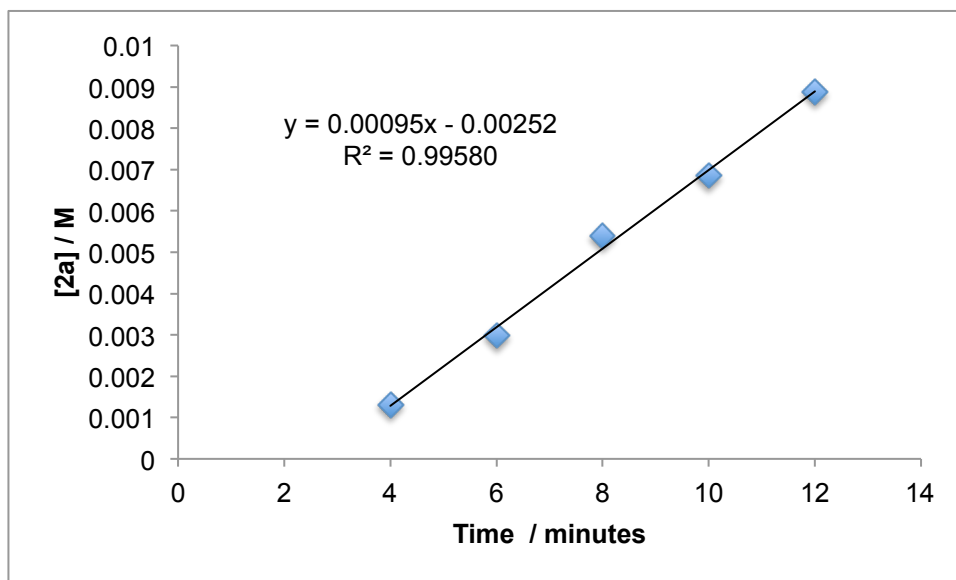
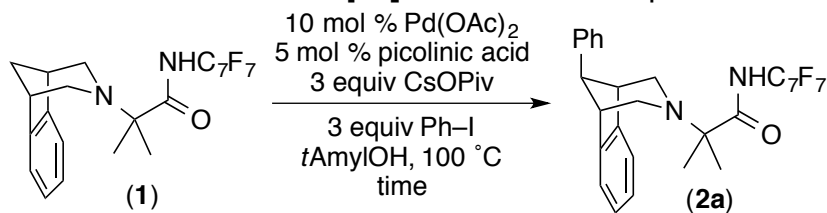


Conditions: **1** (0.12 M), Pd(OAc)₂ (0.012 M), CsOPiv (0.36 M), PhI (0.36 M), quinaldic acid (0.006 M), 0.25 mL *t*AmylOH, 100 °C.

Initial rate with 5 mol% picolinic acid

General Procedure D was used with picolinic acid as the ligand.

Figure 5.22. Plot of initial rate of [2a] versus time with picolinic acid additive.

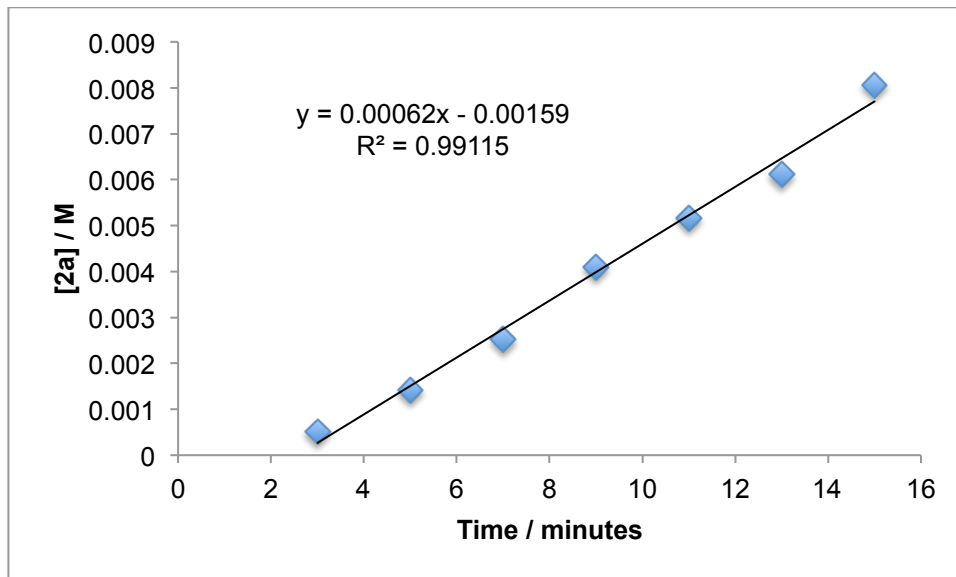
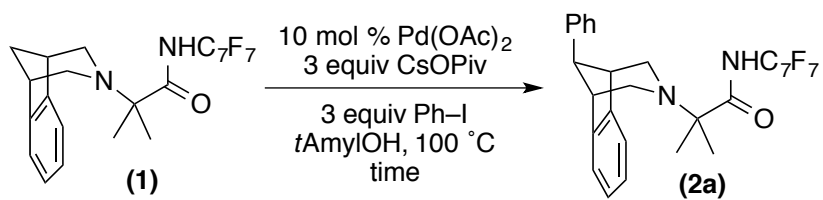


Conditions: **1** (0.12 M), Pd(OAc)₂ (0.012 M), CsOPiv (0.36 M), PhI (0.36 M), picolinic acid (0.006 M), 0.25 mL *t*AmylOH, 100 °C.

Initial rate without ligand

General Procedure D was used without ligand additives.

Figure 5.23. Plot of initial rate of [2a] versus time.

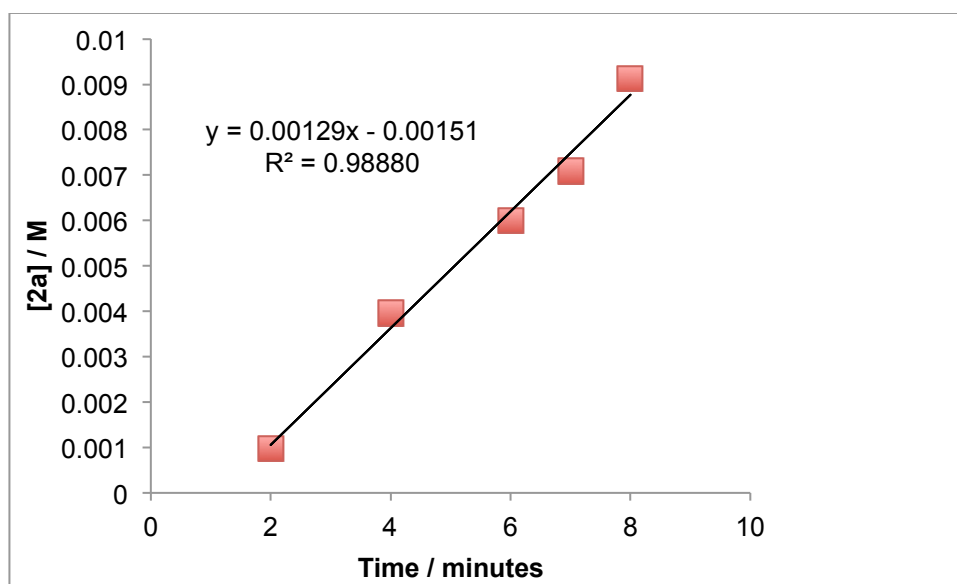
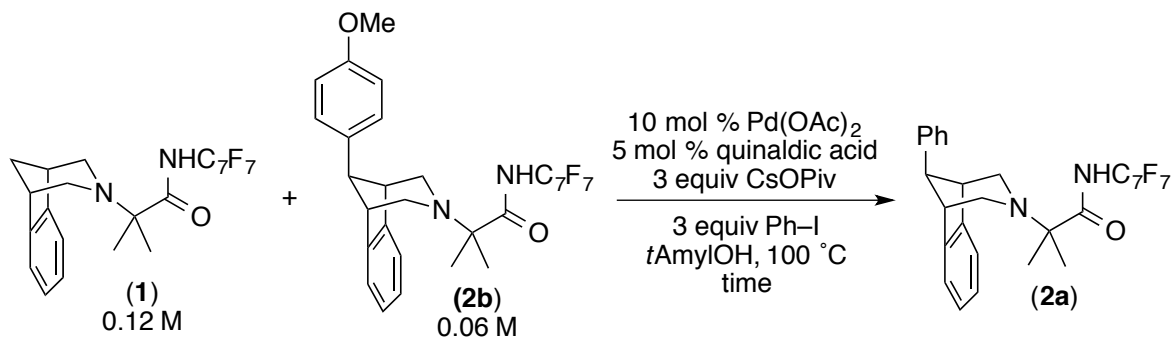


Conditions: **1** (0.12 M), Pd(OAc)₂ (0.012 M), CsOPiv (0.36 M), PhI (0.36 M), 0.25 mL tAmylOH, 100 °C.

Initial rate with addition of product **2b** and 5 mol% quinaldic acid

General Procedure D was used with quinaldic acid as the ligand. Additionally, **2b** (8.5 mg, 0.015 mmol, 0.5 equiv, 0.06 M) was added to each reaction.

Figure 5.24. Initial rate plot of [**2a**] versus time with quinaldic acid in the presence of 0.06 M **2b**.

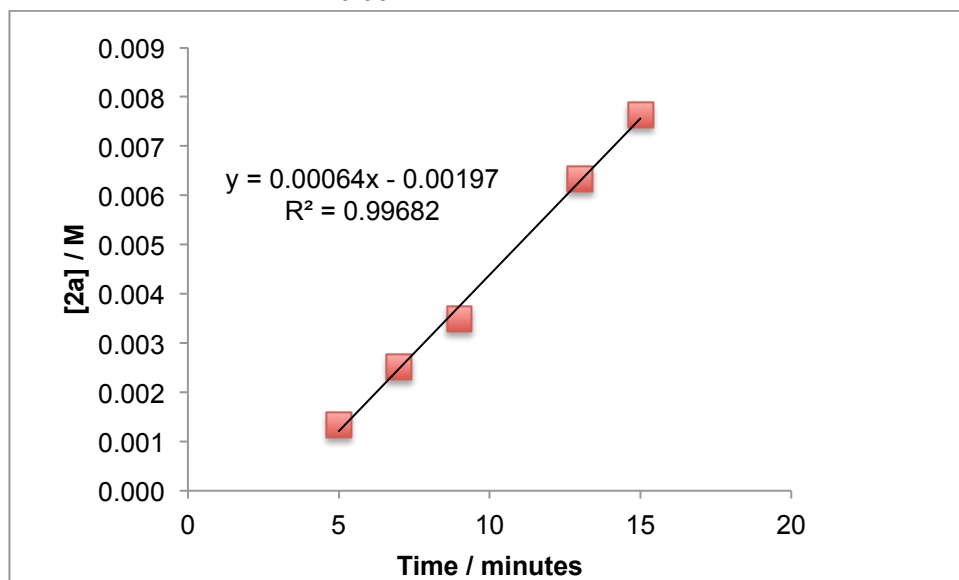
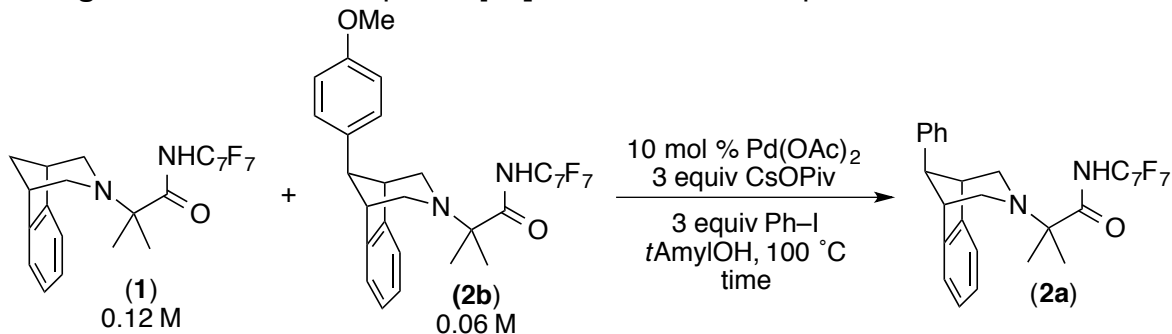


Conditions: **1** (0.12 M), **2b** (0.06 M), Pd(OAc)₂ (0.012 M), CsOPiv (0.36 M), PhI (0.36 M), quinaldic acid (0.006 M), 0.25 mL tAmylOH, 100 °C.

Initial rate with addition of product 2b and without ligand

General procedure D was used without ligand additive. Additionally, **2b** (8.5 mg, 0.015 mmol, 0.5 equiv, 0.06 M) was added to each reaction.

Figure 5.25. Initial rate plot of [2a] versus time in the presence of 0.06 M **2b**.

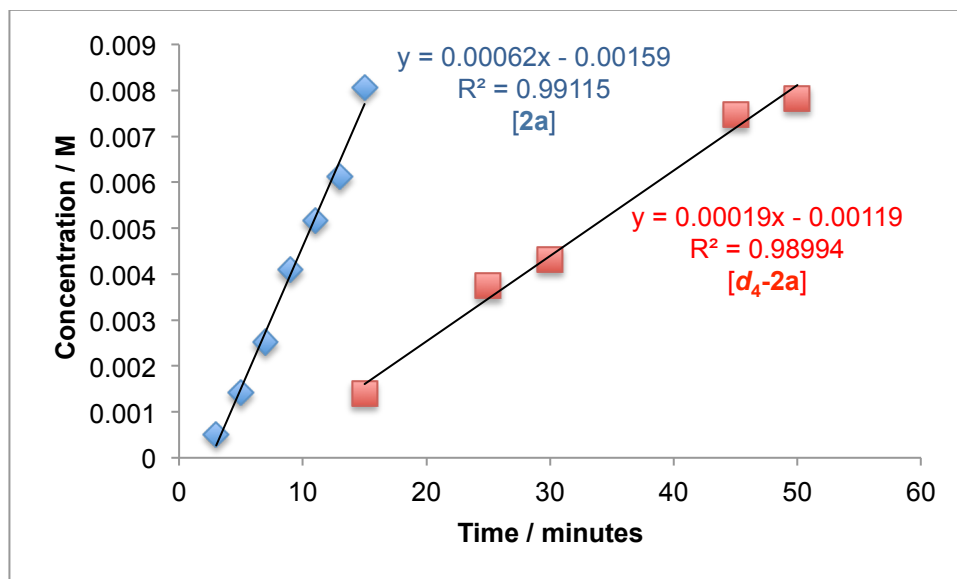
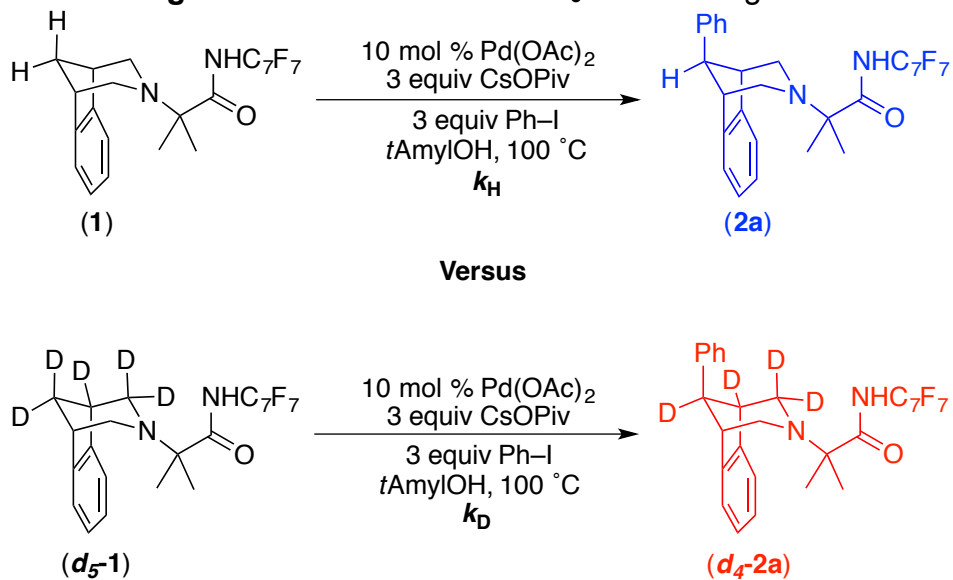


Conditions: **1** (0.12 M), **2b** (0.06 M), Pd(OAc)₂ (0.012 M), CsOPiv (0.36 M), PhI (0.36 M), 0.25 mL tAmylOH, 100 °C.

Kinetic Isotope Effect in substrate 1

KIE without ligand: Intermolecular KIE was performed following **General Procedure D** with addition of **1** (13.8 mg, 0.03 mmol, 1 equiv, 0.12 M) or **d₅-1** (14 mg, 0.03 mmol, 1 equiv, 0.12 M).

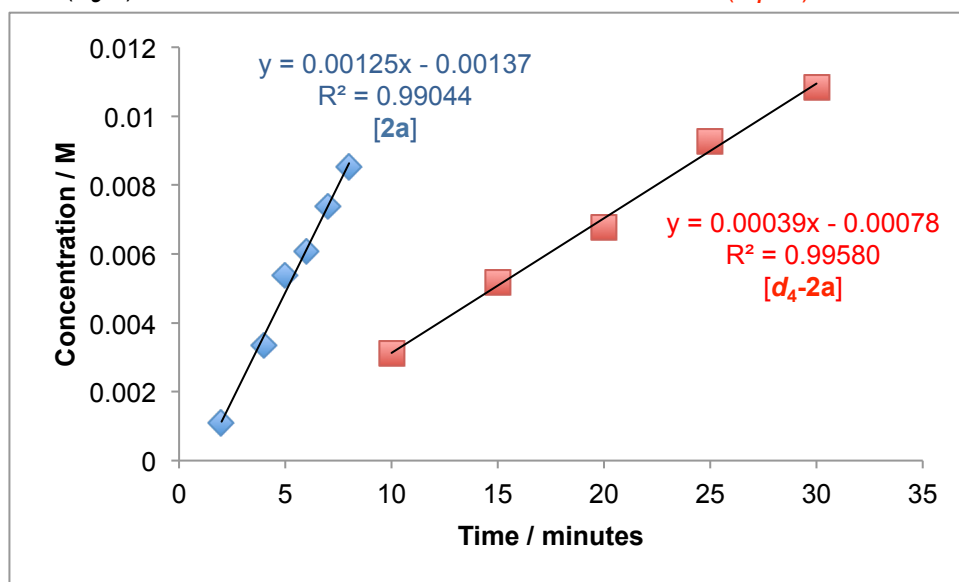
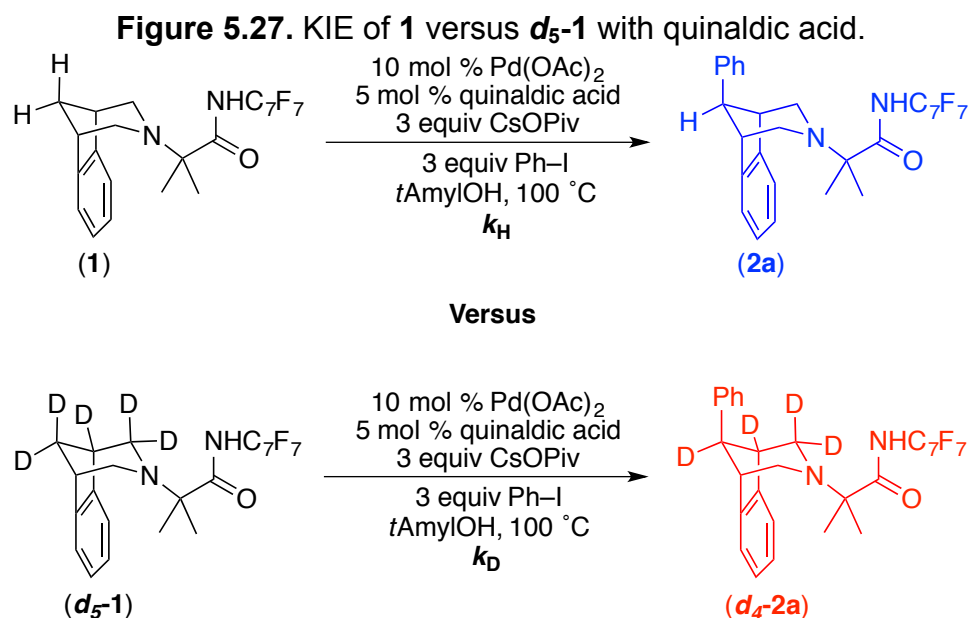
Figure 5.26. KIE of **1** versus **d₅-1** without ligand.



Conditions: **1** (0.12 M) or **d₅-1** (0.12 M), Pd(OAc)₂ (0.012 M), CsOPiv (0.36 M), PhI (0.36 M), 0.25 mL tAmylOH, 100 °C.

$$KIE = \frac{k_H}{k_D} = \frac{0.00062}{0.00019} = 3.3$$

KIE with 5 mol% quinaldic acid: Intermolecular KIE was performed following **General Procedure D** using quinaldic acid and with addition of **1** (13.8 mg, 0.03 mmol, 1 equiv, 0.12 M) or **d₅-1** (14 mg, 0.03 mmol, 1 equiv, 0.12 M).



Conditions: **1** (0.12 M) or **d₅-1** (0.12 M), Pd(OAc)₂ (0.012 M), CsOPiv (0.36 M), PhI (0.36 M), quinaldic acid (0.006 M), 0.25 mL tAmylOH, 100 °C.

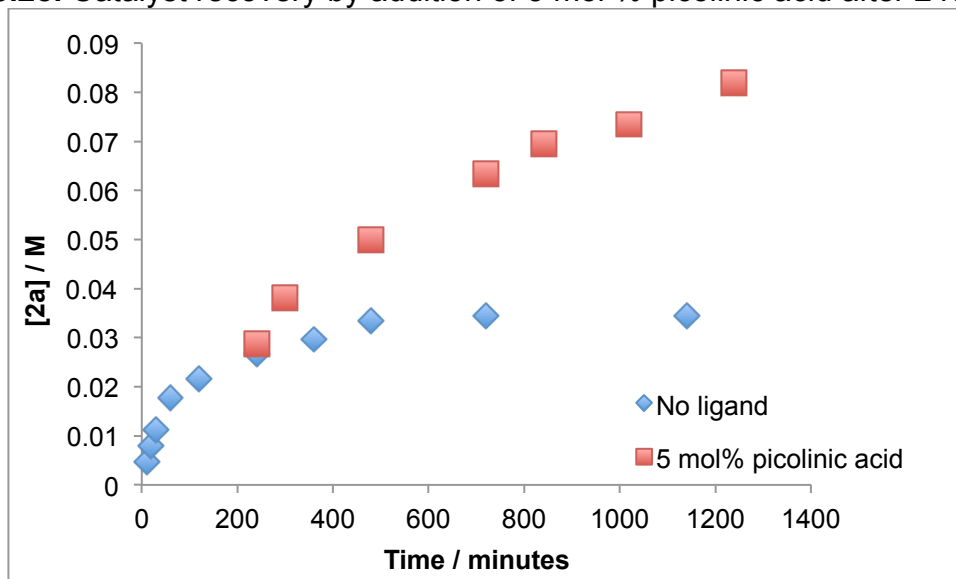
$$KIE = \frac{k_H}{k_D} = \frac{0.00125}{0.00039} = 3.2$$

Catalyst recovery studies

General Procedure E: Under ambient conditions, if ligand was used, a 0.02 M stock solution of picolinic acid (12.3 mg picolinic acid dissolved in 5 mL of MeOH) or quinaldic acid (17.3 mg quinaldic acid dissolved in 5 mL of DCM) was prepared. An aliquot of this solution was transferred to a vial (4 mL capacity, 75 μ L, 0.0015 mmol ligand, 5 mol %). MeOH was removed by heating the open vial to 68 $^{\circ}$ C for 10 minutes or DCM was removed by heating the open vial to 45 $^{\circ}$ C for 5 minutes. To the concentrated carboxylate ligand, a Pd(OAc)₂ aliquot (150 μ L, 0.003 mmol Pd, 10 mol %) of a 0.02 M stock solution (23 mg Pd(OAc)₂ in 5 mL of DCM) was added. DCM was removed by gently heating the open vial to 45 $^{\circ}$ C for 5 minutes. To the vial containing the resulting solid, substrate **1** (13.8 mg, 0.03 mmol, 1 equiv) and CsOPiv (21.1 mg, 0.09 mmol, 3 equiv) were added, followed by PhI (10 μ L, 0.09 mmol, 3 equiv) and *t*AmylOH (0.25 mL). The vial was equipped with a stirbar, sealed with a Teflon-lined screw cap and heated to 100 $^{\circ}$ C in a preheated aluminum block. After four hours (240 minutes), the reaction was removed from the heating source and cooled to room temperature. The reaction mixture was opened to air and solid quinaldic acid (0.260 mg, 0.0015 mmol, 5 mol %) OR picolinic acid (0.19 mg, 0.0015 mmol, 5 mol %) was added (ligand was weighed on a Sartorius ME36S microgram analytical balance). The reaction was then reheated to 100 $^{\circ}$ C. At the desired reaction time (measured by a stopwatch), the reaction was cooled to room temperature and diluted with DCM (2.5 mL). Hydrazine monohydrate (50 μ L) was added and the solution was vigorously stirred for 15 minutes. A 0.2 M stock solution of 1,3,5-trimethoxybenzene (168 mg, 1 mmol) dissolved in DCM (5 mL) was prepared. An aliquot of this solution (150 μ L, 0.03 mmol) was added to the reaction as the GC internal standard. The reaction solution was then filtered through a pipette packed with Celite and was analyzed by GC-FID. The concentration of **2a** over time was used to plot the reaction profiles of Figure 5.13 and Figure 5.28.

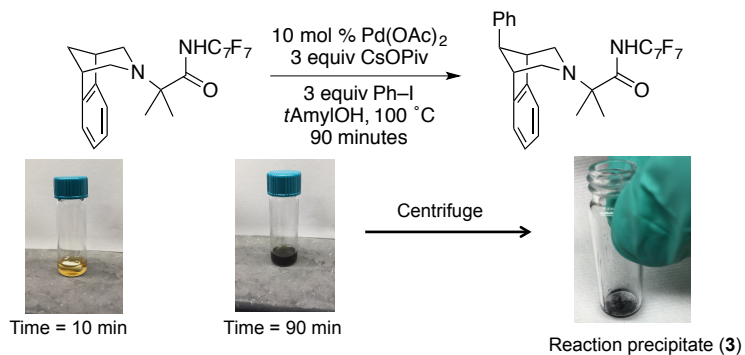
Catalyst recovery with picolinic acid

Figure 5.28. Catalyst recovery by addition of 5 mol % picolinic acid after 240 minutes.



Conditions: **1** (0.03 mmol, 0.12 M), Pd(OAc)₂ (0.012 M), CsOPiv (0.36 M), PhI (0.36 M), 0.25 mL *t*AmylOH, 100 °C, 240 minutes. Then, add picolinic acid (0.006 M) and heat to 100 °C.

Reactivity of Pd species 3

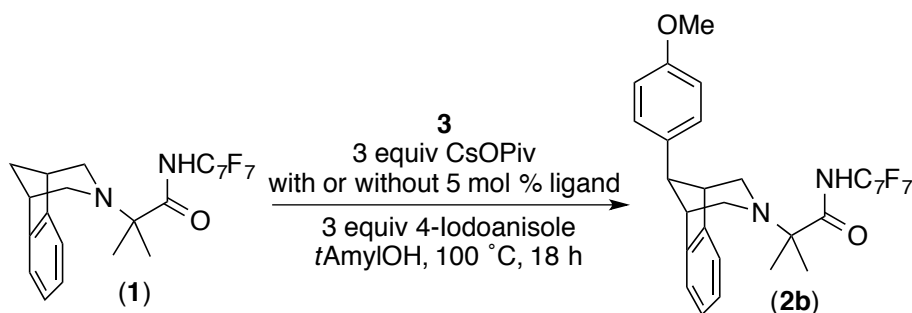


Isolation Procedure for 3: Under ambient conditions, a 0.02 M stock solution of Pd(OAc)₂ (23 mg, 0.1 mmol) dissolved in DCM (5 mL) was prepared. An aliquot of this solution was transferred to a vial (4 mL capacity, 150 μ L, 0.003 mmol Pd, 10 mol %). DCM was removed by gently heating the open vial to 45 °C for 5 minutes. To the concentrated Pd(OAc)₂, substrate **1** (13.8 mg, 0.03 mmol, 1 equiv) and CsOPiv (21.1 mg, 0.09 mmol, 3 equiv) were added, followed by PhI (10 μ L, 0.09 mmol, 3 equiv) and *t*AmylOH (0.25 mL). The vial was equipped with a stirbar, sealed with a Teflon-lined screw cap and heated to 100 °C in a preheated aluminum block. During the course of

90 minutes the reaction color changed from bright yellow to black. At this point, the reaction was removed from the heating source and cooled to room temperature. The stirbar was removed from the vial with a magnetic retriever. The vial was resealed and centrifuged (5000 rpm, 5 minutes). The black precipitate (**3**) settled to the bottom of the vial and the supernatant was carefully removed with a pipette. The precipitate (**3**) was washed with fresh *t*AmylOH (0.1 mL), re-centrifuged, and solvent was removed with a syringe. The remaining precipitate (**3**) was used for subsequent reactions.

Note: If the supernatant was used for subsequent reactions, the supernatant was first passed through a pipette packed with a small piece of glass fiber filter paper.

Reactions with isolated black precipitate **3**:



To the vial containing precipitate **3**, if indicated in Figure 5.14 or Table 5.5, solid quinaldic acid (0.260 mg, 0.0015 mmol, 5 mol%) or picolinic acid (0.190 mg, 0.0015 mmol, 5 mol%) were added (ligand was weighed on a Sartorius ME36S microgram analytical balance). Solid substrate **1** (13.8 mg, 0.03 mmol, 1 equiv), CsOPiv (21.1 mg, 0.09 mmol, 3 equiv) and 4-iodoanisole (21 mg, 0.09 mmol, 3 equiv) were added. To this mixture, *t*AmylOH (0.25 mL) was added. The vial was equipped with a stirbar, sealed with a Teflon-lined screw cap and heated to 100 °C in a preheated aluminum block. After 18 hours, the reaction was cooled to room temperature and diluted with DCM (2.5 mL). Hydrazine monohydrate (50 μ L) was added and the solution was vigorously stirred for 15 minutes. A 0.2 M stock solution of 1,3,5-trimethoxybenzene (168 mg, 1 mmol) dissolved in DCM (5 mL) was prepared. An aliquot of this solution (150 μ L, 0.03 mmol) was added to the reaction as the GC internal standard. The reaction solution was then filtered through a pipette packed with Celite and was analyzed by GC-FID. Yields of **2b** are shown in Table 5.5 along with reaction details.

Reaction with supernatant after removal of precipitate 3:

The supernatant from **Isolation Procedure for 3** was also further reacted as follows: To the vial containing the supernatant, if indicated in Table 5.5, solid quinaldic acid (0.260 mg, 0.0015 mmol, 5 mol %) or picolinic acid (0.190 mg, 0.0015 mmol, 5 mol %) were added (ligand was weighed on a Sartorius ME36S microgram analytical balance). Additional CsOPiv (14 mg, 0.06 mmol, 2 equiv) and PhI (3.5 μ L, 0.03 mmol, 1 equiv) were added. The vial was equipped with a stirbar, sealed with a Teflon-lined screw cap and heated to 100 °C in a preheated aluminum block. After 18 hours, the reaction was cooled to room temperature and diluted with DCM (2.5 mL). Hydrazine monohydrate (50 μ L) was added and the solution was vigorously stirred for 15 minutes. A 0.2 M stock solution of 1,3,5-trimethoxybenzene (168 mg, 1 mmol) dissolved in DCM (5 mL) was prepared. An aliquot of this solution (150 μ L, 0.03 mmol) was added to the reaction as the GC internal standard. The reaction solution was then filtered through a pipette packed with Celite and was analyzed by GC-FID. Yield of **2a** is shown in Table 5.5 along with reaction details.

Table 5.5. Experiments with precipitate **3** and supernatant.

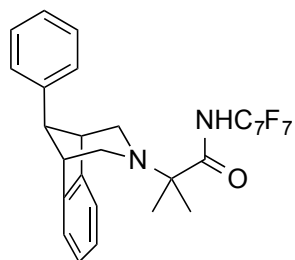
Entry	Ligand		Conversion	Yield 2a	Yield 2b
1	----	3	20%	---	10%
2	quinaldic acid	3	81%	---	47%
3	picolinic acid	3	71%		60%
4	----	supernatant	61%	39%	---
5	quinaldic acid	supernatant	96%	73%	---
6	picolinic acid	supernatant	77%	56%	---

Conditions shown above.

C–H Arylation of substrate **1**

General Procedure F: Isolation of 2a and 2b. A 4-mL vial was charged with solid substrate **1** (115.1 mg, 0.25 mmol, 1 equiv), Pd(OAc)₂ (5.6 mg, 0.025 mmol, 10 mol %), CsOPiv (176 mg, 0.75 mmol, 3 equiv), quinaldic acid (2.2 mg, 0.013 mmol, 5 mol %), iodoarene (0.075 mmol, 3 equiv) and *t*AmylOH (2.1 mL, 0.12 M). The vial was equipped with a magnetic stir bar, sealed with a Teflon-lined screw cap, and heated to an external temperature of 100 °C. After 18 h, the reaction was cooled to room temperature and

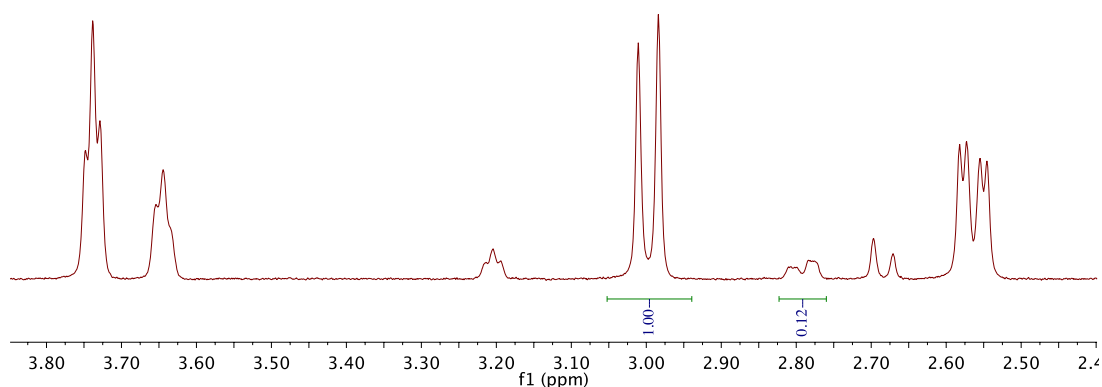
diluted with DCM (1 mL). Hydrazine hydrate (0.7 mL) was added to the solution. The mixture was allowed to stir for 30 min at room temperature to remove Pd from the product. The mixture was filtered through Celite and washed with DCM (10 mL). The volatiles were removed by rotary evaporation and the residue was purified via column chromatography (0% to 10% EtOAc in hexanes) affording the desired product. See each substrate for specific notes.



(**2a**)

Reaction conditions 1: Compound **2a** was isolated in 67% yield as an inseparable mixture with starting material following **general procedure F**.

The yield for compound **2a** was determined by isolating a mixture of recovered starting material **1** and compound **2a** via column chromatography (5% EtOAc in hexanes). The mixture was analyzed by ¹H NMR spectroscopy to determine the ratio of **1:2a** (ca. 0.12:1). This ratio, in combination with the isolated mass of the mixture and the respective molecular masses, was used to determine the yield of **2a** based on the mixture. An excerpt of the NMR used to determine the ratio is below:



Reaction conditions 2: At 120 °C following **general procedure F**, complete conversion of **1** is observed after 18 hours (0.33 mmol scale). Under these modified conditions, pure product **2a** was isolated in 77% yield as a white solid.

Reaction conditions 3: Using previously reported conditions¹⁷ with addition of 20 mol % quinaldic acid, compound **2a** was isolated in 82% yield as a white solid.

Purification by column chromatography (0% to 10% EtOAc in hexanes).

MP: 188-189 °C

R_f: 0.31 (10% EtOAc in hexanes)

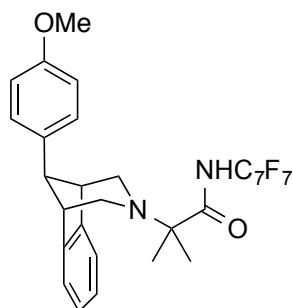
¹H NMR (400 MHz, Chloroform-*d*) δ 7.49–7.37 (m, 3H), 7.32 (m, 2H), 7.30–7.23 (multiple peaks, 3H), 7.12 (m, 2H), 3.74 (m, 2H), 3.65 (m, 1H), 3.00 (d, *J* = 10.7 Hz, 2H), 2.56 (dd, *J* = 10.9, 4.0 Hz, 2H), 1.01 (s, 6H).

¹³C NMR (176 MHz, Chloroform-*d*) δ 176.04, 146.07, 138.93, 128.91, 128.29, 126.78, 126.11, 121.72, 63.58, 51.80, 43.72, 42.43, 21.41.

The carbon resonances corresponding to the perfluoroarene (C₇F₇) in this compound appear as a complex series of multiplets between 105 ppm to 155 ppm as a result of ¹³C/¹⁹F coupling. Due to the complexities of the system, the peaks are not listed. ¹⁹F NMR and HRMS were used to confirm the presence of this ring system.

¹⁹F NMR (376 MHz, Chloroform-*d*) δ –56.08 (t, *J* = 21.7 Hz, 3F), –141.52 (m, 2F), –142.99 (m, 2F).

HRMS (ESI+) [M+H]⁺ Calcd. for C₂₈H₂₄F₇N₂O: 537.1771; Found: 537.1772.



Reaction conditions 1: Compound **2b** was isolated in 68% yield following **general procedure F**.

Reaction conditions 2: At 120 °C following **general procedure F**, complete conversion of **1** is observed after 18 hours (0.33 mmol scale). Under these modified conditions, pure product **2b** was isolated in 81% yield as a white solid.

NMR characterization matches the literature report.¹⁷

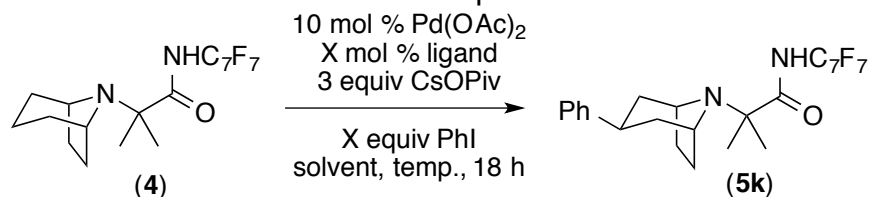
C–H Arylation of 8-azabicyclo[3.2.1]octane (tropane) **4**:

Reaction optimization for tropane **4**.

General procedure G: Under ambient conditions, a 0.02 M stock solution of picolinic acid (12.3 mg picolinic acid dissolved in 5 mL of MeOH) was prepared. An aliquot of this solution was transferred to a vial (4 mL capacity, 75 μ L, 0.0015 mmol ligand, 5 mol %). MeOH was removed by heating the open vial to 68 $^{\circ}$ C for 10 minutes. To the concentrated picolinic acid, a Pd(OAc)₂ aliquot (150 μ L, 0.003 mmol Pd, 10 mol %) of a 0.02 M stock solution (23 mg of Pd(OAc)₂ in 5 mL of DCM) was added. DCM was removed by gently heating the open vial to 45 $^{\circ}$ C for 5 minutes. To the concentrated reaction mixture, solid substrate **4** (12.4 mg, 0.03 mmol, 1 equiv), CsOPiv (21.1 mg, 0.09 mmol, 3 equiv) and PhI (3–45 equiv) were added. The reaction mixture was then diluted with *t*AmylOH (0.25 mL, if indicated in Table 5.6). The vial was equipped with a stirbar, sealed with a Telfon-lined screw cap and heated to the indicated temperature in Table 5.6 in a preheated aluminum block. After 18 hours, the reaction was cooled to room temperature and diluted with DCM (2.5 mL). Hydrazine monohydrate (50 μ L) was added and the solution was vigorously stirred for 15 minutes. A 0.2 M stock solution of 1,3,5-trimethoxybenzene (168 mg, 1 mmol) dissolved in DCM (5 mL) was prepared. An aliquot of this solution (150 μ L, 0.03 mmol) was added to the reaction as the GC internal standard. The reaction solution was then filtered through a pipette packed with Celite and was analyzed by GC-FID. Yield of **5k** is uncalibrated.

In the cases where quinaldic acid was used, a 0.02 M stock solution of quinaldic acid (17.3 mg in 5 mL of DCM) was prepared and an aliquot (75 μ L, 0.0015 mmol, 5 mol %) was added to the 4-mL vial.

Different volumes of ligand stock solution were used depending on the amount of ligand indicated in each entry of Table 5.6.

Table 5.6. Reaction optimization for **4**.

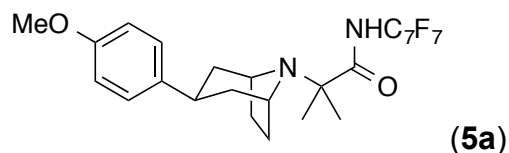
Entry	Ligand (mol %) ^a	Temp	Solvent	PhI (equiv)	Conv.	Yield 5k ^b
1	PA (5)	150 °C	neat	45	> 99%	41
2	PA (10)	150 °C	neat	45	87%	47
3	QA (5)	150 °C	neat	45	97%	31
4	QA (20)	150 °C	neat	45	94%	33
5	PA (5)	140 °C	neat	45	91%	51
6	PA (10)	140 °C	neat	45	51%	21
7	PA (5)	130 °C	neat	45	74%	38
8	PA (10)	130 °C	neat	45	53%	28
9	PA (5)	140 °C	<i>t</i> AmylOH	45	72%	26
10	PA (5)	140 °C	<i>t</i> AmylOH	15	96%	24
11	PA (5)	140 °C	<i>t</i> AmylOH	3	94%	18
12	-----	140 °C	neat	45	47%	4

Conditions from **general procedure G**. ^a PA = picolinic acid; QA = quinaldic acid. ^b Uncalibrated GC yields.

C–H Arylation of Tropane: Scope in Aryl Iodide.

General Procedure H: Under ambient conditions, a stock solution of picolinic acid (24.6 mg, 0.2 mmol) was prepared in methanol (2 mL). An aliquot of this solution was transferred to a vial (4 mL capacity, 50 μ L, 0.005 mmol picolinic acid, 5 mol %). Methanol was removed by heating the open vial to 70 °C for approximately 15 minutes (Note: leftover methanol can lead to Pd-catalyst decomposition). To the concentrated picolinic acid, solid substrate **6** (41.2 mg, 0.1 mmol, 1 equiv), Pd(OAc)₂ (2.3 mg, 0.01 mmol, 10 mol %), CsOPiv (70.2 mg, 0.3 mmol, 3 equiv), and iodoarene (45 equiv) were added. The vial was equipped with a magnetic stirbar, sealed with a Teflon-lined screw cap, and heated to an external temperature of 140 °C. After 18 h, the reaction was cooled to room temperature and diluted with DCM (2.5 mL). Hydrazine hydrate (0.4 mL) was added to the solution. The mixture was allowed to stir for 30 min at room temperature to remove Pd from the product. The mixture was filtered through Celite and washed with DCM (10 mL). The volatiles were removed by rotary evaporation, and the

residue was purified via column chromatography (commonly mixtures of EtOAc:Hex or THF:Hex) affording the desired product. See each substrate for specific notes.



Compound **5a** was isolated in 49% yield as a yellow semi-solid following **general procedure H**.

Purification by column chromatography (silica gel; 0% EtOAc to 5% EtOAc in hexanes)

R_f: 0.1 (5% EtOAc in Hexanes)

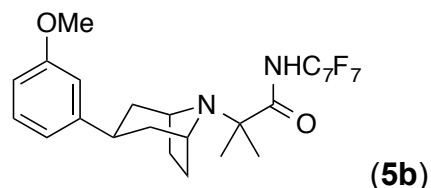
¹H NMR (401 MHz, Chloroform-*d*) δ 9.79 (br s, 1H), 7.13 (d, *J* = 8.6 Hz, 2H), 6.84 (d, *J* = 8.6 Hz, 2H), 3.77 (s, 3H), 3.57 (app. s, 2H), 2.95 (tt, *J* = 10.8, 4.0 Hz, 1H), 1.98–1.79 (multiple peaks, 8H), 1.37 (s, 6H).

¹³C NMR (176 MHz, Chloroform-*d*) δ 176.07, 158.20, 137.35, 128.04, 114.07, 63.96, 57.11, 55.43, 42.92, 34.72, 30.09, 23.90.

The carbon resonances corresponding to the perfluoroarene (C₇F₇) in this compound appear as a complex series of multiplets between 105 ppm to 155 ppm as a result of ¹³C/¹⁹F coupling. Due to the complexities of the system, the peaks are not listed. ¹⁹F NMR and HRMS were used to confirm the presence of this ring system.

¹⁹F NMR (377 MHz, Chloroform-*d*) δ -56.00 (t, *J* = 21.6 Hz, 3F), -141.08 (m, 2F), -143.59 (m, 2F).

HRMS (ESI⁺) [M+H]⁺ Calcd for C₂₅H₂₆F₇N₂O₂: 519.1877; Found: 519.1875.



Compound **5b** was isolated in 60% yield as a colorless oil following **general procedure H**. Purification by column chromatography (silica gel; 0% to 5% THF in hexanes).

R_f: 0.10 (5% THF in hexanes)

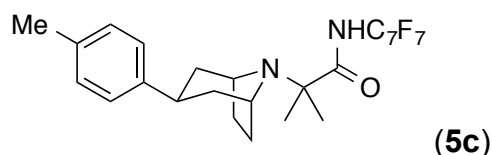
^1H NMR (500 MHz, Chloroform-*d*) δ 7.25 (t, J = 7.8 Hz, 1H), 6.84 (d, J = 7.8 Hz, 1H), 6.82–6.75 (multiple peaks, 2H), 3.82 (s, 3H), 3.62 (app. s, 2H), 3.01 (m, 1H), 2.04–1.82 (multiple peaks, 8H), 1.40 (s, 6H).

^{13}C NMR (176 MHz, Chloroform-*d*) δ 175.66, 159.53, 146.62, 129.27, 119.21, 113.01, 110.98, 63.59, 56.70, 54.91, 42.17, 35.25, 29.71, 23.50.

The carbon resonances corresponding to the perfluoroarene (C_7F_7) in this compound appear as a complex series of multiplets between 105 ppm to 155 ppm as a result of $^{13}\text{C}/^{19}\text{F}$ coupling. Due to the complexities of the system, the peaks are not listed. ^{19}F NMR and HRMS were used to confirm the presence of this ring system.

^{19}F NMR (377 MHz, Chloroform-*d*) δ -56.01 (t, J = 21.6 Hz, 3F), -141.10 (m, 2F), -143.60 (m, 2F).

HRMS (ESI $^+$) [$\text{M}+\text{H}$] $^+$ Calcd for $\text{C}_{25}\text{H}_{26}\text{F}_7\text{N}_2\text{O}_2$: 519.1877; Found: 519.1881.



Compound **5c** was isolated in 40% yield as a colorless oil solid following **general procedure H**.

Purification by column chromatography (silica gel; 0% to 100% DCM in hexanes), followed by a preparative TLC (silica gel; 10% THF in hexanes).

R_f : 0.37 (100% DCM).

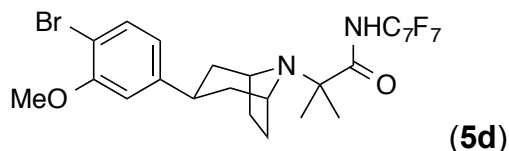
^1H NMR (700 MHz, Chloroform-*d*) δ 7.13 (app. s, 4H), 3.59 (app. s, 2H), 2.99 (m, 1H), 2.32 (s, 3H), 1.99–1.92 (multiple peaks, 2H), 1.90–1.82 (multiple peaks, 6H), 1.39 (s, 6H).

^{13}C NMR (176 MHz, Chloroform-*d*) δ 176.09, 142.24, 136.03, 129.36, 127.05, 63.94, 57.10, 42.76, 35.15, 30.08, 23.88, 21.12.

The carbon resonances corresponding to the perfluoroarene (C_7F_7) in this compound appear as a complex series of multiplets between 105 ppm to 155 ppm as a result of $^{13}\text{C}/^{19}\text{F}$ coupling. Due to the complexities of the system, the peaks are not listed. ^{19}F NMR and HRMS were used to confirm the presence of this ring system.

^{19}F NMR (377 MHz, Chloroform-*d*) δ -56.00 (t, J = 21.6 Hz, 3F), -141.14 (m, 2F), -143.57 (m, 2F).

HRMS (ESI⁺) [M+H]⁺ Calcd for C₂₅H₂₆F₇N₂O: 503.1928; Found: 503.1926.



Compound **5d** was isolated in 46% yield as a yellow oil following **general procedure H**. Purification by column chromatography (silica gel; 0% to 20% THF in hexanes).

R_f: 0.71 (20% THF in hexanes)

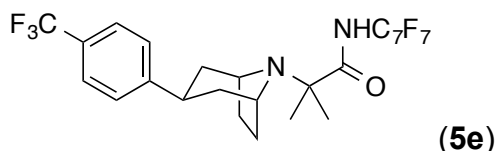
¹H NMR (700 MHz, Chloroform-*d*) δ 9.67 (br s, 1H), 7.45 (d, *J* = 8.1 Hz, 1H), 6.77 (app. s, 1H), 6.72 (dd, *J* = 8.1, 2.0 Hz, 1H), 3.90 (s, 3H), 3.61 (app. s, 2H), 2.99 (tt, *J* = 11.8, 6.2 Hz, 1H), 2.02–1.80 (m, 8H), 1.39 (s, 6H).

¹³C NMR (176 MHz, Chloroform-*d*) δ 175.75, 156.01, 146.29, 133.35, 120.49, 111.19, 109.39, 63.99, 56.99, 56.23, 42.54, 35.67, 30.06, 23.85.

The carbon resonances corresponding to the perfluoroarene (C₇F₇) in this compound appear as a complex series of multiplets between 105 ppm to 155 ppm as a result of ¹³C/¹⁹F coupling. Due to the complexities of the system, the peaks are not listed. ¹⁹F NMR and HRMS were used to confirm the presence of this ring system.

¹⁹F NMR (377 MHz, Chloroform-*d*) δ -55.99 (t, *J* = 21.7 Hz, 3F), -141.02 (m, 2F), -143.80 (m, 2F).

HRMS (ESI⁺) [M+H]⁺ Calcd for C₂₅H₂₅BrF₇N₂O₂: 597.0982; Found: 597.0977.



Compound **5e** was isolated in 47% yield as a white solid following **general procedure H**. Purification by column chromatography (silica gel; 5% THF in hexanes) followed by a preparative TLC (silica gel; 100% CHCl₃).

MP: 100-101 °C

R_f: 0.29 (100% CHCl₃)

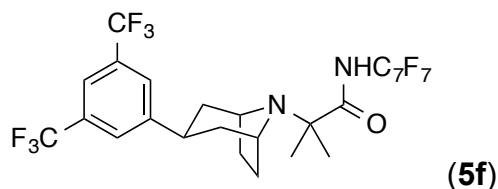
¹H NMR (400 MHz, Chloroform-*d*) δ 9.73 (br s, 1H), 7.55 (d, *J* = 8.1 Hz, 2H), 7.32 (d, *J* = 8.1 Hz, 2H), 3.61 (app. s, 2H), 3.06 (m, 1H), 2.04–1.76 (m, 8H), 1.38 (s, 6H).

^{13}C NMR (176 MHz, Chloroform-*d*) δ 175.64, 149.11, 128.68 (q, $J_{\text{C-F}} = 32.4$ Hz), 127.37, 125.47 (q, $J_{\text{C-F}} = 3.7$ Hz), 124.18 (q, $J_{\text{C-F}} = 271.8$ Hz), 63.83, 56.82, 42.19, 35.42, 29.91, 23.70.

The carbon resonances corresponding to the perfluoroarene (C_7F_7) in this compound appear as a complex series of multiplets between 105 ppm to 155 ppm as a result of $^{13}\text{C}/^{19}\text{F}$ coupling. Due to the complexities of the system, the peaks are not listed. ^{19}F NMR and HRMS were used to confirm the presence of this ring system.

^{19}F NMR (376 MHz, Chloroform-*d*) δ -56.02 (t, $J = 21.7$ Hz, 3F), -62.44 (s, 3F), -140.96 (m, 2F), -143.75 (m, 2F).

HRMS (ESI $^+$) $[\text{M}+\text{H}]^+$ Calcd for $\text{C}_{25}\text{H}_{23}\text{F}_{10}\text{N}_2\text{O}$: 557.1645; Found: 557.1644.



Compound **5f** was isolated in 44% yield as a colorless semi-solid following **general procedure H**. Purification by column chromatography to remove bulk of aryl iodide (silica gel; 5% THF in hexanes), followed by a preparative TLC (silica gel; 8% THF in hexanes). Significant impurities from the preparative TLC binder were observed by ^1H NMR, thus a short column was performed (silica gel; 100% CHCl_3).

R_f : 0.19 (5% THF in hexanes)

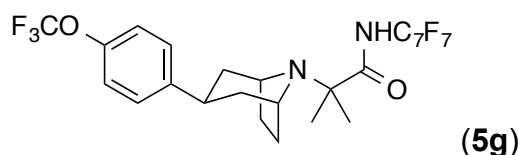
^1H NMR (500 MHz, Chloroform-*d*) δ 9.72 (s, 1H), 7.74 (s, 1H), 7.68 (s, 2H), 3.66 (app. s, 2H), 3.17 (tt, $J = 11.9, 5.9$ Hz, 1H), 2.09–1.78 (multiple peaks, 8H), 1.41 (s, 6H).

^{13}C NMR (126 MHz, Chloroform-*d*) δ 175.53, 147.69, 131.94 (q, $J = 32.9$ Hz), 127.47 (m), 123.51 (q, $J = 272.6$ Hz), 120.63 (m), 64.02, 56.84, 42.28, 35.61, 30.05, 23.84.

The carbon resonances corresponding to the perfluoroarene (C_7F_7) in this compound appear as a complex series of multiplets between 105 ppm to 155 ppm as a result of $^{13}\text{C}/^{19}\text{F}$ coupling. Due to the complexities of the system, the peaks are not listed. ^{19}F NMR and HRMS were used to confirm the presence of this ring system.

^{19}F NMR (471 MHz, Chloroform-*d*) δ -56.01 (t, $J = 21.5$ Hz, 3F), -62.88 (s, 6F), -140.97 (m, 2F), -143.97 (m, 2F).

HRMS (ESI $^+$) $[\text{M}+\text{H}]^+$ Calcd for $\text{C}_{26}\text{H}_{22}\text{F}_{13}\text{N}_2\text{O}$: 625.1519; found 625.1524.



Note: 20 mol % Pd(OAc)₂ was used for this substrate. Compound **5g** was isolated in 34% yield as a light yellow oil following **general procedure H**. Purification by column chromatography (silica gel; 0% to 100% DCM in hexanes).

R_f: 0.77 (100% DCM)

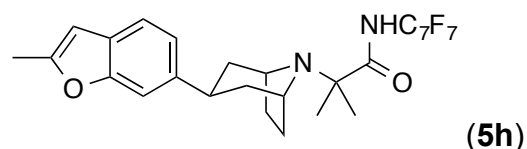
¹H NMR (401 MHz, Chloroform-*d*) δ 7.22 (m, 2H), 7.14 (m, 2H), 3.59 (app. s, 2H), 3.02 (tt, *J* = 11.9, 6.2 Hz, 1H), 2.02–1.76 (m, 8H), 1.37 (s, 6H).

¹³C NMR (176 MHz, Chloroform-*d*) δ 175.71, 147.58 (m), 143.73, 128.23, 121.05, 63.81, 56.84, 42.45, 34.88, 29.92, 23.72.

The carbon resonances corresponding to the perfluoroarene (C₇F₇) and CF₃O are not listed due to complexities in the region between 105 ppm and 150 ppm. ¹⁹F NMR and HRMS were used to confirm the presence of these groups.

¹⁹F NMR (377 MHz, Chloroform-*d*) δ –56.01 (t, *J* = 21.7 Hz, 3F), –57.96 (s, 3F), –140.95 (m, 2F), –143.70 (m, 2F).

HRMS (ESI⁺) [M+H]⁺ Calcd for C₂₅H₂₃F₁₀N₂O₂: 573.1594; found 573.1592.



Compound **5h** was isolated in 54% yield as a colorless oil following **general procedure H**. Purification by column chromatography (silica gel; 0% EtOAc to 10% EtOAc in hexanes).

R_f: 0.1 (5% EtOAc in hexanes)

¹H NMR (700 MHz, Chloroform-*d*) δ 9.88 (br s, 1H), 7.33 (s, 1H), 7.30 (m, 1H), 7.06 (dd, *J* = 8.4, 1.8 Hz, 1H), 6.32 (s, 1H), 3.61 (app. s, 2H), 3.09 (m, 1H), 2.44 (s, 3H), 2.02–1.83 (m, 8H), 1.40 (s, 6H).

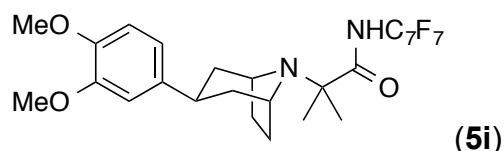
¹³C NMR (176 MHz, Chloroform-*d*) δ 176.11, 156.02, 153.62, 139.47, 129.51, 122.43, 118.21, 110.57, 102.58, 63.95, 57.17, 43.26, 35.57, 30.10, 23.89, 14.24.

The carbon resonances corresponding to the perfluoroarene (C₇F₇) in this compound appear as a complex series of multiplets between 105 ppm to 155 ppm as a result of

$^{13}\text{C}/^{19}\text{F}$ coupling. Due to the complexities of the system, the peaks are not listed. ^{19}F NMR and HRMS were used to confirm the presence of this ring system.

^{19}F NMR (376 MHz, Chloroform-*d*) δ -56.01 (t, J = 21.7 Hz, 3F), -141.15 (m, 2F), -143.59 (m, 2F).

HRMS (ESI⁺) [M+H]⁺ Calcd for C₂₇H₂₆F₇N₂O₂: 543.1877; found 543.1879.



Compound **5i** was isolated in 47% yield as a light yellow oil following **general procedure H**. Purification by column chromatography (silica gel; 0% to 20% THF in hexanes).

R_f: 0.07 (5% THF in hexanes)

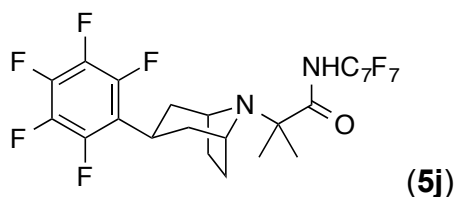
^1H NMR (400 MHz, Chloroform-*d*) δ 6.86–6.72 (multiple peaks, 3H), 3.89 (s, 3H), 3.86 (s, 3H), 3.60 (app. s, 2H), 2.96 (m, 1H), 2.03–1.76 (multiple peaks, 8H), 1.39 (s, 6H).

^{13}C NMR (176 MHz, Chloroform-*d*) δ 175.74, 148.90, 147.49, 137.77, 118.68, 111.29, 110.53, 63.80, 56.90, 55.91, 55.78, 42.69, 35.03, 29.90, 23.69.

The carbon resonances corresponding to the perfluoroarene (C₇F₇) in this compound appear as a complex series of multiplets between 105 ppm to 155 ppm as a result of $^{13}\text{C}/^{19}\text{F}$ coupling. Due to the complexities of the system, the peaks are not listed. ^{19}F NMR and HRMS were used to confirm the presence of this ring system.

^{19}F NMR (376 MHz, Chloroform-*d*) δ -55.97 (t, J = 21.6 Hz, 3F), -141.11 (m, 2F), -143.73 (m, 2F).

HRMS (ESI⁺) [M+H]⁺ Calcd for C₂₆H₂₈F₇N₂O₂: 549.1983; found 549.1990.



Compound **5j** was isolated in 42% yield as a colorless semi-solid following **general procedure H**.

Purification by short silica plug starting at 100% hexanes to remove excess aryl iodide, then 100% EtOAc to collect crude product. After, the crude product was purified by preparative TLC (silica gel; 100% CHCl₃).

R_f: 0.46 (100% CHCl₃)

¹H NMR (700 MHz, Chloroform-*d*) δ 9.73 (s, 1H), 3.62 (app. s, 2H), 3.50 (tt, *J* = 12.2, 6.0 Hz, 1H), 2.23 (app. t, *J* = 7.2 Hz, 2H), 2.00 (m, 2H), 1.86 (m, 2H), 1.75 (m, 2H), 1.38 (s, 6H).

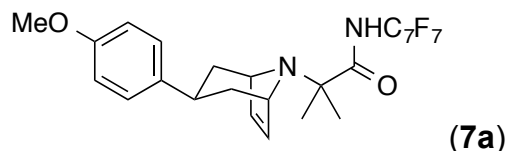
¹³C NMR (176 MHz, Chloroform-*d*) δ 175.86, 63.89, 56.82, 39.16, 29.82, 25.82, 23.79.

The carbon resonances corresponding to the perfluoroarenes (C₇F₇ and C₆F₅) in this compound appear as a complex series of multiplets between 105 ppm to 155 ppm as a result of ¹³C/¹⁹F coupling. Due to the complexities of these groups, the peaks are not listed. ¹⁹F NMR and HRMS were used to confirm the presence of both ring systems.

¹⁹F NMR (377 MHz, Chloroform-*d*) δ -56.04 (t, *J* = 21.7 Hz, 3F), -141.07 (m, 2F), -143.55 (app. d, *J* = 18.4 Hz, 2F), -143.85 (m, 2F), -157.06 (t, *J* = 21.0 Hz, 1F), -162.07 (m, 2F).

HRMS (ESI⁺) [M+H]⁺ Calcd for C₂₄H₁₉F₁₂N₂O: 579.1300; found: 579.1305.

C–H Arylation of other alicyclic amines:



Compound **7a** was isolated in 50% yield as a colorless semi-solid solid following **general procedure H**.

Purification by column chromatography (silica gel; 0% to 5% THF in hexanes).

R_f: 0.19 (5% THF in hexanes)

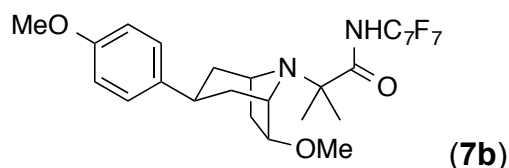
¹H NMR (401 MHz, Chloroform-*d*) δ 7.15 (d, *J* = 8.2 Hz, 2H), 6.85 (d, *J* = 8.2 Hz, 2H), 6.05 (app. s, 2H), 3.88 (app. s, 2H), 3.79 (s, 3H), 2.86 (m, 1H), 1.87–1.76 (multiple peaks, 4H), 1.29 (s, 6H).

¹³C NMR (176 MHz, Chloroform-*d*) δ 175.49, 158.16, 137.40, 130.64, 128.64, 113.99, 64.14, 61.44, 55.40, 35.86, 35.24, 24.20.

The carbon resonances corresponding to the perfluoroarene (C₇F₇) in this compound appear as a complex series of multiplets between 105 ppm to 155 ppm as a result of ¹³C/¹⁹F coupling. Due to the complexities of the system, the peaks are not listed. ¹⁹F NMR and HRMS were used to confirm the presence of this ring system.

¹⁹F NMR (377 MHz, Chloroform-*d*) δ -56.02 (t, *J* = 21.7 Hz, 3F), -141.07 (m, 2F), -143.55 (m, 2F).

HRMS (ESI⁺) [M+H]⁺ Calcd for C₂₅H₂₄F₇N₂O₂: 517.1721; found: 517.1718.



Compound **7b** was isolated in 40% yield as a colorless oil following **general procedure H**.

Purification by column chromatography (silica gel; 0% to 5% THF in hexanes). Minor impurities were observed by ¹H NMR, thus a second column chromatography was performed (silica gel; 2% EtOAc in DCM).

R_f: 0.42 (2% EtOAc in DCM).

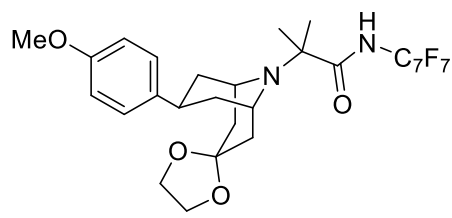
¹H NMR (401 MHz, Chloroform-*d*) δ 10.00 (s, 1H), 7.12 (d, *J* = 8.6 Hz, 2H), 6.86 (d, *J* = 8.6 Hz, 2H), 3.97 (m, 1H), 3.79 (s, 3H), 3.71 (m, 2H), 3.31 (s, 3H), 2.75 (m, 1H), 2.12 (m, 1H), 2.00 (m, 1H), 1.89–1.67 (multiple peaks, 4H), 1.54 (s, 3H), 1.50 (s, 3H).

¹³C NMR (176 MHz, Chloroform-*d*) δ 176.91, 158.32, 137.19, 127.92, 114.16, 85.79, 63.11, 59.76, 56.89, 56.52, 55.44, 39.20, 38.44, 37.96, 35.30, 27.18, 23.33.

The carbon resonances corresponding to the perfluoroarene (C₇F₇) in this compound appear as a complex series of multiplets between 105 ppm to 155 ppm as a result of ¹³C/¹⁹F coupling. Due to the complexities of the system, the peaks are not listed. ¹⁹F NMR and HRMS were used to confirm the presence of this ring system.

¹⁹F NMR (377 MHz, Chloroform-*d*) δ -56.01 (t, *J* = 21.7 Hz, 3F), -141.29 (m, 2F), -143.61 (m, 2F).

HRMS (ESI⁺) [M+H]⁺ Calcd for C₂₆H₂₈F₇N₂O₃: 549.1983; found: 549.1978.



(7c)

Note: 20 mol % Pd(OAc)₂ was used for this substrate. Compound **7c** was isolated in 54% yield as a yellow oil following **general procedure H**. Purification by column chromatography (silica gel; 0% EtOAc to 20% EtOAc in hexanes).

R_f: 0.31 (20% EtOAc in hexanes)

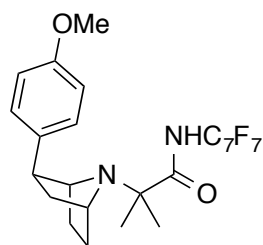
¹H NMR (700 MHz, Chloroform-*d*) δ 10.90 (s, 1H), 7.15 (d, *J* = 8.4 Hz, 2H), 6.87 (d, *J* = 8.4 Hz, 2H), 3.93 (app. s, 4H), 3.80 (s, 3H), 3.63 (app. d, *J* = 10.5 Hz, 2H), 3.27 (m, 1H), 2.44 (t, *J* = 12.6 Hz, 2H), 1.94 (d, *J* = 14.7 Hz, 2H), 1.88 (m, 2H), 1.60–1.52 (multiple peaks, 8H).

¹³C NMR (176 MHz, Chloroform-*d*) δ 177.8, 158.3, 138.1, 128.1, 114.2, 108.7, 64.8, 64.1, 55.4, 46.5, 38.9, 37.6, 31.4, 26.8.

The carbon resonances corresponding to the perfluoroarene (C₇F₇) in this compound appear as a complex series of multiplets between 105 ppm to 155 ppm as a result of ¹³C/¹⁹F coupling. Due to the complexities of the system, the peaks are not listed. ¹⁹F NMR and HRMS were used to confirm the presence of this ring system.

¹⁹F NMR (377 MHz, Chloroform-*d*) δ –56.01 (t, *J* = 18.0 Hz, 3F), –141.57 (m, 2F), –143.82 (m, 2F).

HRMS (ESI⁺) [M+H]⁺ Calcd for C₂₈H₃₀F₇N₂O₄: 592.3088 ; found: 592.3087



(7d)

Note: 5 mol % quinaldic acid was used instead of picolinic acid. Compound **7d** was isolated in 42% yield as a white solid following **general procedure H**.

MP: 97-99 °C

R_f: 0.26 (5% THF in hexanes)

^1H NMR (401 MHz, Chloroform-*d*) δ 9.18 (s, 1H), 7.21 (d, J = 8.3 Hz, 2H), 6.70 (d, J = 8.3 Hz, 2H), 3.80 (m, 1H), 3.65–3.53 (multiple peaks, 4H), 2.91 (app. dd, J = 9.0, 4.4 Hz, 1H), 2.13 (m, 1H), 1.95–1.55 (m, 5H), 1.40 (s, 3H), 1.38 (s, 3H).

^{13}C NMR (176 MHz, Chloroform-*d*) δ 176.35, 157.89, 136.57, 128.03, 113.78, 64.81, 61.14, 56.99, 55.06, 47.83, 37.03, 30.72, 30.13, 25.42, 23.91.

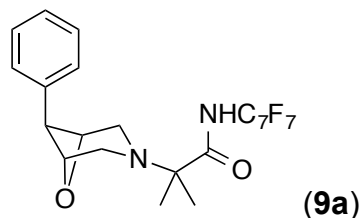
The carbon resonances corresponding to the perfluoroarene (C_7F_7) in this compound appear as a complex series of multiplets between 105 ppm to 155 ppm as a result of $^{13}\text{C}/^{19}\text{F}$ coupling. Due to the complexities of the system, the peaks are not listed. ^{19}F NMR and HRMS were used to confirm the presence of this ring system.

^{19}F NMR (377 MHz, Chloroform-*d*) δ -56.14 (t, J = 21.7 Hz, 3F), -141.93 (m, 2F), -143.61 (m, 2F).

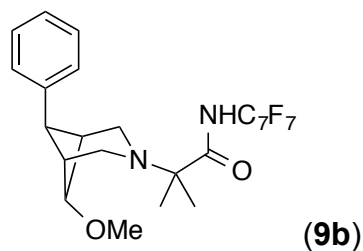
HRMS (ESI $^+$) [$\text{M}+\text{H}$] $^+$ Calcd for $\text{C}_{24}\text{H}_{24}\text{F}_7\text{N}_2\text{O}_2$: 505.1721; found: 505.1720.

Ligand effect on the C–H Arylation of previously reported alicyclic amines

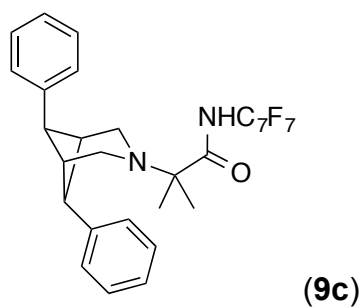
Substrates **8a–8h** were reacted under their previously reported conditions with addition of 5 mol % picolinic acid to the reaction mixture. Products **9a–9h** were isolated as previously reported.¹⁷



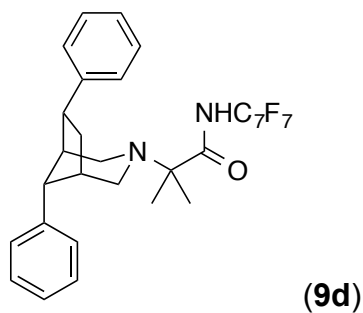
Compound **9a** was isolated in 76% yield. NMR characterization matches literature report. Previous reported yield: 33% yield.¹⁷



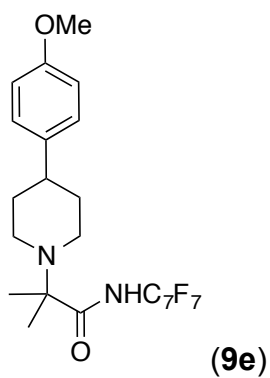
Compound **9b** was isolated in 90% yield. NMR characterization matches literature report. Previous reported yield: 62% yield.¹⁷



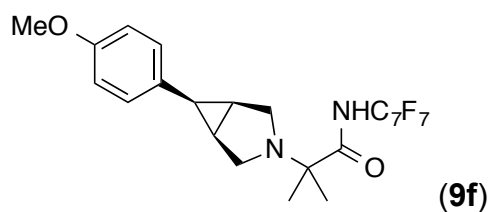
Compound **9c** was isolated in 64% yield. NMR characterization matches literature report. Previous reported yield: 35% yield.¹⁷



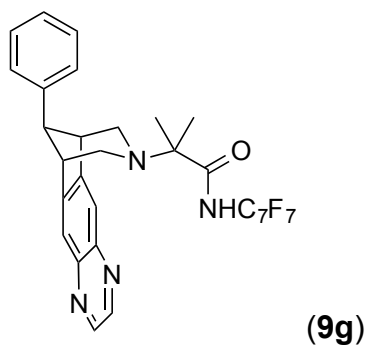
Compound **9d** was isolated in 64% yield. NMR characterization matches literature report. Previous reported yield: 34% yield.¹⁷



Compound **9e** was isolated in 60% yield. NMR characterization matches literature report. Previous reported yield: 55% yield.¹⁷



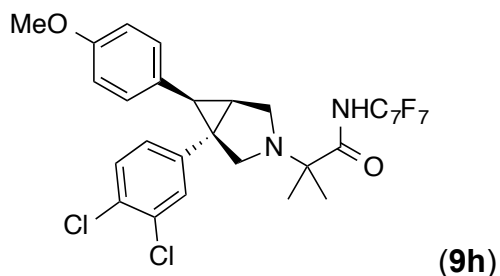
Compound **9f** was isolated in 75% yield. NMR characterization matches literature report. Previous reported yield: 74% yield.¹⁷



Isolated yield using picolinic acid (5 mol %): 68%.

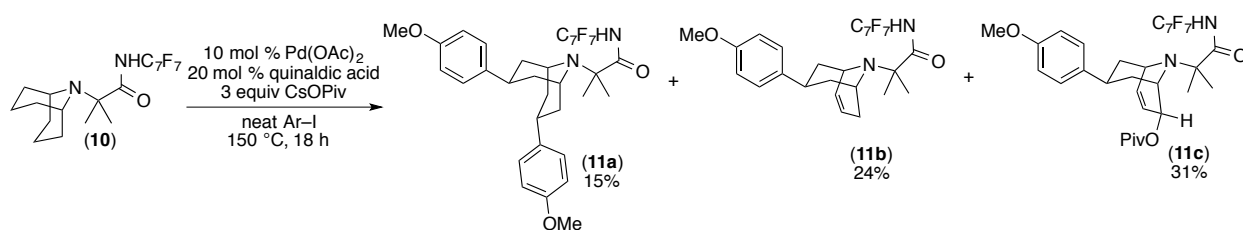
Isolated yield using quinaldic acid (20 mol %): 81%.

NMR characterization matches literature report. Previous reported yield: 45% yield.¹⁷

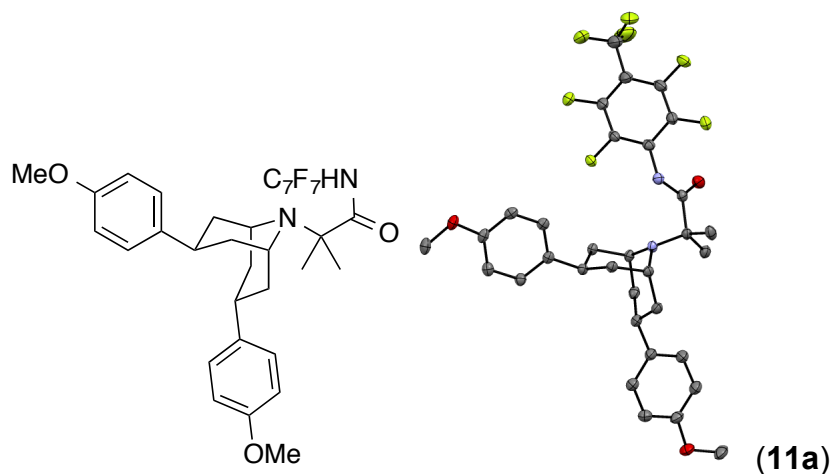


Compound **9h** was isolated in 51% yield. NMR characterization matches literature report. Previous reported yield: 40% yield.¹⁷

C–H Arylation of Azabicyclo[3.3.1]nonane:



Procedure: Under ambient conditions, a 4-mL scintillation vial was charged with solid substrate **10** (40 mg, 0.094 mmol, 1 equiv), Pd(OAc)₂ (2.2 mg, 0.01 mmol, 10 mol %), cesium pivalate (66 mg, 0.28 mmol, 3 equiv), quinaldic acid (3.3 mg, 0.02 mmol, 20 mol %) and 4-iodoanisole (990 mg, 4.23 mmol, 45 equiv). The vial was equipped with a magnetic stir bar, sealed with a Teflon-lined screw cap, and heated to an external temperature of 150 °C. After 18 h, the reaction was cooled to room temperature and diluted with DCM (2.5 mL). Hydrazine hydrate (0.4 mL) was added to the solution and stirred for 30 min at room temperature to remove Pd from the product. The mixture was filtered through Celite and washed with DCM (10 mL). The volatiles were removed by rotary evaporation and the residue was purified via column chromatography (silica gel; 0% to 5% THF in hexanes). Although the column chromatography separated the products (**11a-11c**), minor impurities were observed by ¹H NMR. As such, each of the products were subjected to a preparative TLC (silica gel; 5% THF in hexanes) to afford 15% yield of **11a** as a white solid, 24% yield of **11b** as a colorless oil and 31% yield of **11c** as a white solid.



11a

MP: 170-172 °C

R_f: 0.10 (5% THF in hexanes)

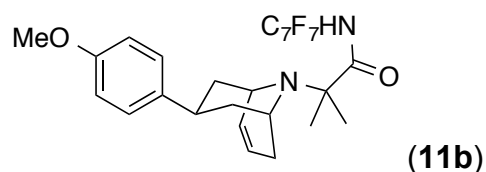
¹H NMR (500 MHz, Chloroform-*d*) δ 9.70 (s, 1H), 7.21 (d, *J* = 8.5 Hz, 4H), 6.89 (d, *J* = 8.5 Hz, 4H), 3.81 (s, 6H), 3.69 (tt, *J* = 12.7, 6.4 Hz, 2H), 3.51 (app. s, 2H), 2.15–1.96 (m, 8H), 1.62 (s, 6H).

¹³C NMR (176 MHz, Chloroform-*d*) δ 176.63, 158.24, 138.93, 127.78, 114.16, 65.27, 55.44, 49.36, 38.38, 37.55, 26.11.

The carbon resonances corresponding to the perfluoroarene (C₇F₇) in this compound appear as a complex series of multiplets between 105 ppm to 155 ppm as a result of ¹³C/¹⁹F coupling. Due to the complexities of the system, the peaks are not listed. ¹⁹F NMR and HRMS were used to confirm the presence of this ring system.

¹⁹F NMR (377 MHz, Chloroform-*d*) δ -56.01 (t, *J* = 21.7 Hz, 3F), -140.95 (m, 2F), -143.56 (m, 2F).

HRMS (ESI+) [M+H⁺] Calcd. for C₃₃H₃₄F₇N₂O₃: 639.2452; found: 639.2444.



11b

R_f: 0.16 (5% THF in hexanes)

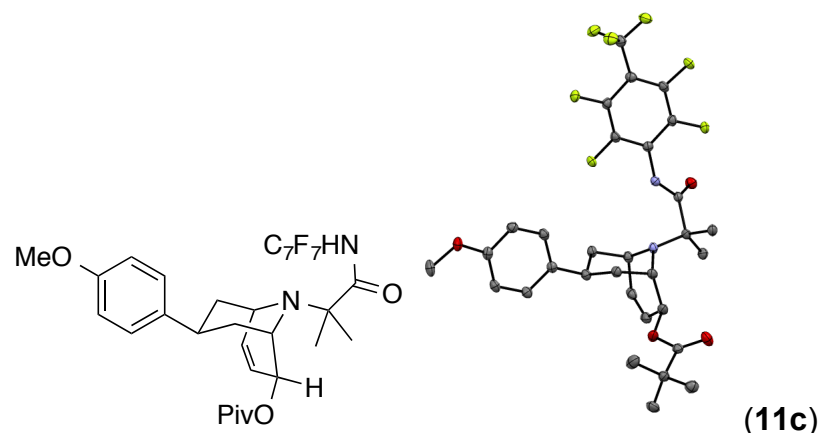
^1H NMR (700 MHz, Chloroform-*d*) δ 9.77 (br s, 1H), 7.15 (d, J = 8.3 Hz, 2H), 6.86 (d, J = 8.3 Hz, 2H), 6.06 (dt, J = 9.9, 3.0 Hz, 1H), 5.92 (m, 1H), 3.79 (s, 3H), 3.61 (s, 1H), 3.42 (s, 1H), 3.21 (tt, J = 12.4, 6.2 Hz, 1H), 2.47 (dd, J = 18.9, 7.0 Hz, 1H), 2.03–1.96 (multiple peaks, 2H), 1.93–1.78 (multiple peaks, 3H), 1.49 (s, 3H), 1.43 (s, 3H).

^{13}C NMR (126 MHz, Chloroform-*d*) δ 176.35, 158.00, 137.55, 130.24, 128.34, 127.87, 113.88, 64.96, 55.26, 50.36, 47.12, 43.59, 37.65, 33.45, 28.75, 24.67, 23.11.

The carbon resonances corresponding to the perfluoroarene (C_7F_7) in this compound appear as a complex series of multiplets between 105 ppm to 155 ppm as a result of $^{13}\text{C}/^{19}\text{F}$ coupling. Due to the complexities of the system, the peaks are not listed. ^{19}F NMR and HRMS were used to confirm the presence of this ring system.

^{19}F NMR (377 MHz, Chloroform-*d*) δ -56.01 (t, J = 21.7 Hz, 3F), -141.09 (m, 2F), -143.74 (m, 2F).

HRMS (ESI+) $[\text{M}+\text{H}^+]$ Calcd. for $\text{C}_{26}\text{H}_{26}\text{F}_7\text{N}_2\text{O}_2$: 531.1877; found: 531.1872.



11c

R_f: 0.13 (5% THF in hexanes)

^1H NMR (700 MHz, Chloroform-*d*) δ 9.47 (s, 1H), 7.14 (d, J = 8.5 Hz, 2H), 6.87 (d, J = 8.5 Hz, 2H), 6.05 (ddd, J = 10.3, 4.6, 1.8 Hz, 1H), 5.95 (dd, J = 10.3, 2.3 Hz, 1H), 5.49 (d, J = 6.8 Hz, 1H), 3.86 (br s, 1H), 3.80 (s, 3H), 3.37 (s, 1H), 3.29 (tt, J = 12.5, 4.5 Hz, 1H), 2.16 (m, 1H), 1.99 (td, J = 12.8, 4.2 Hz, 1H), 1.80 (m, 1H), 1.76 (td, J = 13.3, 4.6 Hz, 1H), 1.55 (s, 3H), 1.46 (s, 3H), 1.24 (s, 9H).

^{13}C NMR (176 MHz, Chloroform-*d*) δ 178.22, 175.53, 158.13, 137.11, 133.64, 127.88, 127.79, 114.00, 67.85, 64.99, 55.25, 51.04, 48.63, 38.87, 36.07, 35.90, 33.24, 27.22, 25.62, 23.44.

^{19}F NMR (377 MHz, Chloroform-*d*) δ -56.03 (t, J = 21.7 Hz, 3F), -140.86 (m, 2F), -143.63 (m, 2F).

HRMS (ESI+) $[\text{M}+\text{H}^+]$ Calcd. for $\text{C}_{31}\text{H}_{34}\text{F}_7\text{N}_2\text{O}_4$: 631.2401; found: 631.2397.

5.6 References

- (1) Vitaku, E.; Smith, D. T.; Njardarson J. T. *J. Med. Chem.*, **2014**, *57*, 10257.
- (2) Fodor, G.; Dharanipragada, R. *Nat. Prod. Rep.* **1994**, *11*, 443.
- (3) (a) Brossi, A.; Cordell, G. A.; Manske, R. H. F.; Rodrigo, R. G. A. *The alkaloids*; 1st ed.; Academic Press: New York, **1995**. (b) Fodor, G.; Dharanipragada, R. *Nat. Prod. Rep.*, **1986**, *3*, 181. (c) Gryniewicz, G.; Gadzikowska, M. *Pharmacol. Rep.* **2008**, *60*, 439. (d) Nocquet, P.-A.; Opatz, T. *Eur. J. Org. Chem.* **2016**, *2016*, 1156. (e) Smith, C. Homotropanes – Synthetic Approaches to the 9-Azabicyclo [4.2.1]nonane/ene Ring System. Ph.D., University of Leicester, **1992**.
- (4) Robinson, R. *J. Chem. Soc., Trans.*, **1917**, *111*, 762.
- (5) (a) Davies, H. M. L.; Saikali, E.; Young, W. B. *J. Org. Chem.*, **1991**, *56*, 5696. (b) Davies, H. M. L.; Matasi, J. J.; Hodges, L. M.; Huby, N. J. S.; Thornley, C.; Kong, N.; Houser, J. H. *J. Org. Chem.* **1997**, *62*, 1095. (c) Reddy, R. P.; Davies, H. M. L. *J. Am. Chem. Soc.* **2007**, *129*, 10312.
- (6) Schultz, D. M.; Wolfe, J. P. *Org. Lett.*, **2011**, *13*, 2962.
- (7) Chen, S.; Bacauanu, V.; Knecht, T.; Mercado, B. Q.; Bergman, R. G.; Ellman, J. A. *J. Am. Chem. Soc.* **2016**, *138*, 12664.
- (8) (a) Singh, S. *Chem. Rev.* **2000**, *100*, 925. (b) Gryniewicz, G.; Gadzikowska, M. *Pharmacological Reports* **2008**, *60*, 439. (c) Hemby, S. E.; Lucki, I.; Gatto, G.; Singh, A.; Thornley, C.; Matasi, J.; Kong, N.; Smith, J. E.; Davies, H. M. L.; Dworkin S. I. *J. Pharmacol. Exp. Ther.* **1997**, *282*, 727.
- (9) Carroll, F. I. *J. Med. Chem.* **2003**, *46*, 1775.
- (10) (a) Cernak, T.; Dykstra, K. D.; Tyagarajan, S.; Vachal; P.; Krska, S. W. *Chem. Soc. Rev.*, **2016**, *45*, 546. (b) Wencel-Delord, J.; Dröge, T.; Liu, F.; Glorius, F. *Chem. Soc. Rev.*, **2011**, *40*, 4740. (c) Neufeldt, S. R.; Sanford, M. S. *Acc. Chem. Res.*, **2012**, *45*, 936. (d) Lyons, T. W.; Sanford, M. S. *Chem. Rev.* **2010**, *110*, 1147.
- (11) (a) Maes, J.; Maes, B. U. W. *Adv. Heterocycl. Chem.* **2016**, *120*, 137-194. (b) Lewis, J. C.; Bergman, R. G.; Ellman, J. A. *Acc. Chem. Res.*, **2008**, *41*, 1013. For radical C–H functionalization reactions see: (c) Dupeyre, R.-M.; Rassat, A.; Ronzaud, J. *J. Am. Chem. Soc.* **1974**, *96*, 6559. (d) Kimura, M.; Ban, Y. *Synthesis*, **1976**, 201. (e) Beddoes, R. L.; Davies, M. P. H.; Thomas, E. J. *J. Chem. Soc., Chem. Commun.* **1992**, 538. (f) Baylis, A. M.; Davies, M. P. H.; Thomas, E. J. *Org. Biomol. Chem.* **2007**, *5*, 3139.
- (12) Pollini, G. P.; Benetti, S.; De Risi, C.; Zanirato, V. *Chem. Rev.* **2006**, *106*, 2434.

- (13) Yu, Y.; Yang, X.-F.; Xu, C.-F.; Ding, C.-H.; Hou, X.-L. *Org. Lett.* **2013**, *15*, 3880.
- (14) Majewski, M.; Lazny, R. *J. Org. Chem.* **1995**, *60*, 5825.
- (15) Sienkiewicz, M.; Wilkaniec, U.; Lazny, R. *Tetrahedron Lett.* **2009**, *50*, 7196.
- (16) (a) Wu, X. *Transition metal-catalyzed heterocycle synthesis via C-H activation*; 1st ed.; Wiley-VCH: Weinheim, 2016. (b) Schultz, D. M.; Wolfe, J. P. *Synthesis*, **2012**, *44*, 351. (c) Thansandote, P.; Lautens, M. *Chem. Eur. J.* **2009**, *15*, 5874. (d) Taylor, A. P.; Robinson, R. P.; Fobian, Y. M.; Blakemore, D. C.; Jones, L. H.; Fadeyi, O. *Org. Biomol. Chem.* **2016**, *14*, 6611.
- (17) Topczewski, J. T., Cabrera, P. J., Saper, N. I.; Sanford, M. S. *Nature* **2016**, *531*, 220.
- (18) (a) McNally, A.; Haffemayer, B.; Collins, B. S. L.; Gaunt, M. J. *Nature* **2014**, *510*, 129. (b) Calleja, J.; Pla, D.; Gorman, T. W.; Domingo, V.; Haffemayer, B.; Gaunt, M. J. *Nature Chemistry* **2015**, *7*, 1009. (c) Willcox, D.; Chappell, B. G. N.; Hogg, K. F.; Calleja, J.; Smalley, A. P.; Gaunt, M. J. *Science*, **2016**, *354*, 851.
- (19) Engle, K. M.; Yu, J.-Q. *J. Org. Chem.*, **2013**, *78*, 8927.
- (20) (a) He, J.; Li, S.; Deng, Y.; Fu, H.; Laforteza, B. N.; Spangler, J. E.; Homs, A.; Yu, J.-Q. *Science* **2014**, *343*, 1216. (b) Wasa, M.; Chan, K. S. L.; Zhang, X.-G.; He, J.; Miura, M.; Yu, J.-Q. *J. Am. Chem. Soc.* **2012**, *134*, 18570.
- (21) Engle, K. M.; Wang, D.-H.; Yu, J.-Q. *J. Am. Chem. Soc.* **2010**, *132*, 14137.
- (22) (a) Ferreira, E. M.; Stoltz, B. M. *J. Am. Chem. Soc.* **2003**, *125*, 9578. (b) Stuart, D. R.; Fagnou, K. *Science* **2007**, *316*, 1172.
- (23) Bandara, H. M. D.; Jin, D.; Mantell, M. A.; Field, K. D.; Wang, A.; Narayanan, R. P.; Deskins, N. A.; Emmert, M. H. *Catal. Sci. Technol.* **2016**, *6*, 5304.
- (24) Baxter, R. D.; Sale, D.; Engle, K. M.; Yu, J.-Q.; Blackmond, D. G. *J. Am. Chem. Soc.*, **2012**, *134*, 4600.
- (25) Kim, D.I.; Schweri, M. M.; Deutsch, H. M. *J. Med. Chem.*, **2003**, *46*, 1456.
- (26) (a) Emmert, M. H.; Cook, A. K.; Xie, Y. J.; Sanford, M. S. *Angew. Chem. Int. Ed.* **2011**, *50*, 9409. (b) Cook, A. K.; Emmert, M. H.; Sanford, M. S. *Org. Lett.* **2013**, *15*, 5428. (c) Chen, G.; Zhuang, Z.; Li, G.; Saint-Denis, T.; Hsiao, Y.; Joe, C.; Yu, J.-Q. *Angew. Chem. Int. Ed.* **2017**, *56*, 1506. (d) Chen, G.; Shigenari, T.; Jain, P.; Zhang, Z.; Jin, Z.; He, J.; Li, S.; Mapelli, C.; Miller, M.; Poss, M.; Scola, P.; Yeung, K.; Yu, J.-Q. *J. Am. Chem. Soc.* **2015**, *137*, 3338. (e) Wasa, M.; Chan, K. S. L.; Zhang, X.-G.; He, J.; Miura, M.; Yu, J.-Q. *J. Am. Chem. Soc.* **2012**, *134*, 18570.
- (27) Valderas, C.; Naksomboon, K.; Fernandez-Ibañez, A. M. *ChemCatChem* **2016**, *8*, 3213.
- (28) Ryabov, A. D. *Chem. Rev.*, **1990**, *90*, 403.
- (29) Smalley, A. P.; Gaunt, M. J. *J. Am. Chem. Soc.* **2015**, *137*, 10632.
- (30) (a) Ryabov, A. D.; Sakodinskaya, I. K.; Yatsimirsky, A. K. *J. Chem. Soc., Dalton Trans.* **1985**, 2629.

(31) (a) Blackmond, D. G. *Angew. Chem., Int. Ed.* **2005**, *44*, 4302. (b) Jinu, S.; Mathew, J. S.; Klusmann, M.; Iwamura, H.; Valera, F.; Futran, A.; Emanuelsson, E. A. C.; Blackmond, D. G. *J. Org. Chem.*, **2006**, *71*, 4711.

(32) Although at the same-excess $[e] = [\text{PhI}]_0 - [\mathbf{1}]_0 = 0.36 \text{ M} - 0.12 \text{ M} = 0.24 \text{ M}$. We maintained the $[\text{PhI}]$ concentration as 0.36 M due to the negligible difference in the $[e]$ constant (0.03 M), as PhI is already in large excess relative to substrate **1** (3 equiv of PhI relative to **1**). To put it in perspective: standard conditions use 10 μL of PhI, the same excess reaction would require 9.25 μL .

(33) (a) Jones, W. D. *Acc. Chem. Res.*, **2003**, *36*, 140. (b) Simmons, E. M.; Hartwig, J. F. *Angew. Chem. Int. Ed.* **2012**, *51*, 3066. (c) Gomez-Gallego, M.; Sierra, M. A. *Chem. Rev.* **2011**, *111*, 4857.

(34) Cook, A. K.; Sanford, M. S. *J. Am. Chem. Soc.* **2015**, *137*, 3109.

(35) Cesium was also observed by ICP.

(36) Leroux, F. R.; Manteau, B.; Vors, J.-P.; Pazenok, S. *Beilstein J. Org. Chem.* **2008**, *4*, 13.

(37) Liu, G.; Wu, Y. *Top. Curr. Chem.* **2010**, *292*, 195.

(38) Davies, D. L.; Donald, S. M. A.; Macgregor, S. A. *J. Am. Chem. Soc.* **2005**, *127*, 13754.

(39) Nocquet, P.-A.; Opatz, T. *Eur. J. Org. Chem.* **2016**, *2016*, 1156.

(40) Simoni, D.; Rossi, M.; Bertolasi, V.; Roberti, M.; Pizzirani, D.; Rondanin, R.; et. al. *J. Med. Chem.* **2005**, *48*, 3337.

(41) O'Donnell, C. J.; Singer, R. A.; Brubaker, J. D.; McKinley, J. D. *J. Org. Chem.* **2004**, *69*, 5756.